Russian Original Vol. 42, No. 4, April 1977

SATEAZ 42(4) 289-398 (1977)

SOVIET ATOMIC ENERGY

АТОМНАЯ ЭНЕРГИЯ
(ATOMNAYA ÉNERGIYA)

TRANSLATED FROM RUSSIAN

CONSULTANTS BUREAU, NEW YORK

SOVIET ATOMIC ENERGY

Soviet Atomic Energy is a cover-to-cover translation of *Atomnaya Énergiya*, a publication of the Academy of Sciences of the USSR.

An agreement with the Copyright Agency of the USSR (VAAP) makes available both advance copies of the Russian journal and original glossy photographs and artwork. This serves to decrease the necessary time lag between publication of the original and publication of the translation and helps to improve the quality of the latter. The translation began with the first issue of the Russian journal.

Consultants Bureau journals appear about six months after the publication of the original Russian issue. For bibliographic accuracy, the English issue published by Consultants Bureau carries the same number and date as the original Russian from which it was translated. For example, a Russian issue published in December will appear in a Consultants Bureau English translation about the following June, but the translation issue will carry the December date. When ordering any volume or particular issue of a Consultants Bureau journal, please specify the date and, where applicable, the volume and issue numbers of the original Russian. The material you will receive will be a translation of that Russian volume or issue.

Subscription
$117.50 per volume (6 Issues)
2 volumes per year

Single Issue: $50
Single Article: $7.50

Prices somewhat higher outside the United States.

CONSULTANTS BUREAU, NEW YORK AND LONDON

227 West 17th Street
New York, New York 10011

Published monthly. Second-class postage paid at Jamaica, New York 11431.

Soviet Atomic Energy is abstracted or indexed in *Applied Mechanics Reviews, Chemical Abstracts, Engineering Index, INSPEC—Physics Abstracts and Electrical and Electronics Abstracts, Current Contents,* and *Nuclear Science Abstracts.*

SOVIET ATOMIC ENERGY

A translation of *Atomnaya Énergiya*

October, 1977

Volume 42, Number 4 April, 1977

CONTENTS

CONTENTS

(continued)

The Russian press date (podpisano k pechati) of this issue was 3/23/1977. Publication therefore did not occur prior to this date, but must be assumed to have taken place reasonably soon thereafter.

THE OPTIMUM RATIO BETWEEN THE OPERATIONAL COMPONENT TIMES OF AN EMERGENCY PROTECTION DRIVE (EPD)

V. P. Petrov

UDC 621.039.5:62-7

Emergency protection drives (EPD's) are widely used in nuclear reactors. Electromagnets (EM's) are used in retaining the safety rods outside the reactor core, while springs attempt to insert them into the core. The operation time of such an EPD is made up of the EM pick-up time (i.e., the time from the instant the the voltage is applied to the EM to the instant the EM armature begins to move) and the travel time of the EPD mechanical system, which amounts to the travel time of the safety rods. As the spring force increases, the travel time of the EPD mechanical system t_{ms} is reduced, while the EM pick-up time increases, as a consequence of which the latter has to be designed for larger forces. Therefore, there is a basis to assume that an optimum ratio between the components exists, which ensures a minimum operating time t_{op} of the EPD.

The aim of this article is to determine this ratio.

It would be helpful to obtain the results for cases in which the displacement of the safety rod is first a function of the instant at which the limiting permissible reactor power is achieved under emergency conditions and, second, a function of a given quantity (a variant that is frequently encountered when developing EPD's).

Let us consider the optimum ratio for the first case. Let us assume that as a result of some cause (e.g., operator error), a surge of positive reactivity arises in the reactor, and the reactor power rises sharply. Figure 1 shows the reactor-power curve for this case. The operating time of the automatic equipment in the emergency protection control system is small in relation to the EPD operating time, and can be assumed to be zero. The EM is energized at instant t_1. At t_2 the EM armature moves and the safety rods begin to enter the reactor core. Because of this the rise rate of the reactor power declines. At instant t_k a negative reactivity equal to ρ_k is introduced by the safety rod, which is sufficient to ensure an end to the power rise. A sharp decrease in power occurs at t_k as the negative reactivity continues to be introduced, e.g., by a brake on the safety rod.

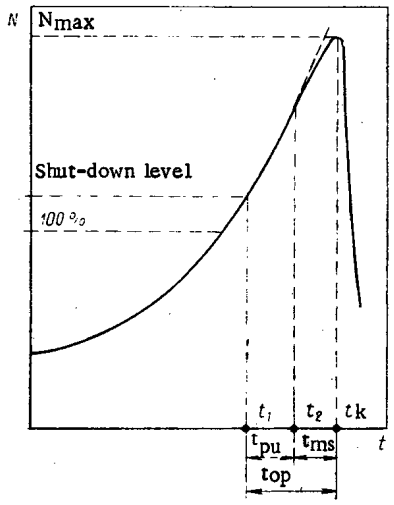

Fig. 1. Diagram showing the shut-down of the reactor after operation of the emergency protection.

Translated from Atomnaya Énergiya, Vol. 42, No. 4, pp. 259-262, April, 1977. Original article submitted December 15, 1975.

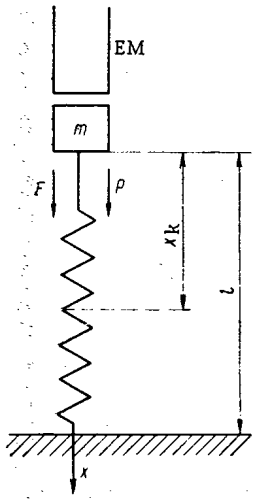

Fig. 2. Diagrammatic representation of a displacement of a safety rod.

The generation of energy which is proportional to the area below the curve (see Fig. 1) represents a danger to the reactor itself. If this energy exceeds the permissible level, then damage could result. According to [1], this energy is proportional to the maximum power N_{max}. Therefore, the t_k represents the instant of danger to the reactor, which corresponds to the attainment of N_{max}.

When deriving the optimum ratio, we assume that the onset of t_k to a first approximation is conditioned only by the negative reactivity ρ_k and does not depend upon the introduction rate.

Let us consider the displacement of the safety rod, of the pull rod connected to the EM, under the influence of the spring force and the mass of the moving system comprising the EPD (Fig. 2). The spring acts over gap l, which equals the displacement of the safety rod in the reactor core up to the initiation of braking. We signify the force of the spring stretched over the length l by F. We signify the mass of the moving system of the EPD together with the safety rod by m, while the corresponding force is P. Let us now consider the displacement of the safety rod in gaseous and liquid media.

If we ignore the effect of the resistance in the gaseous medium on the rod velocity (which is quite permissible, due to the fact that this resistance is small in relation to the spring force), then the expression for determining the travel time of the EPD mechanical system up to the instant the safety rod is inserted by a length x_k, corresponding to the introduction of a negative reactivity equal to ρ_k into the reactor core, has the form

$$t_{ms} = C_1 \sqrt{\beta} \arccos\left(1 - \frac{x^*}{\beta + 1}\right), \tag{1}$$

where

$$C_1 = \sqrt{l/g}; \tag{2}$$

$$\beta = P/F; \tag{3}$$

$$x_k^* = x_k/l; \tag{4}$$

where g is the acceleration due to gravity. Equation (1) is obtained by solving the equation of motion of mass m under the influence of the gravitational and spring forces.

To avoid exceeding the allowable EM surge voltage rating when this is switched off, its winding is shunted by a resistor (Fig. 3a) or stabilitron (Fig. 3b), or other, less usual, connection schemes may be employed. It follows from [2] that the EM pick-up time is directly proportional to the EM constant τ:

$$t_{pu} = C_2 \tau, \tag{5}$$

where C_2 is a function of the EM pick-up current in per unit terms and the magnitude of the surve voltage K, i.e., the ratio of the EM surge amplitude at switch-off to the EM voltage source.

In order to find the relationship between τ and the spring force, let us equate the EM pull force F_{pu}, expressed in terms of the pick-up current I_{pu}, to the sum of spring force F and P. For an unsaturated magnetic system in the EM, this condition can be described in the form [3]:

$$F_{pu} = -0.5 I_{pu}^2 L_{EM}/\delta_0 = -(F + P), \tag{6}$$

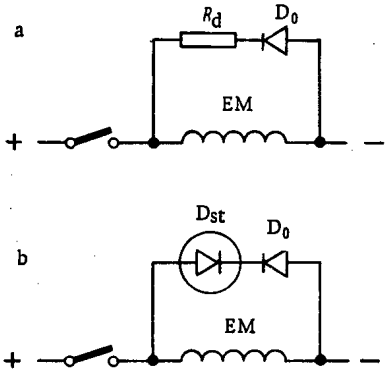

Fig. 3. The most commonly used scheme for disconnecting the EM using: a) a resistance; b) a stabilitron.

where L_{EM} is the EM inductance and δ_0 is the operating air gap in the EM core.

Let us characterize the pull magnitude due to the EM at rated current I_{rtd} in relation to the pull at pick-up current I_{pu} by margin k_m:

$$k_m = F_{rtd}/F_{pu} = (I_{rtd}/I_{pu})^2. \tag{7}$$

Then from (6), and taking (7) into consideration, we obtain

$$\tau = (2\delta_0 k_m/P_{EM})(F+P), \tag{8}$$

where P_{EM} is the EM power; we can define C_2 from the data given in [2] and Eq. (7) (for the scheme of Fig. 3a and b, respectively):

$$C_{2R} = \frac{1}{1+K}\ln\sqrt{\frac{1}{k_m}}; \tag{9}$$

$$C_{2st} = -\ln\frac{K+\sqrt{1/k_m}}{K+1}. \tag{10}$$

From Eqs. (5), (3), and (8) we find that

$$t_{pu} = C_3(\beta+1)/\beta, \tag{11}$$

where

$$C_3 = C_2\frac{2\delta_0 k_m}{P_{EM}}P. \tag{12}$$

We find t_{op} by summing the right-hand sides of Eqs. (1) and (11). By studying these expressions at the extremum for variation of β, we find the conditions for minimum t_{op} (at spring force F_e, i.e., $\beta = \beta_e$)

$$\frac{C_3}{C_1} = \beta_e^2\left[\frac{1}{2\sqrt{\beta_e}}\arccos\left(1-\frac{x_k^*}{\beta_e+1}\right)-\frac{x_k^*\sqrt{\beta_e}}{(\beta_e+1)\sqrt{2x_k^*(\beta_e+1)-x_k^{*2}}}\right]. \tag{13}$$

By defining C_3 from Eq. (13) in terms of C_1, we are able to find the optimum ratio between the operational component times of an EPD for motion of a safety rod in a gas:

$$\frac{t_{pu.e}}{t_{ms.e}} = \frac{\beta_e+1}{2} - \frac{\beta_e x_k^*}{\sqrt{2x_k^*(\beta_e+1)-x_k^{*2}}\arccos\left(1-\frac{x_k^*}{\beta_e+1}\right)}. \tag{14}$$

The relationship of the extremum point β_e to the ratio C_3/C_1 and x_k^*, and also the optimum ratio of β_e and x_k^*, are illustrated by the curves of Fig. 4, which were plotted in accordance with Eqs. (13) and (14). When $\beta_e = 0$, which corresponds to neglecting the small mass of the EPD moving system in relation to the spring force, the optimum ratio is 0.5. The effect of the gravitational force P upon the optimum ratio, up to a tenfold increase of P over the spring force F, is sufficiently small; overall, the optimum ratio is reduced by 18% and equals 0.5 over the range of β from 0 to 0.1.

Since the spring force usually exceeds the gravitational force on the moving system, we are particularly interested in the case where the EM pick-up time is half of the safety rod travel time. To find the spring force F_e corresponding to this condition, together with t_{pu} and t_{ms}, we introduce the gravitational force P for constant C_1 and C_3 into Eqs. (2) and (12) and also take (3) into account; we can then rewrite Eqs. (1), (11), and (13). As a result, we obtain

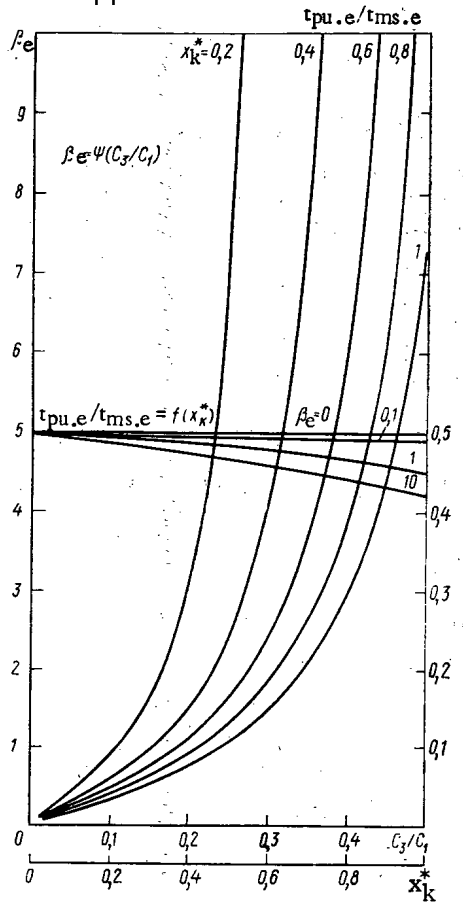

Fig. 4. Relationships of extremum point β_e to C_3/C_1 and x_k^*, and of optimum ratios of $t_{pu.e}/t_{ms.e}$ to x_k^* and β_e.

$$t_{ms} = C_4\sqrt{1/F}; \tag{15}$$

$$C_4 = \sqrt{lm}\arccos(1 - x_k^*); \tag{16}$$

$$t_{pu} = C_5 F; \tag{17}$$

$$C_5 = C_2(2\delta_0 k_m / P_{EM}); \tag{18}$$

$$F_e = \sqrt[3]{\frac{1}{4}\left(\frac{C_4}{C_5}\right)^2}. \tag{19}$$

Figure 5 shows the variations of t_{ms}, t_{pu}, and t_{op} with the spring force for arbitrary units of F^*:

$$F^* = F/F_e \tag{20}$$

It follows from Fig. 5 that the EPD operating time varies very little within the region $F^* = 1$ (which corresponds to F_e). This enables us to somewhat reduce the spring force without greatly affecting the operating time. For example, reducing F^* to 0.65 leads to an increase in the operating time to 5% of its maximum value.

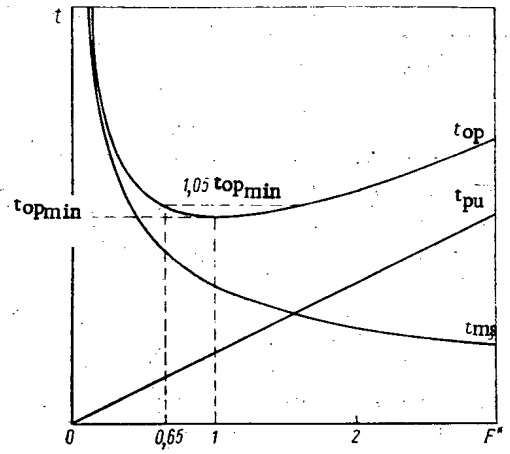

Fig. 5. Variation of pick-up time, safety rod travel time, and EPD travel time in relation to the spring force of the drive.

To obtain the optimum ratio for the case of a safety rod moving through liquid, we have to take into consideration the resistance of the liquid to the rod motion. The gravitational force acting on the moving system of the drive and the force ejecting the safety rod from the liquid can be neglected, which is justified for two reasons:

a) in drives where the rod moves through a liquid, the spring force is usually significantly greater than the gravitational force acting on the moving system of the drive;

b) the force tending to eject the safety rod from the liquid is partially compensated by the gravitational force acting on the moving system of the drive, which greatly reduces its share of the resultant force acting on the rod.

Consequently, the pick-up time of the EM should represent half the travel time of the safety rod for minimum operating time of the EPD as a whole. In this case, Eqs. (15) and (17)-(19) are justified. The effect that the viscosity of the medium has on the travel of the safety rod is reflected in the expression for C_4, which takes on the form:

$$C_{4,\,\text{liq}} = 1.41\mu l\sqrt{l}\int_0^{x_k^*}\frac{dx^*}{\sqrt{2\mu l\,(1-x^*)+m-(2\mu l+m)\exp(-2\mu l x^*/m)}}. \qquad (21)$$

Here

$$\mu = 0.5C_x\rho S,$$

where C_x is the drag coefficient, which depends upon the rod form; ρ, the medium density; S, end-surface area of the safety rod [4].

Equation (21) is obtained for turbulent motion of the rod through the liquid when the rod drag coefficient is proportional to the square of the velocity [4]. Turbulent motion of rod follows from the Reynolds number which, as can be seen from the dimensions of the rod normally used in water-cooled–water-moderated reactors and its travel time, will be of the order 200,000-400,000, which exceeds the limiting value of the Reynolds number (20,000) by a number of times at which laminar flow of a liquid remains possible.

Since the working stroke of the safety rod is a given value, the formulas given earlier are valid. We understand length l as value x_k, i.e., the given length of the operating stroke of the rod. In this case, according to [4], $x_k^* = 1$; the optimum ratio remains as before; to obtain a minimum drive operating time, the pick-up time of the EM should equal about half the travel time of the safety rod.

LITERATURE CITED

1. M. A. Schulz, Regulating Nuclear Power Reactors [Russian translation], Izd-vo Inostr. Lit., Moscow (1957), p. 388.
2. V. P. Petrov, Elektrichestvo, No. 8, 50 (1975).
3. A. K. Ter-Akopov, The Dynamics of High-Speed Electromagnets [in Russian], Énergiya, Moscow (1965), p. 47.
4. K. A. Putilov, A Course in Physics [in Russian], Fizmatgiz, Moscow (1962), p. 208.

PRINCIPLES INVOLVED IN THE DESIGN OF AUTOMATIC CONTROL SYSTEMS FOR THE DISTRIBUTION OF ENERGY IN CHANNEL REACTORS

I. Ya. Emel'yanov, E. V. Filipchuk, P. T. Potapenko, V. G. Dunaev, and N. A. Kuznetsov

UDC 621.039.562:621.039.517

During the widespread development of nuclear power over recent years, both in the USSR and abroad, work has been carried out on the development of computer-based automatic control systems employing reactors. Regardless of the computer's drawbacks as a means of control, including first and foremost its inadequate reliability, it is being used more and more in the design of reactors. Almost all reactors built throughout the world over the last 5-8 years, and all reactors at present under design, have incorporated computers in their automatic monitor and control systems. Check systems based on "objective" computers have been used on the second units at the Beloyarsk and Novovoronezh nuclear power stations and a similar system has been installed on the Leningrad nuclear power station for monitoring the operation of the power unit incorporating reactor type RBMK.

One of the important and urgent questions concerning the operation of the computer complexes of automatic control systems for reactors is the creation of a mathematical base for their operation. The difficulty here lies not only in the size of the program but also in the creation and experimental processing of effective monitor and control algorithms.

The problems of mathematical processing for the signals from transducers within the reactor have been well-enough tested out under operational conditions in [1]. Some questions concerned with the design of direct digital control of reactor power distribution have been considered in [2]. At the same time, there have been practically no publications in non-Soviet literature concerned with the development of algorithms for the optimum control of energy distribution.

Statement of the Problem. The balancing of energy distribution, designed to bring the average power and thermal loading near to the maximum, is the basis of the modern approach to controlling large reactors.

Reducing the radial coefficient of imbalance in energy distribution enables us to achieve practically the same increase in reactive power, increased burnup, and ensure the maintenance of a given margin up to critical thermal loads.

Among the control problems that make it necessary to use manual optimization of the energy distribution in reactors type RBMK, we would do well to pick out the following:

1. obtaining a basic optimally balanced energy distribution;
2. controlling the regulation of the rods so as to maintain the regulating rods within their most effective range, particularly when load is being reapplied after a shut down;
3. the compensation of local disturbances caused by overloading fuel channels, when the location of the disturbance and its magnitude are usually known beforehand;

In general, the problem of controlling energy distribution consists in maintaining some desired distribution under steady-state and transient conditions, which is assigned to the computer as the conditions for achieving maximum power and reliability from the heat-engineering standpoint.

Translated from Atomnaya Énergiya, Vol. 42, No. 4, pp. 263-267, April, 1977. Original article submitted May 3, 1976.

As the optimum condition for the type RBMK reactor is a uniform distribution, the control problem can best be formulated as the minimization of any deviations of energy generation in each discrete control region from the mean level. As a measure of this deviation, we use the quadratic form

$$I = \sum_{k=1}^{N} \{\Phi(k) - \overline{\Phi}(k)\}^{\mathrm{T}} \{\Phi(k) - \overline{\Phi}(k)\},$$

where k = 1, 2, ...; N is a discrete time; $\Phi(k)$ and $\overline{\Phi}(k)$ are vectors of deviation from the mean value with a scale defined by the number of check points; Q is the positively defined weight matrix for the forms of energy distribution, a special case of which is equal to the identity matrix.

We should note that the quadratic relationship of the functional to the value of $\{\Phi(k) - \overline{\Phi}(k)\}$ has the effect that the functional varies little with small variations in energy output. This is an advantage insofar as small (apparent) variations in energy output can be due to inaccuracies in measurement.

In [3] are formulated a number of safety requirements, which must be observed when developing specific control schemes for reactors. When we are considering control functions suitable for assignments to the computer, we should take safety in reactor operation as the basic criterion.

The computer must be entrusted to carry out those functions which, while they are sufficiently important, can still be carried out manually or by means of analog regulators should the computer fail.

From this standpoint, the energy distribution control problem is very suitable for assignment to the computer. On the one hand, the balancing of energy distribution for large reactors is a necessary condition of their operation, while optimizing the position of the regulating rods is a difficult multidimensional problem, whose solution reduces essentially to sorting through a large number of variants. The quality and speed of solution depends in large measure on the operator test. The use of a computer for generating recommendations on optimum strategy for control to a great extent takes the burden from the operator and enables a more uniform distribution of energy to be achieved. On the other hand, failure of the computer or its control program should not give rise to a fault situation, as its function in this case would override the operator.

From consideration of the safety of the regulation system, it would be advisable to base this on the heirarchical principle, using self-consistent regulating equipment with a self-consistent memory in the lowest level of the heirarchy. The normal state of the computer as an element of the higher level of the control heirarchy would be one in which there is no output signals [3]. From this point of view, the best operating mode for the computer would be the "operator advisory" mode.

To design energy distribution control systems we must have enough information on the state of the object being controlled. We must then postulate that all questions connected with the mathematical processing of the signals from the transducers within the reactor are solved on the basis of method [1], while the reactor has a computer-based system of monitoring which operates in real time.

The problem consists in developing a control algorithm for a given number of regulating rods whose position is known, which enables us to find the optimum control, taking engineering limitations into consideration, for a reasonable expenditure in computer time and data storage capacity.

Formulating the Control Problem. Let us assume that the energy distribution is measured digitally in n regions, while r regulating rods are used for control purposes.

For the steady-state condition, the process of measurement at the monitor points gives rise to displacements of the regulating rods. This can be described by the equation

$$\Phi(k+1) = \Phi(k) + C(k)\,\delta u(k), \tag{1}$$

where $\Phi(k)$ is the n-dimensional vector of energy distribution; $\delta u(k)$ is the r-dimensional vector of control; $C(k)$ is the static transfer matrix of the zone.

Under these circumstances, due to the corresponding choice of time interval $[t_k, t_{k+1}]$ between two sequential regulating influences, the rapid processes linked, e.g., with temperature variations of the fuel elements, with the displacements of the rods, and the inertia of the transducers, are completed during this interval, whereas the contamination by xenon and the temperature of the graphite have not changed.

The transfer matrix $C(k)$ can be obtained for a given physical design of reactor or it can be determined from measurements by means of transducers within the reactor. The variations of state $\delta\Phi(k) = C(k)\delta u(k)$, observed at the end of the transient, represent linear conversions of the measured positions of the rods,

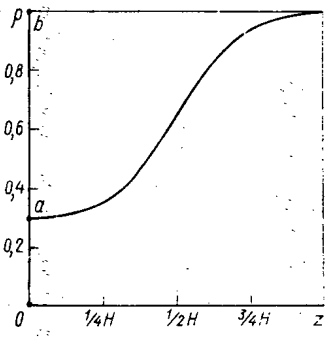

Fig. 1. Calibration characteristic of the control channel.

expressed in reactivity units $\delta u(k)$, with conversion operator

$$C = \begin{pmatrix} \frac{\delta\Phi_1}{\delta u_1} & \cdots & \frac{\delta\Phi_1}{\delta u_r} \\ \cdots & \frac{\delta\Phi_i}{\delta u_j} & \cdots \\ \frac{\delta\Phi_u}{\delta u_1} & \cdots & \frac{\delta\Phi_u}{\delta u_r} \end{pmatrix}.$$

The elements of the transfer matrix $C = \delta\Phi_i/\delta u_j$ can be determined from known pairs of vectors $\{\delta\Phi(k); \delta u(k)\}$ [4].

We can see from the physical concepts involved that matrix $C(k)$ exists and is unique for any conditions of operation of the reactors. However, inaccuracies in measurement and significant spread of the vector pair $\{\delta\Phi(k); \delta u(k)\}$ affect its numerical dependence. Furthermore, the transfer matrix depends upon the actual state of the process; we therefore have to restore (adapt) its elements periodically, replacing the initial data by new data which more closely approximate to the real conditions of operation. When doing this, we stipulate that vectors $\delta\Phi$ and δu belong to regions of linearity and effectiveness, respectively, and that among vectors δu we have at least one r that is linearly independent.

The most important cause of variation in matrix C is variation in the effectiveness of the rods with changes in the height of energy distribution. In this regard, there is significant variation in the characteristics of the control channel (Fig. 1). As the height of the energy distribution is a monitored quantity, we can vary the characteristic in relation to variations in the neutron flux and further increase its accuracy with respect to experimental results.

For reactors with zero or positive power coefficients of reactivity, the necessary condition for the existence of a quasistatic C matrix is the presence of an automatic power regulator, while for a reactor with an unstable spatial energy distribution, zone (local) regulators are needed. Therefore, in the future we will propose that the reactor be equipped with an automatic power regulator and (or) a system of zone regulators, and matrix C be obtained as the result of measurements with the automatic regulators in circuit.

As we have already stated, the aim of control consists in minimizing in the general case over an infinite interval of time a functional of the form

$$I = \sum_{k=1}^{N} \{\Phi(k) - \overline{\Phi}(k)\}^{\mathrm{T}} Q \{\Phi(k) - \overline{\Phi}(k)\}.$$

However, if we take into consideration the properties of the object (1) the unknown control strategy breaks down into a series of partial strategies. Over each interval of time, the aim consists in minimizing the sum of the squares of the energy distribution deviations from the mean value, taking the limitations into consideration.

We can assume that the solution to this optimum problem is equivalent to a solution by the least-squares method of the system of equations

$$\Delta\Phi = C\,\Delta u, \tag{2}$$

where $\Delta\Phi$ is the error vector; Δu is the unknown displacement of the regulating rods.

The Control Algorithm. We know that in the absence of limitations, the solution to system (2) can be found with the aid of the pseudoinverse matrix C^+ [5]:

$$\Delta u^{\circ} = C^{+}\Delta\Phi, \tag{3}$$

where

$$C^{+} = (C^{T}C)^{-1}C^{T}.$$

This solution possesses the important property that its norm is minimal. This is particularly important when applied to reactor control, as the optimum equation not only ensures the best equalization of energy generation, but also guarantees the minimum possible displacement of the regulating rods.

In practice, the unknown optimum equation must satisfy a series of engineering limitations, among which the following are the most important:

1. the optimum equation so obtained must not vary the total power of the reactor;
2. limitation on the regulating action. A typical calibration characteristic for a control channel is given in Fig. 1. The nonlinearity we are considering is connected with the fact that the rods in the general case can only be introduced into a channel that has first been filled with water;
3. the power (output steam content) of the individual fuel channels must not exceed the limiting permissible value corresponding to critical heat exchange.

Let us consider the algorithm for operation of the system taking limitations into account. We will not specify the reasons leading to the need to calculate the optimum displacements of the regulating rods; we merely assume that the aim consists in calculating a technologically practicable system of control for a given vector of errors $\Phi - \bar{\Phi}$.

The First Step. We calculate, in accordance with (3), the "ideal" control vector

$$u^{\circ} = u + \Delta u^{\circ} = u + (C^{T}C)^{-1}C^{T}\Delta\Phi,$$

where u is the initial position of the rods.

The Second Step. Taking (1) into account, we determine the desired energy distribution at each monitor point $\Phi_d = \Phi + C\Delta u^{\circ}$ and the total power $\varphi = \sum_{i=1}^{n} \alpha_i \Phi_d$, where α_i are the weight coefficients.

If φ exceeds the given total power φ_0, all the control actions are reduced by a value $\delta\Delta u^{\circ} = (\varphi - \varphi_0)/\sum_{i=1}^{n}\sum_{j=1}^{r} C_{ij}$.

The Third Step. The values of control action so obtained are compared to the permissible actions (see Fig. 1) and the engineering realization of the rod displacement Δu^{p} is determined in the following manner:

$$\text{if} \quad u_i + \Delta u_i^{\circ} \geqslant b, \text{then} \Delta u_i^{p} = b - u_i;$$

$$\text{if} \quad a \leqslant u_i + \Delta u_i^{\circ} < b, \text{then} \Delta u_i^{p} = \Delta u_i^{\circ};$$

$$\text{if} \quad a/2 \leqslant u_i + \Delta u_i^{\circ} < a, \text{then} \Delta u_i^{p} = a - u_i;$$

$$\text{if} \quad u_i + \Delta u_i^{\circ} < a/2, \text{then} \quad \Delta u_i^{p} = -u_i.$$

The Fourth Step. We determine the new desired value of the error vector $\Delta\Phi_d = C\Delta u^{p}$, which further minimizes the variation in control action, corresponding to the effective range of rods

$$\Delta u^{p} = (\tilde{C}^{T}\tilde{C})^{-1}\tilde{C}^{T}\Delta\Phi_d$$

where $\tilde{C}$ is the matrix obtained from C by plotting those columns which correspond to the boundary values of the control effect (points 0, a, and b in Fig. 1).

The Fifth Step. We again determine the desired energy distribution $\Phi_d = \Phi + C\Delta u^{p}$ and compare this with the limiting permissible values. For those channels in which an increase is observed, recommendations are given regarding the increase in the flow of coolant or reduction in the appropriate settings.

As we have already stated, in addition to the problem of calculating the position of the control actuators to ensure the base regime, the need also arises to compensate for disturbances brought about by overloaded fuel channels and maintaining the rods by means of an automatic regulator in the effective range. In similar cases, we have observed undesirable deviations of energy generation in small local zones, and for control purposes, it is advisable to employ criteria of the form

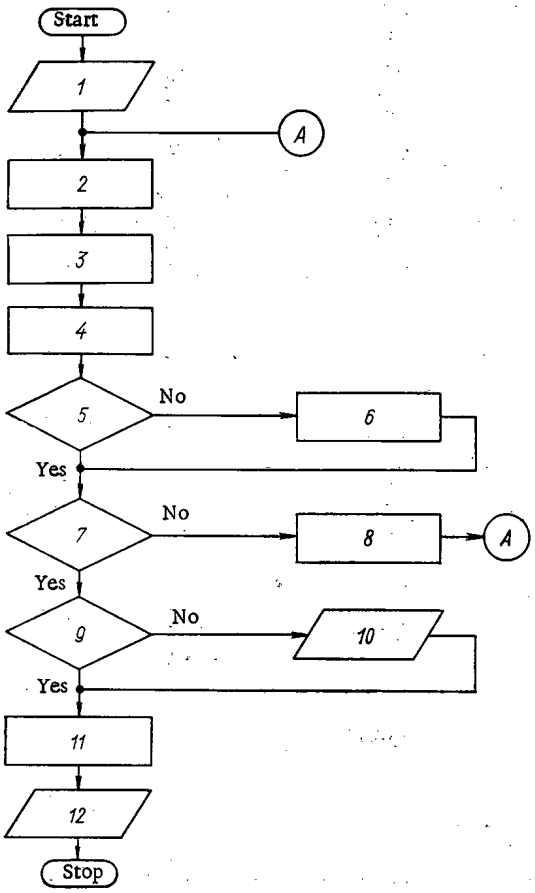

Fig. 2. Structural schematic of control algorithm: 1) input initial position of regulating rods; 2) form matrix of object; 3) determine the error vector; 4) calculate the "ideal" control; 5) summated deviation of energy generation within the dead zone of the total power regulator; 6) calculate the synchronous displacements of the rods; 7) equation in given limits; 8) form the "real" equation; 9) power of channels not exceeding limitation; 10) print numbers of channels with excessive power; 11) calculate displacement of rods; 12) print.

$$I = \sum_{i=1}^{m} (\Phi_i - \overline{\Phi})^2,$$

where i = 1, 2, . . . ; m is the number of monitor points belonging to the local zone.

This problem, in essence, can be solved by the mathematical modeling method, or by prediction of results which lead to the carrying out of the control actions. We should stress that from the calculation point of view, all the problems we are considering are of the same type. Figure 2 shows the structural schematic of the control algorithm we are describing.

Discussion of the Results. The proposed automatic control system for the energy distribution in a reactor type RBMK consists of two basic functional units: systems for identifying the parameters and systems for calculating the optimum position of the regulating rods.

It is assumed that the value of energy generation is estimated by the method described in [1]. The inputs to the system take the form of the indications of transducers in the energy distribution monitor system and the position of the rods, and also the maximum possible local energy generation and the range of rod positions. A characteristic feature of the solution to the problem consists in the significant nonlinearity of the control channel characteristic, which is connected with the fact that the rod can only be introduced into a channel that has first been filled with water. The proposed general algorithm includes the case in which there is no column of water in the safety rod channel, as was the case in the first type RBMK reactor.

The external data for the system comprises the total power of the reactor and the height of the distribution of energy generated. The output data is assumed to be the calculated optimum displacement of the rods and the data for the operator on the desired distribution of energy.

The mathematical description of the process, based upon a static matrix model of the reactor, the elements of which, representing the variation in energy generation at the monitor points, give rise to displacements of the rods, has been experimentally refined by operation of the reactor itself.

The essence of the proposed algorithm for calculating the optimum control system lies in solving by the least-squares method the square matrix equation

$$\Delta\Phi = C\,\Delta u,$$

where $\Delta\Phi$ is the vector of deviation of energy generation from the mean value; Δu is the unknown displacement of the regulating rods.

The limitations given in the form of inequalities are taken into consideration by means of mathematical modeling of the reaction system using the boundary values of the control influences with subsequent solution of the unconditional minimization problem of least dimensionality. Digital modeling of the operation of the system in a typical situation has confirmed the efficiency of the control algorithm.

It should be stressed that the present article has formulated only the basic principles of designing an automatic control system for the energy distribution in a type RBMK reactor. The proposed algorithm can be transformed when enough experience in the use of computers has been accumulated and when a large number of experimental results have been obtained. However, in the initial stage of using computers in the "advisory" mode, the proposed concentration of equations can be very useful, and the algorithm for calculating the optimum positions of the regulating rods could prove to be an effective means of assisting the operator.

LITERATURE CITED

1. I. Ya. Emel'yanov et al., At. Energ., 34, No. 5, 331 (1973).
2. E. V. Filipchuk et al., At. Energ., 39, No. 1, 12 (1975).
3. I. Ya. Emel'yanov and P. A. Gavrilov, in: Experience in the Operation of Nuclear Power Stations and Ways of Furthering the Development of Atomic Power Engineering [in Russian], Vol. 2, Obninsk (1974), p. 288.
4. P. T. Potapenko, At. Energ., 41, No. 1, 25 (1976).
5. F. R. Gantmacher, Applications of the Theory of Matrices, Wiley (1959).

THE APPROXIMATION ERROR AND THE ENERGY DISTRIBUTION IN A REACTOR

L. P. Plekhanov

UDC 621.039.61

The operating efficiency of nuclear reactors, in many respects, depends on the quality of the in-reactor monitoring, to which much attention has recently been devoted [1-7]. References [1, 2, 4-7] consider various aspects of obtaining the detailed energy distribution in the active zone on the basis of physical calculations and approximation of the readings of sensors [1, 2] and their statistical analysis [4-7]. These methods are general and are effective for detailed monitoring of the energy distribution and involve a large volume of computational and experimental work. Reference [3] gives the upper estimate of the error of discrete monitoring, an estimate that is valid for a fairly large number of sensors and positive deviations of the energy distribution from the nominal value.

The present paper proposes a method for estimating the discrete monitoring error which differs from the above-mentioned methods. It is based on the limited nature of the deviations of the unmonitored parameters which determine the neutron field.

Formulation of the Problem. Let the stationary neutron field $\Phi(r)$ be described by the boundary-value problem

$$L(\Phi, \alpha)=0; \quad \Phi(r)=0, \quad r\in S, \tag{1}$$

where L is an operator; $\alpha(r)=\alpha_0(r)+\Delta\alpha(r)$ is a parameter, and S is the boundary of the region.

We take $\Delta\Phi=\Phi-\Phi_0$ to be the deviation of the field from the base distribution $\Phi_0(r)$, obtained for $\alpha=\alpha_0$, and we rewrite the problem as

$$L_0(\Delta\Phi, \alpha_0)=f(\Delta\alpha); \quad \Delta\Phi(r)=0; \quad r\in S, \tag{2}$$

where L_0 is a linear operator in $\Delta\Phi$ and f is an operator. This representation is obtained either directly from Eq. (1) or after expansion of Eq. (1) in powers of $\Delta\alpha$ and $\Delta\Phi$.

The right-hand side of Eq. (2) is subject to a constraint in one of two forms

$$|f[\Delta\alpha(r)]|\geqslant F(r); \tag{3a}$$

$$\int f^2[\Delta\alpha(r)]\,dV(r)\leqslant A^2. \tag{3b}$$

Henceforth all integrals are taken over the region bounded by S. A constraint in the form (3b) is convenience to use, e.g., when analyzing "point" interactions in a reactor, expressed in terms of δ functions.

Let us consider the following points:

1. Approximation of the neutron-field deviation $\Delta\Phi(r)$ by a system of orthonormal functions $\varphi_k(r)$:

$$\Delta\Phi(r)=\sum_{k=1}^{n} c_k\varphi_k(r)+R_n(r), \tag{4}$$

where $R_n(r)$ is the remainder (error) and $c_k=c_k[\Delta\Phi(r)]$ is the expansion coefficient, defined as a linear functional of the approximated function.

2. Reproduction of the field from the measurements of l sensors:

$$\Delta\Phi(r)=\sum_{k=1}^{n} \tilde{c}_k\varphi_k(r)+R_{nl}(r, r_i), \tag{5}$$

Translated from Atomnaya Énergiya, Vol. 42, No. 4, pp. 268-271, April, 1977. Original article submitted October 23, 1975.

where $\tilde{c}_k$ are the approximate values of the coefficients calculated from the measurements and r_i are the coordinates of the sensors.

The remainders in Eqs. (4) and (5) must be evaluated with constraint (3) and with allowance for the measuring error and for the indeterminacy of the sensor coordinates.

Estimation of the Approximation Error and the Choice of Coordinate Functions. The results of the classical theory of approximation [8] are inadequate for solving the problem formulated since only polynomials or trigonometric functions are considered as φ_k and the estimates either give only the order of magnitude by which the remainder decreases as $n \to \infty$ or are too high.

For example, the corollary to the second Jackson theorem for the one-dimensional case states that in the approximation with polynomials of order up to n we have $\max |R_n(x)| \leq M \cdot 6^k/n^k$, where $k \geq 1$ is the order of the differentiability of $\Phi(x)$; $M \geq |\Phi^{(k)}(x)$. For the given problem, $k = 2$ and for $n \leq 6$ this estimate is too high.

The solution of problem (2) can be written as

$$\Delta\Phi(r) = \gamma\Phi^0(r) + \Delta\Phi^1(r); \tag{6}$$

$$\Delta\Phi^1(r) = \int f[\Delta\alpha(\xi)]\, G(r, \xi)\, dV(\xi). \tag{7}$$

Here, $\Phi^0(r)$ is the solution of the homogeneous problem (2) if it is nonzero; γ is a number found from auxiliary conditions (the controller equation, feedback, etc.) and the criticality condition for the perturbed state; and $G(r, \xi)$ is the generalized Green's function, orthogonal to $\Phi^0(r)$. If $\Phi^0(r) \equiv 0$, then $G(r, \xi)$ is the ordinary Green's function of problem (2) [9].

Let us consider separately the estimation for both terms in Eq. (6), respectively, with superscripts 0 and 1:

$$|R_n^0(r)| \leqslant \max|\gamma| \cdot \left|\Phi^0(r) - \sum_{k=1}^{n} c_k [\Phi^0(r)]\, \varphi_k(r)\right|. \tag{8}$$

For the second term from Eqs. (4) and (7) we find

$$R_n^1(r) = \int f[\Delta\alpha(\xi)]\, P_n(r, \xi)\, nV(\xi), \tag{9}$$

where the expression $P_n(r, \xi) = G(r, \xi) - \sum_{k=1}^{n} c_k[G(r, \xi)]\varphi_k(r)$ is the remainder of the approximation of the Green's function $G(r, \xi)$ in the variable r by a chosen system of coordinate functions.

Using the Cauchy – Bunyakovskii inequality, we obtain the following estimates from Eq. (9):

$$|R_n^1(r)| \leqslant \int F(\xi) |P_n(r, \xi)|\, dV(\xi); \tag{10a}$$

$$|R_n^1(r)| \leqslant A\left[\int P_n^2(r, \xi)\, dV(\xi)\right]^{1/2}. \tag{10b}$$

The system of coordinate functions $\varphi_k(r)$ can be chosen from various considerations such as convenience of calculations and physical meaning. Estimates (8) and (10) permit optimization of this choice from the condition of minimum approximation error. The first optimal function is $\Phi^0(r)$, provided it is nonzero; then $R_n^0(r) = 0$. The other functions can be found by minimizing any positive functional of the right-hand sides of inequalities (10). It can be shown, e.g., that in every particular case of self-adjoint operator L_0 and quadratic functional on the right-hand side of inequality (10b), the eigenfunctions of problem (2), taken in the order of increasing modulus of their eigenvalues, are optimal.

Estimation of the Reproduction Error. Suppose that there are l sensors whose maximum measuring error is δ_i and whose coordinates are r_i, with a maximum indeterminacy of δr_i.

We write the equations for determining the coefficients in Eq. (4) from the measured values of the neutron flux with allowance for the errors

$$\Delta\Phi_i + x_i = \sum_{k=1}^{n} c_k \varphi_k(r_i) + R_n(r_i), \quad i = 1, 2, \ldots l, \tag{11}$$

where $\Delta\Phi_i$ is the value of the deviation of the field at the points of measurement and x_i is the sensor error ($|x_i \leq \delta_i$). We solve system (11) by the least-squares method. Then, taking the error of sensor coordinates

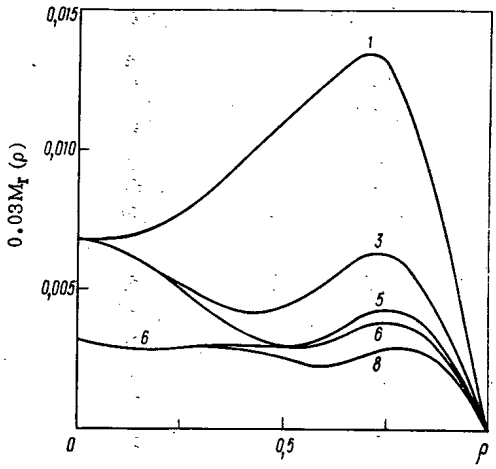

Fig. 1. Estimates of approximation error [$M_r(\rho)$ is the right-hand side of inequality (10b); the numbers denote the value of n].

z_i into account (retaining only the first degree of smallness), we get

$$c_k = \sum_{i=1}^{l} u_{ki} [\Delta\Phi_i + x_i - R_n(r_i)] + \sum_{j=1}^{l} u'_{kij} z_j \Delta\Phi_i, \tag{12}$$

where u_{ki} are coefficients determined by the least-squares method and u'_{kij} are the derivatives of these coefficients with respect to the coordinate r_j. It can be shown that $u'_{kij} = \sum_{m=1}^{n} u_{kj}\varphi'_m(r_j)u_{mi}$.

By $d_i(r) = \sum_{k=1}^{n} u_{ki}\varphi_k(r)$ we denote the "weighting" function of the i-th measurement in reproducing the field. Substitution of the coefficients c_k from Eq. (12) into Eq. (4) yields

$$\Delta\Phi(r) = \sum_{i=1}^{l} \Delta\Phi_i d_i(r) + R_n(r) - \sum_{i=1}^{l} R_n(r_i)\, d_i(r) + \sum_{i=1}^{l} x_i d_i(r) + \sum_{i=1}^{l}\sum_{j=1}^{l}\sum_{m=1}^{n} \varphi'_m(r_j)\, u_{mi} z_j \Delta\Phi_i d_j(r). \tag{13}$$

In this equation the first term is the calculated value of the field, the next two represent the error of discreteness of measurements, which we denote by $R_{discr}(r)$, and the last two terms are, respectively, the reproduction error, due to the sensor error $R_{sens}(r)$, and the indeterminacy of the coordinates, $R_{coord}(r)$. For each error we can give the estimate:

$$|R^0_{discr}(r)| \leqslant \max|\gamma| \cdot |\Phi^0(r) - \sum_{i=1}^{l} \Phi^0(r_i)\, d_i(r)|; \tag{14}$$

$$|R^1_{discr}(r)| \leqslant \int F(\xi) |P_n(r, \xi) - \sum_{i=1}^{l} P_n(r, \xi)\, d_i(r)|\, dV(\xi); \tag{15a}$$

$$|R^1_{discr}(r)| \leqslant A \left\{ \int \left[P_n(r, \xi) - \sum_{i=1}^{l} P_n(r, \xi)\, d_i(r) \right]^2 dV(\xi) \right\}^{1/2}; \tag{15b}$$

$$|R_{sens}(r)| \leqslant \sum_{i=1}^{l} \delta_i |d_i(r)|; \tag{16}$$

$$|R_{coord}(r)| \leqslant \sum_{j=1}^{l} \delta r_j \sum_{i=1}^{l} \Delta_i |d_j(r) \sum_{m=1}^{n} \varphi'_m(r_j)\, u_{mi}|, \tag{17}$$

where Δ_i is the maximum possible deviation of the field at the point r_i; usually Δ_i is known from practice or can be estimated from the inequalities

TABLE 1. Moduli of First Eigenvalues λ_{kj}

j	k				
	0	1	2	3	4
0	0	4,85	13,2	24,8	39,5
1	20,8	39,7	61,6	86,4	114
2	66,8	96,0	127	161	197

$$\Delta_l \leqslant \int F(\xi)\,|\,G(r_l\xi)\,|\,dV(\xi); \tag{18a}$$

$$\Delta_l \leqslant A\left[\int G^2(r_j, \xi)\,dV(\xi)\right]^{1/2}. \tag{18b}$$

Analysis of the relations obtained shows that the right-hand side of inequalities (14) and (15) decrease as n increases and the right-hand sides of inequalities (16) and (17), as a rule, increase as n and l increases. Therefore, there exists a combination of n and l as well as a positioning of sensors which minimize the overall error.

Note that such considerations make it possible to obtain, from the sensor readings, estimates of the functionals of a neutron field such as the integrated power, energy release in any region, etc.

Example. We consider the one-group diffusion equation of a reactor in the form of an infinite circular cylinder in the steady state with a zone of flattened energy distribution, of radius 0.67. This equation is written in terms of deviations

$$\nabla^2\Delta\Phi(\rho,\theta)+\frac{k^0_\infty(\rho,\theta)-1}{M^2}\Delta\Phi(\rho,\theta)=\frac{\Phi^0(\rho)}{M^2}\Delta k_\infty(\rho,\theta);$$
$$\Delta\Phi(1,\theta)=0;\quad k^0_\infty=\begin{cases}1; & \rho\leqslant 0.67,\\ 1+(5.151M)^2; & 0.67<\rho\leqslant 1,\end{cases} \tag{19}$$

where k^0_∞ corresponds to the critical reactor and Δk_∞ corresponds to perturbation; $\Phi^0(\rho)$ is the solution of Eq. (22) for $\Delta k_\infty = 0$ and the condition $\Phi^0(0) = 1$.

Let us now consider Δk_∞ which satisfies the constraint

$$\left\{\int_0^1\int_0^{2\pi}\rho\left[\frac{\Phi^0(\rho)}{M^2}\Delta k_\infty(\rho,\theta)\right]^2 d\rho\,d\theta\right\}^{1/2}\leqslant 0.03. \tag{20}$$

Equation (19) is equivalent to the self-adjoint equation. Therefore, it is desirable to take for the coordinate functions the eigenfunctions (19) determined by well-known methods [10]:

$$\psi_{kj}(\rho,\theta)=\begin{cases}Z_{0j}(\rho)\dfrac{1}{2\pi}, & k=0;\\ Z_{kj}(\rho)\dfrac{\cos k\theta}{\pi};\ Z_{kj}(\rho)\dfrac{\sin k\theta}{\pi}, & k>0,\end{cases} \tag{21}$$

where $Z_{kj}(\rho)$ are the normalized radial parts.

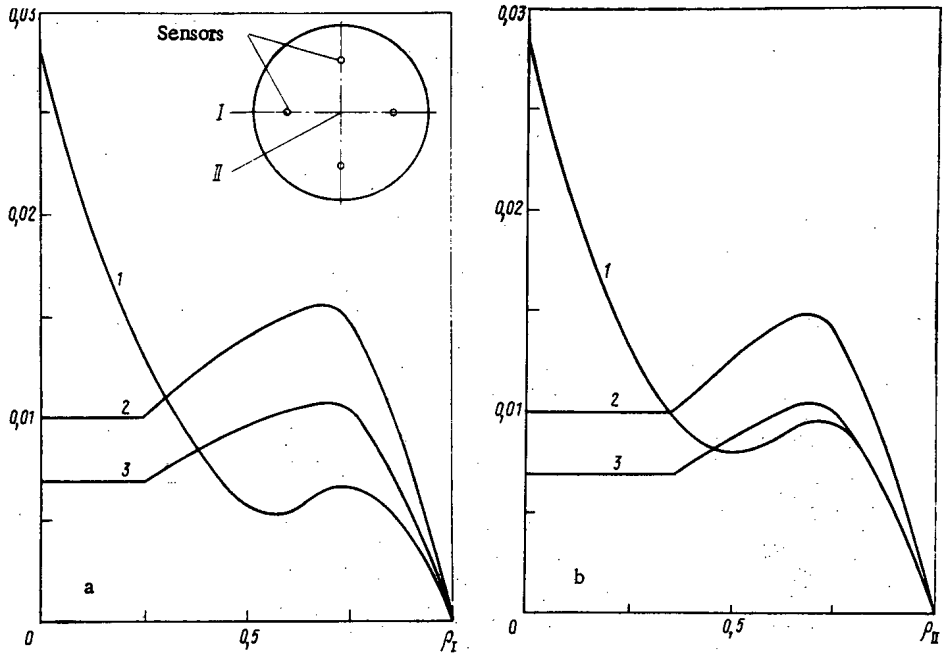

Fig. 2. Estimates of the error in the reproduction of the neutron field along radii I (a) and II (b) as a result of the discreteness of measurements (1) for $\delta_i = \delta r_i = 0$; the sensor error (2); and the indeterminacy of the sensor coordinates (3).

The order of the eigenfunctions is found from Table 1 for the approximations: $k_j = 00$ [function $\Phi^0(\rho)$], 10, 20, 01, 30, 40, 11, etc. Figure 1 takes into account the fact that when $k > 0$ the multiplicity of λ_{kj} is 2 and both functions are taken simultaneously from Eq. (21).

Figure 2 gives the estimates of the error of reproducing the neutron field from the readings of four sensors located at 0.6 radius from the center and taking account of three eigenfunctions [the values of the right-hand sides of inequalities (15b), (16), and (17) are laid off along the ordinate axis]. The sensor error and the indeterminacy of the sensor coordinates were taken to be equal to 0.01. In the case considered, $R^0_{nl}(r, r_i)$ was found to be zero.

LITERATURE CITED

1. T. Hurley, Trans. Am. Nucl. Soc., 9, 262 (1966).
2. W. Legget, Trans. Am. Nucl. Soc., 9, 484 (1966).
3. P. T. Potapenko, At. Energ., 24, No. 4, 340 (1968).
4. I. Ya. Emel'yanov, L. V. Konstantinov, and V. V. Postnikov, At. Energ., 30, No. 3, 275 (1971).
5. I. Ya. Emel'yanov et al., At. Energ., 30, No. 5, 422 (1971).
6. I. Ya. Emel'yanov et al., At. Energ., 34, No. 2, 75 (1973).
7. I. Ya. Emel'yanov et al., At. Energ., 37, No. 6, 451 (1974).
8. P. P. Korovkin, Linear Operators and Approximation Theory [in Russian], Nauka, Moscow (1959).
9. V. V. Stepanov, A Course in Differential Equations [in Russian], Nauka, Moscow (1966).
10. A. Hitchcock, Stability of Nuclear Reactors [Russian translation], Gosatomizdat, Moscow (1963).

REUSE OF POWER PLUTONIUM AND URANIUM AND NEUTRON REGENERATION IN A THERMAL REACTOR

P. I. Khristenko

UDC 621.039:524.46.034.3

Thermal reactors of atomic power stations, operating on enriched 2-3% uranium, utilize only ~0.5% of the natural uranium they require. Thanks to a good neutron balance, heavy-water reactors can utilize from 1 to 1.5% natural uranium.

The conversion of thermal reactors to a plutonium fuel cycle with an equilibrium concentration of the isotopes ^{239}Pu, ^{240}Pu, and ^{241}Pu with ^{238}U and with the necessary addition of ^{235}U, introduced into the fuel in the form of natural uranium [1], substantially increases the utilization of natural uranium. For example, for gas-cooled heavy-water reactors of the KS type [2, 3] the utilization can be brought up to 2-3%. Bearing in mind that more expensive (leaner) uranium ore [4] and spent material from diffusion plants can be used as additions of ^{235}U, in this case the fuel base for thermal reactors is expanded severalfold. Accordingly, the ensured fuel supply for heavy-water reactors is increased many times in comparison with thermal reactors using enriched uranium.

The next stage is the improvement of thermal reactors for fuller utilization of natural uranium may be that of neutron regeneration. A simple method of accomplishing this is to provide thermal reactors with side and end shields of ^{238}U, constituting fuel breeding zones (Fig. 1).

The return of plutonium into the reactor operating in an equilibrium fuel cycle with a multiplication factor of $k = 1.04$-1.06, with no less than 80% of the neutron leakage usefully absorbed in the breeding zone, can further reduce the consumption of natural uranium added in the fuel cycle by a 1.5 factor. The natural-uranium utilization factor of thermal reactors will increase in the same proportion (3-4.5%).

A further increase in neutron regeneration by artificially increasing and maintaining a constant mean concentration of plutonium isotopes in the fuel and absorbing the excess neutrons in the breeding zone is

Translated from Atomnaya Énergiya, Vol. 42, No. 4, pp. 272-276, April, 1977. Original article submitted March 29, 1976.

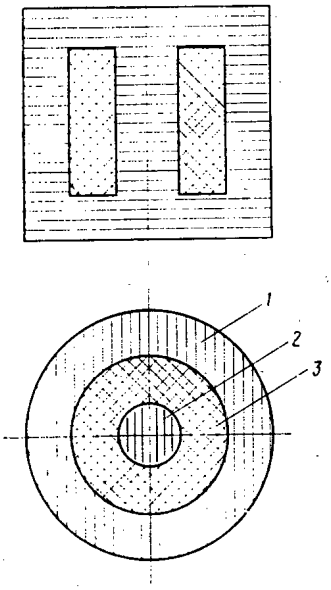

Fig. 1. Diagram of thermal reactor with ^{238}U or ^{232}Th fuel breeding zones: 1, 2) outer and inner (central) fuel breeding zones; 3) active zone of reactor.

advantageous from the point of view of both enhancing the utilization factor for natural uranium and increasing fuel burnup. High fuel enrichment permits resonance absorption in ^{238}U to be increased and this in turn makes it possible to enlarge the fuel charge in the reactor, to increase the reactor power, and to raise the equilibrium content of plutonium in the fuel.

The excess reactivity of the active zone may require a higher neutron escape from the active zone and regeneration of these neutrons; this can be accomplished by using an inner breeding zone in addition to the outer zone (see Fig. 1).

The use of an enriched plutonium fuel will enable fast-neutron fission of uranium to be utilized in greater measure, thus significantly improving the neutron balance. To do this despite the increase in the mass of uranium in the fuel elements, the fuel assembly design should provide for the absorption of excess neutrons (Fig. 2). The central part of an assembly has its area filled with ^{238}U with a high filling factor (β_1); plutonium-enriched fuel is put into the peripheral part, but with the area filled with a low factor of (β_2). The inner and outer shields of the fuel assembly enable the rate of flow of heat-transfer medium through the central and peripheral parts of the fuel assemblies to be controlled during the fuel burnup process.

The use of neutron regeneration and fuel elements ensuring an increased fast-neutron fission factor will enable thermal reactors to burn up to 10-15% of the natural uranium they use (Figs. 3 and 4).

Because of unavoidable uranium losses during chemical processing of fuel elements from the active zone, and especially from the breeding zone, as well as losses during the fabrication of fuel elements, thermal reactors can utilize no more than 60-70% of the uranium. At the same time, thermal reactors are safe and simple, and have been perfected. They are not limited by "fuel-doubling time" in the sense that they themselves can produce the plutonium they need, working on natural uranium in the first period of their operation. This provides a basis for the independent development of a nuclear power industry based on thermal reactors.

The considerable effect from neutron regeneration is due to the utilization of neutron escape to obtain additional ^{239}Pu, the small relative fraction of harmful neutron absorption in the active zone during reactor operation on enriched fuel, the possibility of appreciably raising the level of fast-neutron fission of uranium, and the greater effect of fission of $^{241}Pu(\nu = 2.21)$ in improving the neutron balance at higher plutonium concentrations in the fuel.

The more economically the neutrons are used up in the reactor, the greater the effect from regeneration. The reactor structure should contain breeding zones and the fuel elements should have useful absorbers built into their central part. Therefore, a gas-cooled heavy-water reactor using metallic uranium and magnesium, aluminum, and zirconium alloys as structural materials meets these requirements.

Neutron regeneration enables the amount of ^{235}U added to the fuel to be reduced. Thus, natural uranium is used more efficiently. Estimates of the required additions (concentration ρ_5) of ^{235}U to the fuel, the fuel burnup b per run, and the burnup B per ton natural uranium were obtained from the neutron balance for

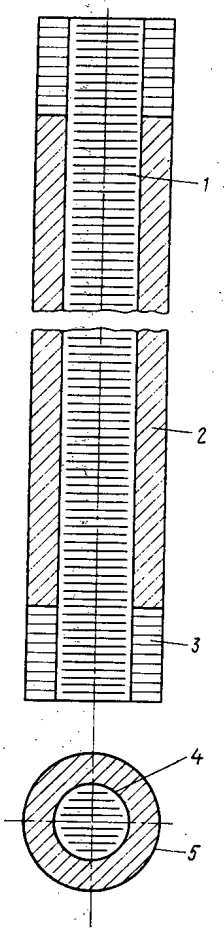

Fig. 2. Diagram of fuel assemblies with central absorbers of ^{238}U or ^{232}Th: 1) ^{238}U or ^{232}Th absorbers; 2) fuel assemblies of enriched fuel; 3) elements of outer breeding zone; 4, 5) inner and outer shields of assembly.

steady-state operation conditions of the reactor with continuous fuel recharging at an average ^{235}U and ^{239}Pu content (ρ_5^{av} and ρ_9^{av} = const; $d\rho_5/dz \neq 0$, $d\rho_9/dz \neq 0$) in the fuel (^{238}U) maintained artificially, by the addition to the fuel of natural uranium and ^{239}Pu which is obtained in the breeding zone and in ^{238}U absorbers.*

Under these conditions the ^{240}Pu and ^{241}Pu content has an average value over the reactor, determined from the conditions $d\rho_0/dz = 0$ and $d\rho_1/dz = 0$.

Estimates were made for the cell of the central channels of the active zone of the KS-150 reactor [3]. The lattice spacing was thus chosen. Plutonium-enriched uranium was placed in the peripheral part of the assembly, and the quantity and uranium filling factor did not change ($\beta_1 = 0.24$). Absorbers of ^{238}U were put in the central part of the assemblies with a filling factor of $\beta_2 = 0.5$, thus increasing the channel diameter, reducing the quantity of heavy water in the cell, enhancing resonance capture in ^{238}U, raising the level of equilibrium concentration of plutonium, and increasing fast-neutron fission.

The estimates were made for the average ^{239}Pu content in reactor fuel which varied from the equilibrium value up to 1.5. In determining the average fuel composition for the reactor and setting up the neutron balance, we assumed constants corresponding to the thermal conditions of the KS-150 reactor: $\sigma_5^a = 647$; $\sigma_5^f = 552$; $\nu_5' = 2.07$; $I_5^a = 560$; $I_5^f = 402$; $C_8 = 0.581$; $\sigma_9^a = 1225$; $\sigma_9^f = 852$; $\nu_9' = 1.99 \pm 0.01$; $I_9^a = 2510$; $I_9^f = 1510$; $\sigma_0 = 289$; $I_0 = 200$ (without the first resonance level); the first resonance level was $E_0 = 1.06$ eV, $\bar{\gamma}_0 = 1.73 \cdot 10^5$ b; $\Gamma = 0.033$ eV; $E_{ssh} = 0.22$ eV; $\sigma_1^a = 1470$; $\sigma_1^f = 1145$; $\nu_1' = 2.21$; $\sigma_2^0 = 19$; and neutron temperature 425°K.

The neutron balance for the operation of the reactor under steady-state fuel conditions, with some approximations, can be written as

$$(\mu\nu_9' - 2)\bar{\sigma}_9\rho_9 + (\mu\nu_1' - 2)\bar{\sigma}_1\rho_1 + (\mu\nu_9'' - 2)\psi_9 f(z)\varphi\mu + (\mu\nu_5' - 1)\rho_5 + (\mu\nu_5'' - 1)\psi_5 f(z)\varphi\mu = \Sigma q_p' + (\hat{q}_{rp}')y + (q_m + q_e + q) + (a/y),\dagger$$

*The points b_0^a, b_0^b and B_0^a, B_0^b in Fig. 3 characterize the operation of the reaction with minimum neutron regeneration (at the outer boundaries), using fuel with a plutonium concentration close to the equilibrium value.

†The possibility of increasing the fast fission factor between wide limits by increasing the mass of uranium in the reactor channels ensures the reliability of the estimates which are extremely sensitive to errors in the fundamental constants of plutonium.

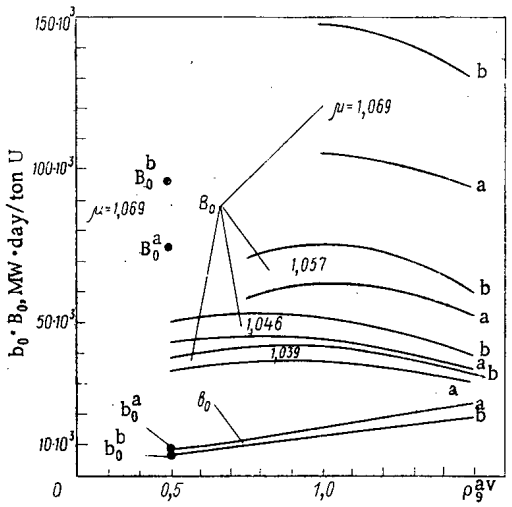

Fig. 3. Plots of b_0 and B_0 vs ρ_9^{av}. Fuel reprocessing losses: a) 5%; b) 3%.

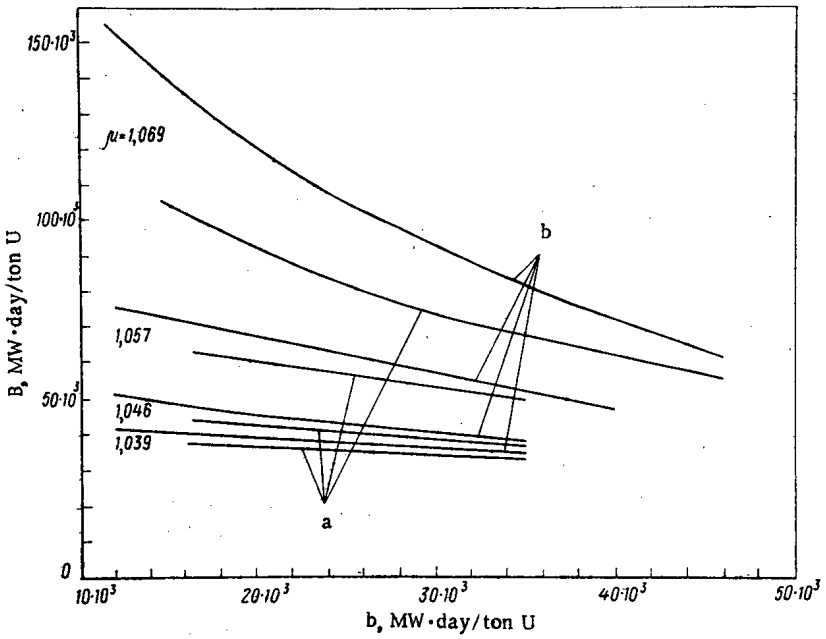

Fig. 4. Plots of B vs b and μ for $\rho_9^{av} = 1$. Fuel reprocessing losses of: a) 5%; b) 3%.

where μ is the fast multiplication factor; $\bar{\sigma}_i$ and ρ_i are the relative cross sections and concentrations of ^{239}Pu, ^{240}Pu, ^{241}Pu, ^{242}Pu, and ^{235}U atoms; ψ_i is the probability of neutron absorption by ^{235}U and ^{239}Pu in the resonance range; ν_i' and ν_i'' are the numbers of neutrons produced during absorption of one neutron by ^{235}U, ^{239}Pu, and ^{241}Pu, respectively, in the thermal and resonance regions; $\Sigma q_p'$ is the thermal absorption in the structural materials, the moderator, xenon, ^{242}P,* etc.; $\hat{q}_{rp}'$† is the absorption in the reactor poisons at a burnup of 10,000 MW·days/ton of U with a height flattening factor of 0.8 and continuous fuel recharging; y is the burnup, 10^4 MW·days/ton of U; q_m are the neutron losses in the moderator and the structural materials of the breeding zone; q_e is the neutron escape from the reactor; and q_0 are the neutrons of the additional reactivity margin.

* Absorption in ^{242}Pu with allowance for the long time required for equilibrium concentration to be established, and the possibilities of it being taken out of the fuel cycle by separation of the fuel according to age and total burnup of ^{240,241}Pu in nonabsorbing fillers has been taken to be equal to 20% of the equilibrium value.

† $\hat{q}_{rp}' \approx 0.09$; ^{135}Xe (0.037) and ^{149}Sm (0.008) have been taken into account in $\Sigma q_p'$.

It has been assumed that q_m, q_e, and q_0 are 10, 20, and 10%, respectively*; a/y is the fraction of neutrons used to make up the losses of ^{239}Pu and ^{240}Pu in the fuel cycle, during the chemical reprocessing, in fabrication of fuel elements, and because of the fission of ^{241}Pu outside the reactor, and is equal to 3 and 5%; about two-thirds is accounted for by losses during the production of plutonium and one-third by the fission of ^{241}Pu.

It has been assumed that all losses of ^{239}Pu, ^{240}Pu, and ^{241}Pu in the external parts of the fuel cycle are made good beforehand in the form of ^{239}Pu in the breeding zone and the absorbers of the reactor (the term a/y on the right-hand side of the balance). These losses are proportional to the mass of plutonium in the fuel; recuperation of the reactor losses is taken into account by the fraction (3 or 5%) of neutron absorption by ^{239}Pu, ^{240}Pu, ^{241}Pu, proportional to the burnup y in a run, as a result of which y enters the right-hand term of the neutron balance (a/y). The quantity a is the product of the absorption of ^{239}Pu, ^{240}Pu, and ^{241}Pu in the reactor by the ratio of masses of ^{239}Pu, ^{240}Pu, and ^{241}Pu lost in the external fuel cycle to the mass of ^{239}Pu and ^{240}Pu which disappears at a burnup of 10,000 MW·day/ton of U.

Since the burnup appears in the numerator of one term of the balance (1) and in the denominator of another, it is meaningful to speak of the optimal value of the burnup per run (b_0) and maximum burnup (B_0) per ton of natural uranium used in the reactor. These values are obtained from the condition that the right-hand side of the balance (1) be a minimum, i.e., that the right-hand side be equal to zero dF/dy = 0, whence

$$y_0 = \sqrt{a/(q'_{rp})^0} \qquad (2)$$

and $b_0 = 10{,}000 \cdot y_0$ MW·day/ton of U.

The burnups per run and per ton of natural uranium used in a cycle are related by

$$B = \frac{1}{x} b,$$

where x is the relative fraction of natural uranium with a ^{235}U content ($\rho_5 = 1$) used in a run; (1 − x) is the fraction of reused spent uranium with an average ^{235}U concentration of $(\rho_5^f)^{av}$. If ρ_5^{in} is the initial ^{235}U content in the fuel, then x can be found from

$$1x + (1-x)(\rho_5^f)^{av} = \rho_5^{in};$$
$$x = [\rho_5^{in} - (\rho_5^f)^{av}]/1 - (\rho_5^k)^{av}.$$

The initial ^{235}U content is defined as

$$\rho_5^{in} = z_1 \rho_5^{av} \frac{1}{1-(1/e^{z_1})},$$

where ρ_5^{av} is the average ^{235}U content in the fuel; z_0 and $z_1 = z_0/\eta$ are the run lengths with and without account for the neutron field inhomogeneities with respect to the height, $\eta_h = 0.8$; $(\rho_5^f)^{av}$ is the final ^{235}U content in the spent fuel, i.e.,

$$(\rho_5^f)^{av} = \rho_5^{in}(1/e^{z_0}).$$

The fuel cycle considered is organized so that part of the uranium depleted in the reactor is removed from the cycle and replaced with natural uranium [the smaller fraction (x)] and part is returned [the larger fraction (1 − x)]. The uranium removed from the fuel cycle, with a ^{235}U content [$(\rho_5^f)^{av} \approx 0.1$] can be reused, at first in absorbers in the central parts of the fuel assemblies, and then in the breeding zones (outer shields). The neutron balance can thus be improved somewhat.

Neutron regeneration in thermal heavy-water reactors would enable the fraction of natural uranium in these reactors to be reduced and a large power generating industry to be created with an ensured supply of fuel for a long time.

If the problem of extracting ^{233}U from thorium is solved in the future, it will be possible also to incorporate thorium into the uranium – plutonium fuel cycle. In this case, an equilibrium concentration of ^{239}Pu, ^{240}Pu, ^{241}Pu with ^{238}U and with an addition of ^{235}U in the form of natural uranium will, as before, be used as the principal fuel. Mainly ^{232}Th (in order to obtain ^{233}U) and partly ^{238}U, withdrawn from the fuel cycle, could be used for the breeding zones and absorbers so as to burn up the ^{235}U and the ^{233}U which remains in it.

Thus, it would be possible to organize a comprehensive closed uranium – thorium fuel cycle. Since appreciably more neutrons are produced in the fission of ^{233}U than in the fission of ^{239}Pu and ^{235}U ($\nu_3' = 2.28$, $\nu_9' = 1.99$, and $\nu_5' = 2.07$), the introduction of thorium (^{233}U) into the fuel cycle could significantly increase the burnup of natural uranium in comparison with the uranium – plutonium fuel cycle considered.

* For the large reactors k is considered to be 1.04-1.05 and these losses are estimated at 1.6-2.0% of $f(z)\mu$.

The uranium – plutonium fuel cycle and the schemes described above for the active zone and fuel elements of a heavy-water reactor are a first approximation to the solution of the problem formulated. Practical realization of the reactors discussed will be possible if, in addition to the high breeding ratio and efficient use of the fuel, they also ensure production of low-cost electricity, i.e., if the barrier of the high costs of chemical fuel reprocessing and fabrication of fuel elements containing plutonium is overcome.

From this point of view, in addition to the high efficiency of uranium utilization in comparison with the cycle with an equilibrium plutonium concentration in the reactor, the cycle with a quasiequilibrium concentration also opens up great possibilities for increasing production of fuel, a considerable proportion of which in this case is made from uranium and enriched with plutonium in the reactor itself.

LITERATURE CITED

1. P. I. Khristenko, At. Energ., 20, No. 1, 26 (1966).
2. V. M. Abramov et al., At. Energ., 36, No. 2, 113 (1974).
3. V. M. Abramov et al., At. Energ., 36, No. 3, 163 (1974).
4. P. A. Petrov and P. L. Khristenko, in: Proceedings of the Seventh International Congress on Power Engineering [in Russian], Vol. 12, Sec. 3, Soviet National Committee (1969), p. 340.

PRESSURE EXCURSION IN FUEL ELEMENTS WITH COMPACT UO_2 DURING THE FIRST POWER EMERGENCE OF A REACTOR

B. V. Samsonov and V. Sh. Sulaberidze

UDC 621.039.524.44:621.039.542.342:621.039.548

Experimental data on the kinetics of gas release in fuel elements with compact UO_2 [1] show that during the first arrival of a fuel element in an operating regime, the gas pressure under the cladding increases sharply, and then falls to a certain steady level during several hours. The increase of pressure is explained, not by heating up of the gas in the fuel element, but by its release from the fuel. This release of gases of technological origin can impair the thermal conductivity of the gap between the fuel and the cladding, filled with helium, in the first hours of operation of the fuel element. In addition, in fuel elements without free space, the increase of pressure may prove to be unacceptable.

The experimental procedure is explained in detail in [1, 2]. The increased quantity of gas under the cladding of the fuel element was determined at each power step by the increase of pressure with increase of the change of gas temperature in a fuel element – sensor system [3]. The fuel was manufactured by the technology accepted for the fuel elements of the water-cooled – water-moderated power reactor (VVÉR) [4].

TABLE 1. Characteristics of Irradiation of Fuel Elements

Fuel element	Av. linear power, W/cm	Calculated temperature, °K		
		surface	center	middle-space
GD-101	~500	~870	~2070	~1520
GD-102	460	1010	2090	1600
GD-104	370	930	1800	1420
GD-107	720	1020	2380	1790
GD-115	720	1020	1980	1630
GD-122	900	1070	2720	2030
GD-124	900	1020	2770	2080
GD-125	960	600	2420	1630
GD-127	720	1020	2380	1790

Translated from Atomnaya Énergiya, Vol. 42, No. 4, pp. 277-279, April, 1977. Original article submitted September 14, 1976.

TABLE 2. Gas-Release Characteristics

Fuel element	Filling		Quantity of gas, 10^{-3} m^3/kg UO_2		Temperature of onset of gas release, °K	
	type of gas	initial press., 10^5 N/m^2	additional release	initial filling	center	middle-space
GD-101	Helium + air	2,45	~ 0,019	~ 0,055	~ 1120	~ 1050
GD-102	Argon	4,90	0,00	0,118±0,0095	—	—
GD-104	»	7,65	0,00	0,185±0,015	—	—
GD-107	Air	0,98	0,020±0,0026	0,0217±0,0018	1320	1100
GD-115	»	0,98	0,021±0,0023	0,0182±0,0014	1170	1040
GD-122	»	0,98	0,023±0,0023	0,0160±0,00166	1530	1250
GD-124	Argon	3,82	0,00	0,0685±0,0055	—	—
GD-125	Helium	3,43	0,023±0,0069	0,0077±0,0062	1730	1220
GD-127	Air	0,98	~ 0,023	~ 0,02	1810	1170

Results of the Experiments. Table 1 shows the thermal characteristics of nine irradiated fuel elements.

The filling characteristics of the fuel elements, values of the additional gas release, and the calculated temperatures corresponding to those power stages at which the release of gases from the fuel becomes marked, are contained in Table 2.

The change of pressure under the fuel-element cladding during gradual raising of the reactor power is shown in Fig. 1, where it can be seen that on arrival at each new power stage the pressure increases and reaches a maximum simultaneously with the termination of the power increase, i.e., the rate of release of gases from the fuel is determined by the rate of heating up.

Later, a fall of pressure is observed, and in fuel elements filled with air the steady-state pressure is found to be below the initial pressure, but in fuel elements filled with helium, it is almost equal to the initial pressure (Table 3). In fuel elements filled with argon at a pressure of $\sim 3.8 \cdot 10^5$ N/m^2 and higher, no pressure excursion is observed (see Table 2).

Discussion of Results. The results of measuring the yield of gases during the increase of power are processed in the form of the relation

$$\Delta N_i = \Delta N_0 \exp(-E/kT_i), \quad (1)$$

where ΔN_i and ΔN_0 are the additional and total gas releases at the i-th power stage; T_i is the fuel temperature, averaged over the volume, at the i-th power stage. The value of ΔN_i was determined from the relation

$$\Delta N_i = k^{-1}(P_{\max} \Sigma V/T)_i - k^{-1}(P_{\min} \Sigma V/T)_{i-1}, \quad (2)$$

where P_{max} and $P_{min(i-1)}$ are the maximum and minimum pressure values at the i-th and (i − 1)-th power stages; Σ is the pressure, summed over all elements of the fuel-element – sensor system.

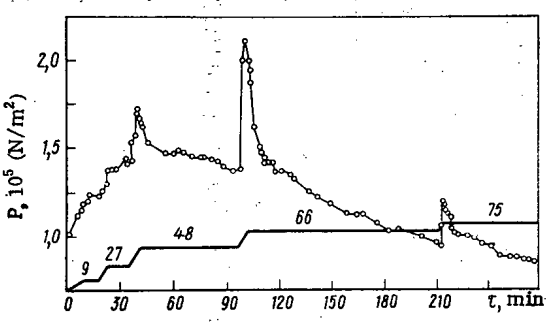

Fig. 1

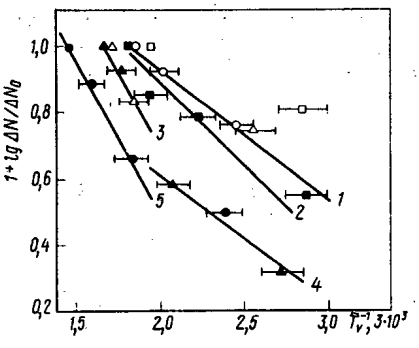

Fig. 2

Fig. 1. Pressure excursion in GD-107 fuel element: ———) reactor power, MW; ○) fuel-element pressure.

Fig. 2. Temperature dependence of yield of gas: ●) GD-122; ○) GD-125; ■) GD-155; ▲) GD-107; □) GD-101; △) GD-127; 1, 4) E = 0.22; 2) 0.26; 3, 5) 0.44 eV/atom.

TABLE 3. Ratio of Quantities of Released and Absorbed Gases

Fuel element	Filling medium	Gas quant. released, m^3/kg UO_2	Absorbed gas			Middle-space temp., °K
			10^{-3}, m^3/kg	release, %	filling, %	
GD-107	Air	0,020	> 0,034	> 170	> 65	1790
GD-115	»	0,021	0,026	124	28	1630
GD-122	»	0,023	0,033	144	63	2030
GD-125	Helium	0,023	0,025	109	2,6	1630

Figure 2 shows the results of this processing. For a temperature of $T_i \leq 1600$°K, the energy of activation E is equal to 0.22-0.26 eV/atom, and when $T_i \geq 1600$°K, $E \approx 0.44$ eV/atom. These values are close to the energies of activation of physical sorption [5].

The error in determining the fuel temperature $\bar{T}_v$, averaged over the volume, is very large ±(15-20)%. Thus, the absolute value of the temperature at nominal power is known with low accuracy. However, its calculation at intermediate stages was carried out by taking account of the relative change of the reactor power. The error in the relative change of reactor power is < ±5%. Thus, the error in the relative change of temperature amounts to ±5%. It is shown in Fig. 2 for points corresponding to intermediate stages of reactor power, and it determines the error in the value of E. The variation of the energy of activation with temperature may be due to desorption of different gases (oxygen, nitrogen, and hydrogen) from the surface of the UO_2.

With further operation at steady power, the gas pressure under the fuel-element cladding decreased. The kinetics of this process are described sufficiently well by the parabolic law

$$[P_{max} - P(\tau)]/P_{max} = a\tau^{1/2}, \quad (3)$$

where P_{max} is the maximum pressure at a given power stage; $P(\tau)$ is the running pressure; τ is the time calculated from the instant when $P(\tau) = P(0) = P_{max}$; and a is a coefficient, connected with the velocity constant of the reaction by the relation $K \sim 0.5a^2$. Assuming that the energy of activation is independent of the temperature, we can write

$$K = K_0 \exp(-E/kT), \quad (4)$$

whence, for T_i and T_j we obtain

$$\ln(K_i/K_j) = -k^{-1}E(T_i^{-1} - T_j^{-1}), \quad (5)$$

where i and j are different reactor power stages. Knowing the ratio K_i/K_j, it is easy to obtain the energy of activation. The value of the coefficient a, determining the velocity constant K, was found by processing the experimental data. Figure 3 shows examples of this processing for three power stages of fuel element GD-107. The relations describing the experimental points were obtained by the least-squares method. It can be seen from Fig. 3 that when $\tau \geq 4$ min, the kinetics of fall of the pressure correspond to the parabolic law.

The energy of activation of this process, found from relation (5), is equal to 0.52 ± 0.01 eV/atom. This is the average value for three power stages of the fuel element GD-107. The error in calculating the temperatures T_i and T_j has not been taken into account here, as already discussed.

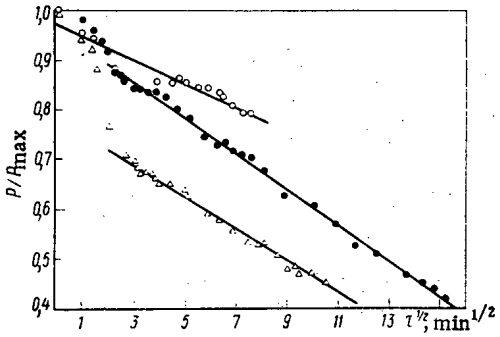

Fig. 3. Kinetics of fall of pressure in fuel element GD-107, with a power of: 48 (○); 66 (△); and 75 MW (●).

It should be noted that when the fuel element is filled with helium (GD-125), the coefficient a for the same temperature is found to be a factor of several less than in the case of fuel elements filled with air (GD-107).

Thus, repeated absorption of the gases released from the UO_2 during the first arrival of the fuel element at power, is due to a heterogeneous chemical reaction with diffusion kinetics. It can be confirmed that the reaction takes place on the effective surface of the UO_2, and not on the inside surface of the 1Kh18N9T steel cladding with a temperature of $\leq$(400-500)°K.

It has been shown that a pressure excursion in fuel elements with compact UO_2 during the first emergence of power is caused by desorption from the surface of the fuel, of gases of technological origin. The release became marked with a middle-space temperature of the fuel of 1050-1250°K. The total quantity of gas released amounted to $\approx 2 \cdot 10^{-5}$ m^3/kg UO_2. Repeated absorption of the gases is due to their chemical interaction with the fuel.

LITERATURE CITED

1. B. V. Samsonov et al., At. Energ., 40, No. 4, 390 (1976).
2. B. V. Samsonov et al., in: Operating Experience with Nuclear Power Stations, and Routes for the Further Development of Nuclear Power Generation [in Russian], Vol. 2, Izd. FÉI, Obninsk (1974).
3. B. V. Samsonov et al., Discoveries, Inventions, Industrial Standards, and Commodity Symbols [in Russian], Izd. TsNIIPI and TÉI, No. 41, Moscow (1973), p. 183.
4. A. S. Zaimovskii et al., At. Energ., 30, No. 2, 226 (1971).
5. S. J. Gregg and K. S. Sing, Adsorption, Surface Area, and Porosity, Academic Press (1967).

FIELD-EMISSION MICROSCOPY AND EMISSIVE PROPERTIES OF URANIUM

A. L. Suvorov

UDC 537.585

The advantages of applying field-emission microscopy techniques to uranium [1] are quite obvious, as this could provide additional information about the interaction of various materials with an uncontaminated uranium surface, about the processes of adsorption, desorption, and surface migration as related to the packing of various crystallographic faces, and about the details of allotropic transitions ($\alpha \rightleftharpoons \beta$ and $\beta \rightleftharpoons \gamma$ transitions). Of considerable importance also are the emissive properties of uranium: the electron work functions of the various phases and for different degrees of "purity" of the emitting surface. Finally, an analysis of low-frequency fluctuations of the field emission current [2] can probably provide important information on the nature of interaction of heavy charged particles (e.g., ionized gas molecules) with the uranium surface covered with a layer of atoms of definite species.

Field-emission studies of uranium (or, rather, of UO_2) have been first indirectly mentioned by Müller [3] who has shown a field-emission pattern of UO_2 film on tungsten without providing any experimental details. In a detailed study of emissive properties of uranium films on a tungsten emitter, Collins and Blott [4, 5] calculated the work function with respect to tungsten using a well-known method (measurement of the point potentials at equal field-emission currents for a pure surface and a surface covered with a uranium film). The work functions φ obtained in [4] (3.60 ± 0.03, 3.53 ± 0.03, and 3.43 ± 0.03 eV for α, β, and γ phases, respectively) hardly agree with the values obtained by other techniques (a brief review is given in [6]). A partial reason for this discrepancy is the fact that the majority of these works have been carried out in unsatisfactory vacuum conditions. An important part also is played by the method used in preparing the raw surface (the "kind" of the sample: bulk or film, the nature of film crystallization, its thickness, etc.). The first field-emission patterns of uranium points have been obtained [7] in autoionic microscopic analysis of uranium; little attention has been paid to the technique of producing detailed patterns.

Translated from Atomnaya Énergiya, Vol. 42, No. 4, pp. 280-285, April, 1977. Original article submitted July 26, 1976.

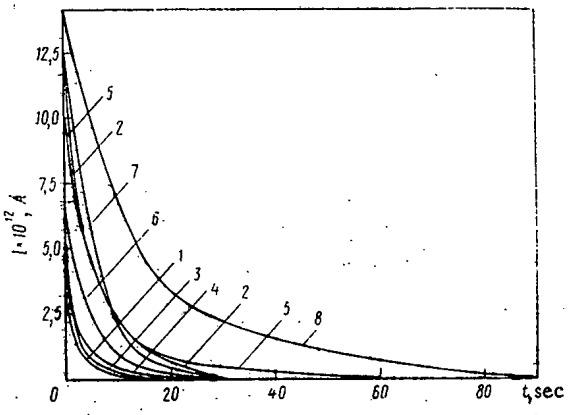

Fig. 1. Field-vaporization current as a function of time in decontamination of the uranium point surface in a reverse field, U = const: 9.25 (1), 9.75 (2), 10.0 (3), 10.5 (4), 10.75 (5), 11.0 (6), 11.25 (7), and 11.6 (8) kV.

Decontamination and Surface Preparation. The experiments were carried out with a conventional field-emission microscope made of glass (of a sealed type). The initial vacuum at the vacuum post was 10^{-7} mm Hg; the final vacuum obtained after sealing the device and evaporating the titanium getter was around 10^{-10} mm Hg. The sample material was 0.2-0.3 mm wire of technically pure natural uranium preannealed for 3 h at ~910°C and cooled in vacuum at a rate of 4 deg/min.

The preparation of a pure and smooth surface on a uranium field-emitter and the study of emissive properties of uranium at high temperatures are associated with certain technical difficulties due principally to the relatively low melting point of uranium. Temperatures more than twice as high as the melting point of uranium are needed to remove the oxygen compounds (in particular, uranium dioxide) that form on the surface of metallic uranium exposed to air [8]. Moreover, this circumstance prevents the use of sufficient heat for degassing the point and its mounting, which also serves as a heater, and impairs the vacuum conditions in the β and, particularly, in the γ temperature range.

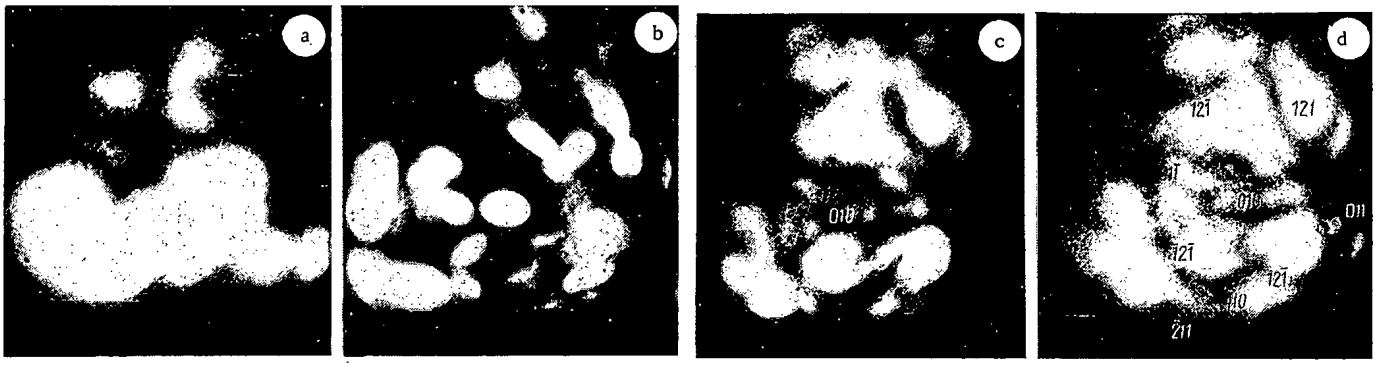

Fig. 2. Field-emission patterns of uranium obtained before (a) and after one (b) and many (c, d) decontamination cycles in a reverse field at t ≈ 150°C.

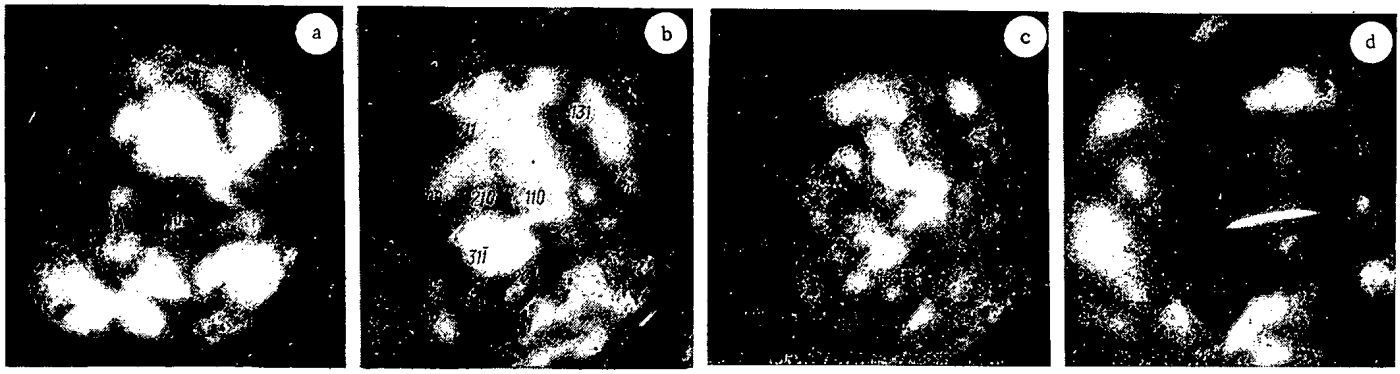

Fig. 3. Field-emission patterns of different crystallographic modifications of uranium: α and β phases (a, b), γ and α phases (c, d) (contaminated surface).

In this work the uranium surface was decontaminated by reverse-field vaporization [9] at room temperature and slight heating of the point (up to ~150°C). Field vaporization was monitored by observing the ion current. Figure 1 shows experimental vaporization – current curves for eight fixed sample potentials as a function of time. For any given sample potential vaporization stops automatically when the point becomes blunt enough for the electric field intensity to fall to $F \leqslant F_e$ (according to estimates [10], the vaporization field of uranium is ~4.35 V/Å). The quality of the surface thus prepared was evaluated from the obtained field-emission patterns. The mean radius R_0 of the point, which is needed for calculating the absolute electron work function averaged over all crystallographic faces $\overline{\varphi}$, was found from the empirical formula $R_0 = U_0/5F$ under the assumption that $F = F_e$, which is justified both by the approximate nature of the empirical expression and the exponential dependence of the vaporization rate on field intensity. It can be assumed that field vaporization ceases almost completely when the field falls slightly below F_e. On the strength of this assumption, the final radius of the point, corresponding to curve 8 in Fig. 1, was taken as equal to ~540 Å. In the last vaporization cycle, the field removes $\sim 7 \cdot 10^8$ atoms (assuming that the vaporization of uranium and other complexes contaminating its surface proceeds via doubly charged ions). This corresponds to more than 100 atomic surface layers. Since the field vaporizes mainly uranium dioxide molecules and atoms or molecules of residual gases adsorbed at the surface (but not pure uranium), the estimated value of F during vaporization and the number of vaporized layers are quite arbitrary. This, however, does not affect the estimates of R_0 provided vaporization removes all foreign materials from the uranium surface and "touches" pure uranium. In a number of cases, radius of the point was evaluated in parallel from shadow patterns in an electron microscope [11]. It was found that the most favorable surface shape is obtained after preliminary vaporization at ~150°C. Nevertheless, it is impossible to smooth out the uranium surface by heating as in the case of high-melting metals.

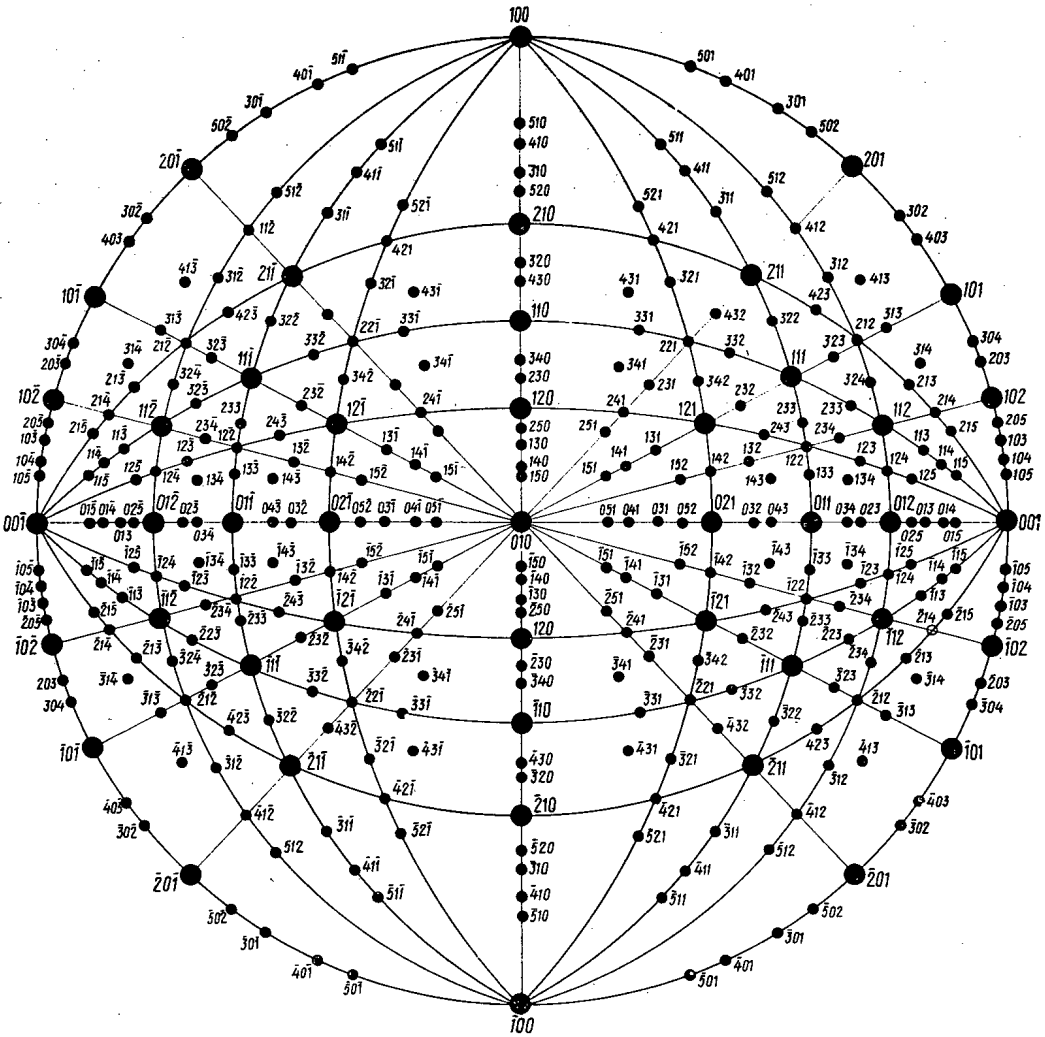

Fig. 4a. Standard stereographic projection of β uranium on the (010) plane.

Pattern Interpretation. Phase Transitions. Figure 2a shows the field-emission patterns of the raw surface (unpurified and unshaped) of α uranium obtained in this work (at room temperature, U = 4.8 kV). The evolution of the surface in the course of decontamination in a reverse field at t ≈ 150°C is shown in Fig. 2b-d; the applied voltage was 3.4 (b), 5.0 (c), and 4.0 (d) kV. In identifying the crystalline faces on the α-phase patterns, and in establishing the orientation of the observed single crystal, we have used the standard crystallographic projections of α uranium calculated in [7]; it has been found that the [010] axis coincides with the sample axis. Even if the obtained field-emission patterns are not entirely satisfactory, the identification of the crystalline structure and the determination of sample orientation, as well as the confirmation of the surface purity provided by them, indicate that the technique has good potentialities. At the same time there is no doubt that the method needs further analysis and development.

The field-emission patterns shown in Fig. 3 illustrate the attempt to analyze the nature of phase transitions in uranium. The pattern in Fig. 3a, corresponding to the α phase, has been obtained immediately after surface decontamination in a reverse field. A gradual increase of sample temperature resulted in a visible and practically instantaneous qualitative change in the pattern at ≤700°C and U = 5.0 kV (Fig. 3b). To decode the resulting pattern of the β phase of uranium we have specially computed the standard stereographic projections of the crystalline structure (tetragonal lattice, a = b = 10.759 Å, c = 5.656 Å; 30 atoms per unit cell).* The most likely projections are shown in Fig. 4. Unfortunately the low quality of the pattern and the absence of certain unformed principal crystallographic faces prevent an unambiguous conclusion about the β phase orientation. The most likely identification is represented in Fig. 3b; the sample axis is parallel to the [110] axis of β uranium.

*The author thanks T. L. Razinkova for running the standard program for stereographic projections of crystals for the β lattice of uranium through a computer.

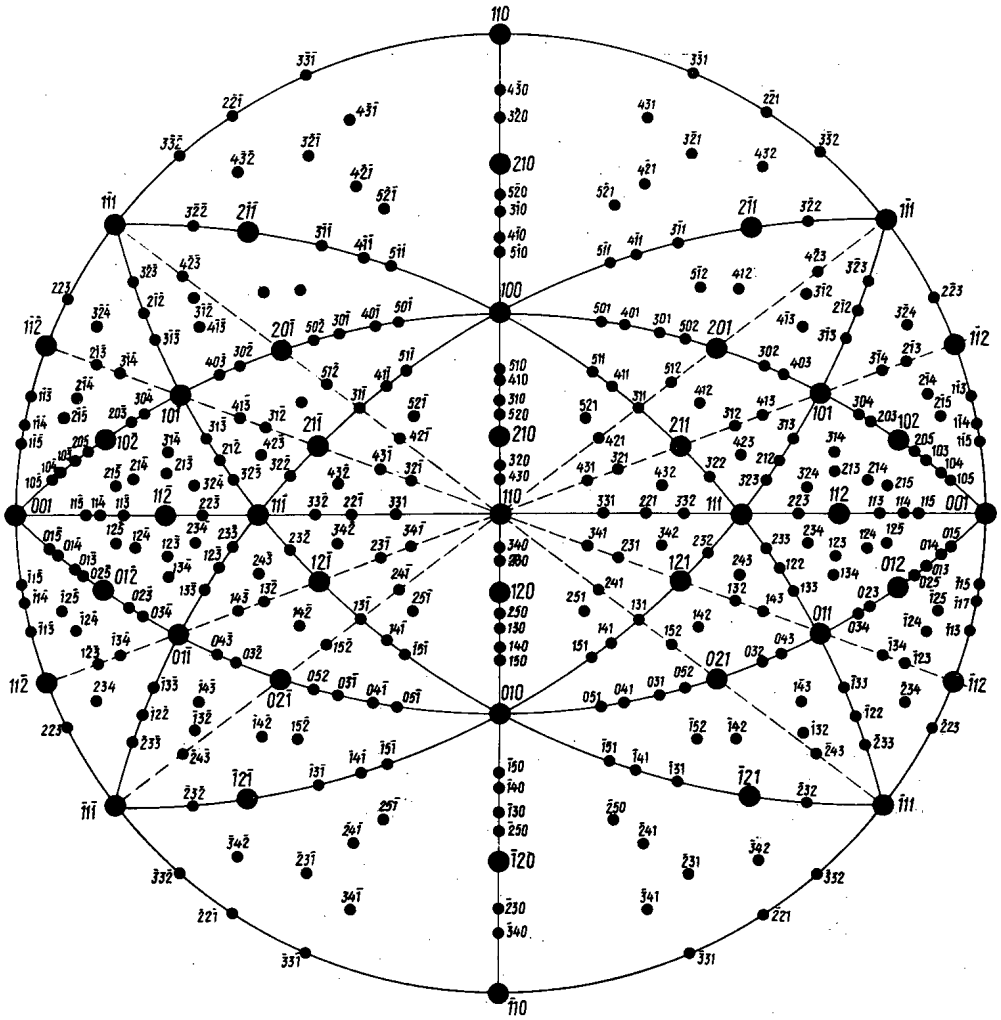

Fig. 4b. Standard stereographic projection of β uranium on the (110) plane.

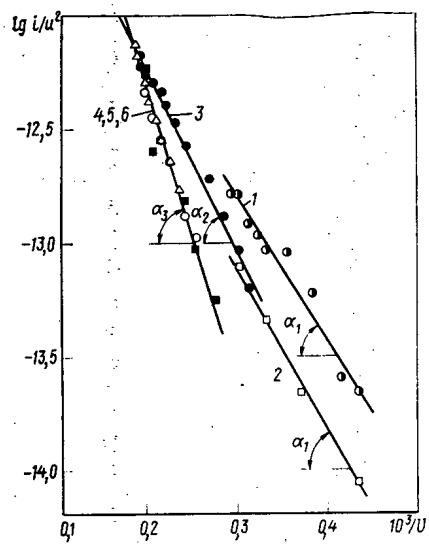

Fig. 5. Fowler – Nordheim curves for a uranium field-emitter (α phase).

The author has no knowledge of experimental data concerning the relative orientation of the different crystalline phases (in particular, α and β phases) of uranium single crystals. A theoretical analysis of the possible orientation relationships (such as made for $\alpha \rightarrow \beta$ zirconium [12]) is a very time-consuming problem, mainly because of the intricacy of the crystalline structure of the initial phases. A study of the texture of rolled uranium bars (polycrystals) indicates [8] that the (010) texture of the α phase of uranium practically vanishes when the sample is heated to β-phase temperature.

Further heating to ~780°C, corresponding to the γ phase range (Fig. 3c, U = 5.0 kV), did not reveal the characteristic bcc structure; this is possibly associated with the deterioration of vacuum conditions in the microscope, resulting in accelerated adsorption of atoms and molecules of residual gases on the sample surface.

Finally, the pattern in Fig. 3d has been obtained after the sample has been cooled to room temperature at U = 5.0 kV without surface decontamination. The subsequent decontamination of the sample surface in a reverse field made it possible to obtain patterns of the type shown in Fig. 2c, d. It should be noted that the β phase of uranium cannot be fixed by abruptly reducing the sample temperature (e.g., by switching off the heating and cooling with liquid nitrogen); this is in complete agreement with the well-known concepts [13].

Electron Work Function. Figure 5 shows Fowler – Nordheim curves corresponding to different states of α uranium surface. Curve 1 (◑) corresponds to a contaminated raw surface of the uranium point; the data for curves 2 (□) and 3 (●) have been obtained after one and two decontamination cycles in a reverse field at t ≈ 150°C and U = 14.0 kV. The decontamination (field vaporization) time was 1.5 min in both cases. As seen in Fig. 5, the slopes of curves 1 and 2 are the same. This means that during the first 1.5 min, field vaporization practically did not change the surface, removing only a fraction of the contaminating materials. Repeated vaporization improved the purity of the point surface: its work function increased by the factor 1.15 [$\bar{\varphi}_1/\bar{\varphi}_2 = (\tan\alpha_1/\tan\alpha_2)^{2/3}$]. Curves 4 (■) and 5 (△) have been obtained after decontaminating the point in a reverse field at t ≈ 150°C and U = 12.5 kV for 4.0 min. The dependence of field-emission current on the point potential was plotted twice, once with an increasing and once with a decreasing voltage. The measurements were taken in a vacuum of $5 \cdot 10^{-9}$ mm Hg. It is seen that the work function $\bar{\varphi}_3$ is now nearly 1.6 times as high as that obtained for the contaminated surface (φ_1). These data lead to a conclusion that field vaporization removes from the surface at least the layers of uranium dioxide and of other molecules adsorbed when the point was exposed to air. Further decontamination cycles in a reverse field at t ≈ 150°C [the data corresponding to curve 6 (○) in Fig. 5 were obtained after applying a vaporizing field of U = 11.0 kV for 10 min] did not change the slopes of the Fowler – Nordheim curves. The work function of α uranium was estimated as ~3.5 ± 0.03 eV (the radius of the point was calculated from the empirical formula).

We have also estimated the ratios of work functions of three allotropic modifications of uranium. In accordance with [14], we measured the point potentials corresponding to one and the same electron current at the temperature ranges of α, β, and γ phases. In the calculation we used the relationship $\bar{\varphi}_{\text{phase I}}/\bar{\varphi}_{\text{phase II}} = (U_1/U_2)^{3/2}$. The following ratios have been obtained: $\bar{\varphi}_\alpha/\bar{\varphi}_\beta \approx 1.03$ and $\bar{\varphi}_\alpha/\bar{\varphi}_\gamma \approx 1.08$ ($\bar{\varphi}_\beta$ was measured at about 700°C, $\bar{\varphi}_\gamma$ at about 780°C). The slight difference between the obtained values and those cited in [4] ($\bar{\varphi}_\alpha/\bar{\varphi}_\beta = 1.02$ and $\bar{\varphi}_\alpha/\bar{\varphi}_\gamma = 1.05$) can be explained in part by the different measuring temperatures (according

to [15] $\bar{\varphi}$ of uranium decreases with increasing temperature) and by the different "kind" of the investigated sample (bulk sample and film). One cannot exclude also the effect of different vacuum conditions.

In conclusion, the author thanks Yu. G. Abov and G. M. Kukavadze for their attention to this work, and A. F. Bobkov and B. Ya. Kuznetsov for participating in the measurements.

LITERATURE CITED

1. R. Gomer, Field Emission and Field Ionization, Harvard Univ. Press, Cambridge (1961).
2. V. A. Kuznetsov and A. L. Suvorov, Radiotekh. Elektron., 19, No. 2, 457 (1974).
3. E. Müller, Ergebn. Exakt. Naturwiss., 27, 290 (1953).
4. R. Collins and B. Blott, Surface Sci., 9, No. 1, 1 (1968).
5. R. Collins and B. Blott, Surface Sci., 13, No. 2, 401 (1969).
6. H. Riviere, in: Surface Properties of Solids [Russian translation], Mir, Moscow (1974), Chap. 4, p. 193.
7. A. L. Suvorov et al., At. Energ., 36, No. 1, 14 (1974).
8. Yu. N. Sokurskii, Ya. M. Sterlin, and V. A. Fedorchenko, Uranium and Its Alloys [in Russian], Atomizdat, Moscow (1971), Chap. 11, p. 222.
9. E. Müller, Phys. Rev., 102, 618 (1956).
10. A. L. Suvorov et al., At. Energ., 38, No. 2, 72 (1975).
11. A. L. Suvorov et al., ibid., No. 6, 412 (1975).
12. W. Burgers, Physica, 1, No. 7, 36 (1934).
13. V. S. Emel'yanov and A. I. Evstyukhin, Metallurgy of Nuclear Fuels [in Russian], Atomizdat, Moscow (1964), p. 49.
14. R. Klein, J. Chem. Phys., 21, 1177 (1953).
15. R. Fry and A. Cardwell, Phys. Rev., 125, 471 (1972).

CREATION OF A WORKING STANDARD OF THERMAL NEUTRON FLUX DENSITY BASED ON THE F-1 REACTOR

É. F. Garapov, A. G. Inikhov,
E. P. Kucheryavenko, S. S. Lomakin,
G. G. Panfilov, V. I. Petrov,
V. V. Khmyzov, and I. A. Yaritsyna

UDC 539.125.52.081.089.68

In the several years after approval by Gosstandart SSSR of the State primary standard of the unit of neutron flux density, a secondary (working) standard was created and certified by the D. I. Mendeleev All-Union Scientific-Research Institute; it is a facility which uses a defined arrangement of neutron isotope sources in a moderator. In the air, spherical working cavity of the facility, with a diameter of 200 mm, an isotropic field of thermal neutrons amounting to $6.70 \cdot 10^7$ neutrons/$m^2 \cdot$ sec is created. This thermal neutron flux density is completely satisfactory for the certification of the majority of detectors usually used in practice, and for determining their efficiency, but is inadequate for certifying instruments over the whole range of thermal neutron flux densities which is required at the present time.

In order to extend significantly the range of the secondary standard created earlier, it was decided to make another standard based on the F-1 reactor, which will be a suitable intermediate stage for connecting with facilities with a high neutron flux density. This will permit the range of the existing standard to be extended to 10^{14} neutrons/$m^2 \cdot$ sec.

The F-1 reactor is a research uranium–graphite reactor, operating on natural uranium [1]. The active zone of the reactor is of approximately spherical shape with a diameter of 6 m and surrounded by a graphite

Translated from Atomnaya Énergiya, Vol. 42, No. 4, pp. 286-289, April, 1977. Original article submitted June 4, 1976; revision submitted August 17, 1976.

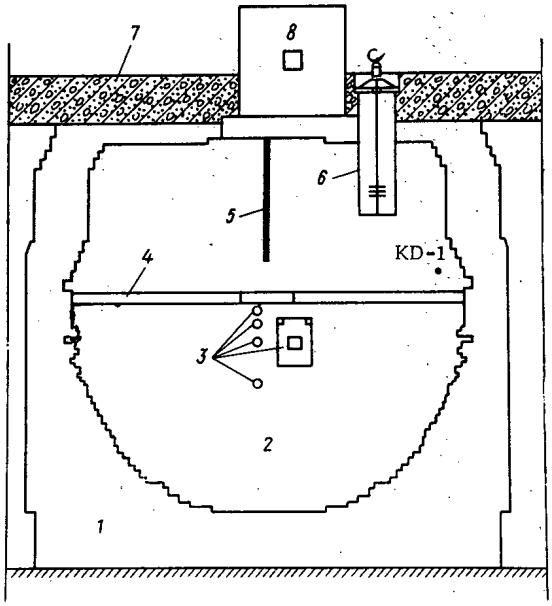

Fig. 1. General layout of the facility based on the F-1 reactor: 1) reflector; 2) active zone; 3, 4) experimental and horizontal channels; 5) control rod; 6) calibration well; 7) shield; 8) thermal column.

reflector of thickness 60-90 cm. The reactor has nine straight-through horizontal channels of different cross section and two wells sunk into the active zone, with cross section 60×60 and 30×30 cm, and also a horizontal channel in the graphite thermal column, which is a prism with dimensions $120 \times 120 \times 240$ cm, adjacent to the reflector.

Three air cavities were certified in the F-1 reactor (Fig. 1): at the center of the horizontal channel passing through the central plane of the reactor; in the channel of the graphite thermal column and in the calibration well with cross section 60×60 cm and with a depth of 130 cm, in which is installed a graphite insert with a central straight-through vertical channel with a diameter of 80 mm.

The cavity in the horizontal channel, with square cross section 10×10 cm, is bounded from the ends at a distance of 20 cm from the center by graphite blocks with a length of 40 cm, and is designed for the calibration of large-sized neutron detectors. In the channel of the thermal column, a field is created with a Maxwell spectrum of thermal neutrons, which have a temperature almost equal to the temperature of the moderator. The channel is rectangular shaped with cross section 18×13.5 cm. The depth of the channel is 180 cm. During irradiation of the detectors, the channel is closed with a graphite plug, 60 cm in length. The detectors being calibrated are arranged in the central cavity of the channels on thin-walled aluminum supports. The support with the detectors can be moved relative to the reactor channel and the thermal column either manually or by means of an electric motor, from the reactor control desk. The error in placing the detectors in the channel is ± 0.5 cm. Also included in the calibration instrument is a chamber, KD-1, of small dimensions with 0.12 mg ^{235}U used as a monitor.

The space-angular characteristics of the field and also its spectral parameters were studied in the certified channels of the F-1 reactor. In order to measure the spatial distribution of the neutrons in the cavities, lutetium, dysprosium, manganese, and indium activation detectors were used. In the horizontal channel and in the channel of the thermal column, these detectors were arranged around the axes of the channels at a distance of 3 cm from one another. The results of the investigations showed that the thermal neutron field is almost invariable over the length of these channels. The thermal neutron flux density distribution over the height of the vertical channel was studied by means of an aluminum rod with recesses located at a different height over 5 cm. The recesses were filled with previously calibrated manganese foils. The relative thermal neutron flux density distribution over the height of the vertical channel is shown in Fig. 2. In order to ensure identical irradiation conditions during certification of the vertical channel, detectors were positioned on an aluminum disk, rotating with a speed of 10 rpm, at a height of 15 cm from the bottom of the well.

For measuring the angular distribution, detectors of two identical dysprosium foils were used, separated by a cadmium disk, 1 mm thick. The anisotropy of the neutron field was determined by the ratio of the activity of these foils with different orientations.

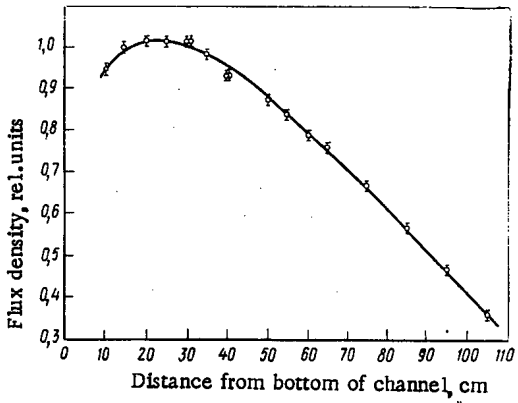

Fig. 2. Thermal neutron flux density distribution over the height of the vertical channel of the insert.

It was found that in the cavity of the thermal column, the neutron flux going below from the side of the active zone exceeds the neutron flux going upwards by a factor of 1.3. In the cavity of the horizontal channel, the neutron field is isotropic.

The spectral parameters of the moderated neutron field (effective temperature of the thermal neutron distribution T_N, Westcott's epithermal parameter r, and the coefficient α, characterizing the deviation of the moderated neutron spectrum from the 1/E law) in the channels of the F-1 reactor were determined by the cadmium ratio method [2] and the method of spectral indices [3]. In the first case, detectors of indium, gold, lanthanum, copper, and manganese were used, and in the second case detectors of lutetium, copper, and manganese were used. The detectors were calibrated in the channel of the thermal column of the F-1 reactor, where the neutron temperature was assumed to be equal to the graphite temperature.

As a result of the measurements by these methods, the following values were obtained for the spectral parameters in the horizontal and vertical channels and in the thermal column, respectively: $T_N = 365 \pm 7$; 334 ± 7; and 293 ± 3°K; $r = 0.058 \pm 0.002$; 0.033 ± 0.002 and $(1.64 \pm 0.08) \cdot 10^{-4}$, and for the horizontal channel $\alpha = -0.010 \pm 0.010$.

Table 1 shows the values of the detector thickness δ, the corrections for absorption of thermal G_{th} and epithermal G_r neutrons, the correction F_{Cd} which takes account of the absorption of epithermal neutrons in the 1-mm-thick cadmium filters, the resonance integrals I', and the activation cross section by thermal neutrons σ_0.

Certification of the channels of the F-1 reactor according to the effective thermal neutron flux density was carried out by means of a comparator, relative to the state primary standard. The effective thermal neutron flux density φ_{th} was taken as the product of the neutron density n_{th} with energies less than the effective limiting energy of cadmium E_{Cd}, and the neutron velocity v_0, equal to 2200 m/sec. The value of the effective thermal neutron flux density, reproduced in the state primary standard, was determined by the method of gold foil activation and at the present time amounts to $5.73 \cdot 10^8$ neutrons/$m^2 \cdot$sec, with a total error of 1% for a confidence coefficient of 0.99% [4]. The spectral parameters of the moderated neutron field determined by the cadmium ratio method are: $T_N = 314 \pm 5$°K; $\alpha = -0.016 \pm 0.008$.

In the measurements, gold foils with 10-mm diameter were used as comparator. The average mass of the foils was 12 mg. The foils were irradiated first of all in the working cavity of the primary standard in

TABLE 1. Detector Parameters and Measured Cadmium Ratios in the Horizontal and Vertical Channels

Detector	δ, mg/cm²	F_{Cd}	G_{th}	G_r	σ_0, b	I', b	R_{Cd} horizontal	R_{Cd} vertical
^{197}Au	16,87	1,02	0,9825	0,547	98,7	1520	2,53	3,48
^{115}In	0,27	1,10	0,9998	0,975	160	2660	2,01	2,74
^{55}Mn	13,87	1,04	0,993	0,926	13,3	8,0	14,3	—
^{63}Cu	18,6	1,00	0,997	0,930	4,5	2,88	14,05	—
^{139}La	2,4	1,00	0,999	1,000	9	7,3	11,8	—

TABLE 2. Values of the Effective Thermal Neutron Flux Density

Reactor power, kW	Readings of regular chamber, fissions	Readings of monitor, pulses/sec	Irradiation position	Mass of foil, mg	Saturation activity, d/min	R_{Cd}	φ_{th}, neutrons/m^2·sec
12	3000	4790	Horizontal channel	12,223	$1{,}287 \cdot 10^9$	2,51	$3{,}499 \cdot 10^{13}$
			Vertical channel	12,664	$1{,}884 \cdot 10^8$	3,44	$0{,}585 \cdot 10^{13}$
			Thermal column	13,735	$1{,}855 \cdot 10^6$	600	$7{,}565 \cdot 10^{10}$
18	4500	7180	Horizontal channel	9,254	$1{,}519 \cdot 10^9$	2,40	$5{,}263 \cdot 10^{13}$
			Thermal column	12,127	$2{,}466 \cdot 10^6$	600	$11{,}363 \cdot 10^{10}$
24	6000	9570	Horizontal channel	11,541	$2{,}456 \cdot 10^9$	2,49	$7{,}032 \cdot 10^{13}$
			Vertical channel	12,781	$3{,}788 \cdot 10^8$	3,45	$1{,}169 \cdot 10^{13}$
			Thermal column	13,127	$3{,}570 \cdot 10^6$	600	$15{,}205 \cdot 10^{10}$
			State standard	13,136	$1{,}601 \cdot 10^4$	6,28	$5{,}73 \cdot 10^8$

1-mm-thick aluminum and cadmium sheaths. Gold foils, similar in mass and area, were irradiated in the channels of the F-1 reactor: at the center of the horizontal channel, at the center of the graphite channel of the thermal column, and at a height of 15 cm from the bottom of the thermal column.

The irradiation time of the foils (150 min) was chosen by calculation, such that the error in determining φ_{th} in consequence of neutrons being present in the variable field at the instant of loading the detectors into the reactor channels did not exceed 0.2%. The activity of the gold foils, irradiated in the standard and in the reactor, was measured on the standard $\beta - \gamma$ and $4\pi\beta - \gamma$ coincidence facilities of the All-Union Scientific-Research Institute. The effective thermal neutron flux density in the reactor channels was determined according to the known effective flux density in the state primary standard, on the basis of the equation

$$\varphi_{th}^{r} = \varphi_{th}^{s} \frac{A^{r} (R_{Cd}^{r} - F_{Cd})\, R_{Cd}^{s} N^{s} g\,(T_{n}^{s})\, G_{th}^{s}\,(T_{n}^{s}\delta^{s})}{A^{s} (R_{Cd}^{s} - F_{Cd})\, R_{Cd}^{r} N^{r} g\,(T_{n}^{r})\, G_{th}^{r}\,(T_{n}^{r}\delta^{r})},$$

where A is the saturation activity in the foil; N is the number of gold nuclei in the foil; R_{Cd} is the cadmium ratio; and g is Westcott's parameter.

Table 2 shows the values of the saturation activity, averaged over the measurement results for three reactor power levels, carried out on the $\beta - \gamma$ and $4\pi\beta - \gamma$ coincidence facilities. The component of the random error, associated with measurement of the foil activity, in all cases did not exceed 0.2%. Table 2 shows the readings of the regular chamber incorporated in the reactor control system, and also the readings of the KD-1 monitor. The operating instability of this monitor chamber during 2 h of continuous reactor operation did not exceed 0.2%.

Table 3 shows the principal components of the random and systematic errors, due to the indeterminacy of the measurement results of the effective thermal neutron flux density in the reactor channels. The total error of the value obtained for the thermal neutron flux density, for a confidence coefficient of 0.99, calculated in accordance with [5], does not exceed 2%.

Additionally, the fast component of the neutron field was investigated by means of threshold detectors of sulfur, indium, and rhodium, and also the exposed dose intensity at the center of the horizontal channel of the F-1 reactor, which was determined by using a slit ionization chamber with a sensitive volume of 2.8 cm^3, calibrated first of all by means of standard γ sources. During operation of the reactor at a power of 24 kW, the

TABLE 3. Errors in Determining the Effective Thermal Neutron Flux Density, %

Quantity	Random	Systematic
Error of standard	—	1,00
A_r	0,2	—
R_{Cd}^{r}	0,3	—
N^{r}	0,1	—
G_{th}^{r}	—	0,2
t_{irr}	—	0,2
t_0	—	$\leq 0{,}3$
Readings of monitor	0,2	—

fast neutron flux density at energies in excess of 3 MeV amounted to $2.6 \cdot 10^{12}$ neutrons/$m^2 \cdot$sec. The exposed dose intensity of γ radiation was 2.2 ± 0.4 R/sec [1].

Thus, the results show that the working standard of the unit of neutron flux density based on the F-1 reactor, in its metrological parameters corresponds to the All-Union verification scheme and can serve as a starting measure for the reproduction of a thermal neutron density in the range from 10^{10} to $7 \cdot 10^{14}$ neutrons/$m^2 \cdot$sec.

LITERATURE CITED

1. É. F. Garapov et al., in: Nuclear Instrument Design, Proceedings of the All-Union Scientific-Research Institute of Instrument Manufacture [in Russian], No. 20, Atomizdat, Moscow (1973), p. 11.
2. O. L. Andreev and E. P. Kucheryavenko, Metrologiya, No. 5, 31 (1974).
3. S. S. Lomakin et al., in: Nuclear Instrument Design, Proceedings of the All-Union Scientific-Research Institute of Instrument Manufacture [in Russian], No. 17, Atomizdat, Moscow (1962), p. 11.
4. I. A. Yaritsyna et al., in: Metrology and Measurement Techniques [in Russian], No. 6, Énergiya, Leningrad (1975), p. 5.
5. K. F. Kudryashova, S. G. Rabinovich, and K. A. Reznik, in: Proceedings of the Metrological Institutes of the SSSR, No. 134 (194), Izd-vo Standartov, Moscow (1972), p. 5.

IONIZING RADIATION DETECTORS BASED ON RADIATION-STABLE CRYSTALLINE SEMICONDUCTORS OF THE In_2Te_3 TYPE

V. M. Koshkin, L. P. Gal'chinetskii, V. N. Kulik, G. K. Gusev, and U. A. Ulmanis

UDC 539.1.08.074.55

The use of semiconductor detectors for dosimetry of high dosages and intensities has been assumed to be impossible in principle, because of the radiation instability and total degradation of the physical parameters under the action of even relatively small doses of ionizing radiation [1]. The effect of an anomalously high radiation stability of a whole class of semiconducting crystals of the In_2Te_3 type was discovered in [2], which made possible the construction of new-in-principle solid-state ionizing radiation detectors.

All methods of detecting ionizing radiations, e.g., calorimetric and colorimetric (with the exception of ionization chambers), are based on measurements of the dose and not the intensity of the flux which, in particular, excludes in principle the possibility of automation of the processes associated with the use of ionizing particles for technological purposes. By comparison with ionization chambers, semiconductor detectors have a number of advantages: high sensitivity, small dimensions, simple construction, low supply voltage, simple matching with measurement amplifiers, etc.

It is shown in [2-5] that the physical parameters – electrical conductivity and its temperature dependence, lifetime of nonequilibrium charge carriers, mobility, concentration of charge carriers, absolute magnitude of photoconductivity, spectral dependence of photoconductivity, spectral coefficient of optical absorption, microhardness – of the semiconducting crystals In_2Te_3, Ga_2Te_3, and Ga_2Se_3 have an anomalously high stability under irradiation by different types of ionizing radiations, in comparison with the well-known semiconductor materials (germanium, silicon, etc.).

Irradiation by fast neutrons ($E_n \geq 1.0$ MeV), $F_n = 1.0 \cdot 10^{18}$ neutrons/cm^2, by fast electrons ($E_n = 100$ MeV), $Fe = 1.0 \cdot 10^{19}$ electrons/cm^2, and by γ quanta (^{60}Co), $F_\gamma = 3.0 \cdot 10^{18}$ quanta/cm^2 does not change the values

Translated from Atomnaya Énergiya, Vol. 42, No. 4, pp. 290-294, April, 1977. Original article submitted June 16, 1976.

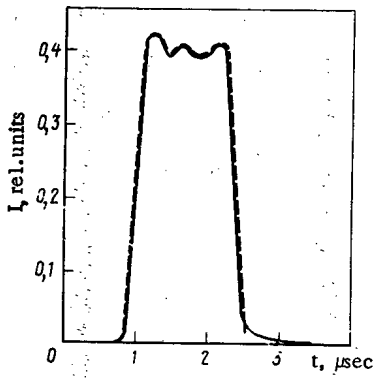

Fig. 1

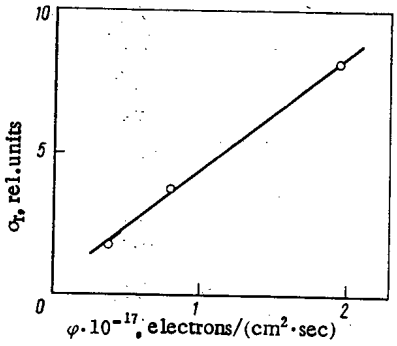

Fig. 2

Fig. 1. Accelerator current pulse (— — —) and voltage pulse in sample (———).

Fig. 2. Dependence of relative radiation conductivity of Ga_2Te_3 on the electron flux density for energy of 275 MeV.

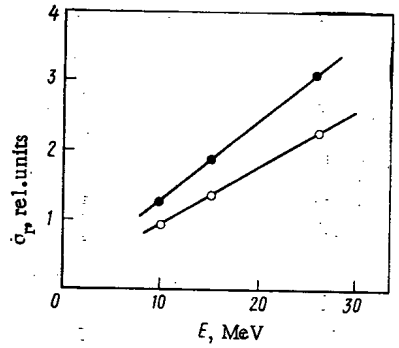

Fig. 3

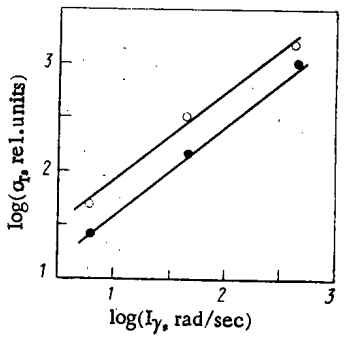

Fig. 4

Fig. 3. Dependence of relative radiation conductivity of Ga_2Te_3 on electron energy for a flux density of $2.8 \cdot 10^{17}$ (○) and $5.6 \cdot 10^{17}$ (●) electrons/cm^2 · sec.

Fig. 4. Dependence of radiation conductivity of Ga_2Se_3 on the dose intensity in the samples 1 (○) and 2 (●).

of these physical parameters within the limits of experimental error. There are still no experimental data, however, according to theoretical calculations [6, 7]; the radiation stability is preserved even at significantly higher fluence values.

The important property of the materials In_2Te_3, Ga_2Te_3, and Ga_2Se_3, in which the impurity atoms are electrically inactive, was investigated experimentally and theoretically in [8-10]. This property predetermines, on the one hand, the high "technologicity" of materials of this type which do not require extreme purification from impurities and, on the other hand, it leads to the fact that the conductivity of these materials always is inherent or close to inherent, as the equilibrium concentration of charge carriers is determined only by the width of the forbidden band. The widths of the forbidden band in In_2Te_3, Ga_2Te_3, and Ga_2Se_3 amount to 1.18, 1.27, and 1.95 eV, respectively. Therefore, all crystals, independently of the technological conditions of preparation, are of high impedance.

In order to use radiation-stable materials as the working elements of detectors, it is necessary that together with radiation stability, some of the parameters should vary inversely as a function of the intensity and energy spectrum of the ionizing radiation, i.e., they should have quite a high sensitivity relative to the parameters of the ionizing radiation.

The present paper is devoted to a study of the possibility of using these materials as the working elements of detectors of different types of ionizing radiations. For this purpose, the radiation conductivity, caused by different types of ionizing radiations, has been investigated.

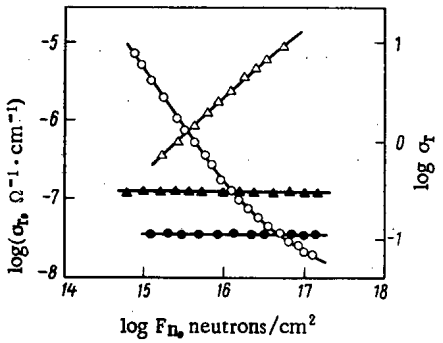

Fig. 5

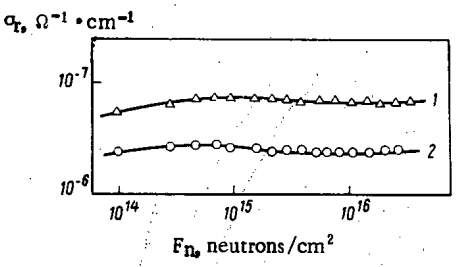

Fig. 6

Fig. 5. Dependence of radiation conductivity on fast neutron fluence during irradiation in the reactor for n–Ge (Δ), CdTe (○), In_2Te_3 (▲), and Ga_2Te_3 (●) for an irradiation temperature of 190°K and a γ-radiation dose intensity of $1.2\cdot10^4$ rad/sec.

Fig. 6. Dependence of radiation conductivity of Ga_2Se_3 on the fast neutron fluence at an irradiation temperature of 330°K and a γ-radiation dose intensity of $1.2\cdot10^4$ rad/sec in samples 1 (Δ) and 2 (○).

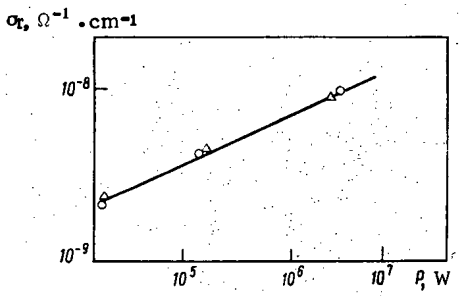

Fig. 7. Dependence of radiation conductivity of Ga_2Se_3 on the reactor power in samples 1 (Δ) and 2 (○).

The tests were carried out on γ facilities with sources of ^{60}Co and ^{137}Cs (E_γ = 1.2 and 0.66 MeV, respectively), on an electron accelerator with energies in the range 10-290 MeV and in the IRT-2000 nuclear reactor.

Fast Electron Detectors. The investigations were conducted on a pulsed electron accelerator. The duration of the electron pulse was 1.5 μsec and the repetition frequency: single, 0.125, 0.25, 12.5, 25, and 50 Hz. The range of energies of the electrons studied was 10-295 MeV, and the range of electron flux densities in the current pulse of the accelerator was 10^{16}-10^{18} electrons/cm^2·sec. During irradiation, compressed air was blown in for cooling the samples. The temperature of the samples was 310 ± 10°K. The dimensions of the samples of In_2Te_3, Ga_2Te_3, and Ga_2Se_3 were 2 × 4 × 5 mm.

A characteristic current pulse in a sample of In_2Te_3, excited by a pulsed stream of electrons with energy 25 MeV, is shown in Fig. 1. Figure 2 shows the dependence of the radiation conductivity σ_r at the point of maximum signal on the electron flux density and Fig. 3 shows the dependence of the radiation conductivity of a Ga_2Te_3 semiconductor on the energy of the fast electrons.

These characteristics of the crystals are unchanged after irradiation with the maximum fluence of fast electrons achieved in these experiments ($F_e = 4\cdot10^{17}$ electrons/cm^2). The lifetime of the nonequilibrium charge carriers is unchanged, which confirms the invariability of the decaying relaxation branch of the radiation conductivity in the samples. Similar results are obtained also on samples of the materials In_2Te_3 and Ga_2Se_3.

The results verify the feasibility of creating radiation-stable spectrometers and detectors for fast electrons, based on materials of the type In_2Te_3.

γ Radiation Detectors. The investigations were carried out on certified γ facilities: a ^{60}Co source (E_γ = 1.2 MeV), dose intensity I_γ = 500 rad/sec; ^{137}Cs source (E_γ = 0.66 MeV), dose intensity I_γ = 50 and 8 rad/sec. Samples of Ga_2Se_3 were investigated. The temperature of the samples during the experiment was 295 ± 5°K. Figure 4 shows the dependence of the radiation current in the crystals of Ga_2Se_3 on the γ-radiation dose intensity. The linear dependence plotted shows the high sensitivity of the Ga_2Se_3 semiconductor crystal to γ radiation; the sensitivity was unchanged after irradiation with a dose of 120 Mrad.

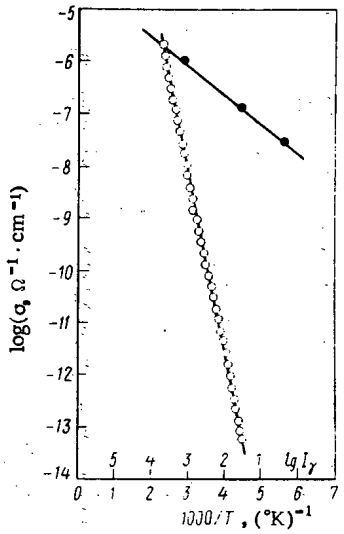

Fig. 8. Dependence of specific conductivity on the reciprocal of the temperature (○) and the radiation conductivity (●) on the γ-radiation intensity for Ga_2Te_3.

Thus, these radiation-stable semiconductor crystals can be used successfully for measurement of γ-radiation dose intensity.

Energy-Release Detectors. Tests were carried out in the horizontal channel of the IRT-2000 nuclear reactor over the temperature range from 190 to 350°K. Figure 5 shows the radiation conductivity of crystals of In_2Te_3 and Ga_2Te_3, induced by the mixed reactor radiation. Similar curves are shown in this same figure for germanium and cadmium telluride, obtained under the same thermal and radiation conditions. It can be seen from the figure that the radiation conductivity of In_2Te_3 and Ga_2Te_3 crystals remains unchanged (with constant reactor power $I_\gamma = 1.2 \cdot 10^4$ rad/sec up to a fluence ($E_n \geq 1$ MeV) of $F_n = 2 \cdot 10^{17}$ neutrons/cm^2. As would be expected, the radiation conductivity n – Ge, CdTe varies significantly as a function of the fast neutron fluence, which confirms the impossibility of measuring a high intensity of steady fluences of ionizing radiations, using classical semiconductor materials.

Figure 6 shows the radiation conductivity of Ga_2Se_3, obtained in the same channel of the reactor at a temperature of 330 ± 20°K. Just as for crystals of In_2Te_3 and Ga_2Te_3, the radiation conductivity of Ga_2Se_3 ($I_\gamma = 1.2 \cdot 10^4$ rad/sec) is invariable with increase of the fast neutron fluence ($E \geq 1$ MeV). The dependence of the radiation conductivity of Ga_2Se_3 crystals on the nuclear reactor power, determined in the same reactor channel, is shown in Fig. 7. The measurements were carried out at a temperature of 330 ± 15°K. The radiation conductivity varies linearly over the power range investigated and remains constant after irradiation with a fast neutron fluence of $F_n = 5.0 \cdot 10^{16}$ neutrons/cm^2.

Based on the data of [11], according to which it is possible to determine the energy release of a reactor by the dose intensity of the instantaneous γ radiation, the conclusion should be drawn that radiation-stable semiconductor crystals can be used as energy-release sensors. It should be stressed that these semiconductors have a high sensitivity to γ flux and excellent time characteristics (fast response ~1 μsec, see Fig. 1), which is particularly important in the automation of reactor control and safety processes.

As In_2Te_3, Ga_2Te_3, and Ga_2Se_3 crystals have an intrinsic (or very close to intrinsic) conductivity and, because of this, a high sensitivity of the specific electrical conductivity to temperature (up to 15%/deg [8]), they can be used for determining energy release by the change of temperature at different points of the reactor.

Figure 8 shows the dependence of the electrical conductivity on the temperature and the radiation conductivity on the γ-flux intensity for Ga_2Se_3. Similar relations were obtained for In_2Te_3 and Ga_2Te_3. It can be seen

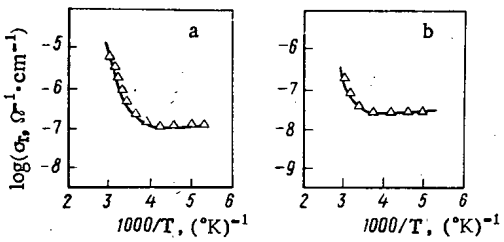

Fig. 9. Temperature dependence of radiation conductivity measured during reactor irradiation.

TABLE 1. Characteristics of Semiconductors of the Type In_2Te_3 and of Detectors Based on Them

Parameter	In_2Te_3	Ga_2Te_3	Ga_2Se_3
Melting point, °C	667	790	1020
Forbidden bandwidth, eV	1.18	1.27	1.95
Specific resistance at 20 °C, Ω·cm	(1-3) 10^6	2-4) 10^7	$3 \cdot 10^8$-$7 \cdot 10^9$
Mobility of charge carriers, $cm^2 \cdot W^{-1} \cdot sec^{-1}$	40 (electrons)	2 (holes)	10 (electrons)
Effective charge of nuclei, zeff	51	44	33
Temperature sensitivity coefficient at T_0 = 20 °C, %/deg	7	10	14
Sensitivity to γ quanta (^{60}Co), A/deg	-	-	10^{-9}
Change of electrical conductivity per unit of flux density of fast electrons with energy 25 ± 0.3 MeV, %/(A/cm^2)*	$6 \cdot 10^6$	$2 \cdot 10^7$	$3 \cdot 10^9$

*The radiation conductivity half-life for detection of pulses of a flux of electrons with energy 25 MeV and a flux density per pulse 5 mA/cm^2 amounts to not more than tens of nanoseconds.

from the figure that for a relatively low temperature and high γ-flux intensity, the working elements operate under γ-detector conditions. At a higher temperature and a relatively low γ-flux dose intensity, the equilibrium thermally induced conductivity exceeds the value of the radiation conductivity, and the sensors operate under thermistor conditions. Over a specified range of temperature and γ-flux dose intensity, it is easy to establish conditions in which the working element can function.

Figure 9 shows the experimentally obtained dependence of the conductivity of In_2Te_3 (a) and Ga_2Te_3 (b) on the temperature directly in the reactor channel for a γ-flux dose intensity of $1.2 \cdot 10^4$ rad/sec. These data are in agreement with the theoretical diagram (see Fig. 8), for a sufficiently low temperature (below 250 and 270°K for In_2Te_3 and Ga_2Te_3, respectively) the conductivity is determined exclusively by the γ-flux dose intensity and is independent of the temperature, but at a higher temperature the electrical conductivity, on the contrary, is independent of the γ flux but is determined only by the equilibrium intrinsic conductivity of the samples at the given temperature.

Thus, crystals of In_2Te_3, Ga_2Te_3, and Ga_2Se_3 can serve as the basis for high-sensitivity energy-release sensors, including local measurements of this parameter. The data given confirm the wide possibilities of using In_2Te_3, Ga_2Te_3, and Ga_2Se_3 as ionizing radiation detectors, and these detectors retain their efficiency after the action (almost infinitely) of high total doses of these radiations.

Table 1 shows the principal physical and experimental parameters of materials of the type of indium sesquitelluride.

The authors thank V. V. Generalov, P. M. Ryabke, Yu. M. Rezanov, É. A. Raitman, and S. S. Dindun for assistance in the experiments.

LITERATURE CITED

1. V. S. Vavilov and N. A. Ukhin, Radiation Effects in Semiconductors and Semiconductor Instruments [in Russian], Atomizdat, Moscow (1968).
2. V. M. Koshkin et al., Fiz. Tverd. Tela, 14, 646 (1972).
3. V. M. Koshkin et al., in: Monocrystals and Techniques [in Russian], No. 6, All-Union Scientific-Research Institute of Instrument Manufacture, Kharkov (1972), p. 97.
4. V. M. Koshkin et al., Radiat. Eff., 29, No. 1, 1 (1976).
5. V. M. Koshkin et al., Solid State Commun., 13, 1 (1973).
6. V. M. Koshkin et al., Fiz. Tverd. Tela, 15, 128 (1973).
7. V. M. Koshkin and Yu. M. Zabrodskii, Fiz. Tverd. Tela, 16, 3480 (1974).
8. V. P. Zhuze, V. M. Sergeeva, and A. I. Shelykh, Fiz. Tverd. Tela, 2, 2858 (1960).
9. V. M. Koshkin, Yu. A. Freiman, and L. V. Atroshchenko, Dokl. Akad. Nauk SSSR, 183, 83 (1968).
10. V. M. Koshkin, L. P. Gal'chinetskii, and A. I. Korin, Fiz. Tekh. Poluprovodn., 5, 1983 (1971).
11. I. Ya. Emel'yanov, L. V. Konstantinov, and V. V. Postnikov, At. Energ., 30, No. 3, 275 (1971).

STATE OF THE ART AND PROSPECTS FOR THE DEVELOPMENT OF TECHNOLOGY OF ATOMIC POWER PLANTS POWERED BY THE WATER-MODERATED – WATER-COOLED REACTOR VVÉR-1000

N. N. Zorev

UDC 621.039.5.53

The equipment of an atomic power plant is characterized by unusual dimensions, difficulty of construction, and exceedingly high demand for quality and reliability. The man-h expenditure is rather large, and the production cycle is fairly long. Thus, the manufacture of a reactor vessel under pressure of power 1000-1300 MW (electrical) in the factories of non-Soviet firms outfitted with up-to-date automated equipment takes up to 2 years.

Ensuring high quality and reliability in the equipment of atomic power plants is a complicated problem involving many factors bearing on the stability and end result of mechanical processes. For instance, the reactor-vessel shell in the water-moderated – water-cooled industrial reactor VVÉR-1000 is produced from ingots of mass up to 190 tons. The diameter of the forged shell reaches 4.7 m. It may have wall thicknesses up to 630 mm, a welded-seam penetration up to 400 mm, and an overall length up to 14 m. The larger the ingot, the more liquation of chemical elements there will be, the more segregation of nonmetallic impurities, and the more shrinkage and porosity in the center. Similarly, the thicker the ingot, the more slowly will hydrogen diffuse with heat treatment, and the more irregular will the plastic deformation be with forging and rolling. In the tempering process, the inner-volume cooling-rate slowdown will impair the microstructure and the strength of the metal. In annealing, heating and cooling time increase for large ingots and embrittlement of the metal takes place. With a large weld penetration, residual deformation, tension, and the probability of other defects sharply increase. Other mechanical processes are also adversely affected by large size and mass.

Besides improving product quality, it is just as important to lower the man-h expenditure, to shorten the production cycle, to eliminate manual labor, all of which are still rather excessive at present, and to economize on metal. This can be done by improving mechanical processes and the technology of manufacture, and by creating new materials and maximally automated factory equipment, especially in the areas of ingot production and welding.

However, the improvement of one mechanical process may slow down subsequent operations with the overall effect of lengthening the production cycle or lowering the quality of the product. Some new methods of deoxidizing liquid steel, for instance, slow down the manufacture of the product by a factor greater than 2, while a highly efficient ingot-slab production method for making reactor vessels which takes up about 6% of the total production cycle shortens the man-h expenditure in press forging but increases it in subsequent welding, thermal and mechanical processing, trimming and dressing, quality control, and repairs, all of which take up a percentage of the total production cycle which is ten times greater. As a result, overall man-h expenditure increases, the production cycle grows longer, and the quality and reliability of the reactor vessel are lowered because the ingot-slab longitudinally welded joints undergo operational stresses which are twice as high as for circumferential joints and because they fall in the zone of maximum radiation exposure. It is clear that if the production cycle is to be shortened and the product quality is to be raised, coordinated improvements must be made in the entire cycle from the smelting of the metal to its mechanical processing, inspection, and testing.

Toward that end, the Central Scientific-Research Institute of Technology, in conjunction with several Scientific-Research Institutes and some industrial plants, developed a coordinated optimization technology for the entire production cycle of the more important large-scale equipment used in the manufacture of the

Translated from Atomnaya Énergiya, Vol. 42, No. 4, pp. 295-303, April, 1977. Original article submitted March 12, 1976.

TABLE 1. Mechanical Properties of Standard Forgings in a Reactor Vessel Made of 15Kh2NMFA Steel (bottom head, thickness under tempering 240 mm)

Kind of heat treatment	Limit of strength σ_b, kgf/mm²	Limit of yield $\sigma_{0.2}$ kgf/mm²	Rel. expansion δ, %	Rel. contraction ψ, %	Limit of strength σ_b, kgf/mm²	Limit of yield $\sigma_{0.2}$ kgf/mm²	Rel. expansion δ, %	Rel. contraction ψ, %	a_H (type IV), kgf·m/cm²	
	20° C				350° C				20° C	−20° C
Tempering from 920°C, soaking for 8 h, cooling in water; annealing at 650°C cooling in air	75,0 73,6	64,5 64,2	22,0 21,6	73,4 74,0	63,2 63,0	55,0 55,0	16,8 16,6	70,0 72,8	18,4 19,4 18,6	21,0 22,0 20,2
Same with reannealing at 625 °C for 25h; at 650°C for 20 h, cooling in the furnace down to 300 °C, then in air	69,2 71,0 69,2 67,5	59,6 62,2 58,6 57,7	25,0 24,0 24,6 25,0	77,3 77,0 77,7 77,0	61,3 61,3 58,8 58,2	53,0 52,6 48,8 49,5	19,0 19,2 19,2 17,0	75,2 76,2 74,6 74,7	27,0 27,5 26,0 27,6	26,3 20,3 20,0 25,0
Normal per specifications	62	50	15	55	55	45	14	50	6	4

VVÉR-1000, including reactor vessels and heads, steam-generator housings, pump casings, volume-compensator and water tanks, armature frames, etc.

Systematic quality control of the product is a necessary aspect of the technology, as it enables us to discover defects in time and to eliminate instabilities in the mechanical process. A nondestructive quality-control system has therefore been introduced along the entire production cycle. The mechanical properties of the finished product are similarly controlled by a sampling system and by methods which determine its stability characteristics.

Optimizing the production cycle alone, however, is not enough. A coordinated optimization of technology, materials, designs, and equipment plays an equally important part in reducing man-h expenditure and in increasing product quality. It is an inescapable scientific and technological fact that with important, large-scale equipment, uncoordinated development of materials, designs, and mechanical processes usually leads to a sharp increase in man-h expenditure and to a decrease in product quality.

New Materials. 15Kh2NMFA steel has been developed and is currently used in the production of the core tanks of the VVÉR-1000. This steel does not require preheating to 200°C for welding, it is less prone to welding defects, and it is tougher (Table 1). Another one of its advantages is its high impact strength. As can be seen in Table 1, with an optimal heat treatment, reactor-vessel bottom-head samples with a sharp transition at −20°C have an impact strength a_H of 20-26.3 kgf·m/cm².

The temperature of the brittle – tough transition, measured in accordance with international standards, reaches −100°C (Fig. 1). In all mechanical properties, 15Kh2NMFA steel surpasses the levels of A508-Class 2

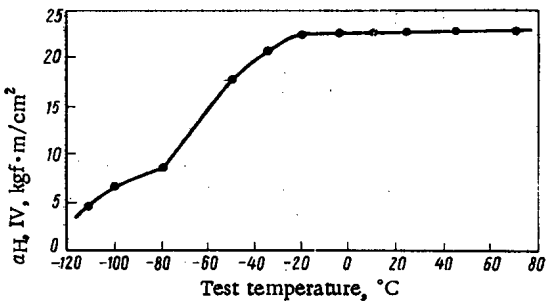

Fig. 1

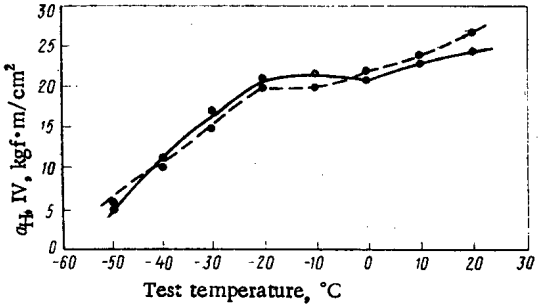

Fig. 2

Fig. 1. Dependence of 15Kh2NMFA steel impact strength on temperature (standard reactor-vessel bottom head).

Fig. 2. Dependence of 10GN2MFA steel impact strength on temperature (shell No. 434165). The solid line indicates the basic heat treatment. The dashed line shows the basic heat treatment and the annealing process over 75 h.

TABLE 2. Mechanical Properties of Standard Shells Made of 10GN2MFA Steel (thickness 150 mm)

Shell no.	Kind of heat treatment	σ_b, kgf/mm²	$\sigma_{0.2}$ kgf/mm²	δ, %	ψ, %	σ_b, kgf/mm²	$\sigma_{0.2}$ kgf/mm²	δ, %	ψ, %	a_H, kgf·m/cm²			
		20°				350°				type I	typeIV	type I	typeIV
										20°		−20°	
434297	920 °C Air	62,5	52,0	25,0	77,0	58,5	47,0	22,4	74,5	29,3	24,6	26,1	19,0
	900 °C Tempering in oil, annealing at 650 °C, reannealing for 74 h									29,3	24,1	24,6	18,6
		63,0	52,5	25,6	76,5	58,5	45,6	24,0	73,5	28,5	26,1	23,9	19,3
		58,6	47,5	27,2	75,0	52,3	38,2	20,4	66,8	33,3	29,3	27,8	23,0
										35,2	25,5	34,1	21,4
		60,0	48,4	25,2	72,5	53,6	39,5	19,4	67,0	34,8	32,1	31,0	26,8
434298	920 °C Air	60,0	53,0	25,0	77,0	54,0	40,0	22,8	74,5	30,5	27,8	21,4	19,7
	900 °C Tempering in oil, annealing at 650 °C, reannealing for 74 h									30,2	27,8	22,9	20,6
		58,0	45,2	27,0	76,5	56,0	50,0	27,0	76,5	31,2	26,8	25,2	19,7
		56,1	45,4	26,4	75,6	52,3	37,7	20,4	70,0	34,1	31,1	31,8	23,9
										35,4	31,9	38,8	22,0
	Norm per specifications	57,3	46,0	30,0	76,5	51,3	35,2	21,0	70,4	34,4	27,8	36,7	24,9
		55	34	16	55	50	30	14	50	8	4,8	4	2

steel and of A533-B steel used for reactor vessels in the USA, the German Federal Republic, Japan, France, and other countries.

For steam-generator housings, volume-compensator and water tanks, and for piping, 10GN2MFA steel has been developed and introduced into the manufacturing process. Its mechanical properties are significantly better than those of 22K steel (Table 2). This steel is even better than the American A533-B steel, since prolonged annealing does not produce significant brittleness (Fig. 2). Thanks to its low carbon content, it is highly effective when welded. Tests have shown that its hardness changes insignificantly in the thermal zone of welding. Its preheating temperature for welding need not exceed 150°C and its post-welding intermediate annealing may be replaced with a "rest period" in the 200-300°C interval during the combined heating. The mechanical properties of large castings up to 270 mm thick made of this steel satisfy the requirements for forged ingots.

In the casting of pump casings and armature frames, 00Kh13NDL stainless steel is used in order to eliminate the time-consuming process of cladding the inner surface with an anticorrosive jacket.

Nickel-free, martensite–ferrite stainless steel 0Kh14MFSe has been developed. It is recommended for the manufacture of separators, and steam superheaters in an atomic power plant equipped with a RBMK-1000 reactor. This steel can also be used for collector pipes and other steam-generator elements in the VVÉR-1000. These are at present made of austenite steel 0Kh18N10T which is prone to cold hardening and corrosive cracking under pressure. It also has a low yield point and requires a large amount of rare nickel in its fabrication.

The man-h expenditure in producing the equipment for the primary circuit of the VVÉR-440 will decrease with the use of technologically effective steels 15Kh2NMFA and 10GN2MFA, which were developed for the VVÉR-1000. In addition, it will soon be possible to standardize base and weld materials as well as many mechanical processes such as smelting, welding, and heat treatment, all of which will also be stabilized.

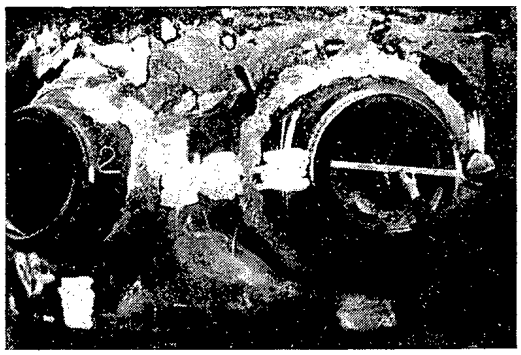

Fig. 3. Reactor-vessel nozzle area with stamped-out nozzles DU-850 in a VVÉR-1000.

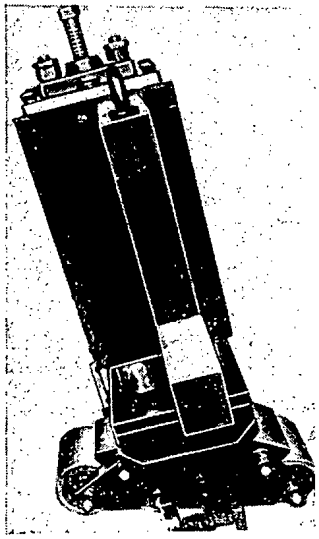

Fig. 4. Device for the follow-up processing of cladding.

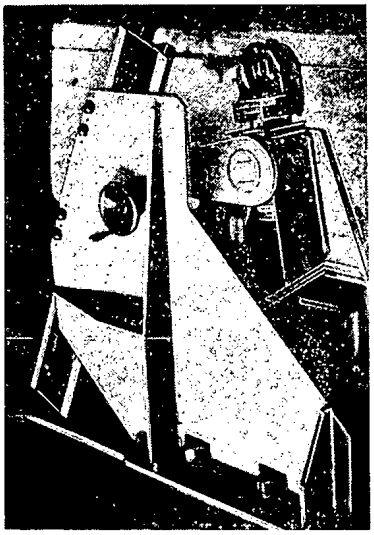

Fig. 5. Device for the follow-up processing of the reactor closure head.

Future improvements in nuclear-power engineering reside in the coordinated optimization of stable operational characteristics and in the technological effectiveness of materials. Insufficient technological effectiveness of materials not only increases production time but also impairs stable operational characteristics.

Coordinated improvement of materials must not be limited to basic chemical compositions. Microimpurities must also be controlled. Just as important is the institution of mechanical processes which ensure the highest stability and operational characteristics of the metal in areas such as smelting, refining of the liquid metal, crystallization guidance, plastic deformation, heat treatment, surface hardening, etc.

New Mechanical Processes. A significant reduction of the man-h expenditure and shortening of the production cycle in the manufacture of the reactor vessel have been effected by the following new processes: stamping-out of vessel nozzles from a wholly forged shell instead of from four 500-mm sections requiring subsequent longitudinal-seam welding (Fig. 3); stamping of reactor closure and bottom heads directly from clad plates, instead of using a complicated process of cladding these heads; electroslag welding-on of fittings, decreasing thus the man-h expenditure involved in welding them on manually; automatic cladding of the vessel-nozzle inner surfaces, thus eliminating defects and improving productivity; two-layered cladding of shells instead of four-layered, shortening thus the man-h expenditure in the cladding cycle; automated heating of the vessel-nozzle zone with electric heaters prior to welding, decreasing thus the unevenness of heat fields.

Induction heating has been introduced in the welding-on of fittings, in the cladding of nozzle inner surfaces, and other welding processes. A new heat-treatment technique shortens the length of tempering almost

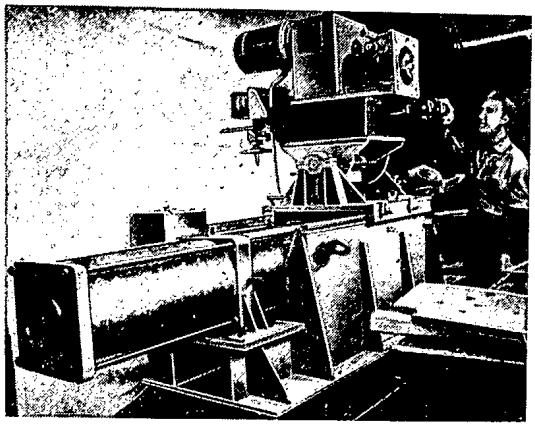

Fig. 6. Cutting device for the processing of the outside welding seams in shells.

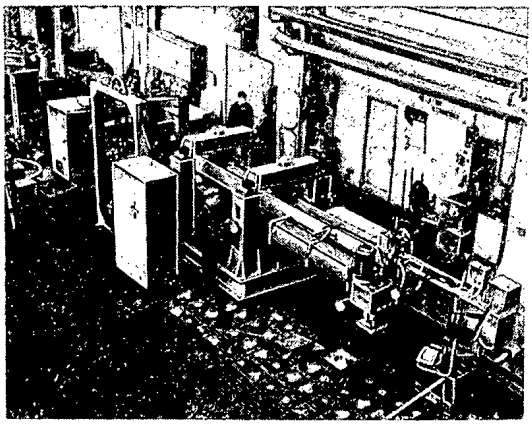

Fig. 7. Cutting device for the processing of the inside welding seams in shells.

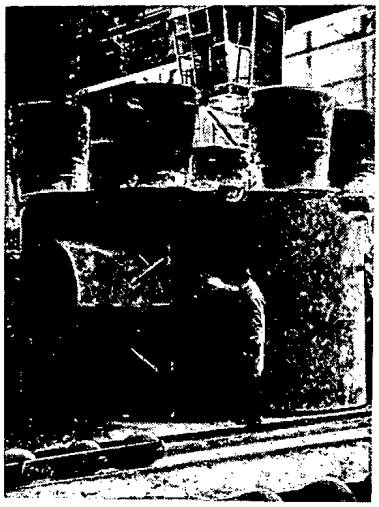

Fig. 8. Casting of a steam-generator nozzle.

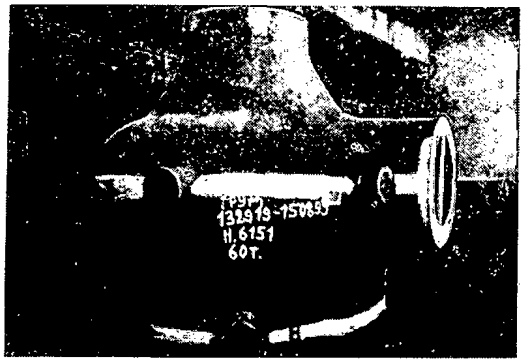

Fig. 9. Casting of a GTsN-195 pump casing.

by half. Thanks to a follow-up mechanical processing of the shells, the amount of metal used is lowered by 10-15%. A similar processing of the closure and bottom head surfaces and cladding (Fig. 4) eliminates manual trimming work (Fig. 5). Threading of the vessel flange with threading heads eliminates the defects of the process, increases the degree of surface finish by 1-2 grades, improves the productivity up to 2.5 times, and lowers the expenditures in manufacturing the object by 5 times.

Mechanizing the machining of the inside and outside seams eliminates hard manual labor (Figs. 6 and 7). The new technology of processing the oval aperture of the protective-pipe grid reduces the man-h expenditure, and with the use of a special device, the productiveness of labor grows by almost four times. The casting of steam-generator nozzles no longer requires special presses, shortens the mechanical processing by 1.5 times, and decreases metal expenditure by 25% (Fig. 8). The casting of GTsN-195 pump casings (Fig. 9) now eliminates forging, stamping, welding, and manual, time-consuming cladding.

The mechanical processes which will soon be introduced in the production of the equipment for the primary systems of atomic power plants include the following: the stamping of radial nozzles in steam generators DU-1200 and DU-850, which eliminates welding, ensures high quality, and cuts the man-h expenditure by half; the cladding of thick plates by spraying with atomized molten metal, which cuts by half the time consumed in cladding these plates by fused-metal surfacing; the cladding of shells with a wide metal strip and of plate sections with a double strip, both of which operations significantly raise the productivity. In the future, the number of plating layers will be reduced to one with the introduction of the ÉP872 nickel alloy strip. Narrow welding of steam-generator circumferential seams shortens the time expenditure by 2.5 times, and the new technology of steam-generator manufacture shortens the production cycle by 1.5 times. The bending of one-piece

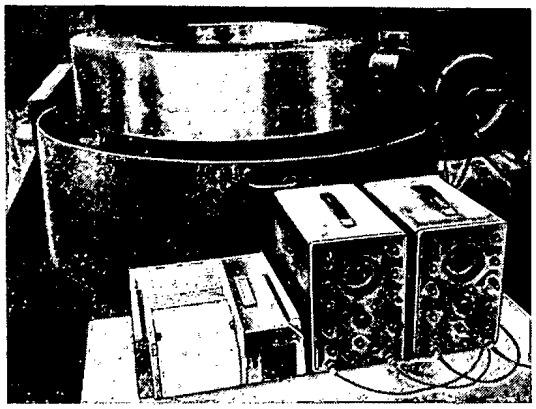

Fig. 10. Automatic device for ultrasonic inspection of shells during the machining process.

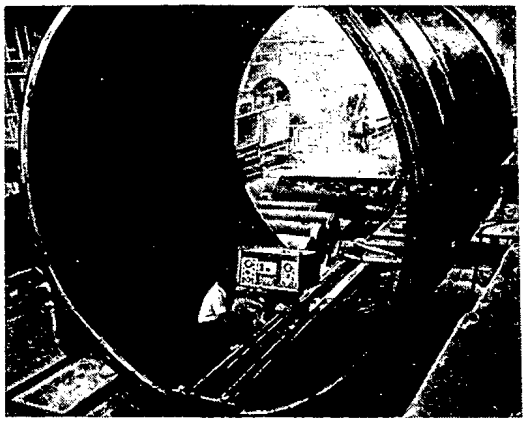

Fig. 11. Automatic device for ultrasonic inspection of welded seams.

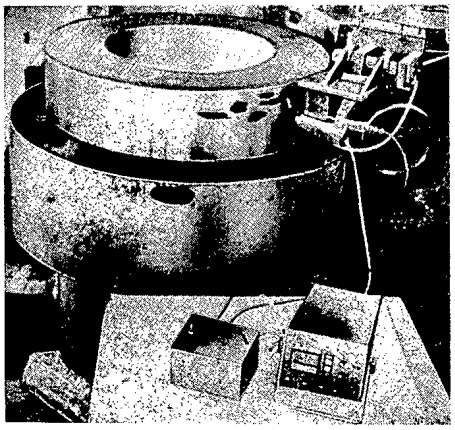

Fig. 12. Automatic device for electromagnetic inspection of shells during the machining process.

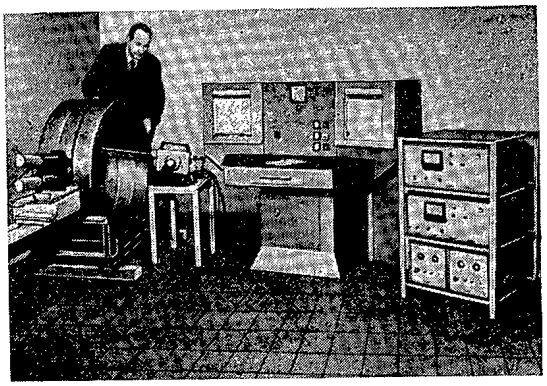

Fig. 13. Automatic installation for γ-ray inspection of welded circumferential seams.

plated tubes by stamping eliminates lengthy manual welding of longitudinal seams and seam plating, and increases the reliability of the tubes. Threaded nozzles in the reactor closure head decrease manual labor, reduce by 1.5 times the general man-h expenditure, eliminate welding defects, and raise the quality and reliability. New welding materials for the reactor vessel, the steam-generator housing, and other machinery in the primary system have been developed and tested. An easily separable welding flux has been developed which eliminates manual slag removal and which lowers the probability of slag inclusion in the welded seam.

The investigation of welded-joint mechanical properties and stability under radiation, performed at the A. A. Zhdanov Izhorsk plant on shells with standard seam penetrations gave results which satisfy existing requirements. Automatic ultrasonic inspection and recording of defects in shells (Fig. 10) and in welded circumferential seams (Fig. 11), and automatic electromagnetic inspection of shell surfaces (Fig. 12) have eliminated manual labor.

The Central Scientific-Research Institute of Mechanical Engineering, in conjunction with other Institutes and factories, solved several production problems in the secondary system of an atomic power plant.

The technology of turbine-cylinder casting, of turbine rotor-disk casting and forging, of prewelding, and precladding induction heating, of smooth-cladding of the disks, of gas-shielded metal arc-welding of root seams, as well as automatic ultrasonic inspection of welded joints, have been developed and introduced.

An automatic γ-ray inspection of welded circumferential seams (Fig. 13) is also being used.

A complex new technology is being introduced which produces rotors for four-pole generators in the fifth unit of the Novovoronezh atomic power plant, forged and welded generator rotors, and electroslag castings of band rings for generators.

Further technological improvement lies in the direction of speeding up the processes, widening the sphere of action, decreasing man-h expenditure, shortening the production cycle, and automating mechanical processes. Equally important is the optimization of mechanical processes and procedures, and their stabilization so as to increase the quality and accuracy of production.

Mechanical processes must be made maximally suitable for automatization, which ensures higher quality because it stabilizes mechanical processes and adjusts them routinely in the most effective way by adaptive guidance based on feedback, with sensing elements controlling the fundamental parameters of the working processes. Direct guidance of mechanical processes by an electronic computer is within sight.

Influence of Basic Industrial Materials on the Quality of Production. Mechanical processes, their parameters and stability, are factors which influence the quality of production, but there are others as well. Often, basic industrial materials play a part, especially in the manufacture of equipment for atomic power plants.

Statistical analysis and experiments have shown that in a reactor vessel it is not the basic chemical composition of the steel which it is made that determines the degree of its resistance to radiation, but the microimpurities it contains. Microimpurities may completely change the properties of the basic alloy components. With a high content in microimpurities, nickel for instance lowers the resistance to radiation, whereas with a low content, it heightens it.

TABLE 3. Microimpurity Content in 15Kh2NMFA Steel (147-ton ingots)

Nature of impurity	Cu	P	As	Sn	Sb
Specification 24-10-00273	0,3	0,02	0,08	—	—
Clean alloy	0,02	0,003	0,002	0,0001	0,001

Microimpurities containing copper, phosphorus, arsenic, or antimony exert the strongest influence on resistance to radiation. Standard industrial-quality norms allow a high content in copper and phosphorus in steel alloys, and they do not limit at all the content in other harmful trace elements such as arsenic, antimony, tin, and lead. 15Kh2MFA steel, however, was given a significantly lower impurity content and as a result its resistance to radiation improved by 15 times. Similarly, 15Kh2NMFA steel was also made very low in impurities, and it became superior, by an entire order of magnitude, to A533-B and A508 Class 2 steels used in the USA, the German Federal Republic, and other countries in the manufacture of reactor vessels (Table 3).

Irradiation of 15Kh2NMFA steel with a $7 \cdot 10^{19}$ nuetrons/cm^2 beam at 290°C shifts the temperature of the brittle – tough transition in a standard alloy by 150°C, and in a clean alloy only by 30°C.

The refractory materials used in the smelting and casting of steel also have a great importance for the quality of the metal. The refractory materials used at the present time do not have the necessary resistance to heat. This leads not only to inefficiency in metallurgical production owing to the frequent necessity for smelting-furnace repairs, but also to an increase in the amount of nonmetallic impurities in the metal. This last shortcoming is especially noticeable in the effect it has on the quality of low-carbon steel which has a lesser yield in the liquid state as a result. When shells made from 10GN2MFA steel, for instance, are x-rayed, they are invariably found to contain nonmetallic inclusions which prove to be aluminum oxides and silicon, the basic components of refractory materials.

The quality of welding materials, i.e., the harmful impurity content of welding wires and fluxes, exercises a strong influence on welded-joint resistance to radiation, and on welded-joint chemical properties and incidence of defects. Thus, when a seam is welded with a wire containing the usual amount of impurities and then irradiated with a beam of $9 \cdot 10^{19}$ neutrons/cm^2 at 290°C, its brittleness transition temperature reaches 370°C, but if the seam is welded with a wire free of impurities, the shift occurs only at 40°C.

Existing industrial standards and production norms for welding materials fall short of the high requirements made necessary by welding important equipment in atomic power plants. The data in Tables 4 and 5 show that in order to increase the quality and reliability of the equipment of an atomic power plant, the existing industrial materials must be made to more stringent requirements. It must be noted that the condition of the initial materials influences not only the quality and reliability of the equipment of an atomic power plant but also the man-h expenditure and the production cycle. Defects which appear in the base metal and in the welded joints lead to rejection of the particular piece of equipment. To repair the defect, long and arduous work must be done, as a rule by hand.

Improving Industrial Equipment. The quickly developing atomic technology requires the creation of new, complicated processes which can be realized only with perfect equipment. In the last few years, the equipment for the Izhorsk and other plants has been developed and manufactured, including automated installations for the welding of circumferential seams under a layer of flux at the reactor nozzle openings; an automatic machine for narrow gas-shielded arc welding; automatic machines for metal surfacing; heat-radiating installations and inductors for the heating of shells and nozzles prior to welding; transformers for electroinductive heating;

TABLE 4. Permissible Harmful-Impurity Content in Welding Fluxes Used on the Equipment of an Atomic Power Plant, %

Flux mark	Harmful-impurity content (USSR stand. or spec., %)		S	P	Cu	As	Sn	Pb	H, cm^3/100g
	P	S							
48-OF-10	0,04	0,04	0,020	0,020	0,3	0,0015	0,0005	0,0005	1
48-OF-6	0,025	0,05	0,020	0,020	0,3	0,0015	0,0005	0,0005	1
AN-42	0,07	0,07	0,020	0,020	0,3	0,0015	0,0005	0,0005	1
AN-17M	0,05	0,05	0,020	0,020	0,3	0,0015	0,0005	0,0005	1

TABLE 5. Permissible Harmful-Impurity Content in Welding Wire Used on the Equipment of an Atomic Power Plant

Welding-wire mark	S	P	Cu	As	Sn	Pb	N_2
Weld-08AA	0,008	0,005	0,03	0,0015	0,0005	0,0005	0,008
Weld-10KhGNMAA	0,008	0,005	0,03	0,0015	0,0005	0,0005	0,008
Weld-10GN1MA	0,008	0,005	0,03	0,0015	0,0005	0,0005	0,008
Weld-08GNMA	0,008	0,005	0,03	0,0015	0,0005	0,0005	0,008
Weld-10GN2MFA	0,010	0,008	0,06	0,0020	0,0010	0,0010	0,010
Weld-16Kh2NMFTA	0,010	0,008	0,06	0,0020	0,0010	0,0010	0,010
Weld-10KhMFT	0,008	0,005	0,03	0,0015	0,0010	0,0010	0,010

feed sources and control panels of heating installations for welding; installations for processing welding seams of outside and inside surfaces of shells; an installation for aggregate dressing and trimming of outside and inside surfaces of shells; a device for follow-up processing of the reactor-closure head and of the built-up metal layer; the thread-cutting head M140 with an automatic disengagement of the cutting plates; a device for the boring of oval apertures in the grid of the protective tubes assembly; automatic machines for the ultrasonic and electromagnetic inspection of shells at the time of mechanical processing; a shielded-metal arc welding automatic machine for the welding of root seams of the turbine rotor in an atomic power plant; installations for automatic ultrasonic inspection of turbine-rotor welded seams, and γ-ray inspection of welded circumferential seams.

The problem of improving the mechanical equipment depends on automatization with a programmed control.

The Influence of Design Effectiveness on Man-Hour Expenditure and Quality. For complicated and important equipment, the effectiveness of design is especially important. In atomic-machine construction, it is necessary to establish as early as in the planning stage the effectiveness of design and to include ways to adjust it. The effectiveness of existing designs for the equipment of atomic power plants must also be raised, paying special attention to the following: the standardization of primary-system vessel diameters and of similar designs for units of different power; elimination of uncoordinated fabrication of the equipment, which hinders the stabilization of mechanical processes and inspection; the elimination of processes requiring manual labor or which lower the quality of the product; discontinuing the fabrication of equipment which hinders the automatization of mechanical processes; the elimination of singularities in construction as these significantly raise the man-h expenditure and lengthen the production cycle.

In order to specialize production and thereby ensure a decrease in time expenditure, an increase in productivity of labor, and a shortening of the production cycle, it is necessary to standardize atomic power plant units of different power.

Let us note also that the increase in unit power of atomic power plant equipment will significantly reduce the man-h expenditure per kilowatt of power. The transition to the production of powerful units will also raise the yearly power output of the equipment. The above also applies to the secondary system.

Conclusions. The equipment of atomic power plants is characterized by unusual dimensions, complicated fabrication processes, high man-h expenditures, and exceptionally high requirements for quality and reliability. To solve new, complicated fabrication problems, it is necessary to further improve the dependable operational characteristics of basic materials as well as their effectiveness, to create new progressive mechanical processes, and high-quality automated equipment. The quality of initial materials making up the alloys, the refractory vessels, the welding wires and fluxes, the ingots, the rolled and complementary equipment, must be improved.

The effectiveness of atomic power plant equipment design must also be improved, and the equipment itself must be maximally standardized. Similarly, materials, designs, all mechanical processes and equipment must be coordinated and optimized.

Specialization in atomic power plant equipment production and the creation of continuous production lines will have a significant effect on quality improvement. The increase of unit power in atomic power plant machinery will substantially increase the output of power in the equipment at the factories.

EXCITED X-RAY FLUORESCENCE ANALYSIS OF A SUBSTANCE BY AN SXRL PROGRAM

S. P. Golenetskii, V. A. Kalugin,
V. I. Sedel'nikov, and N. I. Sukhlova

UDC 550.832.56

An SXRL (selective x-ray radiometric logging) program has been developed for theoretical evaluations of the capabilities of excited fluorescence x-ray analysis of substances. This program makes it possible to calculate the form of the energy spectra of secondary x-ray radiation excited by some source in a medium under study. A distinguishing feature of the program is that it takes detailed account of the interaction of x-ray quanta with the matter in the energy range considered, including the photoeffect with the emission of characteristic quanta, as well as coherent and incoherent scattering with allowance for the binding of elements in atoms [1-4]. The program is written in FORTRAN FM-20 for an M-222 computer.

Spectra calculated according to this program are compared with those obtained experimentally with a Ge(Li) detector. Pure sand with a 1% content served as the medium studied, and the specimen was excited with ^{241}Am radiation ($E_\gamma \approx 59.6$ keV). The experimental and calculated data are in good agreement apart from the region between peaks of coherent and incoherent scattering, which may be due to the nonideal nature of the collimating system in the experiment.

LITERATURE CITED

1. E. Storm and H. Israel, Cross Sections for Interactions of Gamma Rays. A Handbook [Russian translation], Atomizdat, Moscow (1973).
2. E. Storm and H. Israel, Nucl. Data, 47, 565 (1970).
3. H. Hanson et al., "HFS scattering factors," Acta Crystallogr., 17, 1040 (1964).
4. D. Cromer and J. Mann, J. Chem. Phys., 47, 1892 (1967).

PHOTOEMULSION METHOD OF PERSONAL NEUTRON MONITORING

M. M. Komochkov and M. I. Salatskaya

UDC 539.12.08:621.386.82

This paper gives some characteristics of a photoemulsion method of personal neutron monitoring (ppnm), based on recording tracks and stars in K-type nuclear emulsion (20 μ). The sensitivity of the ppnm detector, determining the density of proton tracks per rem of neutrons of various energies incident isotropically in a 2π solid angle, is presented in Fig. 1. The values obtained for the sensitivity with calibration of the detectors with neutrons from a Pu + Be source can be taken to be $A = (1.23 \pm 0.15) \cdot 10^4$ tracks $\cdot$ cm$^{-2} \cdot$ rem^{-1}.

The fact that the readings during irradiation of ppnm detectors, when the contribution of relativistic neutrons to the total equivalent dose exceeds 5%, are too high necessitates corrections to the readings obtained ppnm methods, described in [1]. The corrected readings of ppnm detectors are in good agreement with the readings of other instruments which record the dose more reliably.

The paper presents the results of experiments on the effect of the temperature and the humidity of the ambient air on the preservation of tracks in an emulsion irradiated with neutrons from a Pu + Be source. It

Translated from Atomnaya Énergiya, Vol. 42, No. 4, pp. 304-306, April, 1977.

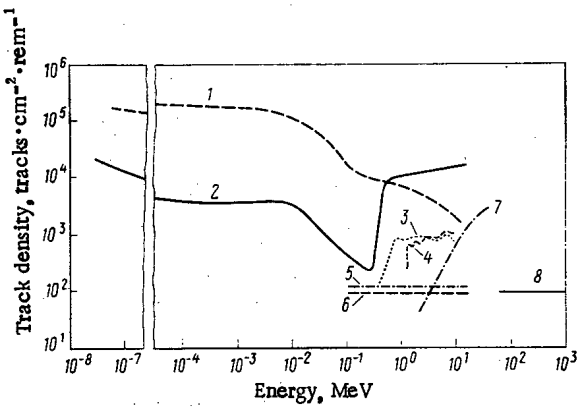

Fig. 1. Sensitivity of various detectors as neutron dosimeters: 1) ^{6}Li thermoluminescent detector; 7) ^{7}Li; 2) ppnm detector; 3) detector of traces of radiation damage with radiators of ^{237}Np; 4, 6) ^{232}Th; 5) ^{7}Li; 8) Bi.

is shown that under ordinary conditions (t = 25°C, relative humidity less than 60%) the number of tracks in irradiated emulsions remains constant when the emulsions are stored for two months. For comparison, Fig. 1 gives the sensitivity of thermoluminescent detectors (tld) and radiation-damage detectors (rdd) to neutrons of various energies, expressed in terms of the number of tracks or equivalent tracks (for the tld) per unit area of detector under radiation with a 1-rem dose [2]. Under actual conditions of work near nuclear-physical installations rdd as well as tld on the whole are inferior to personal neutron monitoring in regard to sensitivity. This circumstance, as well as experience acquired, the accessibility of the method, and the possibility of analyzing the information obtained warrant the assumption that the photoemulsion personal neutron monitoring method will in coming years remain competitive in personal neutron monitoring.

LITERATURE CITED

1. M. M. Komochkov and M. I. Salatskaya, JINR Preprint [in Russian], P16-8175, Dubna (1974).
2. M. M. Komochkov and M. I. Salatskaya, JINR Preprint [in Russian], P16-9780, Dubna (1976).

SOME LAWS GOVERNING NEUTRON SPECTRA BEHIND THE SHIELDING OF PROTON ACCELERATORS

V. E. Aleinikov, V. P. Gerdt, and M. M. Komochkov

UDC 539.125.164

The paper gives the results of studies on measuring the systematizing neutron spectra behind the shielding of high-energy proton accelerators, first published in [1-3]. The studies were based on improved methods of measuring and reproducing spectra and on analysis of the information from spectra beyond shieldings of various compositions as well as analysis of the composition of the shielding, and the upper limit of the neutron energy range.

The spectra were measured with six detectors. Five of them constituted a Bonner spectrometer [3]. The sixth detector was a carbon-containing detector which recorded neutrons by the reaction $^{12}C(n, 2n)^{11}C$. The spectra were reproduced by statistical regularization [4], with allowance for a priori information about the existence of an upper limit of the neutron energy range.

The energy distribution of neutrons behind solid shielding has been studied in greatest detail. Analysis of the results, which are given in Fig. 1, shows that for "hard" spectra the function $E\Phi(E)$, where $\Phi(E)$ is the differential flux density of neutrons of energy E, has a maximum in the high-energy range, at ~100 MeV.

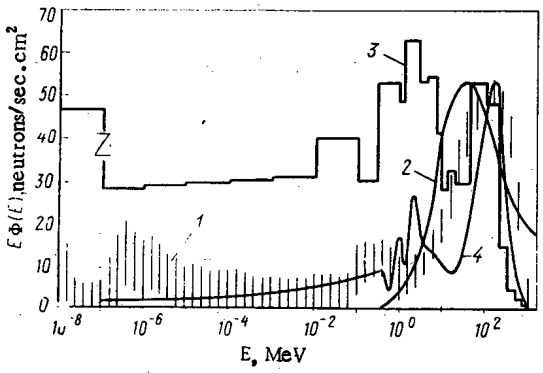

Fig. 1. "Hard" neutron spectra: 1) behind the solid shielding of the JINR synchrocyclotron; 2) behind the shielding of the CERN proton synchrocyclotron [2], rel. units; 3) behind the side shielding of the 800-MeV proton accelerator of the Los Alamos Meson Factory, calculation [5], rel. units; 4) behind 500-g/cm^2 concrete shielding for incident neutrons emitted by a target at 70° relative to the direction of an 18.2-GeV primary proton beam of 18.2 GeV protons, calculation [6].

It is shown that the information obtained about the neutron energy distributions can be used to establish the maximum indeterminacy in the equivalent neutron dose, measured with an instrument which determines the magnitude of the dose in a limited energy interval.

LITERATURE CITED

1. M. Weinstein et al., Rep. HASL-223 (1970).
2. R. Thomas, in: Proc. IAEA "Neutron monitoring for radiation protection purposes," Vienna, Dec. 11-15 (1972), Vol. 1, p. 327.
3. V. E. Aleinikov, V. P. Gerdt, and M. M. Komochkov, Proceedings of the Fourth All-Union Meeting on Charged-Particle Accelerators [in Russian], Vol. II, Nauka, Moscow (1975), p. 240.
4. L. S. Turovtseva, IPM Preprint [in Russian], Moscow (1975).
5. H. Israel and D. Cochron, in: Proceedings of the Second International Conference on Accelerator Dosimetry and Experience, Stanford, California (1969), p. 341.
6. E. K. Gel'fand et al., Tr. Radiotekh. Inst., No. 22, 242 (1975).

DATA ON THE RADIOACTIVE CONTAMINATION OF THE BIOSPHERE IN HUNGARY

Szabo Andras

UDC 551.510.3:614.876

Systematic monitoring of the radioactivity of food products began in Hungary in 1960 and 12 institutes now participate in this work. Table 1 lists the radioactive contamination of some food products. The data indicate that the radioactivity of the food products is of natural origin.

In 1974 radiometric studies were made of the food that a person needs in a day. It was found that each day the human organism ingests substances with a mean activity of 2 nCi, of which ^{90}Sr accounts for 17 pCi/day. These data are in good agreement with those for other European countries.

The discriminatory factor of the milk–feed link was determined from measurements of the radioactivity of feed and milk. From 1965-1975 the average discriminatory factor for ^{90}Sr was 0.13, which means that the ^{90}Sr content in the milk is less than in the feed.

A peak in the radioactivity of food products in Hungary was observed in 1961-1964 after which the level of radioactive contamination decreased significantly and has practically not changed since 1968-1970. The

TABLE 1. Results of Radiometric Measurements of Food Products in Dyör – Sopron Region in 1972-1974, pCi/g Dry Substance

Product	Activity		
	total	^{40}K	^{90}Sr
Apple	7,2	6,2	0,4
Pear	7,0	6,1	0,3
Peach	5,7	3,6	0,7
Grapes	12,1	11,8	0,1
Cabbage	22,1	21,4	0,3
Potatoes	13,1	11,5	0,4
Cucumber	2,1	1,9	0,1
Bread	2,3	1,9	0,1
Ham	4,6	4,5	0,0
Sliced sausage	4,7	4,4	0,1
Egg white	11,3	9,0	0,7
Egg yolk	2,4	1,2	0,5

radioactive contamination of food products is not high; usually, it is an order of magnitude lower than the activity of natural radioactive isotopes.

LETTERS TO THE EDITOR

α-RADIATION MEASUREMENT OF BERYLLIUM COATING THICKNESS

M. A. Belyakov and É. P. Terent'ev

UDC 621.039.164

In radioisotopic thickness gauges used for the measurement of coatings, one usually employes the scattering of β particles or the excitation of x rays [1, 2]. These instruments are used for measurements of the thickness of heavy-element coatings (Fe, Cu, Sn, Cr, etc.). A characteristic of light elements (Be, B, F, Li) is the higher yield of secondary radiation from the nuclear reaction (α, n, γ), viz., 80, 24, 10, and 2.6 neutrons, respectively, per 10^6 ^{210}Po α particles.

The nuclear reaction in beryllium, ^{9}Be(α, n, γ)^{12}C, is accompanied by hard γ radiation at 4.45 MeV. Measurement of secondary radiation from this reaction can be used for determination of beryllium and for measurement of the thickness of thin films and foils [1-3]. An interesting possibility is the use of the (α, n, γ) nuclear reaction for determination of the thickness of beryllium coatings which are widely used in nuclear-physics equipment, e.g., coating for the windows of scintillation and proportional counters for "soft radiation," etc. [4].

A block diagram of the appropriate equipment is shown in Fig. 1. The α source is ^{210}Po contained in a holder. Beneath the source is the beryllium-coated material and a γ-ray detector in a lead housing. The signal from the detector is fed to an amplifier-discriminator and then to counting equipment.

The α particles irradiate the beryllium coating with the yield from the α, n, γ secondary reaction varying as a function of coating thickness. Radiation accompanying the reaction is measured by the detector and acts as a measure of coating thickness. An NaI(Tl) scintillation crystal 40 × 40 mm in size was used as a detector.

In order to eliminate the effect of γ radiation from ^{210}Po (E_γ = 800 keV), measurements were made with a discrimination threshold of 1.2 MeV.

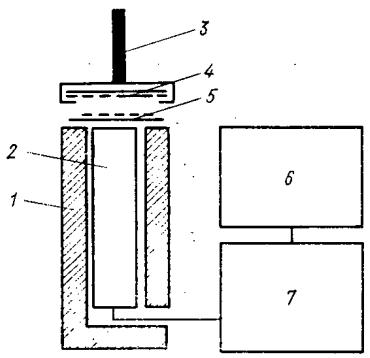

Fig. 1

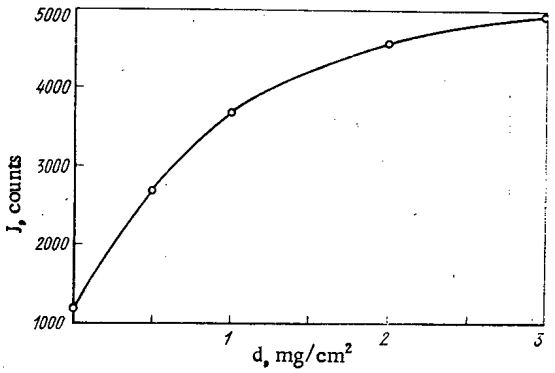

Fig. 2

Fig. 1. Block diagram of equipment for measurement of beryllium coatings: 1) lead housing; 2) γ-ray detector; 3) source holders; 4) α source; 5) beryllium-coated material; 6) counting equipment; 7) amplifier-discriminator.

Fig. 2. Dependence of secondary γ radiation from the ^{9}Be(α, n, γ)^{12}C reaction on thickness of beryllium coating.

Translated from Atomnaya Énergiya, Vol. 42, No. 4, pp. 307-308, April, 1977. Original article submitted January 7, 1976.

TABLE 1. Accuracy of Coating-Thickness Measurements

Range of measurement, mg/cm²	Rms error,* mg/cm²	Range of measurement, mg/cm²	Rms error,* mg/cm²
0,03—0,5	0,01	1,0—2,0	0,10
0,5—1,0	0,02	2,0—3,0	0,20

*Calculated from the expression $\sigma = \sqrt{J}/(\Delta J/\Delta d)$, where J is counts and $\Delta J/\Delta d$ is measurement sensitivity.

Figure 2 shows the dependence of γ-ray counts from the secondary radiation of the $^{9}Be(\alpha, n, \gamma)^{12}C$ reaction on the thickness of the beryllium coating. The measurements were made on beryllium-coated Lavsan films.

A measurement time of 10 min was chosen with a source activity of 1.5 mCi. The accuracy of coating-thickness measurements is shown in Table 1.

LITERATURE CITED

1. S. V. Rumyantsev et al., X- and γ-Ray Flaw Detection [in Russian], Atomizdat, Moscow (1969), pp. 224-247.
2. R. I. Plotnikov et al., Fluorescence X-Ray Radiometric Analysis [in Russian], Atomizdat, Moscow (1973), p. 217.
3. É. Segre, Experimental Nuclear Physics, Wiley (1959).
4. I. P. Plaksin et al., At. Energ., 13, No. 4, 374 (1962).

MINIATURE FISSION CHAMBERS FOR INVESTIGATION OF NEUTRON FIELDS

V. V. Bol'shakov

UDC 621.039.516.4:621.039.512.45

Commercially produced fission chambers cannot be used in the study of neutron fields in critical assemblies which simulate research reactors such as VVR-M, IRT, etc. since the dimensions of the chambers are greater than the gaps between fuel element tubes and individual fuel-element assemblies. Saturation with structural elements leads to perturbation of the neutron fields at points of measurement. The traditional cylindrical form of the sensitive element of a chamber does not permit resolution of details in the neutron flux distribution pattern since integration of neutron flux occurs over the volume occupied by the cylindrical radiator of the detector.

The fission chambers developed (Fig. 1) were made up in the form of miniature cylinders of nickel or stainless steel 1.7 × 0.1 mm (Fig. 1a) and 4.5 × 0.2 mm (Fig. 1b) in diameter. The converters were made of ^{235}U, ^{233}U, ^{239}Pu, ^{237}Np, ^{10}B, and ^{6}Li. Coatings were deposited on an aluminum backing by brazing and electrodeposition. The chambers were filled by the method described in [1, 2]. Chambers 4.5 mm in diameter were supplied with removable cadmium shields. The electrical capacity of a chamber was ~5 pF. Signals with amplitudes from tens to hundreds of microvolts were fed to an amplifier over an RK-75-1.5-11 cable 2.5 m long. The amplifier was located in the tank for the critical assembly.

The instrumental energy spectrum of fission fragments from the fission chambers was recorded on the Didad analyzer. The counting characteristics of the chambers show a plateau starting at an electrode voltage

Translated from Atomnaya Énergiya, Vol. 42, No. 4, pp. 308-309, April, 1977. Original article submitted January 27, 1976.

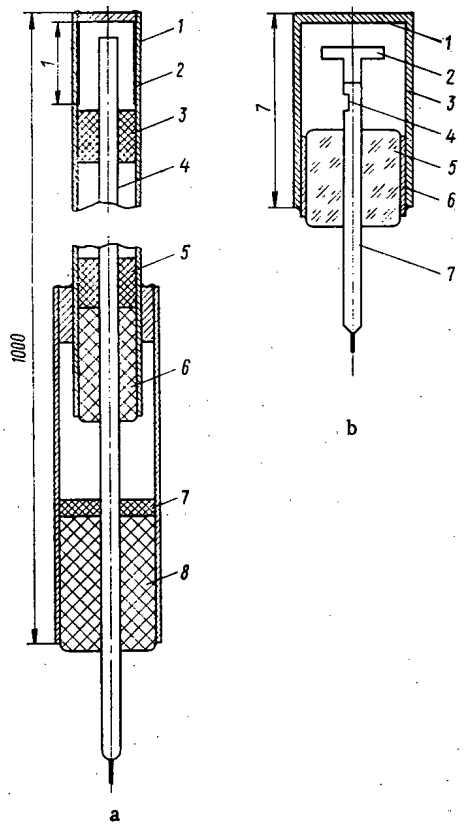

Fig. 1. Fission chambers: a – 1) housing; 2) radiator, fissile material; 3, 5, 7) insulators, Teflon; 4) anode, evacuation tube, nickel; 6, 8) insulators, epoxy resin; b – 1) radiator, fissile material; 2) anode, brass; 3) housing, stainless steel; 4) opening for evacuation and filling; 5) insulator, glass; 6) sleeve, Kovar; 7) tube for evacuation and filling, Kovar.

of 100 V (Fig. 2). The sensitivity of fission chambers with ^{235}U converters (1 mg/cm^2) for thermal neutrons was $\sim 10^{-4}$ counts · cm^2/neutron and varied with the use of converters of corresponding thickness.

For measurements in regions of a critical assembly with significantly differing neutron flux densities, chambers were used with radiator thicknesses of 0.05, 0.5, 1.0, and 2.0 mg/cm^2, which made it possible to avoid over-loading of amplification channels. The assembly was activated insignificantly during a measurement and no difficulties arose in subsequent operations with the fuel elements. Thin-walled tubes acted as guides for the chambers. A mechanical system for synchronous displacement provided simultaneous use of more than ten chambers. The chambers 4.5 mm in diameter can be used at temperatures up to 300°C and those 1.7 mm in diameter at room temperature. Information from PP9-2M counting equipment was extracted by the use of an electronic switch on a BZ-15 digital printer.

The fission chambers underwent lengthy testing in the horizontal beam of the VVR-MAN SSSR reactor at a neutron flux density of 10^7–10^8 neutrons/cm^2·sec. The chamber parameters did not change after continuous operation for several weeks. Neutron distribution in structural gaps between individual fuel elements can be measured with the chamber having a diameter of 1.7 mm.

The sensitive volume of a chamber is bounded by the radiator surface. This volume is negligibly small for a chamber 4.5 mm in diameter and there is practically no distortion during measurement of neutron fields

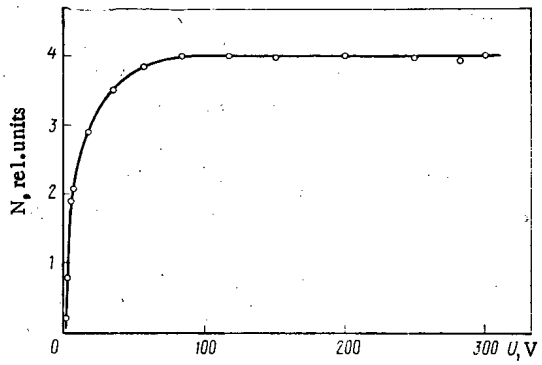

Fig. 2. Counting rate as a function of chamber voltage.

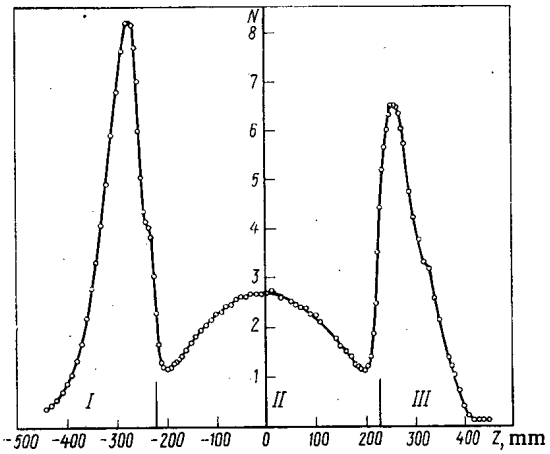

Fig. 3. Distribution of ^{235}U fission rate over height of a critical assembly obtained with a fission chamber 1.7 mm in diameter ($N \cdot 10^{13}$ is the number of counts): I, III) reflector; II) core.

over the height of an assembly. The chambers, which are 1.7 mm in diameter, have a sensitive volume defined by a cylinder 1 mm high and 1.3 mm in diameter and make it possible to obtain practically undistorted neutron distributions in regions of a critical assembly with maximum neutron flux density gradients (Fig. 3).

The distribution of the ^{235}U fission rate corresponds within a constant factor to the distribution of energy release and of neutron flux density in that part of the core volume within which fuel concentration and neutron spectrum are constant. In core regions where the neutron spectrum varies (e.g., the core region adjacent to a reflector or a water trap), the distribution of the ^{235}U fission rate does not correspond to the distribution of energy release or neutron flux since a blocking effect is observed at the fuel elements and the chamber radiators, made of an insignificantly thick layer of uranium, are practically transparent to the neutrons.

The error in measurements with the chambers is 2-5% and is determined by the statistical counting error, the inaccuracy of chamber position, and additional systematic errors.

The author is deeply grateful to K. A. Koneplev, R. G. Pikulik, A. N. Erykalov, E. K. Malyshev, I. A. Reformat-skaya, Yu. P. Konavalov, A. N. Dolinin, A. V. Romanov, and B. M. Aleksandrov for assistance.

LITERATURE CITED

1. A. B. Dmitriev, E. K. Malyshev, and I. A. Reformat-skaya, Prib. Tekh. Eksp., No. 4, 55 (1968).
2. W. Abson, P. Salmon, and S. Pyrah, in: Proceedings of the IEE Symposium on Design, Performance, and Use of Fission Counters, Paper N 2546M (1958).

DETECTION EFFICIENCY OF Si(Li) DETECTORS FOR 0.05-1.25-MeV γ RAYS

V. A. Kozhemyakin and G. I. Shul'govich

UDC 539.1.074

Interest has arisen recently in the use of Si(Li) detectors for γ-ray dosimetry and radiometry. Pulse-height discrimination is used for operation in the most sensitive pulsed mode in order to eliminate counts resulting from detector and preamplifier noise. The presence of a discrimination threshold has a significant effect on detection efficiency – one of the most important detector parameters. In a number of cases the evaluation of this effect brings undoubted advantage by eliminating experimental checks of considerable volume and complexity. Methods were proposed for calculation of the detection efficiency of silicon p – i – n detectors [1, 3]. However, they were not applicable in those cases where the energy of Compton electrons and photoelectrons were less than, or commensurate with, the energy equivalent of the discrimination threshold. This deficiency can be eliminated if one takes into account the broadening of line shape because of noise in the detection system.

Detection efficiency is the ratio between the number of recorded γ rays and the number of incident γ rays:

$$\varepsilon = N_{\text{rec}}/N_{\text{inc}} = N_{\text{rec}}/N_0 S, \tag{1}$$

where N_0 is the γ-ray flux and S is the area of the sensitive surface of the detector.

The number of recorded γ rays (counts) can be calculated if one knows the number of secondary Compton electrons and photoelectrons, N_e^c and N_e^p, which are produced in the interaction of γ ratiation with the material in the sensitive volume of the detector. Although the Compton process is predominant in silicon, it is impossible to neglect the photoeffect in the low-energy region. Clear evidence of this is the instrumental spectra obtained with p – i – n silicon detectors having a sensitive region of thickness W = 1.4 mm and an area of 0.8 mm^2 from various γ-ray sources (Fig. 1). In a volume element dv = dxdS of the detector, a parallel beam of γ rays at the depth x forms $N_0 \exp\left(-\sum_i \mu_i l_i\right) \exp\left(-\mu x\right) n_e \sigma\left(E_\gamma\right) dSdx$ Compton electrons where $_e\sigma(E_\gamma)$ is the effective

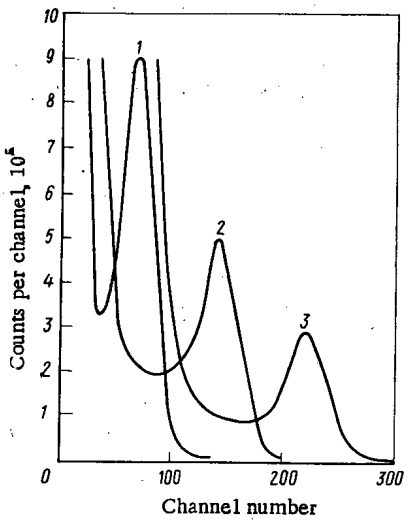

Fig. 1. Instrumental spectra obtained with Si(Li) detector for γ radiation from ^{241}Am (1), ^{57}Co (2), and ^{141}Ce (3) at energies E = 59, 122, and 145 keV, respectively.

Translated from Atomnaya Énergiya, Vol. 42, No. 4, pp. 309-311, April, 1977. Original article submitted April 1, 1976.

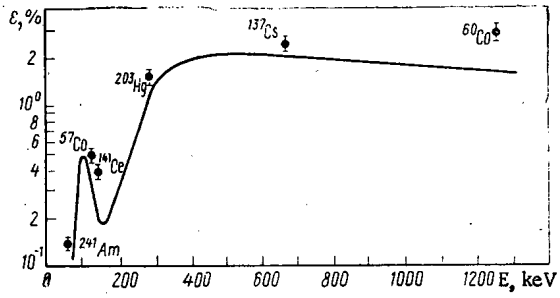

Fig. 2. Dependence of detection efficiency on γ-ray energy: ———) calculation; ●) experiment.

Compton interaction cross section per electron; $n = \rho N_A (Z/A)$ is the number of electrons per unit volume of the detector; ρ is the density of the detector material; N_A is Avogadro's number; Z is atomic number; A is atomic mass; μ and μ_i are the γ-ray linear attenuation coefficients for the material in the sensitive volume and for the i-th structural element of thickness l_i in the housing of the detector; E_γ is the quantum energy.

The number of Compton electrons in the energy interval from E to E + dE can be defined as

$$N_0 \exp\left(-\sum_i \mu_i l_i\right) \exp(-\mu x)\, n\, (d_e\sigma/dE)\, dS\, dx,$$

where $d_e\sigma/dE$ is the differential cross section per energy interval which shifts an electron from E to E + dE.

According to [4],

$$\frac{d_e\sigma}{dE} = \frac{\pi r_0^2}{\alpha^2 m_0 c^2}\left\{2 + \left(\frac{E}{E_\gamma - E}\right)^2 \left[\frac{1}{\alpha^2} + \frac{E_\gamma - E}{E_\gamma} - \frac{2}{\alpha}\left(\frac{E_\gamma - E}{E}\right)\right]\right\},$$

where r_0 is the classical radius of the electron and α is the quantum energy in m_0c^2 units.

Assuming that the electrons lose their energy completely in the sensitive region, the number of counts caused by the Compton effect can be defined as

$$dN_c^C = N_0 \exp\left(-\sum_i \mu_i l_i\right) \exp(-\mu x)\, n\, (d_e\sigma/dE)\, \Phi(E, E_t, E_n)\, dS\, dx. \quad (2)$$

In Eq. (2), the function $\Phi(E, E_t, E_n)$ is a pulse-detection probability which is a function of the electron energy E, of the energy equivalent E_n of the noise in the detector – preamplifier system, and of the discrimination threshold E_t and which is defined as

$$\Phi(E, E_t, E_n) = \frac{1}{\sqrt{2\pi}} \int_{-\infty}^{2.35(E-E_t)/E_n} \exp(-u^2/2)\, du.$$

Integrating Eq. (2) with respect to x, S, and E, we obtain an expression for the number of counts produced by the Compton effect:

$$N_c^C = N_0 S\,[1 - \exp(-\mu W)] \exp\left(-\sum_i \mu_i l_i\right) \frac{1}{\mu} n \int_0^{E_{max}} \frac{d_e\sigma}{dE} \Phi(E, E_t, E_n)\, dE, \quad (3)$$

where $E_{max} = E_\gamma[2\alpha/(1 + 2\alpha)]$ is the maximum energy of the Compton electrons.

In similar fashion, we obtain an expression for the number of counts produced by the photoeffect:

$$N_c^p = N_0 S\,[1 - \exp(-\mu W)] \exp\left(-\sum_i \mu_i l_i\right) (1/\mu)\, \tau \Phi(E_p, E_t, E_n), \quad (4)$$

where τ is the linear attenuation coefficient for the photoeffect in the detector material; E_p is the energy of the photoelectron. The total number of γ-ray counts is $N_c^C + N_c^p$. Then with Eqs. (1), (3), and (4) taken into consideration, the expression for calculation of detection efficiency takes the following form

$$\varepsilon = [1 - \exp(-\mu W)] \exp\left(-\sum_i \mu_i l_i\right) \frac{1}{\mu}\left[\tau \Phi(E_p, E_t, E_n) + n \int_0^{E_{max}} \frac{d_e\sigma}{dE} \Phi(E, E_t, E_n)\, dE\right]. \quad (5)$$

Computed results for $\varepsilon(E_\gamma)$ in the γ-ray range 0.05-1.25 meV, where E_t = 90 keV and E_n = 30 keV, and W = 1.4 mm, are shown graphically in Fig. 2. Shown there for comparison are experimentally obtained values of detection efficiency for a DKD-G-1 commercial detector of domestic manufacture having the same values of

W, E_n, and E_t. The measuring system included a charged-sensitive preamplifier with an intrinsic noise level of ~2 keV, a linear amplifier and integral discriminator of an LP-4840 multichannel pulse-height analyzer, and a ChZ-32 electronic computing frequency meter. The discrimination threshold was set with an error of no more than ±5% in accordance with data from an energy calibration performed in the spectrometer mode (see Fig. 1). The activities of the γ-ray sources were known to be better than ±7%. As follows from Fig. 2, satisfactory agreement is observed between experimental and theoretical data. The existing discrepancy is of a systematic nature and may result from the fact that the computational equation (5) does not include the contribution from secondary electrons reaching the sensitive region from the "dead layer."

LITERATURE CITED

1. M. L. Gol'din, K. R. Pater-Razumovskii, and F. V. Virnik, At. Energ., 34, 121 (1973).
2. S. N. Vasil'ev and M. I. Chistakov, in: Nuclear Instrument Construction [in Russian], No. XIII, Tr. SNIIP, Atomizdat, Moscow (1970), p. 3.
3. A. A. Petushkov and V. A. Manchuk, Med. Radiologiya, 71, 52 (1971).
4. K. Siegbahn (editor), Alpha-, Beta-, and Gamma-Spectroscopy [Russian translation], Atomizdat, Moscow (1969).

USE OF 11-MeV PROTONS FOR ACTIVATION ANALYSIS

B. V. Zatolokin, I. O. Konstantinov, and N. N. Krasnov

UDC 539.171.12

In the irradiation of elements with $Z \geq 20$ by protons with energies $E_p \leq 11$ MeV, the (p, n) reaction has the largest cross section (hundreds of millibarns), the value for the (p, γ) reaction cross section is of the order of a millibarn [1], the cross section for the (p, α) reaction is small because of the Coulomb barrier for emerging particles [2, 3], and the (p, 2n) and (p, pn) reactions have high energy thresholds for most nuclei. The relatively simple pattern of activation of elements with $Z \geq 20$ explains to a considerable degree the interest evidences in recent years by many investigators in the use of protons with energies ≤11 MeV for analytic purposes.

Methods have been described for the determination of Ti [4-7], V [7, 8], Fe [9], Zn [7], Zr [10, 11], and Nb [12]. One paper [13] was devoted to the determination of the contaminants B, N, Na, Cr, Se, Br, and Cd in water. The possibilities of determining 50 elements from their activation by 10-MeV protons were discussed in [14-18]. Depending on experimental conditions, the limits of impurity detection in these papers were 10^{-4}-10^{-7}%, which is completely sufficient for the solution of many practical problems.

In order to calculate impurity concentration by an absolute method and to evaluate the limit of detection for a given impurity in activation analysis with charged particles, it is well known that it is necessary to know the thick-target yield of a radioisotope [19, 20], which for protons with an initial energy of 11 MeV is determined from the expression

$$Y = 6.25\lambda n \int_{11}^{0} \frac{\sigma(E)}{dE/d(\rho x)} dE, \quad (1)$$

where Y is the yield of the radioisotope, disintegrations/sec·μA·h; λ is the decay constant for the radioisotope, h^{-1}; n is the atomic concentration of a given isotope, atoms/g; σ(E) is the cross section for the nuclear reaction, cm^2; $dE/d(\rho x)$ is the stopping power of the element, MeV/g·cm^2.

For a target consisting of a natural mixture of stable isotopes, the yield depends only on the initial energy of the protons. Since the energy of charged particles is measured rather simply and accurately,

Translated from Atomnaya Énergiya, Vol. 42, No. 4, pp. 311-314, April, 1977. Original article submitted April 16, 1976.

TABLE 1. Radioisotopic Yields for Irradiation of Thick Targets of Natural Isotopic Composition by Protons with Energies of 8-11 MeV, disintegrations/sec·μA·h

Element	Radioisotope	E_p, MeV							K
		8,0	8,5	9,0	9,5	10,0	10,5	11,0	
Ca	^{44}Sc	0,9	1,1	1,2	1,4	1,5	1,7	1,8	7
Ca	^{44m}Sc	0,3	0,4	0,5	0,6	0,7	0,9	1,0	5
Ca	^{48}Sc	2,0	2,1	2,3	2,4	2,6	2,7	2,9	5
Sc	^{45}Ti	3,4	4,1	4,8	5,7	6,7	7,8	9,3	8
Ti	^{48}V	1,6	2,1	2,8	3,5	4,3	5,1	6,0	6
V	^{51}Cr	3,4	4,2	5,0	6,0	7,0	7,9	8,8	6
Cr	^{52}Mn	0,37	0,64	0,92	1,3	1,8	2,3	2,9	6
Cr	^{54}Mn	2,6	3,3	4,1	2,8	5,6	6,1	6,6	3
Fe	^{56}Co	0,37	0,92	1,3	2,2	2,8	3,7	4,4	5
Cu	^{65}Zn	0,92	1,1	1,3	1,6	1,9	2,2	2,5	5
Zn	^{66}Ga	1,1	1,9	3,0	4,0	5,3	6,5	8,1	7
Ga	^{69}Ge	1,6	2,0	2,3	2,7	3,2	3,8	4,5	7
Ge	^{72}As	0,6	1,0	1,3	1,6	2,0	2,7	4,0	7
Ge	^{74}As	0,6	0,7	1,0	1,2	1,6	2,2	2,9	6
Rb	^{85}Sr	0,5	0,6	0,8	0,9	1,0	1,2	1,4	6
Rb	^{85m}Sr	1,8	2,3	2,8	3,3	3,8	4,3	5,0	8
Rb	^{87m}Sr	0,5	0,6	0,7	0,8	0,9	1,0	1,2	8
Sr	^{86}Y	1,5	2,5	3,5	4,5	6,0	7,5	9,5	6
Y	^{89}Zr	0,7	0,9	1,2	1,4	1,8	2,4	3,2	7
Nb	^{93m}Mo	0,5	0,9	1,7	2,7	3,8	5,3	7,2	6
Mo	^{95m}Tc	0,9	1,2	1,5	1,9	2,3	2,8	3,8	4
Mo	^{96}Tc	0,6	0,8	1,0	1,3	1,6	1,9	2,3	6
Cd	^{111}In	0,9	1,3	1,7	2,2	2,9	3,5	4,4	6
Sn	^{117}Sb	1,3	1,7	2,3	3,1	3,9	4,9	6,2	7
Sn	^{181m_1}Sb	0,3	0,4	0,85	1,3	1,9	2,8	4,1	7
Sn	^{120B}Sb	0,11	0,19	0,32	0,48	0,74	1,0	1,5	5
Sn	^{122}Sb	0,27	0,41	0,55	0,7	0,89	1,1	1,2	6
Sn	^{124}Sb	1,5	2,1	2,8	3,5	4,2	5,0	5,6	4
Sb	^{121}Te	2,6	3,1	4,0	5,1	6,5	8,1	9,9	5
Sb	^{121m}Te	1,4	1,8	2,5	3,4	4,5	5,9	7,6	4
Sb	^{123m}Te	0,29	0,38	0,52	0,66	0,82	1,0	1,2	5
Cs	^{133m}Ba	1,4	2,2	3,1	4,3	5,8	7,5	9,9	6
W	^{182m}Re	0,45	0,75	1,3	2,2	3,4	4,9	7,4	6
W	^{183}Re	0,25	0,45	0,65	1,0	1,8	3,0	4,8	4
W	^{184}Re	0,95	1,7	2,8	4,3	5,8	7,4	8,8	4
Pb	^{206}Bi	0,35	0,55	0,8	1,2	1,8	2,7	3,6	5

radioisotopic yield values obtained in preliminary experiments can be used subsequently in the performance of multielement activation analysis.

In this paper, experimentally determined yields are presented for 36 radioisotopes formed by the irradiation of 21 elements with protons having energies of 8-11 MeV.

Analysis of the dependence of the (p, n)-reaction yield on atomic number of the target nucleus made it possible to determine, for example, matrices for instrumental activation analysis of an iron impurity, which is an often encountered impurity in pure metals used as target materials for the production of radioisotopes in a cyclotron.

Sample irradiation was performed in the extracted beam of the 150-cm cyclotron at FEI (Obninsk). The proton energy was measured with a silicon surface-barrier detector and the current with a microammeter. Aluminum absorbers were used to change the proton energy; the energy loss in the absorbers was calculated from the data in [21].

The activity of the irradiated samples was measured on a scintillation γ spectrometer with a NaI(Tl) crystal 70 mm in diameter and 70 mm high and on a semiconductor spectrometer with a Ge(Li) detector 22 cm^3 in volume. The spectrometers were calibrated for efficiency by means of standard sources from a set of standard spectrometric gamma sources.

Calculation of radioisotopic yield was based on the formula

$$Y = \lambda B / I\,[1 - \exp(-\lambda t)], \qquad (2)$$

where B is the activity of the radioisotope at the end of irradiation, disintegrations/sec; I is the irradiation current, μA; t is the irradiation time, h.

In the calculation of activity, the decay characteristics of the radioisotopes were taken from [22].

Table 1 shows the results of radioisotopic yield measurements. The error of the absolute value is ±15%. Linear interpolation can be used for a variation in proton energy within the limit of 0.5 MeV. The radioisotopic yield values at 11 MeV agree within the limits of experimental error with yield values obtained by integration of the excitation functions for the appropriate (p, n) nuclear reactions: ^{45}Sc(p, n)^{45}Ti [23, 24]; ^{48}Ti(p, n)^{48}V [25]; ^{51}V(p, n)^{51}Cr [26, 27, 23]; ^{52}Cr(p, n)^{52}Mn [26]; ^{56}Fe(p, n)^{56}Co [28, 29]; ^{65}Cu(p, n)^{65}Zn [26, 30]; ^{89}Y(p, n)^{89}Zr [31, 32]; ^{111}Cd(p, n)^{111}In [26]; ^{115}Sn(p, n)^{115}Sb [33].

The resultant values of radioisotopic yields for thick targets were used for qualitative analysis of the dependence of the (p, n)-reaction yield on the atomic number of the target nucleus. For this purpose, we transform Eq. (1) to the following form:

$$Y = \lambda K J(A, Z), \tag{3}$$

where K is the isotopic abundance; $J(A, Z) = 3.8 \cdot 10^{36} \frac{1}{M} \int_{11}^{0} \frac{\sigma(E)\,dE}{dE/d(\rho x)}$ is the yield of radioactive atoms per microcoulomb of incident protons normalized to an abundance K = 1 (M is the atomic mass of the element). It is obvious that the yield L(A, Z) of the (p, n) reaction is the sum of the yields of radioactive atoms in ground and isomeric states formed as the result of the (p, n) reaction:

$$L(A, Z) = \Sigma J(A, Z). \tag{4}$$

The yields L(A, Z) for the (p, n) reaction for thick targets and protons with an initial energy of 11 MeV were calculated from Eqs. (3) and (4) using experimental values of Y. The following published data on (p, n) reaction cross sections were also used: ^{52}Cr(p, n)^{52m}Mn [26]; ^{63}Cu(p, n)^{63}Zn [26]; ^{119}Sn(p, n)^{119}Sb [33]; ^{140}Ce(p, n)^{140}Pr [37]; ^{160}Gd(p, n)^{160}Tb [32]; ^{197}Au(p, n)^{197}Hg [38]; ^{209}Bi(p, n)^{209}Po [2]; ^{60}Ni(p, n)^{60}Cu [34]; ^{68}Zn(p, n)^{68}Ga [34]; ^{133}Cs(p, n)^{133}Ba [35]; ^{142}Ce(p, n)^{142}Pr [37]; ^{181}Ta(p, n)^{181}W [38]; ^{197}Au(p, n)^{197m}Hg [38]; ^{112}Cd(p, n)^{112,112m}In [36].

Figure 1 shows values of the yield L(A, Z) for the (p, n) reaction as a function of the atomic number of the target nucleus. We point out the following features of this dependence:

1) a significant decrease in yield (by a factor of 10-15) with increase in atomic number from 40 to 200 which results from the decrease in the cross section σ(E) for the (p, n) reaction because of the increase in the Coulomb barrier with increasing Z and also from the decrease in the atom concentration n;

2) the change in yield follows the same law as the mean neutron excess (N − Z)/A. Note that the same behavior was observed for neutron yields from thick targets bombarded with protons at 18 and 32 MeV [39];

3) a sharp drop in yield is observed in comparison with neighboring isotopes at the isotopes $^{54}_{24}$Cr, $^{56}_{26}$Fe, and $^{142}_{58}$Ce in which the number of neutrons exceeds the magic numbers of 28 and 82 by two neutrons, respectively;

4) the yield for the isotopes $^{60}_{28}$Ni, in which the number of protons is equal to the magic number 28, is also less than that of neighboring isotopes with the exception of isotopes with N = 28 + 2.

Equations (3), (4), and Fig. 1 make it possible to evaluate the upper limit of radioisotopic yield for irradiation of a thick target with 11-MeV protons and, based on this evaluation, to determine the matrices in which an instrumental method for the determination of one or another impurity is possible. For example, one of the widespread technical impurities in pure metals used as target material for production of radioisotopes in a cyclotron is iron, which can be determined instrumentally from the radioisotope ^{56}Co in the following matrices: Be, B, C, O, F, Na, Mg, Al, Si, P, S, Cl, Ar, K, Ca, Sc, Mn, Co, Ni, Ga, Se, Br, Y, Nb, Rh, Ag, Ba, Ce, Pr, Tl, Dy, Ho, Hf, Ta, Ir, Au, Tl, Bi.

The yield of radioactive atoms per microcoulomb as a function of atomic number (see Fig. 1) is practically equal to the neutron yield from a thick monoisotopic target irradiated by 11-MeV protons since the (p, n) reaction is the dominant reaction. These values for the neutron yields can be used to evaluate matrix activation by secondary neutrons by taking into account their energy spectrum and angular distribution [40].

Activation analysis using protons with energies $E_p \leq 11$ MeV by an absolute method requires a knowledge of radioisotopic yields for thick targets. Knowledge of the yields makes it possible to plan an experiment in optimal fashion, to determine impurity concentration, to estimate its limit of detection and the necessary

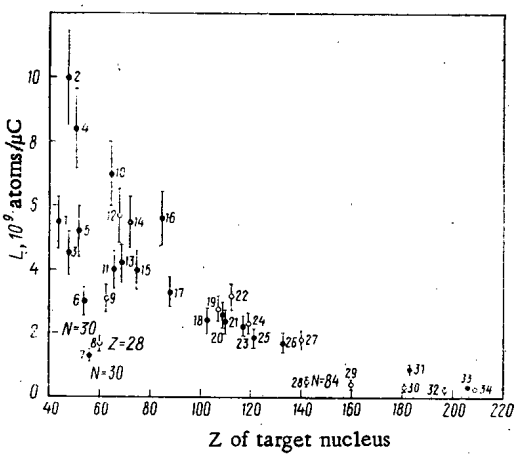

Fig. 1. Yields L(A, Z) of the (p,n) reaction for 11-MeV protons: ●) this work; ○) data of others; irradiated isotopes: 1) ^{44}Ca; 2) ^{48}Ca; 3) ^{48}Ti; 4) ^{51}Y; 5) ^{52}Cr; 6) ^{54}Cr; 7) ^{56}Fe; 8) ^{60}Ni; 9) ^{63}Cu; 10) ^{65}Cu; 11) ^{66}Zn; 12) ^{68}Zn; 13) ^{69}Ga; 14) ^{72}Ge; 15) ^{75}As; 16) ^{85}Rb; 17) ^{88}Sr; 18) ^{103}Rh; 19) ^{107}Ag; 20) ^{109}Ag; 21) ^{110}Cd; 22) ^{112}Cd; 23) ^{117}Sn; 24) ^{119}Sn; 25) ^{121}Sb; 26) ^{133}Cs; 27) ^{140}Ce; 28) ^{142}Ce; 29) ^{160}Gd; 30) ^{181}Ta; 31) ^{183}W; 32) ^{197}Au; 33) ^{206}Pb; 34) ^{209}Bi.

decontamination factor for interfering radioisotopes when doing radiochemistry. Further measurements of radioisotopic yields will make it possible to construct a complete system of constants for proton activation analysis.

LITERATURE CITED

1. B. Cohen, Phys. Rev., 100, 206 (1955).
2. C. Andre et al., Phys. Rev., 101, 645 (1956).
3. M. Furukawa, Nucl. Phys., 77, 565 (1966).
4. E. Schweikert and P. Albert, C. R., Ser. C, 262, 87 (1966).
5. B. S. Mazitov and S. Mukhammedov, in: Activation Analysis [in Russian], Fan, Tashkent (1971), p. 212.
6. L. Zelst, J. Radioanal. Chem., 12, 129 (1972).
7. N. Krasnov et al., J. Radioanal. Chem., 16, 395 (1973).
8. J. Debrun, J. Barrandon, and P. Albert, in: Uses of Cyclotrons in Chemistry, Metallurgy, and Biology, Butterworths, London (1970), p. 354.
9. E. Schweikert and P. Albert, C. R., Ser. C, 262, 342 (1966).
10. D. Riddle and E. Schweikert, Anal. Chem., 46, 395 (1974).
11. S. Kormali and E. Schweikert, J. Radioanal. Chem., 22, 139 (1974).
12. J. Tomita and H. Saisho, Nature, No. 195, 1189 (1962).
13. S. Bankert, S. Bloom, and G. Santer, Anal. Chem., 45, 692 (1973).
14. J. Debrun and J. Barrandon, J. Radioanal. Chem., 17, 291 (1973).
15. J. Barrandon, J. Debrun, and A. Kohn, J. Radioanal. Chem., 16, 617 (1973).
16. J. Barrandon et al., Anal. Chim. Acta, 73, 39 (1974).
17. J. Debrun et al., Anal. Chem., 47, 637 (1975).
18. P. Benaben, J. Barrandon, and J. Debrun, Anal. Chim. Acta, 78, 129 (1975).
19. N. N. Krasnov, At. Energ., 26, 284 (1969).
20. N. Krasnov, Intern. J. Appl. Rad. Isotopes, 25, 223 (1974).
21. C. Williamson, J. Boujot, and J. Picard, Rap. CEA-R-3042 (1966).
22. W. Bowman and K. Macmurdo, Atomic Data and Nuclear Data Tables, 13, Nos. 2, 3 (1974).
23. G. Dell, W. Ploughe, and H. Hausman, Nucl. Phys., 64, 513 (1965).
24. R. Thomas and W. Bartolini, Nucl. Phys., A106, 323 (1968).
25. S. Tanaka, Atomic Energy Soc. Jpn., 1, 171 (1959).
26. J. Wing and J. Huizenga, Phys. Rev., 128, 280 (1962).
27. G. Chodil et al., Nucl. Phys., A93, 648 (1967).

28. S. Tanaka and M. Furukawa, J. Phys. Soc. Jpn., 14, 1269 (1959).
29. I. Jenkins and A. Walin, Nucl. Chem., 32, 1419 (1970).
30. R. Colle et al., Phys. Rev., C9, 1819 (1974).
31. G. Saha and N. Portile, Phys. Rev., 144, 962 (1966).
32. C. Birattari, Nucl. Phys., A201, 579 (1973).
33. E. A. Skakun et al., Izv. Akad. Nauk SSSR, Ser. Fiz., 34, 2174 (1970).
34. V. A. Muminov et al., in: Nuclear-Physics Methods of Analysis [in Russian], Fan, Tashkent (1974), p. 50.
35. P. P. Dmitriev, G. A. Molin, and M. V. Panarin, At. Energ., 35, 61 (1973).
36. K. Otozai et al., Nucl. Phys., 80, 335 (1966).
37. M. Furukawa, Nucl. Phys., A90, 253 (1967).
38. L. Hansen et al., Nucl. Phys., 30, 389 (1962).
39. Yuin-Kwei Tai et al., Phys. Rev., 109, 2086 (1958).
40. V. K. Daruga et al., Preprint FÉI-225, Obninsk (1970).

FAST-NEUTRON RADIATIVE CAPTURE CROSS SECTION FOR ^{242}Pu

A. A. Druzhinin, V. K. Grigor'ev,
A. A. Lbov, S. P. Vesnovskii,
N. G. Krylov, and V. N. Polynov

UDC 539.125.5.17

In the construction of fast reactors it is important to know the energy dependence of the cross section for radiative capture of neutrons by heavy isotopes of plutonium, particularly ^{242}Pu. Published data for such cross sections in the neutron energy region around 1 MeV are extremely unsatisfactory and are mainly limited to estimates and calculations. This situation was mainly caused by the lack of sufficient amounts of enriched isotopes and of appropriate sources of monoenergetic neutrons needed for differential measurements. In view of that, this paper gives the results of activation measurements of the neutron radiative capture cross section of ^{242}Pu nuclei for a spectrum similar to the fission neutron spectrum.

Plutonium enriched in ^{242}Pu to 99.7 mass % was used as the initial material. The plutonium solution was placed in a quartz container and evaporated to dryness following which the container was sealed with a quartz lid and covered with a layer of cadmium 1 mm thick. The amount of plutonium in each container was 50-100 μg.

The prepared samples were irradiated at the center of a fast pulsed reactor with a neutron spectrum characterized by the following energy distribution: 0-0.1 MeV, 3.0%; 0.1-0.4 MeV, 20.1%; 0.4-0.9 MeV, 26.9%; 0.9-1.4 MeV, 15.0%; 1.4-3.0 MeV, 23.8%; above 3.0 MeV, 11.2%. Neutron fluence at the sample position was $\sim 3 \cdot 10^{14}$ neutrons/cm^2 and was measured with "long" counters previously calibrated against a fission chamber. In each irradiation, the neutron flux was additionally determined from activation of gold foils placed with the plutonium samples. The effective activation cross section of the gold for this neutron spectrum was 150 ± 15 mb.

The irradiated plutonium samples underwent radiochemical analysis. The plutonium was leached from the quartz container with nitric acid. The solution was passed through a 1 × 8 Dowex resin in nitric acid form. The plutonium was desorbed from the column with 0.5 M HCl. Finally, the plutonium was purified on a 1 × 8 Dowex resin in thiocyanate form. The plutonium in the form of a thiocyanate complex was adsorbed on an anionite. The column was subsequently washed with a weakly acid solution of 1 M ammonium thiocyanate and a small amount of water; the plutonium was then desorbed with 0.3 M HCl. For removal of the small amount of thiocyanate ions, the eluate was passed through a column filled with 1 × 8 Dowex resin in chloride form. After the column, the solution was collected on a platinum backing and dried. The resultant target was not

Translated from Atomnaya Énergiya, Vol. 42, No. 4, pp. 314-315, April, 1977. Original article submitted April 20, 1976.

TABLE 1. Basic Experimental Results

Irradiation No.	Sample No.	Fluence, neutrons/cm^2	Amount of ^{242}Pu on target, atoms	Amount of ^{243}Pu on target, atoms	Measured cross section, mb	Average cross section, mb
I	1	$3,4\cdot10^{14}$	$2,91\cdot10^{16}$	$1,44\cdot10^{6}$	146	140 ± 17
II	2	$4,0\cdot10^{14}$	$5,63\cdot10^{16}$	$3,36\cdot10^{6}$	149	
	3	$4,0\cdot10^{14}$	$5,66\cdot10^{16}$	$3,28\cdot10^{6}$	145	
III	4	$3,0\cdot10^{14}$	$11,93\cdot10^{16}$	$4,5\cdot10^{6}$	126	
	5	$3,0\cdot10^{14}$	$10,11\cdot10^{16}$	$3,6\cdot10^{6}$	125	

measured. Such a technique provided a plutonium decontamination factor of $\sim10^6$ for fission products and of $\sim10^4$ for americium, and a chemical yield of plutonium of $\sim30\%$. Separation time was about 5 h. The irradiated gold foils were dissolved in aqua regia.

As a result of radiative capture of neutrons by ^{242}Pu nuclei, short-lived ^{243}Pu is formed which decays to the long-lived ^{243}Am by β decay with a half-life of 4.958 ± 0.005 h [1]. A β counter with a scintillating plastic (53×1 mm) was used to measure the absolute activity of ^{243}Pu as was done in [2]. An aluminum filter 30 μ thick was used to eliminate α-particle counts from the plutonium. The effect of low-energy x and γ radiation from the plutonium was reduced by selection of an appropriate discrimination level in the single-channel pulse-height analyzer. Calibration of the β counter for the selected measurement geometry was performed in the following manner. A sample of the original plutonium was irradiated in a sufficiently high flux of thermal neutrons so that the β activity of the ^{243}Pu formed was far greater than the α activity of the original plutonium. After radiochemical treatment of the irradiated plutonium by the method described above, targets were prepared in parallel for measurements of the absolute β activity of ^{243}Pu in a $4\pi\beta$ flow counter and for measurements with the β scintillation counter. A comparison of the readings of both counters established that the detection efficiency of the β scintillation counter was $20\pm1\%$.

Measurements of the β activity of the irradiated plutonium samples were made continuously with the β scintillation counter over a period of ~50 h after the end of irradiation. Before this period, the counter recorded only a constant background activity which was less than 2% of the sample activity at the beginning of measurement. These data were analyzed by the method of least squares on a Mir-1 computer. In all cases, after subtraction of the constant background component, a component was isolated with the half-life of ~5 h assigned to ^{243}Pu. No components with other half-lives were observed. The measured half-life of the ^{243}Pu was 5.1 ± 0.2 h, which agrees with other data [1]. Identification of ^{243}Pu was also made from the maximum energy of the β spectrum by means of a β scintillation spectrometer with an anthracene crystal. The value obtained (580 ± 10 keV) is in good agreement with the published value (578 ± 10 keV) [1]. After measurement on the scintillation counter, all the plutonium was washed off the platinum target backing with acid and the content of the original ^{242}Pu in the resultant solution determined. For this purpose, α spectrometry and absolute counting of α particles in an ionization chamber with plane electrodes were used. The absolute activity of the irradiated gold foils was determined by $4\pi\beta$ counting.

The results are shown in Table 1. Measurement errors were mainly determined by the uncertainty in the value for the fluence and in the amount of ^{243}Pu on a target.

There is actually no data on the dependence of the cross section for the ^{242}Pu(n, α)^{243}Pu reaction on fast-neutron energy. In a single experimental paper [3], a value of 490 mb is given for this cross section for the spectrum of the fast reactor 4000-1. Conversion of this value to the neutron spectrum used in this work yields ~130 mb, which agrees with the measured value (140 ± 17 mb). A calculated dependence on neutron energy for this reaction cross section is given in [4]. The cross section was calculated from the resonance parameters in the neutron range 1 keV-1 MeV. At higher energies up to 15 MeV, the authors assumed equality of the neutron radiative capture cross sections in ^{242}Pu and ^{238}U. Use of the data in [4] for a neutron spectrum similar to the fission-neutron spectrum leads to a value of ~150 mb, which agrees with the measured value here. Approximately the same value is obtained by using the calculated data in [5].

LITERATURE CITED

1. V. M. Gorbachev, Yu. S. Zamyatnin, and A. A. Lbov, Fundamental Characteristics of Heavy-Element Isotopes [in Russian], Atomizdat, Moscow (1975).
2. N. I. Ivanova et al., At. Energ., 30, 369 (1971).

3. H. Kronberger, in: Proceedings of the IAEA Panel on Use of Plutonium for Power Production, Vienna, Dec. 7-12, 1964, p. 56.
4. S. Yiftah et al., in: Proceedings of the IAEA Symposium on Fast Reactor Physics, Karlsruhe, Oct. 30-Nov. 3, 1967, Vol. I, p. 123.
5. P. Kasten, At. Energy Rev., 8, 473 (1970).

ANALYSIS OF HEAVY ELEMENTS THROUGH THE ABSORPTION JUMP IN AN INTERFERING ELEMENT

M. B. Énker, L. I. Shmonin, G. E. Kolesov, and V. I. Cherevko

UDC 543.422.8:543.52

At the present time, x-ray radiometric methods are being developed and extensively used for the analysis of heavy elements which are based on measurements of the fraction of γ radiation from two monoenergetic radioisotopic sources transmitted through a layer of the sample; the quantum energies of the two are close but are respectively higher and lower than the energy of the absorption jump in the element being determined. This method makes it possible to determine selectively the content of elements of high or medium atomic weight in media of complex composition [1]. However, the condition for the selection of emitter energy is too rigorous in many cases and it is very difficult to choose appropriate γ emitters.

Samples being analyzed can often be represented as a three-component mixture consisting of the element being determined, an interfering (selectively absorbing) element, and a lighter filler with slightly varying effective atomic number. It is then promising to use a method of analysis in which the absorption jump of the interfering element is used. The physical premises of the method consist of the following. If a layer of sample with a surface density m, consisting of two heavy elements with concentrations C_A and C_M, respectively, in a light filler, is alternately exposed to γ-ray fluxes with different energies E_1 and E_2 (or one measures the intensity of sample transmission for radiation in two energy intervals of a "continuous" spectrum), the intensity of the unabsorbed radiation for a "good" geometry measurement is

$$I_1 = I_0 \exp\left[-(\mu_A - \mu_H)_1 C_A - (\mu_M - \mu_H)_1 C_M - (\mu_H)_1\right] m,$$
$$I_2 = I_0 \exp\left[-(\mu_A - \mu_H)_2 C_A - (\mu_M - \mu_H)_2 C_M - (\mu_H)_2\right] m, \quad (1)$$

where μ_A, μ_H, and μ_M are the γ-ray mass attenuation coefficients for the separate components of the mixture; the subscripts 1 and 2 correspond to radiation with the quantum energies E_1 and E_2, respectively.

Considering the nonuniqueness of the dependence of μ on radiation energy in the region of the absorption jump, the energies of the test radiation can be selected so that $(\mu_M - \mu_H)_1 = (\mu_M - \mu_H)_2$.

In that case, the value of the ratio I_1/I_2 becomes

$$\varkappa = \exp\left[C_A(\Delta\mu_A - \Delta\mu_H) + \Delta\mu_H\right] m \quad (2)$$

TABLE 1. γ-Ray Energies for Analysis of Element Content

Energy, keV	Pb	Ba	Sb
E_1/E_2	1,68	2,03	2,3
E_2	50—88,0	20,0—37,4	16,0—30,5
E_1	88—155	37,4—69,0	30,5—58,0

Translated from Atomnaya Énergiya, Vol. 42, No. 4, pp. 315-316, April, 1977. Original article submitted May 31, 1976.

TABLE 2. Dependence of $\varkappa$ on Element Determined and Interfering Element

Element determined													Interfering element		
Pb, %					Ba, %$BaSO_4$					Sb, g/liter			Ba, %$BaSO_4$	Pb, %	Ba, g/liter
0	20	40	60	80	0	20	40	60	80	0	23,4	47,6	0—80	0—80	0—92
1,0	5,62	27,0	98,0	218	1,0	1,95	4,14	3,30	17,4	1,0	3,7	6,3	1±0,1	1±0,1	1±0,1

and does not depend on the concentration of the second impurity heavy element. Here,

$$\Delta\mu_A=(\mu_A)_2-(\mu_A)_1;\quad \Delta\mu_H=(\mu_H)_1-(\mu_H)_2.$$

Assuming that the dominant process in the attenuation of γ radiation near the absorption jump is the photoeffect, and roughly considering $\mu \sim E^{-3}$ (E is the γ-ray energy), one can write for the selection of emitter energies or of energy detection intervals $E_1/E_2 \approx S^{1/3}$, where S is the absorption jump for M.

Then the relative sensitivity $Q_\varkappa = \Delta\varkappa/(\varkappa\Delta C)$ of the determination of the component being analyzed can be evaluated from the expression

$$Q_\varkappa = m\,[(E_1/E_2)^3-1]\,[(\mu_A)_1-(\mu_H)_1]. \qquad (3)$$

Comparing Eq. (3) with the well-known expression for relative sensitivity in the traditional method [2], one can see that the value $Q_\varkappa$ in the proposed method is practically the same since the factor $[(E_1/E_2)^3 - 1]$ is equivalent to $(S - 1)$ but is for the interfering element.

Table 1 shows calculated estimates for the ratios and measurement limits E_1 and E_2 for the selection of γ emitters (energy intervals) for the analysis of lead (barium), antimony (barium), and barium-containing products. The filler was simulated with calcium carbonate.

Products of such composition are difficult to analyze by any of the presently existing radioisotopic methods but are easily analyzed by the proposed method of measurement. The optimal thickness m_0 of a layer is selected in accordance with the minimum statistical measurement error, for example [2].

Experimental studies by the described method were performed on artificial powdered mixtures and solutions containing the specified components in various ratios. The radiation detector used was a scintillation spectrometer employing a sodium iodide crystal (18×10 mm), an FÉU-31 photomultiplier, and a single-channel differential analyzer. Primary radiation sources were ^{241}Am (E = 59.6 keV) and ^{153}Gd (E ≈ 100 keV) for barium analysis in media containing lead, and also ^{241}Am and ^{241}Am with an intermediate iodide target for lead or antimony analysis in mixtures containing barium.

Measurements made in a geometry with highly collimated radiation on heavy-metal ore samples and processing products confirmed the possibility of complete elimination of the effect of the impurity element for a broad range of its concentration. For example, variation of lead content in a sample from 0 to 80% had practically no effect on the value of $\varkappa$, while $\varkappa$ increases as the content of the analyzed element increases (Table 2). In this case, the maximum sensitivity of the determination of the analyzed metal for an instrumental error of no more than 1% in the measurement of $\varkappa$ and with a 0.95 confidence factor for the determination of lead and barium was 0.1 and 0.4%, respectively, in the powdered samples and in the antimony solution (0.2 g/liter).

Thus the analytic method described expands the analytic possibilities of γ-absorption analysis in the determination of elements for which the selection of optimal emitters is practically impossible in the traditional x-ray radiometric absorption method, as in the analysis of lead, for example.

The complete elimination of the effect of an interfering impurity on the results of determinations in the proposed method without additional sample preparation makes it possible to analyze in reliable fashion complex ore samples and samples of heavy-metal processing products and solutions in which the concentration of the interfering element is many times greater than the content of analyzed elements.

LITERATURE CITED

1. V. I. Kokolevskii et al., in: Radiation Technology [in Russian], No. 8, Atomizdat, Moscow (1972).
2. A. L. Yakubovich et al., Nuclear-Physics Methods in the Analysis of Raw Minerals [in Russian], Atomizdat, Moscow (1969).

CALCULATION OF ELECTRON CONVERSION INTO POSITRONS AT 0.2-2 GeV

V. A. Tayurskii

UDC 539.124.6

The production of intense positron beams is essential for devices with clashing $e^- - e^+$ beams and also for a number of other physics problems. Positron beams are usually obtained by conversion of electrons. To produce an e^+ beam with minimal emittance, the electron beam must be well focused and a target of heavy material must act as a converter. Striking the target of the converter, the electrons produce an electron – photon cascade in it. A small part of the total number of positrons in the cascade escape from the converter and a certain fraction of them can be used experimentally. In the development of a conversion system, it is necessary to obtain the maximum number of positrons of given energy in a definite phase volume of a receiver, which, for a storage ring, is set by the transverse acceptances ε_r and ε_z. For calculation of the optimal conversion system, data are needed for the energy spectra of the positrons and also for the magnitude and shape of the beam emittance ε_+.

In the energy region considered, there are individual measurements of $d^2N^+/dE_+d\Omega$ [1-3]. In Monte Carlo calculations of the $e - \gamma$ shower in lead [4-6], overall characteristics of the electrons and positrons in the cascade were obtained. One can only estimate dN_+/dE_+ and ε_+ roughly for the positrons with the aid of these data.

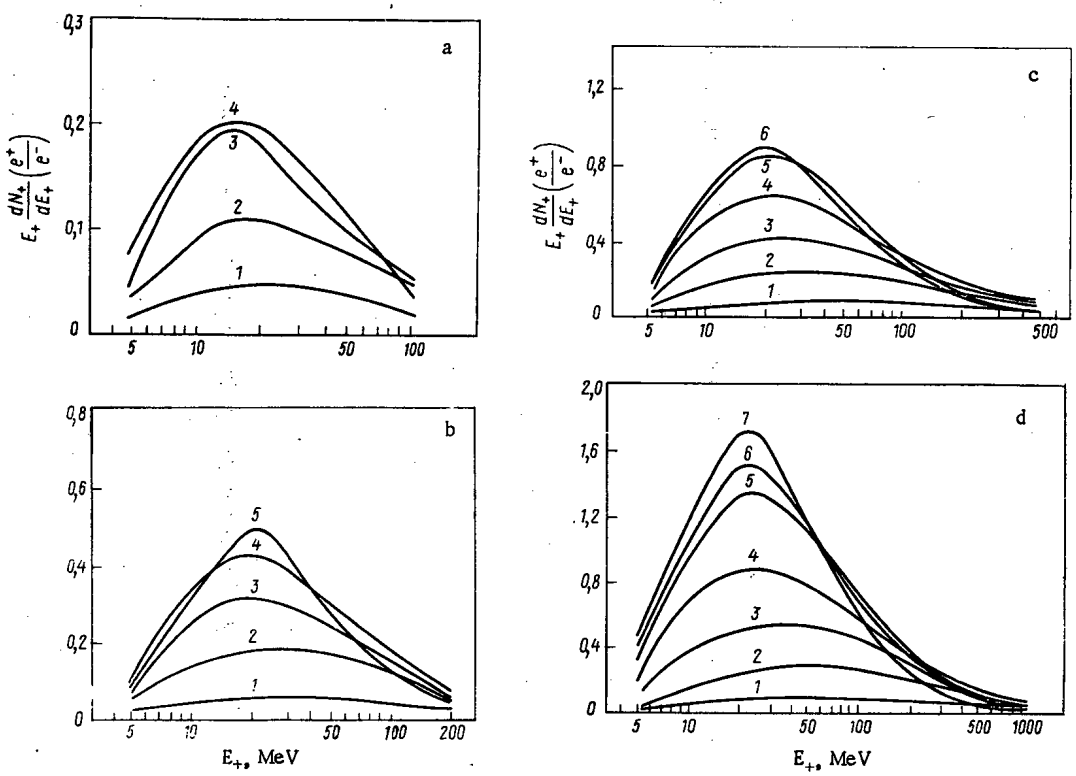

Fig. 1. Energy spectra of positrons emerging from a target in the forward direction in the solid angle $\Omega = 2\pi$ per incident electron and for various converter thicknesses: 1) $T = 0.5\ X_0$; 2) $1\ X_0$; 3) $1.5\ X_0$; 4) $2\ X_0$; 5) $2.5\ X_0$; 6) $3\ X_0$; 7) $3.5\ X_0$.

Translated from Atomnaya Énergiya, Vol. 42, No. 4, pp. 317-319, April, 1977. Original article submitted April 14, 1976; revision submitted October 8, 1976.

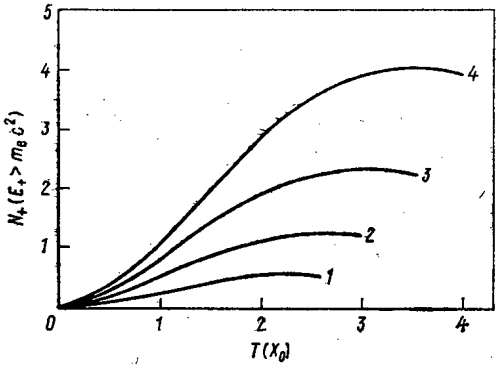

Fig. 2

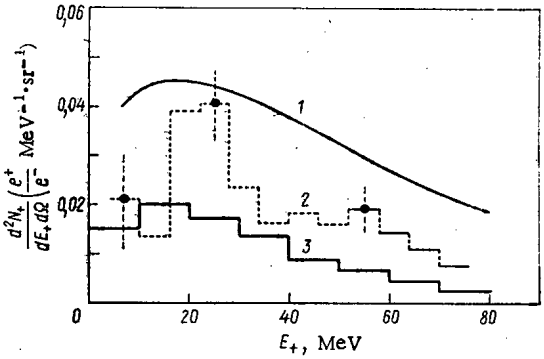

Fig. 3

Fig. 2. Total yield of positrons of all energies in the forward direction in the solid angle $\Omega = 2\pi$ per incident electron as a function of converter thickness for $E_- = 0.2$ (1), 0.5 (2), 1 (3), and 2 GeV (4).

Fig. 3. Comparison of calculations with measurements [1] and calculations [11] for $E_- = 220$ MeV and $T = 1.81\ X_0$: 1) experiment [1], lead; 2) calculation [11], lead (● – individually calculated points); 3) Monte Carlo calculation, tungsten.

This paper presents the results of Monte Carlo calculations of the positron energy spectra and also of the average values $\langle \theta_x^2 \rangle$ of the positron angular distributions for initial energies $E_- = 0.2$, 0.5, 1, and 2 GeV and for tungsten targets with thicknesses $T = (0.5\text{-}3.5)X_0$ (here and below, lengths are given in radiation lengths; for tungsten, $X_0 = 0.35$ cm [7]). The calculations were performed using the program [8] with certain improvements. The basic features of the computer program agree with those in the programs described in [4-6]. As an initial condition, it was assumed that a point beam of electrons was normally incident on the surface of a broad converter.

Positron spectra and $\langle \theta_x^2 \rangle$ for a given energy E_- were calculated for positron energies 5 MeV $\leq E_+ \leq E_-/2$. In the calculations, results were averaged over an energy interval $\Delta E_+ \approx 0.3 \langle E_+ \rangle$. Calculations at various energies E were performed for target thicknesses from $T = 0.5X_0$ to $T \approx T_{max}(E_-)$ [see Eq. (1)] in steps $\Delta T = 0.5X_0$. Figure 1 shows spectral curves for $E_+ dN_+/dE_+$ drawn within the limits of statistical error from calculated histograms for $E_- = 0.2$ (a), 0.5 (b), 1 (c), and 2 (d) GeV and various values of T. Figure 2 gives curves for the number $N_+(E_+ > m_e c^2)$ of positrons emerging from a target as a function of its thickness. The curves were obtained by approximate integration of computed spectra. The converter thickness for which the yield is a maximum is given within 10% by the expression

$$T_{max}(E_-) \approx 0.51 \ln E_- - 0.6, \quad (1)$$

where E_- is the energy of the electron beam, MeV (200 $\leq E_- \leq$ 2000 MeV). The fraction of low-energy positrons in a spectrum increases as the target thickness increases and $N_+(E_+ > m_e c^2)$ is determined mainly by the low-energy portion of the spectrum. Therefore, Eq. (1) gives the maximum target thickness for selection of optimum conversion conditions. The transverse emittance of a positron beam increases with target thickness. If $\varepsilon_+(T_{max}) \gg \varepsilon_r, \varepsilon_z$, the maximum number of positrons captured in a storage ring can be assured at a converter thickness $T \ll T_{max}$ (if the initial electron beam has a phase volume $\varepsilon_0 \gtrsim \varepsilon_+$, it is necessary to take it into account in ε_+ when calculating optimal conversion conditions).

In order to calculate the phase ellipse of the positron beam and the coefficient for capture in a storage ring [9], the quantities $\langle x^2 \rangle$, $\langle \theta_x^2 \rangle$, and $\langle x\theta_x \rangle$ are needed. Values of $\langle \theta_x^2 \rangle$ are given here. Data for $\langle x^2 \rangle$ and

TABLE 1. Dependence of $\langle \theta_x^2 \rangle$ (rad^2) on E_+ and T

T	E_+, MeV							
	5	10	20	50	100	200	500	1000
0,5	0,37	0,15	0,049	0,010	0,0028	0,00061	0,0001	0,00003
1	0,32	0,19	0,072	0,015	0,0067	0,0010	0,00021	0,00005
1,5	0,35	0,22	0,11	0,027	0,0074	0,0018	0,00027	0,00009
2	0,32	0,21	0,11	0,031	0,011	0,0022	0,00035	0,00011
2,5	0,34	0,22	0,12	0,034	0,0084	0,0019	0,00028	0,01018
3	0,33	0,23	0,12	0,036	0,011	0,0032	0,00047	0,00012
3,5	0,36	0,27	0,12	0,035	0,012	0,0029	0,00057	0,00009

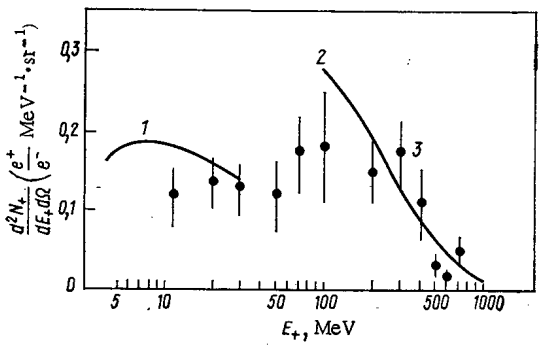

Fig. 4. Comparison of calculations with measurements [2, 3]: 1) experiment [2]; 2) experiment [3]; 3) Monte Carlo calculation (●), tungsten.

$\langle x\theta_x \rangle$ are contained in [10]. The quantity $\langle \theta_x^2 \rangle$ is practically independent of E_- and therefore the average value for $E_- = 0.2$-2 GeV is given in Table 1. With the aid of the data in Fig. 1 and Table 1, one can roughly estimate the double differential positron spectrum at an angle $\theta = 0°$,

$$d^2N_+(0°)/dE_+ d\Omega \approx (1/2\pi \langle \theta_x^2 \rangle)(dN_+/dE_+). \quad (2)$$

The equation given, which is valid for a Gaussian distribution over an angle, underestimates the positron yield by a factor of 1.5-2 in the present case. This is associated with the fact that the distributions over θ_x (and over x) obtained in the calculations were somewhat narrower Gaussians (with the calculated $\langle \theta_x^2 \rangle$ and $\langle x^2 \rangle$) in the central region and somewhat broader in the "tails." The statistical errors of the values given in Table 1, which were determined from the number of positrons arriving in the energy interval ΔE (over which the averaging was performed), and also the errors of the spectral curves in Fig. 1 were about 15% on the average. For limiting positron energies $E_+ \sim 5$ MeV and $E_+ \sim 0.5E_-$, the error was ~25%.

In Figs. 3 and 4 the calculated results are compared with experimental data [1-3] and with calculations [9] for the positron yield $d^2N_+/dE_+d\Omega$ at $\theta = 0°$ from heavy targets. In Fig. 3, calculated data (for tungsten) are compared with measurements [1] and calculations [11] for $E_- = 220$ MeV and $T = 1.81X_0$ (11.6 g/cm^2 of lead). The figure shows that the data calculated by the Monte Carlo method fall between the measurements [1] and calculations [11] but are closer to [11]. Note that the calculations [11] should underestimate the yield e^+ for $T > 1X_0$ since only positrons of the primary generation were considered in them. In the Monte Carlo calculations, the points $d^2N_+/dE_+d\Omega$ were calculated for $d\Omega = 3.8 \cdot 10^{-3}$ sr as in the measurements [1]. In Fig. 4, calculated data are compared with experimental data [2, 3]. Measurements of $d^2N_+/dE_+d\Omega$ were made in [2] for $E_- = 1$ GeV and targets of lead with a thickness $T = 2.9X_0$ at various angles θ_0. The spectrum $d^2N_+/dE_+d\Omega$ was measured in [3] at $\theta = 0°$ for $E_- = 640$ and 1220 MeV and a tantalum converter with thicknesses $T = (0.5\text{-}3)X_0$. Calculations of $d^2N_+/dE_+d\Omega$ at $\theta = 0°$ for $E_- = 1220$ MeV and $T = 3X_0$ are compared with these data. The calculated points were computed for a solid angle $d\Omega = 4.2 \cdot 10^{-4}$ sr as in [3]. As is clear from Fig. 4, satisfactory agreement within the limits of measurement error (~15%) between the calculations and the data of [3] is observed. The difference between the low-energy portion of the calculated spectrum and the data of [2] is obviously associated with experimental errors. On the whole, the data from our calculations are in satisfactory agreement with earlier measurements [1-3] and calculations [11].

Calculation of a positron energy spectrum and of the second moments of a distribution function for a single (E_-, T) mode takes up to 1 h on a BÉSM-6 computer. Calculations with good statistics for the double differential spectra require a considerable increase in computing time with the existing program. For that reason, such calculations were only performed for comparison with other data.

In conclusion, the author is grateful to B. V. Chirikov for a number of valuable comments.

LITERATURE CITED

1. T. Aggson and I. Burnod, Int. Rap. LAL-27, Orsay (1962).
2. H. De Staebler, Preprint SLAC TN-65-23 (1965).
3. I. A. Grishaev et al., Ukr. Fiz. Zh., 13, 1926 (1968).
4. H. Messel et al., Nucl. Phys., 39, 1 (1962).
5. H. Nagel, Z. Phys., 186, 319 (1965).
6. M. Ya. Borkovskii and S. P. Kryglov, Yad. Fiz., 16, 349 (1972).

7. O. I. Dovshenko and A. A. Pomanskii, Tr. FIAN, 26, 166 (1964).
8. F. M. Izraelev et al., Preprint JINR 63-73, Novosibirsk (1973).
9. T. A. Vsevolozhskaya, Preprint JINR 75-35, Novosibirsk (1975).
10. V. A. Tayurskii, Preprint JINR 76-36, Novosibirsk (1976).
11. H. Ferdinande et al., Preprint Rijksuniversiteit Gent FR68-1/1 (1968).

DETERMINATION OF ABSOLUTE γ YIELDS IN α DECAY OF ^{243}Am

D. I. Starozhukov, Yu. S. Popov, and P. A. Privalova

UDC 539.163

A nitric acid solution of ^{243}Am obtained by chemical and radiochemical purification [1] was used in this work. Methods of source preparation and of radiometric measurement are reported in [1] also. The isotopic composition of the source as determined by α and mass spectrometry [2] was 92.0 ± 0.30 and 7.98 ± 0.30% in terms of the spectrum and 99.476 ± 0.019 and 0.524 ± 0.019% in terms of mass for ^{243}Am and ^{241}Am, respectively. No other masses were observed. Specific α activity was determined by measurements in a $4\pi\alpha$ flow counter of targets prepared by deposition on a backing film (a colloid film ~10 $\mu g \cdot cm^{-2}$ thick) of the initial solution after parallel mass dilutions. In addition, the americium concentration was established from the results of mass and complexometric determinations [3]. The value of the specific activity $Q_{\alpha 243}$ of the solution was calculated as the weighted mean of the results of these methods of measurement.

The following half-lives were used in the calculations (Table 1): 7380 ± 34 yr [2] for ^{243}Am and 432.8 ± 3.1 yr [1] for ^{241}Am.

For measurements on a Ge(Li) spectrometer, 23 samples were prepared in a geometry similar to the geometry of standard spectrometric γ sources. Deposition of ^{243}Am in a layer 2 $\mu g \cdot cm^{-2}$ thick on a polyethylene backing 0.3 mm (27 $mg \cdot cm^{-2}$) thick made it possible to neglect self-absorption and absorption of short-wave γ radiation in the backing. To check the representativeness of the prepared samples, the mass of the prepared source was compared with the α activity for each individual sample. Relative measurements were carried out on a NaI(Tl) detector at 170 and 260 mm from the face of the detector in order to eliminate differences in measurement geometry. The error in the determination of the mass of a sealed source was no more than ±1%.

The γ spectra from the samples were measured on a spectrometer with a Ge(Li) detector with a volume of 30 cm^3, a Langur SES 2-03 spectrometric instrument, and an AI-4096 pulse-height analyzer. The instrumental resolution of the spectrometer was 3 keV for the ^{137}Cs γ line. A working γ spectrum is shown in Fig. 1.

TABLE 1. Determination of Specific Activity of ^{243}Am Solution

Method of determination	$Q_{\alpha 243}$, dis/sec • g
$4\pi\alpha$ measurements and semiconductor α spectrometry	60101±601
$4\pi\alpha$ measurements, mass spectrometry, and known $T_{\alpha 241}$ and $T_{\alpha 243}$	59895±599
Complexometry, mass spectrometry, and known $T_{\alpha 243}$	60015±660
Weighted mean	60000±270

Translated from Atomnaya Énergiya, Vol. 42, No. 4, pp. 319-322, April, 1977. Original article submitted June 4, 1976.

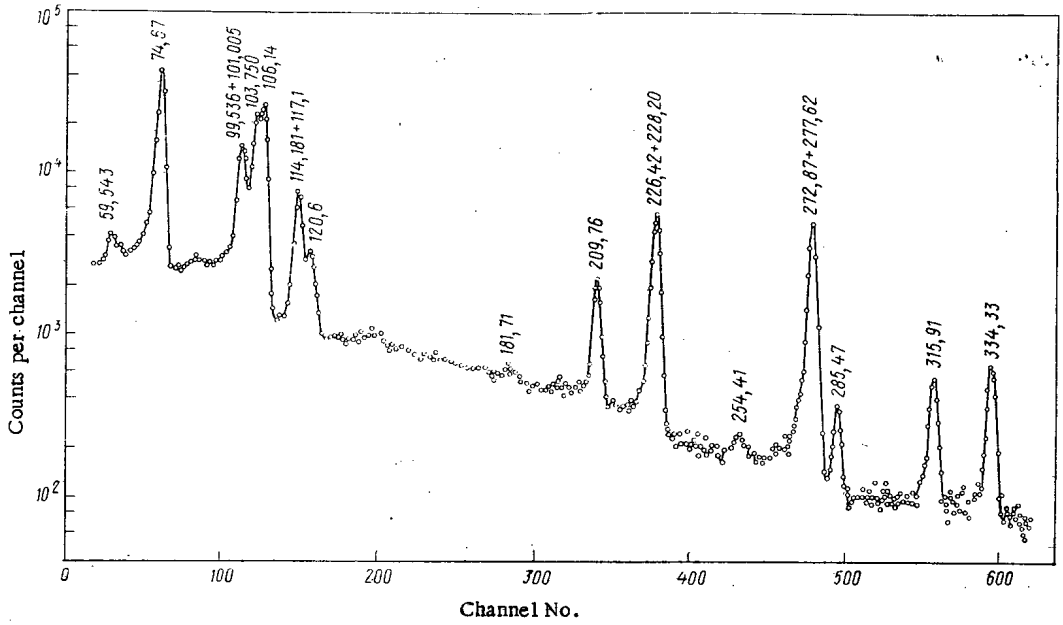

Fig. 1. γ-Ray spectrum from test sample.

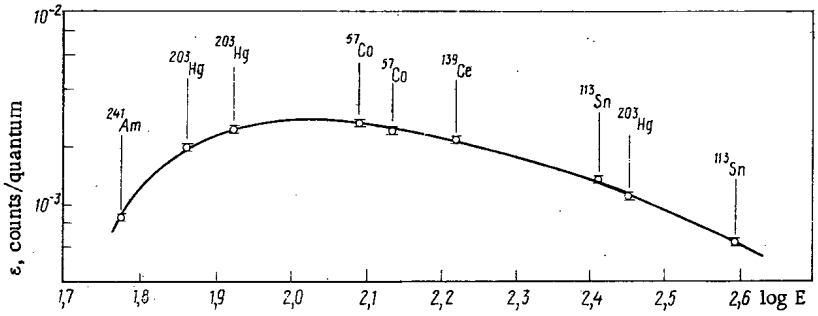

Fig. 2. Dependence of detector efficiency on γ-ray energy.

TABLE 2. Absolute γ-Line Yields in the α Decay of ^{243}Am, %

Radition source	E, keV	Ewan, 1959 [18]	Hyde, 1964 [22]	Davies, 1965 [23]	Lederer, 1967 [9]	Aleksandrov, 1969 [27]	Ewan, 1972 [24]	Ahmad, 1972 [25]	Yurova, 1974 [26]	This work
^{243}Am	74,67				50	73±3		66,0±3,0		59,1±4,0
PuK_{α_2}	99,536							14,5±0,6		0,72±0,08
NpK_{α_1}	101,005									13,50—0,06
PuK_{α_1}	103,750							22,2±0,8		19,7±0,8
^{239}Np	106,14	22,78						27,8±0,9		26,6±1,0
NpK_{β_1}	114,181									2,5±0,3
PuK_{β_1}	117,1		0,5			0,64±0,25		8,9±0,4		5,8±0,4
^{239}Np	120,6							2,77±0,10		2,53±0,12
^{239}Np	209,76	4,08		3,40				3,42±0,10		3,36±0,14
^{239}Np	226,42									0,24±0,03
^{239}Np	228,20	12,68		11,73				11,4±0,3		11,78±0,44
^{239}Np	277,62	14,076		14,076			14,5±0,4	14,5±0,4	14,1±0,4	15,0±0,5
^{239}Np	285,47	0,629		0,816				0,76±0,02		0,93±0,06
^{239}Np	315,91	1,496		1,496				1,52±0,05		1,63±0,07
^{239}Np	334,33	1,989		2,057				1,95±0,07		2,1±0,1

The spectrometer was calibrated by means of three sets of standard spectrometric γ sources having an error of $\pm 3\%$ in the determination of absolute activity. Nuclear-physics constants from [4-17] were used in calculating the values of the photoefficiency. The resultant efficiency curve (Fig. 2) was described by an empirical formula – a polynomial of fifth power in the argument log E (E is the γ-line energy, keV). The rms error of the photoefficiency for each γ line (3-6%) was calculated with allowance for the errors in the determination of the number of counts under a photopeak, the absolute value of the γ-line yield, and the determination of the activity of a γ standard for a 95% confidence interval.

Working samples and standards from the set of standard spectrometric γ sources were measured in a fixed geometry at 125 mm from the detector which was selected in order to produce optimum spectrometer loading and to reduce the error resulting from differences in measurement geometry. Areas under photopeaks in all measurements were determined on a BÉSM-4M computer with a program which made it possible to analyze overlapping photopeaks. The absolute values of γ-line yields were calculated by the least-squares method. The accuracy of the resultant values was determined mainly by the accuracy in the determination of the area under photopeaks, which is nicely illustrated by weak and overlapping γ lines where the error amounted to 10-12%, and to a lesser extent by the error in the determinations of photoefficiency and absolute activity of the samples.

The energy values of the γ lines studied were taken from [18-21]. The results of this work, which are given in Table 2 in comparison with known data, are in good agreement within the limits of error with the results of [25].

LITERATURE CITED

1. V. G. Polyukhov et al., At. Energ., 36, 319 (1974).
2. V. G. Polyukhov et al., At. Energ., 37, 357 (1974).
3. E. M. Piskunov, A. G. Rykov, and G. A. Timofeev, Byull. Izobret., No. 33, 178 (1973).
4. L. Brown and R. Progst, J. Inorg. Nucl. Chem., 30, 2591 (1968).
5. F. Oetting and S. Gunn, J. Inorg. Nucl. Chem., 99, 2659 (1967).
6. T. Yamasaki and J. Hollander, Nucl. Phys., 22, 525 (1965).
7. R. Mowatt, Nucl. Instrum. Methods, 70, 237 (1969).
8. G. Eicholz and J. Krzyzewski, Canad. J. Phys., 34, 1167 (1956).
9. C. Lederer, J. Hollander, and J. Perlman, Tables of Isotopes, Wiley, New York (1967).
10. J. Campbell and L. McNells, Nucl. Instrum. Methods, 98, 433 (1972).
11. J. Cork, M. Brice, and L. Schmid, Phys. Rev., 99, 703 (1955).
12. J. Geiger et al., Nucl. Phys., 68, 352 (1965).
13. R. Wille and R. Fink, Phys. Rev., 118, 242 (1960).
14. R. Greenwood and E. Brannen, Phys. Rev., 122, 1849 (1961).
15. R. Girgis and R. Van Lieshout, Physica, 24, 672 (1958).
16. S. Burson, Phys. Rev., 115, 188 (1959).
17. W. Phillips and J. Hopkins, Phys. Rev., 119, 1315 (1960).
18. G. Ewan et al., Phys. Rev., 116, 950 (1959).
19. K. Blinowska et al., Nucl. Phys., 55, 331 (1964).
20. B. Maier, Z. Phys., 184, 143 (1965).
21. G. Nelson, B. Saunders, and W. John, Phys. Rev., 188, 4 (1969).
22. E. Hyde, J. Perlman, and G. Seaborg, The Nuclear Properties of the Heavy Elements, Vol. II, Prentice-Hall, Englewood Cliffs, New Jersey (1964).
23. D. Davies and J. Hollander, Nucl. Phys., 68, 161 (1965).
24. G. Ewan and M. Wahlgram, Nucl. Instrum. Methods, 99, 337 (1972).
25. J. Ahmad and M. Wahlgram, Nucl. Instrum. Methods, 99, 333 (1972).
26. L. N. Yurova et al., At. Energ., 36, 51 (1974).
27. B. M. Aleksandrov, O. I. Grigor'ev, and N. M. Shimanskaya, Yad. Fiz., 10, 14 (1969).

VARIATION OF THERMAL CONDUCTIVITY OF A GAS MIXTURE UNDER THE FUEL-ELEMENT JACKET DURING BURN-UP

V. S. Yamnikov and L. L. Malanchenko

UDC 621.039.546:536.23

Rod-type fuel elements with fuel in the form of sintered UO_2 pellets are employed in water-moderated – water-cooled (VVÉR) and RBMK reactors. The temperature level in the fuel is, in the main, determined by the thermal load, the thermal conductivity of UO_2, and the thermal conductivity of the jacket – fuel interface (α_{O-T}). The magnitude of α_{O-T} and the character of its variation while the fuel element is in use in turn depend on many factors [1], in great measure on the thermal conductivity of the gaseous medium under the fuel-element jacket.

The empty space under the fuel-element jackets of power reactors is filled with helium or a mixture of helium with argon at normal or elevated pressure [2, 3]. When a fuel element is in service, fission-product gases, consisting mainly of krypton and xenon, are formed under the fuel-element jacket. Thus, the gas mixture under the jacket consists of the filling gas and the krypton and xenon formed; the composition, and hence the thermal conductivity, of the mixture changes continuously.

The volume of the fission-product gases liberated under the jacket is calculated by the formula

$$V_i = (22.4/N_A)\, nY_i J\omega G = 0.1056 Y_i J\omega G, \quad (1)$$

where V_i is the volume of the i-th gas under normal conditions, cm^3; N_A is Avogadro's number; n is the number of fissions corresponding to a burn-up of 1 MW·day and is equal to $2.84 \cdot 10^{21}$ fissions/MW·day [4]; J is the average burn-up in a fuel element, MW·day/ton U; Y_i is the yield of krypton and xenon isotopes during fission of ^{235}U, 0.04 and 0.26, respectively; ω is the fraction of fission-product gases liberated under the fuel-element jacket; and G is the uranium charge in the fuel element, kg.

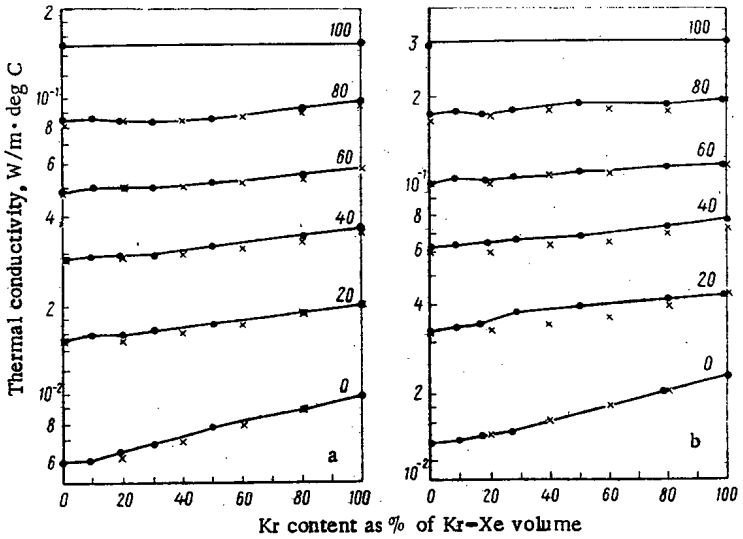

Fig. 1. Thermal conductivity of He – Kr – Xe mixture at: a) 29 and b) 520°C (the numbers next to the curves indicate the helium content, %); ●) experiment; ×) calculation.

Translated from Atomnaya Énergiya, Vol. 42, No. 4, pp. 322-324, April, 1977. Original article submitted June 7, 1976.

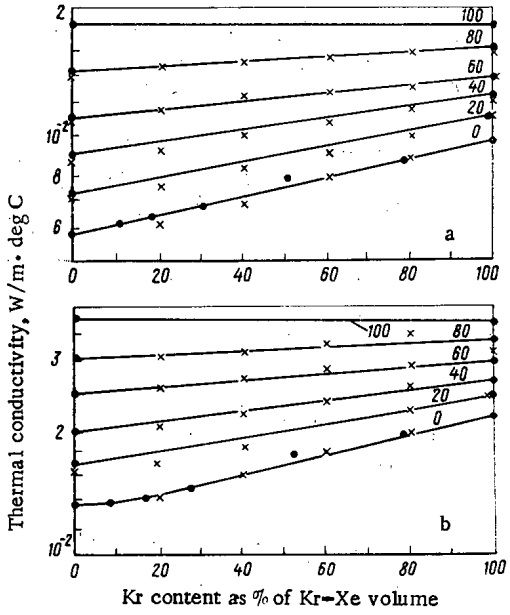

Fig. 2

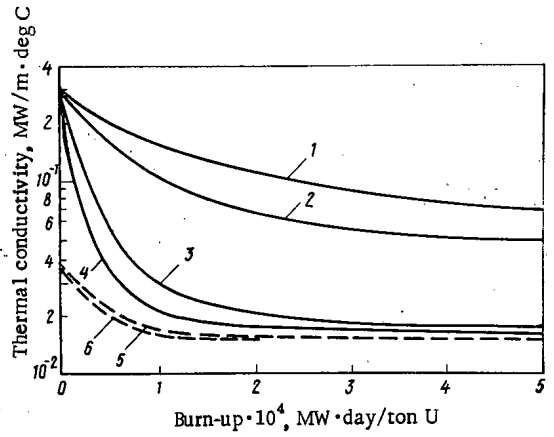

Fig. 3

Fig. 2. Thermal conductivity of Ar–Kr–Xe mixture at: a) 29 and b) 520°C (the numbers next to the curves indicate the argon content, %); ●) experiment; ×) calculation.

Fig. 3. Variation of thermal conductivity of gas mixture at 500°C under fuel-element jacket as function of initial filling and liberation of fission-product gases $\omega = 0.25$ (1, 3, 5) and $\omega = 0.50$ (2, 4, 6): 1, 2 and 3, 4) helium, $P_{init} = 2$ and 0.1 MPa; 5, 6) argon, $P_{init} = 0.1$ MPa.

A number of authors calculate the thermal conductivity of the gas mixture by using the formula [5, 6]:

$$\lambda_{mix} = \sum_{i=1}^{n} \left(\lambda_i/1 + (1/x_i) \sum_{\substack{j=1 \\ j \neq i}}^{n} A_{ij} x_j\right), \tag{2}$$

where λ_{mix} and λ_i are, respectively, the thermal conductivity of the gas mixture and its components, and x are the volume fractions of gases in the mixture.

As applied to fuel elements, this formula should be considered for a ternary and a quaternary mixture. In particular, for a quaternary mixture it is of the form

$$\lambda_{mix} = \frac{\lambda_1}{1 + A_{12}(x_2/x_1) + A_{13}(x_3/x_1) + A_{14}(x_4/x_1)} + \frac{\lambda_2}{1 + A_{21}(x_1/x_2) + A_{23}(x_3/x_2) + A_{24}(x_4/x_2)} + \\ + \frac{\lambda_3}{1 + A_{31}(x_1/x_3) + A_{32}(x_2/x_3) + A_{34}(x_4/x_3)} + \frac{\lambda_4}{1 + A_{41}(x_1/x_4) + A_{42}(x_2/x_4) + A_{43}(x_3/x_4)}. \tag{3}$$

Theoretical formulas and an empirical method are suggested for calculating the coefficients A_{ij}; in the empirical method, A_{ij} are found with the aid of the experimental values of the thermal conductivities for given compositions of binary gas mixtures [5-7]. The various methods give different values but the choice of coefficients for binary mixtures is not unique, i.e., there is a region in which all pairs of values A_{12} and A_{21} give good agreement with experimental data [6-8].

To calculate the thermal conductivity of a gas mixture under the fuel-element jacket we considered binary mixtures of helium, krypton, xenon, and argon. On the basis of experimental data on the thermal conductivity of binary mixtures of these gases [9], we obtained the following values of A_{ij} by the empirical method:

$$A_{12} = 2.7; \quad A_{13} = 3.6; \quad A_{14} = 2.0;$$
$$A_{21} = 1.7; \quad A_{23} = 0.6; \quad A_{24} = 0.2;$$
$$A_{31} = 0.5; \quad A_{32} = 3.5; \quad A_{34} = 0.8;$$
$$A_{41} = 2.2; \quad A_{42} = 2.6; \quad A_{43} = 1.9$$

(in the subscripts helium is denoted by 1, krypton by 2, xenon by 3, and argon by 4).

Taking these coefficients into account, we calculated the thermal conductivity of the ternary mixtures He–Kr–Xe and Ar–Kr–Xe. The calculation is compared with the published experimental data [9] in Figs. 1

and 2, from which the calculated experimental values of the thermal conductivity are seen to be in good agreement for all combinations of compositions by volume. We are not aware of any experimental data on the thermal conductivity of the quaternary mixture He – Ar – Xe – Kr.

Thus, the thermal conductivity of the medium under the fuel-element jacket with account for the initial filling with helium or helium – argon mixture and liberation of fission-product gases under the jacket (for $x_2 \approx 0.15x_3$ since $Y_{Kr} \approx 0.15Y_{Xe}$), is found from the following relations:

with an initial filling of helium

$$\lambda_{mix} = \frac{\lambda_1}{1{,}0+4.0(x_3/x_1)} + \frac{\lambda_2}{5.0+11.3(x_1/x_3)} + \frac{\lambda_3}{1{,}5+0{,}5(x_1/x_3)}; \quad (4)$$

with an initial filling of a helium – argon mixture

$$\lambda_{mix} = \frac{\lambda_1}{1.0+4.0(x_3/x_1)+2.0(x_4/x_1)} + \frac{\lambda_2}{5.0+11.3(x_1/x_3)+1.3(x_4/x_3)} + \frac{\lambda_3}{1.5+0.5(x_1/x_3)+0.8(x_4/x_3)} + \frac{\lambda_4}{1.0+2.2(x_1/x_4)+2.3(x_3/x_4)}. \quad (5)$$

Figure 3 gives the plot of the thermal conductivity of the gaseous medium under the fuel-element jacket as a function of the initial filling, liberation of fission-product gases, and burn-up as applied to the fuel element of the VVÉR-1000 reactor [10].

The pressure of the gas mixture under the fuel-element jacket increases to 10-20 MPa. Experimental data on the thermal conductivity of the gas mixture are not available. However, it is known that the pressure in the limits 10-20 MPa has an insignificant effect on the thermal conductivity of pure gases at temperatures exceeding 300°C. Therefore, it may be recommended that the thermal conductivity of a mixture be calculated at elevated pressure by Eqs. (4) and (5), where the thermal conductivity of pure gases is taken at the mixture temperature and pressure.

Experimental determination of the thermal conductivity of the quaternary mixture He – Kr – Xe – Ar at various pressures and temperatures makes it possible to refine this relation for calculation of the thermal conductivity of a gas mixture.

LITERATURE CITED

1. V. S. Yamnikov and L. L. Malachenko, At. Tekh. Rubezhom, No. 2, 21 (1969).
2. R. Holzer and H. Knaab, Kerntechnik, 14, No. 11, 519 (1972).
3. H. Ferrari, Trans. Am. Nucl. Soc., 12, 554 (1969).
4. A. D. Galanin, Theory of Thermal-Neutron Nuclear Reactors [in Russian], Atomizdat, Moscow (1959).
5. N. V. Tsederberg, Thermal Conductivity of Gases in a Liquid [in Russian], Gosénergoizdat, Moscow (1963).
6. A. G. Shashkov and R. N. Abramenko, Thermal Conductivity of Gas Mixture [in Russian], Énergiya, Moscow (1970).
7. S. Saxena and P. Tondon, J. Chem. Eng. Data, 16, No. 2, 212 (1974).
8. S. Saxena and G. Gupta, J. Chem. Eng. Data, 15, 99 (1970).
9. H. Ubisch et al., in: Proceedings of the Second International Conference, Vol. 7, Geneva (1968), p. 697.
10. A. S. Zaimovskii et al., At. Energ., 30, No. 2, 226 (1971).

OPTIMAL CONDITIONS FOR SHUTTING DOWN A REACTOR FOR A GIVEN SHUTDOWN TIME

S. A. Vasil'ev, V. I. Pavlov, and V. D. Simonov

UDC 621.039.516

A characteristic feature of the operation of thermal power plants involved in power regulation is that they are shut down for 5-8 h during the night. If the power-generating unit of an atomic power plant is operated in this manner, there may be constraints because the xenon poisoning of the reactor at the end of the shutdown period exceeds the existing reactivity excess.

It is known [1] that the character of the xenon processes in a nuclear reactor can be controlled by choosing the conditions of power-variation before the shutdown. Conditions which are realized in the shortest time are preferable. Accordingly, the problem is to choose the optimal method of shutting down the reactor for a known period.

Figure 1a gives the phase-plane plots of the curves abo_1f_10, keo_2f_20, do_3f_30, and gf_40 of the changes in the concentrations of ^{135}I and ^{135}Xe, normalized to the fission macrosection ($x^{(1)}$ and $x^{(2)}$, respectively) during an instantaneous reduction in the power of the reactor whose state is characterized by points a, k, d, and g on curve ξ of iodine and xenon equilibrium states. The position of points d and k can be chosen so that the time of travel along the trajectories do_3f_3 and eo_2f_2 is equal to the given reactor shutdown time t_{sh} (this is possible for a reasonable shutdown time and reactivity excesses). Then, it follows from the time dependence of the xenon concentration after the total power reduction that the straight line de is the locus of the initial points of the trajectory corresponding to the final power level $x_k^{(3)} = 0$ and ending at the time $t = t_{sh}$ with the constraint $x^{(2)} = x_{max}^{(2)}$ which is determined by the reactivity excess of the reactor.

The equation of the straight line de is of the form

$$x^{(2)} = x_{max}^{(2)} \exp(\lambda_2 sh) + \lambda_1/(\lambda_2 - \lambda_1)\, x^{(1)} \{1 - \exp[(\lambda_2 - \lambda_1) t_{sh}]\}, \quad (1)$$

where λ_1 and λ_2 are the decay constants of ^{135}I and ^{135}Xe. If the moment at which the line de is reached is taken for $\tau = 0$, then when $\tau \geq t_{sh}$ the condition

$$x^{(2)} \leqslant x_{max}^{(2)} \quad (2)$$

is satisfied and this ensures that the reactor can be brought up to nominal power.

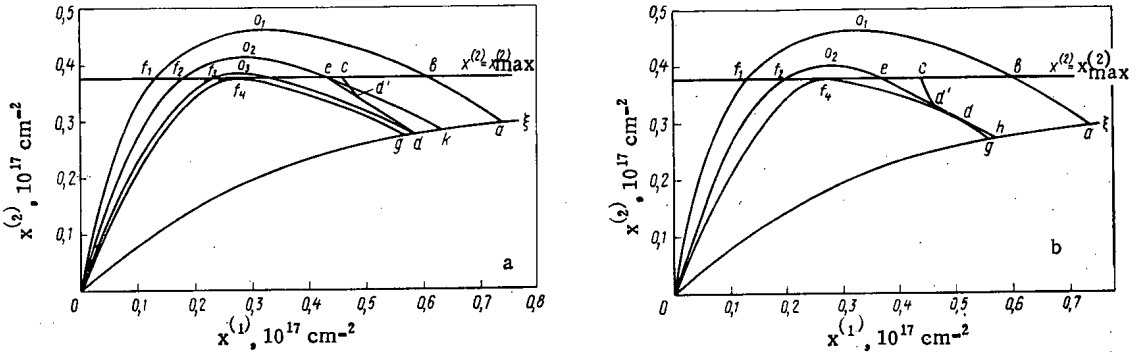

Fig. 1. Optimal trajectory of power reduction for: a) $t_{sh} > t_{gf_4}$ and b) $t_{sh} < t_{gf_4}$.

Translated from Atomnaya Énergiya, Vol. 42, No. 4, pp. 324-325, April, 1977. Original article submitted June 16, 1976.

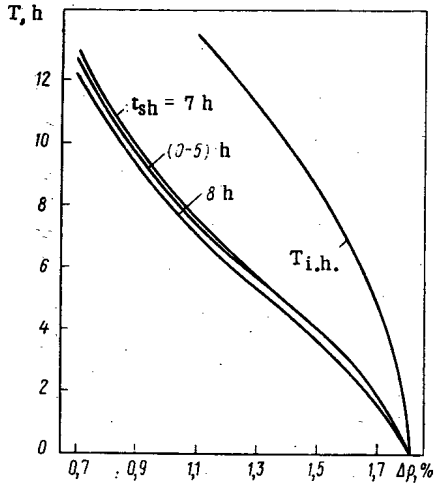

Fig. 2. Power-reduction time as a function of the excess reactivity and duration of reactor shutdown.

Thus, the problem comes down to finding the temporally optimal trajectory of the transition from the initial equilibrium state (point a) to the straight line de, determined by the duration of the shutdown, given the constraints

$$x^{(2)}(t) \leqslant x^{(2)}_{max};\ x^{(3)}_{min} \leqslant x^{(3)}(t) \leqslant x^{(3)}_{max}. \qquad (3)$$

In this formulation the problem is analogous to that of the speed of response considered in [2]. Therefore, we shall look for the solution on the trajectories *a*bcd' (see Fig. 1a), consisting of three segments: *a*b, the segment of minimum allowable power ($x^{(3)}_{min}$); bc, the segment of variable power ($x^{(3)}(t)$), ensuring that the xenon concentration is equal to its maximum limiting value; and cd', the segment of maximum allowable power ($x^{(3)}_{max}$).

The position of the straight line de in the phase plane is determined by the reactivity excess and the relation between the time t_{sh} and t_{gf_4} (f_4 is the point of tangency of the curve gf_40 and the straight line $x^{(2)} = x^{(2)}_{max}$). Figure 1a corresponds to the case when $t_{sh} > t_{gf_4}$, and Fig. 1b to the case $t_{sh} < t_{gf_4}$. The straight line edh can can be shown to touch the curve gf_{40} if the condition $t_{df_4} = t_{sh}$ is satisfied. With the straight line ed in this position it may turn out that the curve dg is reached much more quickly than the straight line ed is and, in the process, condition (2) is satisfied. The segment dh, which is intersected during the transition to dg, cannot be chosen as the "goal" owing to violation of condition (2). Therefore, when $t_{sh} < t_{gf_4}$, the optimal trajectory should end at the line edg.

These results of the optimization of the trajectory of power reduction were obtained on the basis of a one-group point model of the water-moderated – water-cooled reactor under the assumption that the power could be changed in steps. The optimality was verified by the maximum principle [3]. Figure 1b gives the time of the optimal power-reduction regime as a function of the reactivity excess and the planned shutdown time. The point of intersection of the curves with the abscissa axis gives the value of the reactivity excess at which the reactor does not fall into the "iodine" hole. For a shutdown time of t_{sh} = 0-5 h, at all values of the reactivity excess considered the optimal transition is the one to the curve dg (Fig. 2), i.e., in the range 0-5 h the duration of the shutdown does not affect the duration of the optimal transition, but after the power reduction it is still possible to increase the power at any moment without limitation. When $t_{sh} > 5$ h, the optimal transition time decreases (for t_{sh} = 8 h the decrease is ~0.5 h for the entire range of values of excess reactivity), but there are limitations on an increase in power when $\tau < t_{sh}$ (see Fig. 1).

Figure 2 shows the dependence of the time that the reactor remains in the "iodine hole" ($T_{i.h.}$), i.e., the time of travel along the trajectory bo_1f_1 from the reactivity excess. Comparison of this relation with the optimal power-reduction time indicates it is advisable to employ the regime considered.

LITERATURE CITED

1. A. P. Rudik, Nuclear Reactors and the Pontryagin Maximum Principle [in Russian], Atomizdat, Moscow (1971).
2. V. M. Desyatov, V. I. Pavlov, and V. D. Simonov, At. Energ., 40, No. 6, 464 (1976).
3. L. S. Pontryagin et al., Mathematical Theory of Optimal Processes [in Russian], Fizmatgiz, Moscow (1965).

FAST-ELECTRON TRANSFER IN LAMELLAR MATERIALS

B. A. Kononov, Yu. M. Stepanov, and A. P. Yalovets

UDC 539.124.17

The Monte Carlo method is traditionally used to calculate radiation transfer in inhomogeneous media. However, the numerical analysis method considered in [1, 2] for calculating fast-electron transfer enables the existence of planar interfaces in the medium to be taken into account easily. The idea of including the planar interfaces is developed in the present paper for the case when electron transfer is considered in an absorber consisting of plates with various effective atomic numbers. This method is based on the solution of an integral Boltzmann kinetic equation written for a model of sections in the continuous slowing-down approximation [1]. A similar Boltzmann equation can also be written for the "continuous trajectories" model [3, 4] which encompasses the fluctuations in the ranges of particles and, as shown in the papers mentioned, permits the functionals of the flux to be calculated with a high degree of accuracy. Therefore, the problem is tackled here within the framework of this model.

Thus, let us consider fast-electron transfer in a lamellar absorber of thickness $d = \sum_{i=1}^{i_{max}} \Delta z_i$, the planes z_0 and z_m being the free surfaces of the absorber; Δz_i is the thickness of the i-th layer; and i_{max} is the total number of layers. Then the transport equation, written within the framework of the "continuous trajectories" model, is of the form

$$I(z, u; T) = \int_{4\pi} d\Omega' G(u; u', \Delta, T, z) \int_0^\infty ds\omega(s; \Delta, T+\Delta, z)\, I(z-su', u'; T+\Delta) + \\ + \int_0^\Delta d\Delta' \int_{4\pi} d\Omega' G(u; u', \Delta', T, z) \int_0^\infty ds\omega(s; \Delta', T+\Delta', z)\, Q(z-su', u', T+\Delta'), \quad (1)$$

where z is the electron coordinate; u' and u are the cosines of the angles between the electron momenta and the 0z axis before and after scattering, respectively; I(z, u; T) is the density of electrons of kinetic energy T in the phase space {z, u}; $\omega(s; \Delta, T, z)ds$ is the probability that an electron of energy T, having lost an energy of Δ, travels a path of s to s + ds; $G(u; u', \Delta, T, z)du$ is the probability of an electron of energy T being scattered from the direction u' in the range of directions du about u after traversing a path s, in accordance with the probability $\omega(s; \Delta, T, Z)$; Q(z, u, T) is a function of the source of fast electrons. As shown in [3], the function $\omega(s; \Delta, T) = \varphi(\lambda)(d\lambda/ds)$, where $\varphi(\lambda)$ is the universal Landau function; λ is a dimensionless parameter; $G(u; u', \Delta, T) \approx g(u; u', \langle s \rangle, T)$, where $\langle s \rangle = \Delta/B(T)$ and B(T) are the specific energy losses and the function $g(u; u', \langle s \rangle, T)$ describes the probability of particles of energy T being scattered from u' to u after traveling a path $\langle s \rangle$, and can be obtained on the basis of the theory of multiple scattering.

It is seen from Eq. (1) that the geometry of the problem is taken into account through the coordinate dependence of the functions which describe the spread of the mean free paths and the scattering. Before solving Eq. (1), we go over to a new variable in the traversed path s and, therefore, to a new variable in the coordinate z through the relation

$$d\tilde{s} = ds/R_0(z); \quad (2)$$

$$d\tilde{z} = dz/R_0(z), \quad (3)$$

where $R_0(z) = \int_0^{T_0} dT_0/B(T, z)$ is the total mean free path of electrons of energy T_0 in the substance of the layer to which coordinate z belongs. The function $\omega(s; \Delta, T, z)$ can be recast into

Translated from Atomnaya Énergiya, Vol. 42, No. 4, pp. 326-328, April, 1977. Original article submitted July 5, 1976.

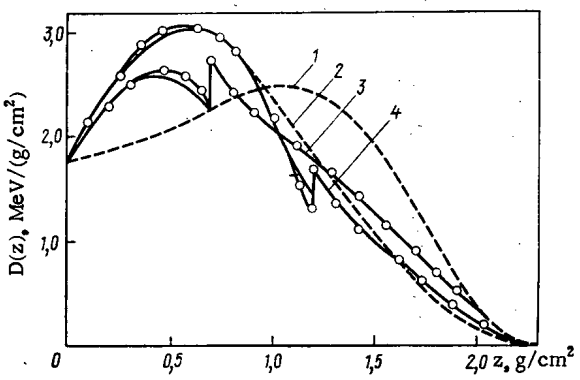

Fig. 1. Distribution of energy loss by electrons with initial energy of 4 MeV: — — —) semifinite absorber; 1) carbon; 2) copper; ———) two-layered absorber (copper + carbon); 3, 4) Δz_{Cu} = 0.7 and 1.2 g/cm², respectively (results of present paper); ○) results of [7].

$$\omega(s;\ \Delta,\ T,\ z) = [Z(z), A(z)]\,\omega^*(s;\ \Delta,\ T), \tag{4}$$

where Z and A are the effective atomic number and mass number of the substance at the depth z.

From Eq. (2) and (4) it follows that $\omega(s; \Delta, T, z)R_0(z) = \tilde{\omega}(\tilde{s}; \Delta, T)$, this new function being independent of the type of substance apart from a logarithmic dependence on the ionization potential. Then, in the new variables the Boltzmann equation (1) is in the form

$$\tilde{I}(\tilde{z},\ u;\ T) = \int_{4\pi} d\Omega' g(u;\ u'\langle\tilde{s}\rangle,\ T,\ \tilde{z}) \int_0^\infty d\tilde{s}\tilde{\omega}(\tilde{s};\ \Delta,\ T+\Delta)\tilde{I}(\tilde{z}-\tilde{s}u',\ u';\ T+\Delta) +$$
$$+\int_0^\Delta d\Delta' \int_{4\pi} d\Omega' g(u;\ u',\langle\tilde{s}'\rangle,\ T,\ \tilde{z}) \int_0^\infty d\tilde{s}\tilde{\omega}(\tilde{s};\ \Delta',\ T+\Delta')\tilde{Q}(\tilde{z}-\tilde{s}u',\ u',\ T+\Delta'), \tag{5}$$

where $\tilde{I}(\tilde{z}, u; T) = I[z(\tilde{z}), u; T]R_0[z(\tilde{z})]$.

Equation (5) describes electron transfer in a medium that is homogeneous with respect to slowing-down properties and inhomogeneous with respect to scattering properties. It should be noted that a similar change of variables was used earlier in [5, 6]. For a lamellar medium, the dependence of the scattering probability on the coordinates can be written as

$$g(u;\ u',\langle\tilde{s}\rangle,\ T,\tilde{z}) = \begin{cases} (2\pi)^{-1}\delta(u'-u), & \tilde{z}<\tilde{z}_0;\ \tilde{z}>\tilde{z}_m; \\ g^{(1)}(u;\ u',\langle\tilde{s}\rangle,\ T), & \tilde{z}_0\leqslant\tilde{z}\leqslant\tilde{z}_1; \\ \cdots\cdots\cdots\cdots\cdots \\ g^{(m)}(u;\ u',\langle\tilde{s}\rangle,\ T), & \tilde{z}_{m-1}\leqslant\tilde{z}\leqslant\tilde{z}_m, \end{cases} \tag{6}$$

where $g^{(i)}(u; u', \langle\tilde{s}\rangle, T)$ is the scattering probability in the substance of the i-th layer.

Equation (5) was solved by expanding the sought function in a Fourier – Legendre series:

$$\tilde{I}(\tilde{z},\ u;\ T) = \sum_{l=0}^{\infty}\frac{2l+1}{4\pi}P_l(u)\left\{\frac{\tilde{a}_{0l}(T)}{2}+\sum_{k=1}^{\infty}[\tilde{a}_{kl}(T)\cos\pi kz+\tilde{b}_{kl}(T)\sin\pi kz]\right\}. \tag{7}$$

In this case Eq. (5) goes over into a system of recurrence formulas for the coefficients $\tilde{a}_{kl}(T)$ and $\tilde{b}_{kl}(T)$. The steps in the solution and the features of the calculation are discussed in detail in [2, 3].

The functionals of the flux were calculated by a BÉSM-4 computer by the method described. The program enables calculations to be performed for an absorber with as many as five layers, the computation of one set of functionals not taking more than 20 min.

It should be noted that the use of the Fourier expansion in solving Eq. (5) with ten terms in series (7) does not yield results of satisfactory accuracy if the thickness of any layer is less than $(0.15\text{-}0.2)N_0$ or if there are more than five layers.

Figures 1 and 2 give the calculated distributions of the energy loss and of thermalized electrons and compare them with the results of [7]. Our results and those of [7] are in agreement almost everywhere, only slight differences being observed near the interfaces and at small depths.

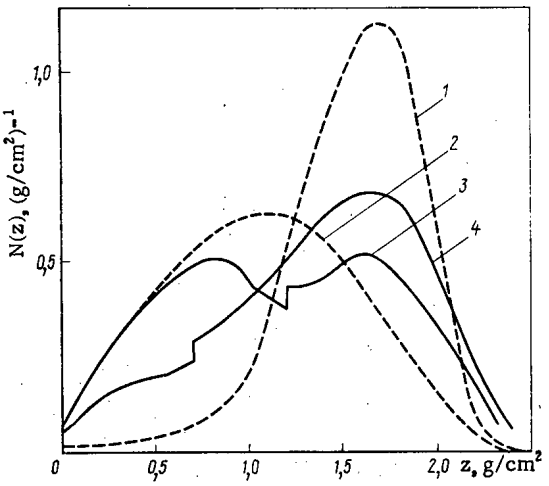

Fig. 2

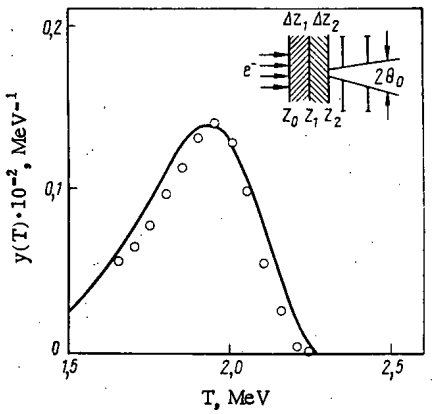

Fig. 3

Fig. 2. Distribution of thermalized ions with initial energy of 4 MeV (notation as in Fig. 1).

Fig. 3. Energy distribution of electrons beyond a two-layered target (copper + carbon): ———) calculation; ○) experiment. In top corner, geometry of experiment at $T_0 = 2.9$ MeV; $\Delta z_1 = 0.36$ and $\Delta z_2 = 0.24$ g/cm^2.

The distributions of energy losses and thermalized electrons were calculated by the formulas:

$$D(z) = R_0^{-1}(z) \int_{4\pi} d\Omega \int_{T_{th}}^{T_{max}} dT \tilde{I}[\tilde{z}(z), u; T]; \tag{8}$$

$$N(z) = R_0^{-1}(z) \int_{4\pi} d\Omega \tilde{I}[\tilde{z}(z), u; T_{th}], \tag{9}$$

where T_{th} is the threshold electron energy at which the residual range can be neglected.

The behavior of the distribution of the energy lost by fast electrons has been discussed in [7]. The discontinuities in the distributions are due to the differences in the specific energy losses in the layers.

The existence of discontinuities in the distribution of thermalized electrons in inhomogeneous absorbers (Fig. 2) was somewhat surprising. However, if the distribution N(z) is expressed in terms of the differential flux $\Phi(z, T)$, which is a continuous function of the coordinates, it is clear that the discontinuity at the interface is due to the fact that the differential cross section of energy loss, $\Sigma_s(T \to T)$, depends on the atomic number of the substance:

$$N(z) = \int_{T_{th}}^{T_{max}} dT \Phi(z, T) \int_0^{T_{th}} dT' \Sigma_s(T \to T'). \tag{10}$$

The results of comparison of the calculated energy spectrum y(T) beyond a two-layered target with experimental data are presented in Fig. 3. The spectrum y(T) was calculated by the formula

$$y(T; z_2) = [B(T) R_0]^{-1} 2\pi \int_{u_0}^{1} du u \tilde{I}[\tilde{z}(z_2), u; T], \tag{11}$$

where $u_0 = \cos\theta_0$.

The electron energy distribution beyond the two-layered target was studied experimentally with a magnetic spectrometer which had a resolution of 0.1%. The source used was a betatron with a half-width of the external-beam spectrum that was less than 2% and a divergence angle of the beam on the target of less than 1° in both planes. The systematic error in determining the magnitude of the external-beam energy does not exceed ±1.6%. The entrance angle $2\theta_0$ of the spectrometer is 2°.

The results testify to the effectiveness of this method of taking the inhomogeneity of the medium into account. The economy and simplicity of the method justify the conclusion that it is useful in solving transport problems for multilayered absorbers.

In conclusion, the authors express their gratitude to O. B. Evdokimov for his useful discussion.

LITERATURE CITED

1. O. B. Evdokimov, Izv. Vyssh. Uchebn. Zaved., Fiz., No. 1, 17 (1973).
2. O. B. Evdokimov and A. Yalovets, Nucl. Sci. Eng., 55, 67 (1974).
3. A. P. Yalovets, Candidate's Dissertation, Tomsk (1973).
4. A. A. Vorob'ev and A. P. Yalovets, At. Energ., 36, No. 3, 208 (1974).
5. A. M. Kol'chuzhkin, At. Energ., 25, No. 3, 442 (1968).
6. A. M. Kol'chuzhkin, I. N. Shevtsova, and K. A. Dergobuzov, Izv. Vyssh. Uchebn. Zaved., Fiz., No. 8, 52 (1968).
7. A. V. Plyasheshnikov, Candidate's Dissertation, Tomsk (1974).

TESTING THE BIOLOGICAL SHIELDING OF THE REACTOR OF THE BILIBINSK NUCLEAR POWER PLANT

V. Yu. Ifraimov, V. N. Mironov, A. P. Suvorov, Yu. V. Kharizemenov, S. G. Tsypin, and A. I. Shul'gin

UDC 621.039.538.7

The thickness of the biological shielding of channel-type reactors, in particular those of the Bilibinsk nuclear thermal power plant, is determined in the lateral direction primarily by γ-capture radiation produced in the walls of the reactor vessel and circular water tank (Fig. 1), where there is a comparatively high thermal-neutron flux density. Therefore, to verify the computational techniques it was of great interest to measure the spatial distribution of the γ-ray dose rate over the entire thickness of the side shield of the reactor. This is the first time such data are being published.

Calculation of the transmission of active-zone and secondary γ ray through the dense shield was carried out according to the GAMMA-3 program for a plane geometry, employing a method of ray analysis with allowance for the build-up of scattered radiation [1]. The results of the calculations were corrected to take account of the size of the sources (active zone and reactor vessel) and the annular geometry of the part of the side biological shield that is closest to the reactor (vessel and water tank). Much attention was paid to the temperature correspondence of real and computational models.

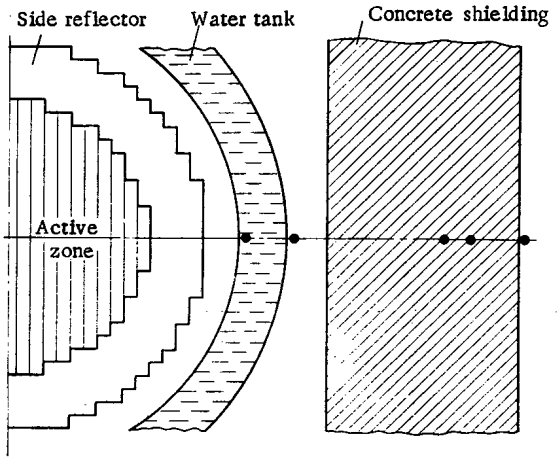

Fig. 1. Side biological shielding: ●) detection points.

Translated from Atomnaya Énergiya, Vol. 42, No. 4, pp. 328-329, April, 1977. Original article submitted July 22, 1976.

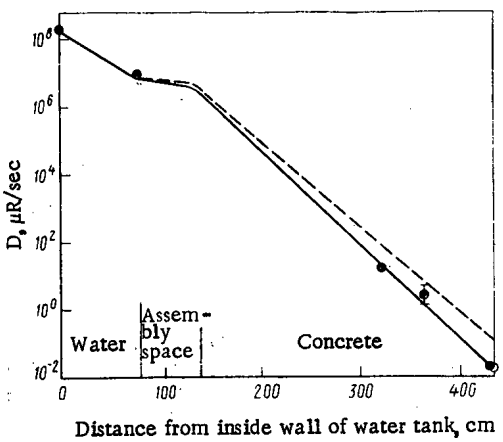

Fig. 2

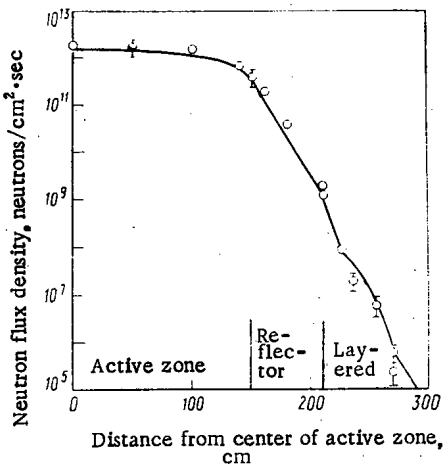

Fig. 3

Fig. 2. Spatial distribution of γ-ray dose rate in side biological shield: ●) experiment; — — —) calculation for plane geometry; ———) calculation taking account of cylindrical geometry and corrections for presence of reinforcing steel in concrete.

Fig. 3. Spatial distribution of neutron flux density in top biological shield: ○) experiment; ———) calculation.

The experimental data on the dose-rate distributions were obtained for γ rays inside and beyond the water tank during reactor operation at zero power ($\sim 10^{-3}$% of the nominal) and in the concrete shielding, at nominal power. We note that, according to the results of the calculations presented, the γ-ray dose rate in the side biological shield in the first case proved to be 20-30% higher than in the second when converted to the nominal rate. This is explained primarily by the temperature dependence of the radiative-capture cross section.

The experimental and calculated γ-ray dose rates $\dot{D}$ in the side biological shielding of the Bilibinsk nuclear power plant at the level of the center of the active zone are presented in Fig. 2. Comparison of the experimental (30% error) and the calculated data shows that they are in good agreement, the differences not exceeding 50% with an attenuation factor of $\sim 10^8$, and indicates that the geometry of the biological shield and the reinforcing steel in the concrete must be taken into account in the calculations. The overall correction for the detection points located beyond the side shield is as much as five.

The top biological shield of the reactor of the Bilibinsk plant is denser than the side shield since it is pierced by numerous fuel channels and safety-rod and control-rod channels. Moreover, because of the quite stringent temperature limitations, graphite and cast iron are used here in the form of multilayered shielding.

The experimental studies of the upper biological shield were conducted in hollow cells of the fuel channels with the aid of special suspensions which, in particular, made it possible to imitate a layered shield of cast iron and graphite. The spatial distribution of the flux density of neutrons with an energy of $E \geqslant 2$ MeV was measured (Fig. 3). The experimental data were reduced to 1 W of reactor power.

The neutron radiation fields in the active zone and the biological shield were calculated in the P_2 approximation for plane geometry (21 groups) according to program 9M [2] with allowance for the presence of the structural steel of fuel channels and control-rod and safety-rod channels in the upper reflector. The experimental and calculated data (see Fig. 3) are in satisfactory agreement with each other.

LITERATURE CITED

1. M. A. Luk'yanov et al., in: Studies on the Problems of the Physics of Shielding of Atomic Power Plant Reactors [in Russian], PK IAÉ CEV, Moscow (1974), p. 108.
2. G. I. Marchuk, Methods of Calculation of Nuclear Reactors [in Russian], Gosatomizdat (1961).

ANALYSIS OF SOLID LUBRICATING COATING BY PROTON-STIMULATED X RAYS

A. G. Strashinskii, G. K. Khomyakov, N. V. Serykh, I. T. Ostapenko, and R. V. Tarasov

UDC 539.1.074.55

In the preparation of products from refractory compounds such as borides, carbides, nitrides, etc. by hot pressing in graphite press-forms, use is frequently made of solid lubricating coatings, especially the refractory oxides Al_2O_3, BeO, ZrO_2, etc., which are deposited as ground powder from an aqueous suspension onto the walls of the press form and are baked onto graphite.

The purity of solid lubricating coatings has a significant effect on their properties. Moreover, impurity elements from the coating inevitably enter the product in the process of hot pressing and as a result the properties of the product to some extent depend on the quantity of impurity it receives from the lubricating coating. The chemical composition of the lubricating coatings employed must, therefore, be determined.

Proton-stimulated characteristic x rays can be used for elementary analysis of specimens of solid lubricating coatings [1]. In the given case specimens were irradiated with a 2.5-MeV proton beam for 10-30 min at a current of $\sim 10^{-8}$ A on the specimens. The energy resolution of the spectrometer was 270 eV with respect to the 6.4-keV line. The experimental technique was described earlier in [2-4]. The specimens of lubricant (Table 1) were in the form of plates of thickness greater than the proton range. Polyvinyl alcohol was used as the binder.

The instrumental line profile was used in the analysis of the spectra obtained. No allowance was made for the dependence of the line width on the energy of the x-ray quanta. A linear approximation of the background lines was carried out in the region of the peak analyzed.

The magnitude of the useful signal N_S at the characteristic radiation peak is the difference of two quantities

TABLE 1. Materials Studied

Solid lubricating coating	Grade, GOST, TU
Al_2O_3	MRTU-6-09 No. 2046-64 (AP)
ZrO_2	VTU UKhKP-16-59 (pure)
BN	STU 71-341-65
Natural graphite	MRTU-6-09-4004-67 (pure)
Aquadag	V-O, GOST 5245-50

TABLE 2. Results of Analysis of Specimens Studied

Substance	Impurity content, mass %										
	Cl	K	Ca	Ti	Cr	Fe	Cu	Zr	Ta	W	Pb
Al_2O_3	$5.6 \cdot 10^{-2} \pm 5\%$	—	$5.5 \cdot 10^{-3} \pm 10.5\%$	$1.9 \cdot 10^{-1} \pm 2.3\%$	—	$3.2 \cdot 10^{-2} \pm 6.4\%$	—	$3.8 \cdot 10^{-2} \pm 7\%$	—	—	—
ZrO_2	—	$2.3 \cdot 10^{-1} \pm 3.6\%$	$3.5 \cdot 10^{-1} \pm 2.7\%$	—	—	$7.7 \cdot 10^{-2} \pm 5\%$	—	—	$1.4 \cdot 10^{-2} \pm 4\%$	—	—
BN	—	—	$5.3 \cdot 10^{-2} \pm 2.3\%$	$1.5 \cdot 10^{-2} \pm 6\%$	$5.6 \cdot 10^{-2} \pm 4.2\%$	$1.6 \cdot 10^{-1} \pm 3\%$	—	$5.8 \cdot 10^{-1} \pm 8.3\%$	—	—	—
Natural graphite	$1.1 \cdot 10^{-1} \pm 2.7\%$	$5.5 \cdot 10^{-2} \pm 2.2\%$	$1.2 \cdot 10^{-1} \pm 2.5\%$	—	—	$4.7 \cdot 10^{-1} \pm 2.7\%$	$2.8 \cdot 10^{-3} \pm 28\%$	—	—	$2.8 \cdot 10^{-3} \pm 29\%$	$6 \cdot 10^{-4} \pm 40\%$
Aquadag	$4.8 \cdot 10^{-1} \pm 2.1\%$		$9.5 \cdot 10^{-2} \pm 2\%$	$2.3 \cdot 10^{-3} \pm 17\%$	$3.4 \cdot 10^{-3} \pm 16\%$	$2.4 \cdot 10^{-1} \pm 2.5\%$	—	$1.7 \cdot 10^{-2} \pm 50\%$	—	$9.6 \cdot 10^{-2} \pm 5\%$	$4.3 \cdot 10^{-3} \pm 36\%$

Translated from Atomnaya Énergiya, Vol. 42, No. 4, pp. 329-331, April, 1977. Original article submitted August 11, 1976.

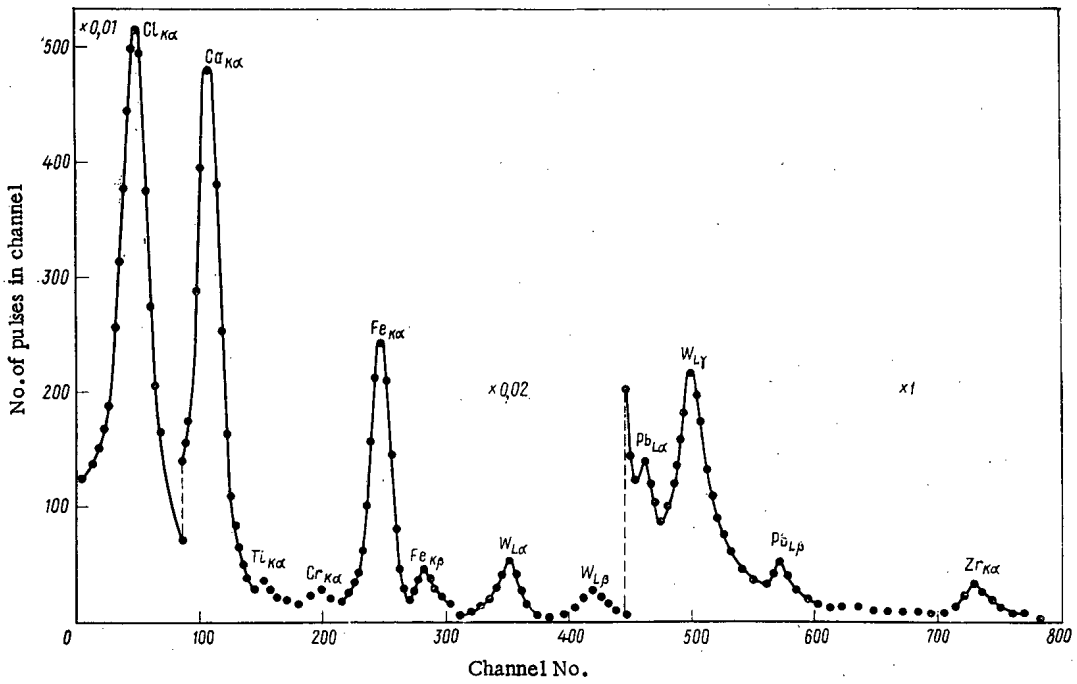

Fig. 1. Spectrum of x-ray radiation from elements detected in Aquadag.

$$N_s = N_{s+b} - N_b$$

where N_{s+b} is the total number of counts in the characteristic radiation peak and N_b is the number of background counts under the given peak.

The relative error of an individual measurement was calculated from the formula

$$\varepsilon_s = \frac{\sqrt{N_{s+b} + N_b}}{N_{s+b} - N_b} \cdot 100\%.$$

Reference spectra from copper vacuum-evaporated onto mica were used in the quantitative determination of the impurity [3]. In this case the relative error was

$$\varepsilon_s = \sqrt{\varepsilon_{obs}^2 + \varepsilon_{ref}^2} \cdot 100\%.$$

Table 2 lists the results of single analyses of five specimens of solid lubricating coatings (confidence coefficient 95%). The statistical errors and the error of determining the quantity of substance in the reference standard make the principal contribution to the total error, especially in those cases when the impurity content in the specimen lies at the limit of sensitivity of the method.

Figure 1 shows the spectrum of the x-ray radiation from elements detected in Aquadag. It must be noted that in some spectra it is not possible to isolate weak lines which lie in the range of the continuous retarding background and near intensive lines of other elements. Therefore, it is difficult to say anything about the presence of titanium and chromium in natural graphite, since their weak lines are obscured by intensive peaks from calcium and iron. Moreover, natural graphite evidently has traces of molybdenum (no more than 10^{-5} mass %), i.e., at the limit of the sensitivity of the method. Indium may be present in such quantity in the analyzed boron nitride. The graphite impurity, which is always present in zirconium with a content of 10^{-2}-10^{-3} mass %, cannot be detected in an analysis of ZrO_2 with a high tantalum content. The difference between the energy of the tantalum and hafnium L_α lines is 250 eV and it was therefore not possible to separate the weak hafnium line near the intense tantalum line.

Improving the spectrometer's energy resolution by 150-200 eV allows more precise impurity detection.

LITERATURE CITED

1. F. Folkmann et al., Nucl. Inst. Methods, 119, 117 (1974).
2. A. G. Strashinskii et al., At. Energ., 36, No. 5, 401 (1974).
3. A. G. Strashinskii et al., At. Energ., 39, No. 4, 283 (1975).
4. G. K. Khomyakov et al., Prib. Tekh. Eksp., No. 2, 139 (1975).

NONSTATIONARY DISTRIBUTION FUNCTIONS OF PARTICLES RETARDED IN MATTER

Yu. A. Medvedev and E. V. Metelkin

UDC 621.039.512.4

A method of calculating a nonstationary distribution function has been presented in [1]. Instead of the actual energy spectrum of particles scattered in an individual collision, about which very little theoretical and experimental information is available, the method uses certain measured energy moments of that spectrum. The dependence of these moments on the energy was not specified in the process of solution and the final result is valid for any form of this dependence. The expression from [1] for the distribution function can, therefore, be used to describe elastic moderation of neutrons with allowance for the thermal motion of nuclei of the medium and also to describe moderation with inelastic processes. In this case the following conditions [1] should be satisfied: $\Delta(E) \ll E$ and $\gamma(E) \ll \nu(E)$, where $\Delta(E)$ is the mean energy loss in one collision; $\gamma(E)$ is the frequency of collisions accompanied by absorption; and $\nu(E)$ is the frequency of collisions of slowing-down particles, accompanied by scattering.

In calculating the distribution function in [1], use was made of only two independent energy moments of the spectrum of particles scattered in one collision.

The present paper generalizes the method presented in [1] into one which takes account of the effect independent higher-order energy moments have on the distribution function of slowing-down particles.

How particles from a pulsed, monoenergetic source uniformly distributed with respect to space slow down in a homogeneous medium is described by the Boltzmann kinetic equation [2]:

$$\partial f(E, t)/dt + [\nu(E) + \gamma(E)] f(E, t) = \int_0^\infty \nu(E') P(E' \to E) f(E', t)\, dE' + \delta(t)\,\delta(E - E^+). \tag{1}$$

Here, f(E, t)dE is the number of particles of energy E in the interval dE at the instant t; $P(E' \to E)$ is the probability that as a result of collision a slowing-down particle passes near E in a unit energy interval; E^+ is the energy of particles emitted by the source; and $\delta(x)$ is the Dirac delta function.

In solving Eq. (1), we use the following moments of the function $P(E' \to E)$:

$$b_n^n(E') = \int_0^\infty [E' - \Delta(E') - E]^n P(E' \to E)\, dE, \tag{2}$$

where

$$\Delta(E') = \int_0^\infty (E' - E) P(E' \to E)\, dE. \tag{3}$$

The function $P(E' \to E)$ can be recast into

$$P(E' \to E) = \frac{1}{2\pi} \int_{-\infty}^{\infty} dk P(E', k) \exp\{ik[E' - \Delta(E') - E]\}, \tag{4}$$

where

$$P(E', k) = \int_{-\infty}^{\infty} dE\, P(E' \to E) \exp\{-ik[E' - \Delta(E') - E]\}. \tag{5}$$

Translated from Atomnaya Énergiya, Vol. 42, No. 4, pp. 331-333, April, 1977. Original article submitted August 11, 1976.

Since it follows from Eqs. (5) and (2) that

$$b_n^n(E') = \frac{1}{(-i)^n} \frac{\partial^{(n)}}{\partial k^n} P(E', k)|_{k=0}, \tag{6}$$

the function P(E', k) can be expressed in terms of the moments b_n^n:

$$P(E', k) = \sum_{n=0}^{\infty} \frac{(-ik)^n}{n!} b_n^n(E'). \tag{7}$$

Equations (2) and (3) imply that $b_0^0 = 1$ and $b_1^1 = 0$.

Using Eqs. (4) and (7), we can rewrite the integral on the right-hand side of Eq. (1) as

$$\int_{-\infty}^{\infty} \nu(E') P(E' \to E) f(E', t)\, dE' = \frac{1}{2\pi} \int_{-\infty}^{\infty} dk \int_{-\infty}^{\infty} dE' \nu(E') f(E', t) \times$$

$$\times \exp\{ik[E' - \Delta(E') - E]\} \sum_{n=0}^{\infty} \frac{(-ik)^n}{n!} b_n^n(E'). \tag{8}$$

Expanding the functions on the right-hand side of Eq. (8) in a Taylor series about the point E_0, which is a root of the equation $E_0 - \Delta(E_0) - E = 0$, and substituting the resulting expressions into Eq. (8), we get

$$\int dE' \nu(E') P(E' \to E) f(E', t) = \sum_{m=0}^{\infty} \sum_{s=0}^{\infty} \sum_{q=0}^{\infty} \sum_{p=0}^{\infty} \frac{(m+s+p+2q)!}{m!s!q!(m+s+q+p)!} \times$$

$$\times \frac{C_{p,q}}{[1-(d\Delta/dE_0)^{m+s+p+2q+1}]} [\partial^{(m)}(\nu f)/\partial E_0^m] \frac{\partial^{(s)}}{\partial E_0^s} b_{m+s+p+q}^{m+s+p+q}, \tag{9}$$

where

$$C_{0q} = \left(\frac{1}{2} \frac{d^2\Delta}{dE_3^2}\right);$$

$$C_{p,q} = 2P(d^2\Delta/dE_0^2) \sum_{k=1}^{p} (kq - p + k)(d^{(k+2)}\Delta/dE^{k+2})\, C_{p-k} \frac{1}{(k+2)!}; \quad p \geqslant 1.$$

Suppose that there is no absorption of particles during the slowing down, i.e., suppose that $\gamma = 0$. The solution of Eq. (1) is found in the form [3, 1]:

$$f(E, t) = \exp\left\{\frac{1}{\eta} \varphi_-(E, t) + \varphi_0(E, t) + \ldots\right\}, \tag{10}$$

where η is an appropriate dimensionless small parameter [1].

When we use Eqs. (1), (9), and (10) and equate the terms of zero order in η, we get the following equation to define the function φ_-:

$$\frac{1}{\nu} \frac{\partial \varphi_-}{\partial t} \sum_{k=0}^{\infty} \frac{(-1)^k}{k!} \Delta^k \left(\frac{\partial \varphi_-}{\partial E}\right)^k + \sum_{k=1}^{\infty} \frac{(-1)^k}{k!} \Delta^k \left(\frac{\partial \varphi_-}{\partial E}\right)^k = \sum_{k=2}^{\infty} \frac{1}{k!} b_k^k \left(\frac{\partial \varphi_-}{\partial E}\right)^k. \tag{11}$$

Since particles are focused according to energy [3, 1] as they slow down, we seek the solution of Eq. (11) in the form

$$\varphi_-(E, t) = -\frac{K(t)}{2}\left[\frac{\varepsilon_m(t)}{E} - 1\right]^2 - \frac{L(t)}{3}\left[\frac{\varepsilon_m(t)}{E} - 1\right]^3 - \ldots \tag{12}$$

Repeating the procedure presented in detail in [1], we find that, as before, the functions ε_m and K are given by Eqs. (35) and (36) from [1], where we must now use the value of b_2^2 instead of b^2. The function L is given by Eq. (37) from [1], in which Q' should be replaced by

$$\tilde{Q}' = Q' - K^3(t)(b_3^3 \varepsilon_m / 6\varepsilon_m^3 \Delta), \tag{13}$$

and P' and Q' are given by the previous expressions from [1] in which, too, b_2^2 should be used instead of b^2.

With absorption, when we repeat the procedure presented in detail in [1], we find that the function φ_- is given by the expressions from [1] in which b^2 should be replaced by b_2^2 and the expression for the function L should have the appropriate correction (13).

The moments b_n^n for $n \geq 4$ do not enter the expression for the functions $\varepsilon_m(t)$, K(t), and L(t) and affect only the values of the subsequent terms in the series in Eq. (12) which are necessarily calculated in parallel

with the function φ_0 from Eq. (10). The latter function is of such an order of smallness that the procedure is quite involved.

Let us establish the relation between the expressions for the function $P(E' \to E)$ used in [1] and in the present paper. By Eq. (6) the function $P(E', k)$ can be written as

$$P(E', k) = \exp\left\{\sum_{n=2}^{\infty} \frac{(-ik)^n}{n!} A_n(E')\right\}, \tag{14}$$

where $A_2 = b_2^2$; $A_3 = b_3^3$; $A_4 = b_4^4 - 3(b_2^2)^2$, etc.

On substituting Eq. (14) into Eq. (4), we get

$$P(E' \to E) = \frac{1}{2\pi} \int_{-\infty}^{\infty} dk \exp\left\{ik[E' - \Delta(E') - E] + \sum_{n=2}^{\infty} \frac{(-ik)^n}{n!} A_n(E')\right\}. \tag{15}$$

Setting $A_n = 0$, from Eq. (15) we find that in this case

$$P(E' \to E) = \delta[E' - \Delta(E') - E]. \tag{16}$$

If $A_n = 0$ for $n \geq 3$, i.e., if the higher-order moments (b_4^4, etc.) are expressed in terms of b_2^2, then it follows from Eq. (15) that

$$P(E' \to E) = \frac{1}{\sqrt{2\pi} b_2(E')} \exp\left\{-\frac{[E' - \Delta(E') - E]^2}{2b_2^2(E')}\right\}. \tag{17}$$

Equations (16) and (17) were used to solve Eq. (1) in [1].

Performing the calculations in accordance with Eqs. (2) and (3), we can easily establish that the moment b_3^3 is zero for elastic spherically-symmetric scattering in the center-of-mass system. Therefore, the function L(t) calculated in [1] by using Eq. (17) for this particular case was in agreement with the corresponding value obtained earlier in [1], where the specific form of the corresponding function $P(E' \to E)$ was used in the calculation.

The authors express their gratitude to M. V. Kazarnovskii for his valuable comments and useful discussion.

LITERATURE CITED

1. Yu. A. Medvedev et al., At. Energ., 38, No. 3, 156 (1975).
2. A. M. Weinberg and E. Wigner, Physical Theory of Neutron Chain Reactors, Univ. of Chicago Press (1958).
3. M. V. Kazarnovskii, Proceedings of the P. N. Lebedev Institute of Physics, Academy of Sciences of the USSR, 11, 176 (1959).

ENERGY LOSSES OF SLOW IONS IN ORGANIC MEDIUM FOR ELASTIC NUCLEAR COLLISIONS

S. P. Kapchigashev and V. V. Duba

UDC 539.1

At present we know of two sets of experimental data which require detailed consideration of the energy exchange of heavy charged particles moving in a medium at low velocity ($V \leq V_0 = 2.183 \cdot 10^8$ cm/sec): the increase in the mean ionization energy in gases as the particle velocity decreases [1-3]; the higher sensitivity of biomolecules [4, 5] and polymers to radiation damage [6, 7] by slow heavy particles than to damage by energetic particles ($V > V_0$).

Such effects are due to the fact that besides ionization and excitation of atoms and molecules of the medium, a significant role in energy exchange by slow ions is played by processes of atomic and molecular displacement as a result of elastic nuclear collisions. Elastic processes should play an important role in radiation damage to biological and chemical systems since atomic displacement may lead to a direct and more sensitive change in the structure of macromolecules than ionization and excitation.

The present paper calculates the energy of protons and C, N, and O ions expended on elastic nuclear collisions when the particles are stopped in nitrogen and tissue-equivalent gas. This energy is determined from the formula

$$g(E) = \frac{I}{E} \int_0^E S_n(E')\, dE' / [S_n(E') + S_e(E')],$$

where $S_n(E')$ and $S_e(E')$ are the specific energy losses for elastic processes (scattering in the field of atomic nuclei) and inelastic processes (interaction with atomic electrons) [8, 9], respectively, for particles of energy E'.

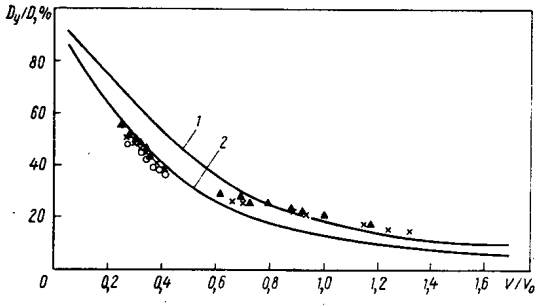

Fig. 1

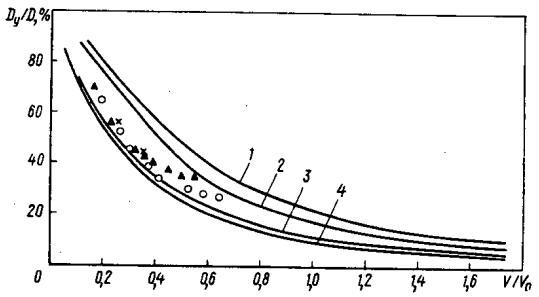

Fig. 2

Fig. 1. Fraction of nitrogen-ion energy expended on elastic nuclear collisions, D_y/D, in nitrogen and the value $[W(E) - W_\beta]/W(E)$: 1, 2) $= D_y/D$ in the $f_1(E)$ and $f_5(E)$ approximations, respectively; ○, ×, ▲) $[W(E) - W_\beta]/W(E)$ for C, N, and O ions in nitrogen [1], respectively.

Fig. 2. Fraction of carbon and oxygen ion energy expended on elastic nuclear collisions, D_y/D, in tissue-equivalent gas and the value $[W(E) - W_\beta]/W(E)$: 1, 3) oxygen; 2, 4) carbon D_y/D in the $f_1(E)$ and $f_5(E)$ approximations; ○, ▲) $[W(E) - W_\beta]/W(E)$ for C and O, respectively, in methane; ×) $[W(E) - W_\beta]/W(E)$ for oxygen ions in tissue-equivalent gas.

Translated from Atomnaya Énergiya, Vol. 42, No. 4, pp. 333-334, April, 1977. Original article submitted September 14, 1976.

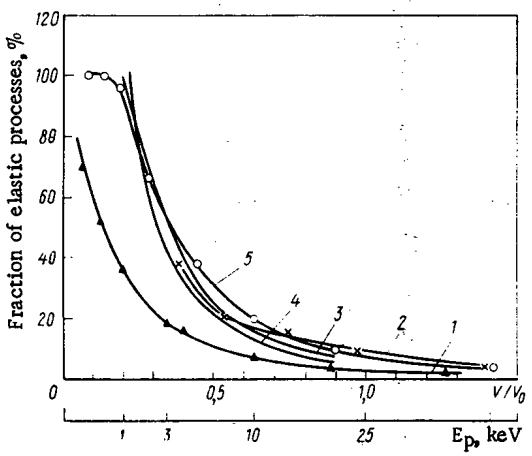

Fig. 3. Fraction of proton energy expended on elastic nuclear collisions, D_y/D, in tissue-equivalent gas, and value of $[W(E) - W_\beta]/W(E)$: 1) calculation [8]; 2) $[W(E) - W_\beta]/W(E)$ [3]; 3) calculation based on data on dE/dX [11]; 4) calculation based on model in [12]; 5) D_y/D [13].

Besides using the theory [8], we found the value for protons as follows: $S_n(E')$ was determined according to the Bohr theory [10] and $S_e(E')$ was taken from [11], where the energy lost by particles for electron collisions was found from the experimental data on the dependence of the effective charge of an ion on its energy. The energy expended by protons on elastic collisions in tissue-equivalent gas was also calculated by a model [12] according to which this energy is numerically equal to the mass of the impinging ion, in keV.

Figures 1 and 2 present the results of calculations of the energy lost in elastic processes when nitrogen ions are slowed down in nitrogen (Fig. 1) and carbon and oxygen ions in tissue-equivalent gas (Fig. 2). Curves 1 in Fig. 1 and 1 and 2 in Fig. 2 were obtained with the assumption that secondary, tertiary, and other recoil atoms lose energy in the medium only in elastic processes [$f_1(E)$ approximation]. Corrections for the probability of energy loss by recoil atoms in inelastic processes were introduced into the f_5 approximation by the method described in [1].

It is seen from the figures that the fraction of energy (D_y/D) that heavy ions expend in media on elastic nuclear collisions is in good agreement with the fraction by which the mean ionization energy of these ions W(E) exceeds the ionization energy of electrons W_β for the range $V/V_0 < 0.4$-0.6. When the ion velocity is above $0.6\ V_0$, the value of D_y/D falls off more rapidly than $[W(E) - W_\beta]/W(E)$ does. It follows from Fig. 3 that the values of D_y/D calculated according to the model in [8] differ significantly from the data on the fraction by which the ionization energy is exceeded as found in [3] and other papers. Yet the results of calculations based on the Bohr theory and [11], as well as those of [13], agree with $[W(E) - W_\beta]/W(E)$, where the scattering of protons on hydrogen atoms was approximated by the Coulomb potential, just as the interaction of heavy atoms was described by the Thomas – Fermi potential in the theory in [8].

Thus, as the velocity of ions decreases, the energy lost on elastic nuclear collisions rises sharply. The rise in the mean ionization energy as the ion velocity decreases is due to the energy lost on elastic scattering for $V/V_0 < 0.4$-0.6. The small difference between D_y/D and $[W(E) - W_\beta]/W(E)$ for $V/V_0 > 0.6$ is evidently due to the nature of the velocity dependence of the energy lost by ions on excitation of atoms and molecules of the medium.

LITERATURE CITED

1. J. Dennis, Rad. Eff., 8, 87 (1971).
2. J. MacDonald and G. Sidenius, Phys. Letters, 28A, 543 (1969).
3. B. Leonard and J. Boring, Rad. Res., 55, 1 (1973).
4. H. Jung, Z. Naturforsch., 20, 8 (1965).
5. J. Sutcliffe and D. Watt, in: Proceedings of the Fourth Symposium on Microdosimetry, Italy (1973), p. 477.
6. S. P. Kapchigashev et al., in: Problems of Microdosimetry [in Russian], V. I. Ivanova (editor), No. 2, Atomizdat, Moscow (1974), p. 57.

7. S. P. Kapchigashev et al., At. Energ., 38, No. 1, 50 (1975).
8. J. Lindhard et al., Kgl. Danske Vid. Selskab. Matfys. Medd., 33, No. 10, 1 (1963).
9. V. V. Yudin, Dokl. Akad. Nauk SSSR, 207, 325 (1972).
10. W. Snyder and J. Neufeld, Rad. Res., 6, 67 (1957).
11. J. Neufeld and V. Snyder, in: Proceedings of the Symposium on Particular Problems of Dosimetry [in Russian], Gosatomizdat, Moscow (1962), p. 33.
12. F. Seitz, Radiation Effects in Solids [Russian translation], IL, Moscow (1960).
13. V. A. Naumov et al., Radiobiologiya, 15, No. 2, 233 (1975).

DETERMINATION OF THE EFFECTIVE ENERGY CUT-OFF OF GADOLINIUM AND CADMIUM

I. R. Merkushev

UDC 621.039.51

The cadmium cover and the methodology of the cadmium ratio is usually used to suppress activation due to thermal neutrons [1]. The methodology of the cadmium ratio cannot be used to study the neutron flux in high-temperature nuclear reactors where as a cover a foil material must be used which has a high cross section for thermal neutrons and a melting point higher than cadmium (e.g., for gadolinium $T_m = 1320°C$).

In this work are presented the results of calculations and experiments on the determination of the effective energy cut-off of gadolinium as related to the use of a gadolinium cover and the methodology of the gadolinium ratio. Calculations for a cadmium cover were also made and were compared with literature values. The effective energy cut-off can be represented in the form

$$E_{co}=4\left\{\int_0^\infty \Delta\left(\frac{E}{kT}\right)E_2\left(\mu_a[E]\delta\right)\frac{dE}{E^{3/2}}\right\}^{-2},$$

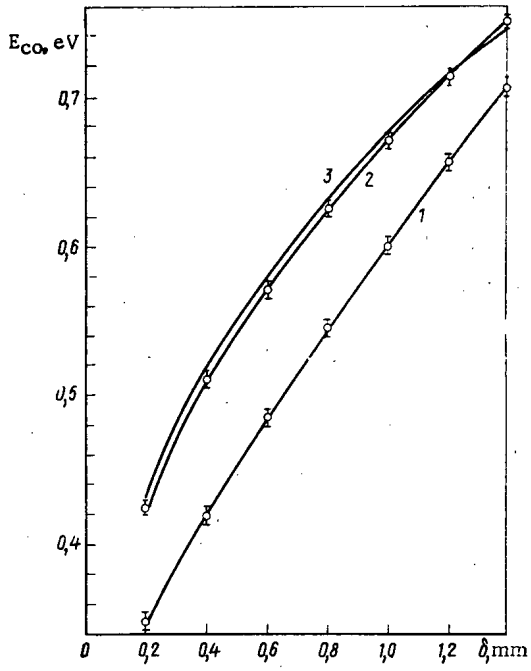

Fig. 1. Dependence of the effective energy cut-off of gadolinium (1) and cadmium (2) on the cover thickness; 3) results of [1] for cadmium.

Translated from Atomnaya Énergiya, Vol. 42, No. 4, p. 335, April, 1977. Original article submitted December 1, 1976.

where $\Delta(E/kT)$ is a function of the transition region of neutron energy which has the same shape for the majority of real moderations, k is Boltzmann's constant, T = 293.6°K (20.4°C), kT = 0.025 eV, E_2 is Plachek's second-order function, $\mu_a(\tilde{E})$ is the macroscopic cross section, and δ is the thickness of the cover foil.

To calculate Plachek's function and the effective energy cut-off, a program was composed, written in FORTRAN (monitoring system DUBNA) [2], and solved on the BÉSM-6 computer. The results of calculations of the dependence of the effective energy cut-off of thin 1/V gadolinium and cadmium absorbers, in an isotropic neutron field, on the thickness of the corresponding cover foils are presented in Fig. 1.

The error for the determination of the effective energy cut-off reaches 5% and is basically due to the errors connected with the cross sections of gadolinium and cadmium. The ratio of energy cut-offs of gadolinium to cadmium changes from 1.20 ± 0.01 to 1.05 ± 0.05 for cover thicknesses varying from 0.2-1.4 mm.

To check the results of calculations experimentally, the gold foils were irradiated in the F-1 reactor at the I. V. Kurchatov Atomic Energy Institute using known thermal neutron fields. The thickness of the cadmium and gadolinium cover was 0.5 and 0.8 mm, respectively. The errors connected with the activity measurements and with the thermal neutron flux density were equal to 3 and 5%, respectively. The values of the neutron flux density, $(8.4 \pm 0.4) \cdot 10^9$ neutrons/(cm^2 · sec), determined by the gadolinium and cadmium ratios and by the monitor, are in a satisfactory agreement, considering the experimental errors [3]. The energy cut-off for a 0.5-mm-thick cadmium shield is equal to the energy cut-off of a 0.8-mm-thick gadolinium foil, $E_{co}^{Cd} = E_{co}^{Gd} = 0.54$ eV.

Consequently, the experiments with gold foils have confirmed the correctness of the theoretical calculations for gadolinium and cadmium.

LITERATURE CITED

1. K. Beckurts and K. Wirtz, Neutron Physics, Springer-Verlag (1964).
2. Program Library in FORTRAN, Appendix 1 to the Manual for the BÉSM-6 Computer [in Russian], Izd. Inst. At. Energ., Moscow (1971).
3. Document on Measuring Devises Based on the F-1 Reactor [in Russian], VNIIFTRI (1973).

AUTOMATIC EIGHT-CHANNEL UNIT FOR RECORDING TRACER ACTIVITY

S. S. Volkov, V. P. Koroleva,
N. I. Kurakov, E. B. Martynov,
and L. A. Chernov

UDC 539.1.074:681.32

It is well known that the relative activation method is used extensively in the study of nuclear reactors and in a number of other fields such as biology, chemistry, geology, dosimetry, and nuclear physics. In these cases it is necessary to measure large batches of radioactive tracers and it is the efficiency in work with such tracers that in large measure determines the recording capabilities of the unit.

The most common Soviet-manufactured detector apparatus are one- and two-channel systems [1-3] recording the activity of irradiated specimens (either in sequence of two at a time), one of which is a standard specimen. Multichannel systems which have been proposed [4] require continuous monitoring and allowance for the differences in channel efficiency.

The objective of the present paper is to create a multichannel unit for efficient measurement of the activity of specimens in a run of physical measurements in critical assemblies. The principal feature of the

Translated fron Atomnaya Énergiya, Vol. 42, No. 4, pp. 336-337, April, 1977. Original article submitted November 3, 1976.

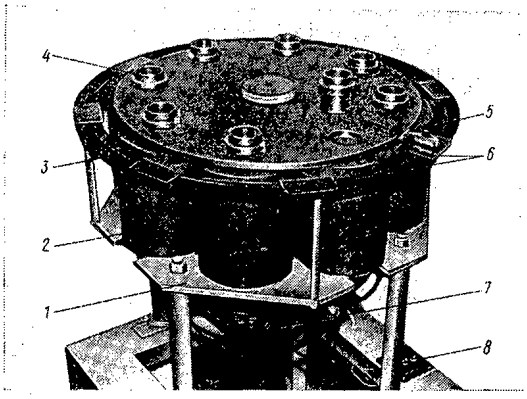

Fig. 1. General view of automatic unit: 1) fixed pedestal; 2) scintillation detector in lead shield; 3) turntable; 4) specimen holder; 5) magnet; 6) cutoff switch; 7) mechanical drive with maltese mechanism; 8) turntable rotation angle selector.

unit developed is its capability to measure the activity of eight tracers at one time without allowance for the difference in detection-channel efficiency and without introducing corrections for radioactive decay. This is achieved by rotating the tracers above the detectors to effect a number of rearrangements so that the activity of each specimen is measured by all detectors in succession. The operating principle of the unit [5] can be demonstrated by referring to the example of measurement of the activity of two tracers (one of them being the monitor M) in a two-channel system. After two cycles of measurements we have an experimental relation between the activity of the specimen and that of the monitor:

$$a_1'/a_M' = \sqrt{a_1\varepsilon_A\theta_1 a_1\varepsilon_B\theta_2/a_M\varepsilon_B\theta_1 a_M\varepsilon_A\theta_2} = a_1/a_M, \quad (1)$$

where a_1 and a_M are the activities of the tracers at the time t_0; ε_A and ε_B are the registration efficiencies of counters A and B; θ_1 and θ_2 are factors taking account of the radioactive decay in the time t_0 up to the beginning of the measurement and during it. It is seen from Eq. (1) that the registration efficiencies and the time factors cancel out. The expression for the ratio of the activity of specimens to that of the monitor in the eight-channel unit is of the form

$$a_i/a_M = \sqrt[8]{N_{i1}N_{i2}\ldots N_{i8}/N_{M1}N_{M2}\ldots N_{M8}}, \quad (2)$$

where i is the specimen number, i = 1-8 (i = 1 is the monitor); $N_{i(1-8)}$ and $N_{M(1-8)}$ are the recorded counts from the i-th specimen or from the monitor M in detectors 1-8. The number of channels (8-10) in units of this kind is optimal from the point of view of facility of operation, satisfactory cycle duration with low loss of radiation intensity per cycle, and provision of a sufficient volume of information (eight measurements for each specimen in each cycle).

Figure 1 presents a general view of the unit which comprises the following basic subassemblies. The mechanical subassembly consists of a fixed pedestal on which are mounted eight detectors spaced uniformly 45° apart on a circle of diameter 40 cm, and a turntable for holders with active specimens. Also mounted on the fixed pedestal is the mechanical drive (electric motor with reducing gear) which is connected to the turntable by means of a maltese mechanism. The latter ensures that the turntable can be put precisely in eight positions. Moreover, with its sinusoidal law of variation of the angular velocity the maltese mechanism helps stop the turntable smoothly and reduces its vibrations to a minimum.

The eight detectors are scintillation counters (FÉU-13 photomultipliers) with NaI(Tl) crystal (40 mm diameter × 40 mm height) for recording gamma quanta or with a stilbene crystal (40 × 10 mm) for beta particles. The detectors are shielded by lead cylinders with walls ~35 mm thick. To reduce the background lead blocks are installed on the turntable around the specimen holders. Such shielding is sufficient to eliminate the effect of the activity of neighboring specimens (a specimen activity corresponding to a counting rate of $5 \cdot 10^3$ counts/sec practically does not change the background in the neighboring specimen container).

A "Pechat'" rack (built by the Central Intermediate Production Shop, Joint Institute of Nuclear Research, Dubna) functions as an "intermediate memory." It contains 10 independent scaling channels, two of which are reserves. The information from the detectors is accumulated and stored in the Pechat' rack in the form of

pulses. The rack parameters are: capacity of each channel, 2^{18} pulses; speed, ~0.1 sec; and information-transfer time to the next measuring complex, ~200 μsec.

Once it has been collected from the Pechat' rack, the information is transferred to an immediate-access magnetic memory of the measuring complex [6], from which it is transferred onto perforated tape for computer processing and also to a teletype for checking.

The remote-control panel controls the automatic operation of the turntable with specimens, timer, and rack. In one complete 360° rotation (one cycle) of the turntable with specimens we obtain 64 numbers of seven ratios, normalized to the monitor.

Let us consider the order in which the automatic unit operates. When the active specimens have been placed in the holders with the turntable in the initial position, the START button on the remote control panel switches on the scalers of the Pechat' rack and the timer. After the registration time, set by the timer, the accumulation of information ceases. A timer signal about the completion of the count proceeds to the motor of the turntable which changes the position of the specimens by a specified angle. The unit has provision for rotating the turntable through various angles (45, 90, and 180°) for operation with fewer specimens. During the time that the specimens are being moved (1-2 sec) the information from the Pechat' rack is recorded in the immediate-access memory of the measuring complex. As soon as the turntable has rotated through the specified angle, the timer and the rack are started automatically with subsequent recording of the results in the immediate-access memory. Such motions of the turntable are continued automatically until it has rotated 360°. To repeat the cycle it is sufficient to press the START button on the control panel. Upon completion of the required number of cycles, the operator changes the specimens. This multichannel unit has a time advantage of roughly tenfold in comparison with two-channel systems.

LITERATURE CITED

1. G. Ya. Vasil'ev et al., in: Metrology of Neutron Radiation in Reactors and Accelerators [in Russian], Vol. 1, Izd. Standartov, Moscow (1972), p. 259.
2. E. M. Lobanov, P. I. Chalov, and U. Mamyrov, At. Energ., 21, No. 3, 304 (1966).
3. B. G. Egiazarov et al., At. Energ., 21, No. 3, 252 (1966).
4. A. M. Gurevich and N. N. Konovalov, Prib. Tekh. Éksp., No. 5, 263 (1975).
5. Yu. M. Shalashov, At. Energ., 18, No. 3, 282 (1965).
6. L. A. Matalin, Zh. Narai, and S. I. Chubarov, Methods of Data Logging and Processing in Nuclear Physics and Engineering [in Russian], Atomizdat, Moscow (1968), p. 435.

THE FINE STRUCTURE OF THE FISSION YIELDS OF HEAVY NUCLEI

K. A. Pietrzak (Petrzhak), E. V. Platygina, and V. F. Teplykh

UDC 539.173.3:546.791.3

The fine structure of the mass-distribution curve of products, i.e., the anomalous deviation of the separate fission yields from the smooth relation, is a characteristic feature of the low-energy fission of most nuclei of the actinide region. Since the discovery of this effect, many hypotheses have been advanced to explain these anomalies [1-5]. At the present time it is generally assumed that the source of the fine structure lies in the filled shells of the fission fragments, i.e., that the formation of fission fragments with the magic number of nucleons is preferential.

In the present paper the mass-spectrometric method is used to measure the relative yield of xenon isotopes in the region A = 131-135 amu during the fission of certain nuclei by 14-MeV neutrons and bremsstrahlung γ quanta with a maximum energy of 15 and 20 MeV for the accelerated electrons. The relative yield has been renormalized to the absolute yield wherever some sort of information was available about the absolute fission yield in this range of masses (Table 1).

The results obtained indicate that the fine structure is conserved with a maximum at A = 134 amu to an excitation energy $E^* \sim 21$ MeV of the fissioning nucleus for ^{235}U and ^{239}Pu and does not confirm the data of the

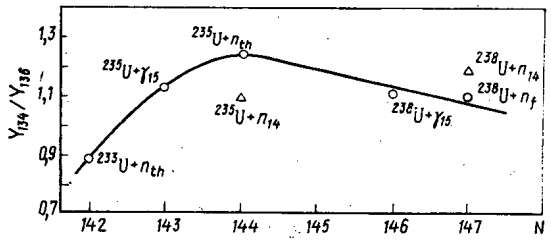

Fig. 1. Dependence of fine-structure quantity Y_{134}/Y_{136} on number of neutrons in fissioning nucleus for uranium isotopes: ○) for fissionable nucleus at $E^* = 6$-10 MeV [7, 10, and present paper]; △) for compound nucleus at $E^* = 19$-21 MeV [8 and the present paper].

TABLE 1. Yield of Xenon Isotopes in Fission of Heavy Nuclei by 14-MeV Neutrons and γ Quanta

Fissioning nucleus	Energy, MeV	Isotopic composition, %				Y_{134}/Y_{136}
		^{131}Xe	^{132}Xe	^{134}Xe	^{136}Xe	
$^{235}U+n$	14,7	20,75±0,3 4,03	25,05±0,4 4,86	28,35±0,4 5,51	25,85±0,4 5,02	1,10
$^{235}U+\gamma$	15	17,65±0,35	23,1±0,45	31,45±0,6	27,8±0,55	1,18
$^{239}Pu+n$	14,7	20,5±0,3 3,77	24,9±0,3 4,58	28,5±0,3 5,24	25,75±0,3 4,74	1,12
$^{239}Pu+\gamma$	20	20,75±0,15	25,00±0,25	29,2±0,4	24,15±0,2	1,21
$^{239}Pu+\gamma$	15	21,85±0,15	25,65±0,1	27,3±0,15	25,2±0,15	1,08
$^{232}Th+n$	14,7	14,15±0,3 2,05	18,8±0,3 2,70	28,7±0,75 4,73	28,25±0,4 5,50	0,75

Translated from Atomnaya Énergiya, Vol. 42, No. 4, pp. 337-338, April, 1977. Original article submitted November 11, 1976.

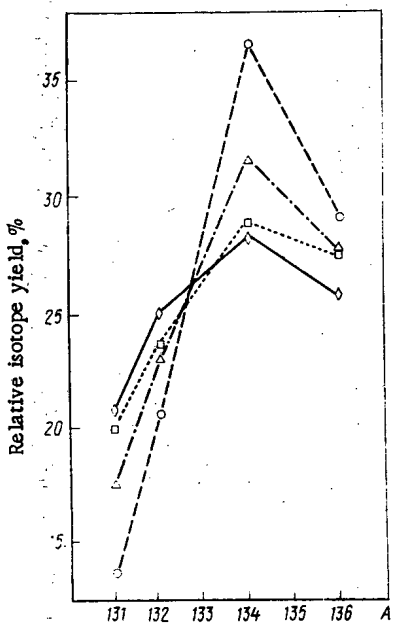

Fig. 2. Mass spectra of xenon isotopes during fission of ^{235}U by neutrons and γ quanta: ○) $^{235}U + n_{th}$; ◇) $^{235}U + n_{14}$; △) $^{235}U + h\nu_{15}$; □) $^{235}U + h\nu_{20}$.

radiochemical measurements of Broom about the existence of a structure when ^{232}Th is fissioned by 14-MeV neutrons [6].

Analysis of the experimental results on photofission and the data in the literature [7] on fission with low-energy neutrons revealed that the fine-structure quantity (Y_{134}/Y_{136}) depends on the number of neutrons in the compound nucleus. Thus, in the case of uranium isotopes the fine structure increases as we approach the fissioning nucleus with 144 neutrons (Fig. 1). On the basis of this relation, obviously, we can explain the observed variations in the fine structure of the mass spectra of fission fragments as the excitation energy of the fissioning nucleus increases. According to estimates by Ford and Lechman [9], the fission of ^{239}U with the preliminary emission of one neutron (n, nf) is observed even at a compound-nucleus excitation of ~12 MeV, and at an energy exceeding 13.5 MeV is comparable with high-temperature fission. The contribution of the (n, 2nf) reaction becomes significant at $E^* > 20$ MeV and with an excitation of ~23 MeV the (n, f), (n, nf), and (n, 2nf) fission cross sections are equally probable.

From these positions it is possible to explain the variation in the fine structure as the excitation energy of the fissioning ^{239}U atom increases [8]. If emissive fission occurs, one may expect the fine structure to be conserved or even to increase somewhat as the excitation of this nucleus increases. In this case there may be fission of ^{237}U and ^{238}U nuclei for which, in accordance with the relation given, the fine structure is greater (see Fig. 1).

The observed decrease in the fine structure for fission of ^{235}U by 14-MeV neutrons is in good agreement with the hypothesis adopted. There should be significant contribution from the fission of ^{235}U nuclei which have less structure. This is confirmed by the similarity of the mass spectra in the mass range A = 131-136 amu during fission of ^{235}U by γ quanta with a maximum energy of 20 MeV (the mean excitation energy of the fissioning nucleus in this case is ~12.5 MeV) and by 14.7-MeV neutrons (Fig. 2).

LITERATURE CITED

1. D. Wites et al., Can. J. Phys., 31, 419 (1963).
2. L. Glendenin, Phys. Rev., 75, 337 (1949).
3. A. Wahl, Phys. Rev., 99, 730 (1955).
4. H. Farrar and R. Tomlinson, Can. J. Phys., 40, No. 8, 943 (1962).
5. J. Terrell, Phys. Rev., 127, 880 (1962).
6. K. Broom, Phys. Rev., 133, No. 4B, 874 (1964).
7. A. Walker, in: Proc. "Panel fission product nucl. data," Bologna, Nov. 26-30 (1973), Rev. paper 11a, p. 285.
8. K. A. Pietrzak (Petrzhak), V. F. Teplykh, and M. G. Pan'yan, Yad. Fiz., 11, No. 6, 1178 (1970).
9. G. Ford and R. Lechman, Phys. Rev., 137, B826 (1965).
10. K. A. Pietrzak (Petrzhak) et al., Yad. Fiz., 14, No. 5, 950 (1971).

HYDRAULIC RESISTANCE TO FORCED TWO-PHASE FLOW OF HELIUM IN NARROW CHANNELS

V. I. Deev, Yu. V. Gordeev,
A. I. Pridantsev, V. I. Petrovichev,
and V. V. Arkhipov

UDC 621.039.534.36:532.529:532.58

Large superconducting magnets with forced circulation of coolant through hollow combined conductors have a number of advantages over magnets immersed directly in a bath of liquid helium [1]. In choosing the parameters of the coolant and the cryogenic equipment in the first case, it is important to make a correct estimate of the hydraulic resistance to the flow of helium in the narrow channels of the cooling system. The development of methods to calculate the pressure loss in a single-phase isothermal flow has been adequate. However, the known methods of determining the hydraulic resistance for single-phase flows with significantly varying properties and for two-phase flows are based on approximate models or are empirical. The calculational relations recommended for these cases are based mainly on experimental data for ordinary (noncryogenic) liquids. Data on the hydraulic resistance in a two-phase flow of helium [2, 3] show that the pressure drop calculated using a homogeneous model of the flow may differ significantly from the experimental results.

The present work gives the results of measurements of hydraulic resistance in forced upward motion of a two-phase flow of helium in a vertical stainless-steel tube of internal diameter 1.6 mm and total length around 750 mm.

The motion of the working medium along the tube was produced by discharge under pressure of liquid helium from a liquid cryostat of volume around 35 liters. After total vaporization of the helium, it was heated to room temperature in the gaseous part of the loop, passed through the flow-rate measurement section, and fed to a gas holder. To eliminate oscillations of the flow due to hydrodynamic instability of the two-phase flow, the working-tube inlet was provided with a local resistance which could be adjusted within certain limits.

The pressure loss due to friction was investigated on an adiabatic portion of the tube, of length 259 mm. The pressure was regulated by means of an annular chamber, an aperture of diameter 0.4 mm communicating with the internal cavity of the tube. The measuring section was preceded by a heated section and a section of hydrodynamic stabilization of length 60 mm.

The pressure drop in the experimental tube was measured by a differential manometer of membrane type with an inductive transformer of motion into dc voltage. The inlet and outlet pressures were determined from the readings of manometers of the same type and sampling manometers. The helium flow rate was recorded by gas counters and a calibrated diaphragm. The helium temperature at the tube inlet was determined by a germanium resistance thermometer. The enthalpy at the inlet to the measuring section was changed by heating the flow in the preceding section. The current and voltage at the electrical heater and all the readings of temperature, pressure, and flow rate of the helium were transferred to tape by an automatic recording instrument.

To confirm that the chosen procedure is adequate for measuring and determining the hydraulic characteristics of an experimental channel with a flow of a single-phase medium, preliminary experiments were carried out for various gases (helium, argon, nitrogen) at room temperature and for helium at low temperature (liquid and superheated vapor). The Reynolds number in these experiments varied from 10^2 to $5 \cdot 10^5$. The dependence of the coefficient of hydraulic frictional resistance on the Reynolds number in laminar flow ($10^2 < \mathrm{Re} < 2.3 \cdot 10^3$) was in good agreement with Poiseuille's law. For turbulent flow ($\mathrm{Re} > 3 \cdot 10^3$), the experimental data were described by the Colbrook – White formula, which takes into account the effect of channel roughness

Translated from Atomnaya Énergiya, Vol. 42, No. 4, pp. 339-340, April, 1977. Original article submitted March 5, 1976.

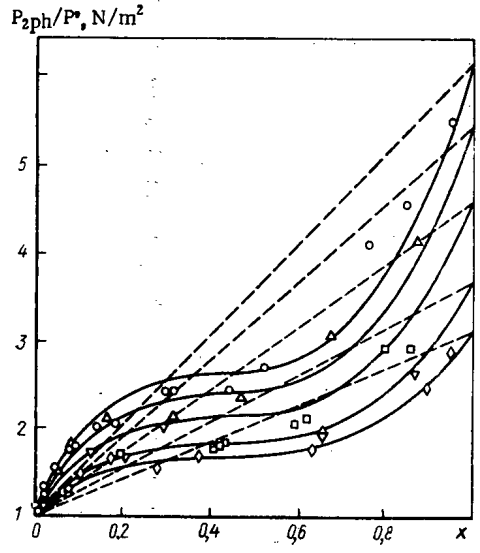

Fig. 1

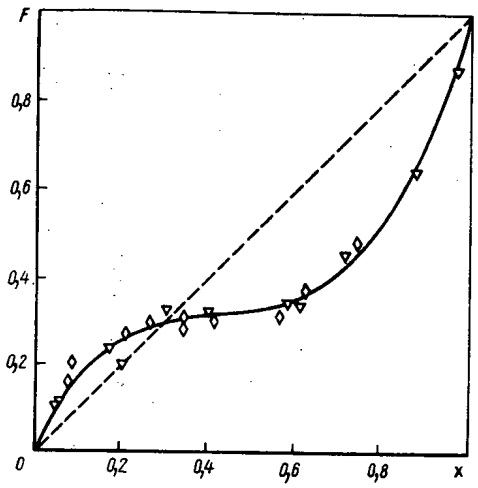

Fig. 2

Fig. 1. Effect of vapor content of two-phase flow on relative pressure drop due to friction: P, 10^{-5} N/m²; ○) 1; △) 1.2; □) 1.4; ▽) 1.6; ◇) 1.8; the dashed lines were calculated for a homogeneous mixture.

Fig. 2. The dependence of F on x for a two-phase flow of helium: ▽) $w\rho$ = 245 kg/m²·sec; ◇) 375; the dashed line was calculated for a homogeneous mixture.

on the coefficient of hydraulic resistance. Comparison of the experimental results with the Colbrook – White formula showed that the experimental tube has an equivalent roughness of 1 μ. In the intermediate region of Reynolds numbers ($3 \cdot 10^3 < Re < 2 \cdot 10^4$), the Blasius formula for smooth tubes also gives a good description of the experimental results (in this range of Re, the tube may be regarded as hydraulically smooth).

Experiments to determine the hydraulic resistance for two-phase flow of helium were carried out in series with the same values of the mass flow rate and pressure in the experimental tube but different values of the vapor content in the two-phase flow. The results covered a range of mass flow rates $w\rho$ = 100-400 kg/m²·sec, of pressure $P = (1\text{-}1.8) \cdot 10^5$ N/m², and of vapor content x = 0-1.

The mass vapor content in the flow was determined from the thermal-balance equation with the parameters of the helium at the tube inlet. The hydraulic frictional resistance was calculated as the difference between the total measured pressure drop at the measuring section and the hydrostatic pressure head. Since at present no data are available on the true volumetric vapor content in a two-phase flow of helium, the hydrostatic pressure head was calculated using the vapor content measured in the flow.

The curves in Fig. 1 show the ratio of the frictional pressure loss in a two-phase flow of helium ΔP_{2ph} to the pressure loss in a single-phase flow $\Delta P'$ as a function of the mass vapor content in the flow for a constant mass flow rate 170 kg/m²·sec and various pressures in the tube. The experimental data are seen to deviate from the results calculated for a homogeneous mixture in the intermediate range of vapor contents.

In the equations that are widely used in practice, the difference between the real pressure drop in a two-phase flow ΔP_{2ph} and that calculated for a homogeneous mixture ΔP_{hom} is taken into account by introducing in the Darcy – Weisbach formula a correction factor $\Psi = \Delta P_{2ph}/\Delta P_{hom}$ [4]. For vapor content x < 0.3, as follows from Fig. 1, $\Delta P_{2ph} > \Delta P_{hom}$ ($\Psi > 1$), while at higher vapor contents $\Delta P_{2ph} < \Delta P_{hom}$ ($\Psi < 1$).

Another method of representing experimental data on hydraulic resistance in a two-phase flow was proposed in [5]. This involves the function $F(x) = (\Delta P_{2ph} - \Delta P')/(\Delta P'' - \Delta P')$, where ΔP_{2ph} is the frictional pressure loss in a two-phase flow, while $\Delta P'$ and $\Delta P''$ are the frictional pressure losses for single-phase flow of liquid and vapor at the saturation line. It is evident that F = 0 when x = 0 and F = 1 when x = 1. If the hydrualic-resistance coefficient is constant, F(x) = x for a homogeneous mixture. It follows from Fig. 2 that the results of experiments for two values of the mass flow rate at a pressure $1.4 \cdot 10^5$ N/m² are described by a single function F(x), which is significantly different from the curve calculated for a homogeneous mixture.

Analysis of the complete set of experimental data in Fig. 2 shows that the dependence F(x) provides a good generalization of the experimental results for various values of mass flow rate and pressure. As a result the following equation, based on the definition of F(x) given above and the formula for single-phase flow, can be recommended for the calculation of the frictional resistance in a two-phase flow of helium in narrow channels

$$\Delta P_{2ph}=\xi' \frac{l}{d} \frac{(w\rho)^2}{2\rho'} \left\{1+F(x)\left[\frac{\xi''}{\xi'} \frac{\rho'}{\rho''}-1\right]\right\} \quad (1)$$

where l and d are the channel length and diameter; ρ' and ρ'' are the density of liquid and vapor at the saturation line; ξ' and ξ'' are the coefficients of hydraulic resistance of the given channel for a flow of only liquid or vapor with the total mass flow rate of the mixture. In practical calculations, the value of F(x) may be read from the graph in Fig. 2 for the appropriate value of the mass vapor content in the flow x. Comparison of results obtained from Eq. (1) and experiment shows that the discrepancy does not exceed ±15% over the whole range of parameter values investigated.

LITERATURE CITED

1. V. Keilin et al., Cryogenics, 10, No. 3, 224 (1970).
2. Cryogenics, 9, No. 1, 36 (1969).
3. A. De La Harpe et al., Adv. Cryog. Eng., 14, 170 (1969).
4. O. M. Baldina et al., Proceedings of the I. I. Polzunov Scientific-Research Institute for the Design and Planning of Boilers and Turbines (TsKTI), Rotary-Turbine-Construction Series [in Russian], No. 59, Leningrad (1965), p. 72.
5. V. Borishansky et al., Int. J. Heat Mass Transfer, 16, No. 6, 1073 (1973).

INFORMATION

FOURTH SESSION OF THE JOINT SOVIET – AMERICAN COMMISSION ON COOPERATION

V. A. Vasil'ev

The Fourth Session of the Joint Soviet – American Commission on Cooperation in the Peaceful Use of Nuclear Energy was held at Erevan during Dec. 7-9, 1976. The session heard reports from each side on cooperation in the following areas: controlled thermonuclear fusion, fast-breeder reactors, and the investigation of the fundamental properties of materials; the reports presented the main results of Soviet – American scientific – technical cooperation for 1976 and offered proposals from both sides for cooperative projects in 1977. In addition, there was discussion at the session of the possibility of extending cooperation and, in particular, proposals for the testing of an American steam generator at the BN-350 reactor at Shevchenko and several other organizational matters.

The Soviet delegation to the session consisted of the Chairman of the State Committee for the Use of Atomic Energy (GKAÉ), A. M. Petros'yants; the deputy to the minister of power and electrification of the USSR, A. I. Maksimov; deputies of the Chairman of the GKAÉ, I. G. Morozov and A. G. Meshkov; the deputy of the director of the I. V. Kurchatov Institute of Atomic Energy, E. P. Velikhov; the director of the Institute of Theoretical and Experimental Physics, I. V. Chuvilo; the director of the Erevan physics institute, A. Ts. Amatunin; and the deputy of the Chairman of the State Planning Commission of the Armenian SSR, Yu. I. Khodzhamiryan. The American delegation consisted of the Chairman of the US Energy Research and Development Administration (ERDA), R. Simens; deputies of the Chairman, R. Hersch and N. Sivering; President of the US Association of Universities, J. Teip; head of the ERDA Board of the Development and Demonstration of Reactors, E. Bekdzhord; and executive secretary and section head of ERDA, B. Hill. Other participants in the work of the session were representatives of the GKAÉ Board of International Relations, the US Committee on the licensing of reactors, and the US Embassy in Moscow.

The session was held in the conference hall of the Praesidium of the Armenian Academy of Sciences. Its participants were greeted by the deputy of the President of the Soviet of Ministers of the Armenian SSR, K. A. Gambaryan. In his address he noted, in particular, that the problems discussed at the session were of great interest for Armenian physicists and energy specialists, because the first Armenian nuclear power station was nearing completion at Zakavkaz.

The discussion and debate occurring in the course of the Fourth Session was thoroughly businesslike and constructive. Both sides expressed a high opinion of the major results of the previous year's cooperation.

Reporting on the work of fast-breeder reactors, A. G. Meshkov and E. Bekdzhord noted the efficiency of the working conferences and seminars in 1976, which dealt with such pressing problems as the dangers of fast-breeder reactors with sodium coolant, and improvement in reliability and accident-prevention measures in using the steam generators of these reactors. An exchange of samples of constructional materials was begun and the results of physical calculations of standard reactors were also exchanged.

The program of cooperation on fast-breeder reactors in 1977 envisaged further expansion in the range of problems that are the subject of joint discussion and joint experimental investigation.

By mutual agreement, cooperation in 1976 on controlled nuclear fusion centered mainly on problems associated with the development of thermonuclear systems with magnetic containment of plasma, and the design, on this basis, of a reactor to demonstrate, in principle, the feasibility of controlled thermonuclear fusion. Whereas in previous years the two sides had been largely concerned with exchanging detailed information on the state of investigation and development in the USSR and the USA, in 1976 there was scientific and technical cooperation on a wide range of problems. The 1976 program of cooperation was characterized by

Translated from Atomnaya Énergiya, Vol. 42, No. 4, pp. 341-342, April, 1977.

the participation of specialists from both sides in experiments based at existing Soviet and American thermonuclear centers, and also by the creation of special groups and the calling of working conferences on the basic scientific – technical problems of the demonstration reactor and the development of design principles for its main elements. Altogether, 23 joint projects were undertaken.

The 1977 program of cooperation on controlled thermonuclear fusion agreed upon at the session includes 33 joint projects, of which half are associated with the experimental and theoretical investigation of methods of containing and heating plasmas in various magnetic systems, a quarter with the development and testing of elements of the demonstration thermonuclear reactor, and the remaining quarter with the solution of engineering problems of controlled thermonuclear fusion. The cooperation program envisages an increase not only in the number of joint projects, but also in the number of participating Soviet – American organizations. Thus, in the USSR, participant bodies include scientific – technical organizations of the Academy of Sciences of the USSR such as the A. A. Baikov Institute of Metallurgy and the High-Temperature Institute, as well as the Institute of Physics of the Academy of Sciences of the Georgian SSR.

Cooperation of Soviet – American scientists and specialists on the study of the fundamental properties of materials has a long and healthy tradition. Until recently, however, this cooperation was restricted mainly to investigations in nuclear and elementary-particle physics and to exchange of experimental data on the acceleration of charged particles. In 1976 the two sides agreed to examine together the possibility of developing scientific and technical cooperation in such important regions as the physics of solids and the use of nuclear-physics methods in allied fields of science and in applied investigations. All this was expressed in the cooperation program for 1977 agreed at the session. In particular, it was agreed to exchange delgations of specialists on the use of synchrotron radiation and also on the use of pulse neutron beams and beams of accelerated ions in materials science.

In discussing the results obtained in the 1976 program, the two sides noted with satisfaction the high scientific level of the joint experiments, carried out at the accelerator of the Fermi National Laboratory in Batavia (USA). In the experiments, effective use was made of the gas jet target developed at JINR and also of the cloud chamber prepared by Soviet specialists which is highly accurate and reliable in operation. At the beginning of 1977, one of the beams of the Batavia accelerator, which, at 500 BeV, is the most powerful in the world, tests were begun of a promising detector of very-high-energy particles based on the use of transitional radiation. This detector and its operating principle were developed at the Erevan physical institute.

After the conclusion of the session, the American delegation visited the Armenian nuclear power station, the Erevan physical institute, the P. N. Lebedev Physics Institute and the High-Temperature Institute of the Academy of Sciences of the USSR, the I. V. Kurchatov Institute of Atomic Energy, and the BN-350 fast reactor at Shevchenko. In the course of these visits, the American delegation was brought up to date on Soviet work in elementary-particle physics, nuclear power, and laser thermodynamic fusion, were shown Tokamak-type installations and magnetohydrodynamic generators, and could discuss specific problems of Soviet – American scientific – technical cooperation with leading Soviet scientists and specialists at the organizations visited.

The Fourth Session was concluded in an atmosphere of complete mutual understanding between the two sides. The attitudes and proposals of the participants on both sides were informed by a concern to make sound progress and to eliminate the remaining difficulties, mainly of an organizational character. This businesslike attitude and concern for the further development and strengthening of Soviet – American cooperation is reflected in the final document resulting from the session, the Protocol of the Fourth Session, which was signed on behalf of the two sides by A. M. Petrosyan and R. Simens.

FIFTH ALL-UNION CONFERENCE ON CHARGED-PARTICLE ACCELERATORS

V. A. Berezhnoi

The conference, which took place on Oct. 5-7, 1976, at Dubna, was attended by representatives of all the interested organizations in the USSR, and also 39 scientists from 12 other countries. At the two plenary sessions devoted to current trends in the development of accelerators (chairmen A. A. Vasil'ev and A. A. Naumov) only review papers were presented.

Following a well-established tradition, the papers presented at the first plenary session were devoted to the most urgent lines of physical research and the requirements for the next generation of accelerators. These papers were presented by A. A. Logunov, B. A. Arbuzov, and G. N. Flerov (on the prospects for the development of high-energy physics and the physics of heavy ions).

Much interest was aroused by material on superhigh-energy accelerators and especially by a report on the successful start-up of the CERN 400-GeV proton synchrotron. Future projects were considered in papers on the accelerator – accumulator complex of the Institute of High-Energy Physics (IFVÉ), including reports on opposing pp beams using a method of electronic cooling developed at the Institute of Nuclear Physics of the Siberian Branch of the Academy of Sciences of the USSR (and now recognized around the world) and on the next stage in the development of the accelerator complex of the Fermi National Laboratory at Batavia (USA). It is also necessary to note the work being carried out at Batavia on energy doubling.

The delegates at the conference were very interested in papers on the implementation of the PETRA project (German Federal Republic) and on installations with opposed e^-e^+ beams at the Institute of Nuclear Physics of the Siberian Branch of the Academy of Sciences of the USSR. Other papers that were received with interest dealt with the start-up of one of the largest isochronous cyclotrons in Europe, the U-240 machine of the Institute of Nuclear Research of the Academy of Sciences of the Ukrainian SSR, and with the course of development of annular injectors for the IFVÉ accelerator and cyclic accelerators for obtaining powerful neutron beams.

At present, various lines of physical research are associated with the acceleration of heavy ions, in which there has been considerable progress in recent years. At Darmstadt (German Federal Republic), there is the UNILAC universal linear accelerator, in France the GANIL project is beginning, and at the Laboratory of Nuclear Development of JINR the powerful U-400 isochronous cyclotron is under construction. Operating these installations at their design parameters will allow beams of heavy ions (up to uranium) of high intensity to be obtained. Several papers at the session were devoted to the improvement of existing equipment, and also new accelerator designs capable of generating beams of heavy ions of energy several hundred MeV/nucl.

In recent years, the LAMPF (USA), SIN (Switzerland), and TRIUMF (Canada) high-intensity meson generators have begun operation, while the meson generator of the Institute of Nuclear Research of the Academy of Sciences of the USSR and the high-current phasotron of the Laboratory of Nuclear Development of JINR are under construction. These and other matters were discussed in sessions on cyclic and linear high-current proton accelerators.

The SIN and TRIUMF cyclic meson generators have gradually achieved the design parameters on intensity, and serious progress is noted in the work of the Los Alamos National Laboratory (USA), where a linear accelerator is stably operating with a mean current 100 μA and where beams of protons and H^- ions are simultaneously accelerated. Reports that were received with interest dealt with the development of the supercyclotron, a high-current meson generator of the next generation, the "F" installation, and other accelerators of various descriptions. The progress achieved in the investigation of accelerators with high-frequency focusing (IFVÉ)

Translated from Atomnaya Énergiya, Vol. 42, No. 4, pp. 342-343, April, 1977.

and high-current linear meson-generator accelerator of the Institute of Nuclear Research of the Academy of Sciences of the USSR was noted.

Papers on equipment with opposed e^-e^+ beams aroused the interest of the conference delegates, in connection with the latest discoveries (J and ψ particles, etc.). Machines of this kind at present under construction are the VÉPP-4 (USSR), the PEP (USA), and the PETRA (Germany Federal Republic); the DCI machine (France) is at the start-up stage, and even larger designs are under development. The VÉPP-4, PEP, and PETRA machines complement one another (as regards the working region of energy and the possibilities of physical experiments) and, with their completion, it will be possible, in the years to come, to operate with energies in the range $2 \cdot (4\text{–}19)$ GeV in the center-of-mass system. The possibility of carrying out experiments on opposing beams with transverse polarization (VÉPP-2M, SPEAR) is of great interest for physics.

In experiments on electronic cooling at the Institute of Nuclear Physics of the Siberian Branch of the Academy of Sciences of the USSR, rapid compression of the phase volume of the cooled particles is observed, which gives good prospects for the creation of opposing pp beams of high intensity. At CERN, the method of stochastic cooling is being developed, which will probably be added to the method of electronic cooling in the future.

Further progress in accelerator science and technology is associated with the development of methods of radiation protection. At the session devoted to these problems, papers of note were those on the radiational stability of materials (IFVÉ) and methods of calculation of the radiation fields close to a proton accelerator and behind protective shielding (Radioengineering Institute of the Academy of Sciences of the USSR).

There has been considerable success in developing ion sources and in improving and developing direct-action accelerators. A representative of HVEC (USA) gave an interesting paper on the prospects for the development of a tandum accelerator, which noted, in particular, that accelerators of 20, 25, and 30 MeV are beginning construction. In a review paper, a representative of JINR concluded that in the coming years new types of source will significantly enlarge the possibilities in the field of multicharge-ion accelerators.

At the session on particle dynamics in accelerators and accumulators, the most important paper reported recent results in collective methods of acceleration (Physics Institute, Academy of Sciences of the USSR), drawn from the proceedings of the second symposium at Dubna. Most of the papers dealt with increase in intensity in cyclic accelerators by various methods of imposing coherent and incoherent instability; by this means it is possible to optimize the beam intensity and to ensure reliable operation of the equipment.

Further development of accelerator technology would be difficult or even impossible without the use of superconductivity. This and other topics were considered in the session on magnetic systems, including superconducting systems. A report on the development of superconducting systems in the USA, the German Federal Republic, France, and the USSR aroused much interest. Progress in creating such systems was much assisted by the fact that by correct choice of the construction and the technology of preparation the so-called aging effect can be practically eliminated.

Conference delegates were particularly interested in the session on increasing the efficiency of the use of accelerators in physical experiments. Papers of note dealt with methods of attaining superhigh energies for accelerator beams, possibilities of formation and separation of beams of secondary particles (IFVÉ), and properties of secondary-particle channels of meson generators built in the USSR (Institute of Nuclear Research, Academy of Sciences of the USSR). A paper from the Argonne National Laboratory (USA) reporting recent results on the acceleration of polarized protons in a synchrotron with zero gradient caused some excitement.

Particular mention must be made of the session devoted to the use of accelerators in medicine, applied research, and industry, which presented a startling picture of the introduction of accelerators into the world of practical human activity. These issues were discussed by scientists of the NIIÉFA and other organizations. News of work devoted to problems of the use of synchrotron radiation came from England, the USA, and the USSR (Institute of Nuclear Physics of the Siberian Branch of the Academy of Sciences of the USSR).

At the session on the modernization of existing accelerators, attention centered on a paper describing the increase in intensity of the IFVÉ accelerator to $5 \cdot 10^{12}$ protons/pulse, which must be regarded as an important achievement. Other papers of note dealt with the operation of the synchrotron of the Institute of Theoretical and Experimental Physics after reconstruction and the increase in intensity of the JINR synchrophasotron to $1.2 \cdot 10^{12}$ protons/pulse. A delegate from CERN read a paper reporting successes achieved with the booster accelerator in terms of intensity and reliability. The overall conclusion to be drawn from the session is that

the construction of new accelerators and the modernization of old machines is proceeding on a reliable theoretical base.

Results on the development of a powerful electron accelerator, which has applications both within and outside accelerator technology, were reported in the session on superhigh-current pulse accelerators. Work proceeding in a number of research organizations in the USSR has allowed the time range of the current to be extended to tens of microseconds and important results have been obtained on reducing the dimensions of individual units of the high-current accelerator.

It appeared at the session on the automation of accelerators and accumulators that a qualitatively new level of automation has been reached, as a result of the wide use of elements with a high degree of integration, the use of a third-generation computer, and the development of complex high-level languages in the programs provided for the experiments.

It is intended to publish the proceedings of the Fifth All-Union Conference on Charged-Particle Accelerators in 1977.

THIRD SESSION OF THE SOVIET — AMERICAN COORDINATION COMMISSION ON FAST REACTORS

A. F. Arifmetchikov

At the session, which took place during Oct. 20-22, 1976, at Tbilisi (USSR), the results of cooperation since the second session (Washington, Nov. 1975) were reported, and the program for 1977-1978 was developed. The Soviet and American sides exchanged information on the present state and future prospects of work on fast reactors with sodium coolant.

Soviet — American Cooperation

In the period between sessions the following joint activities had taken place.

1. A seminar was held on the safety of fast reactors at the Argonne National Laboratory in Jan. 1976. In discussing the work of the seminar, the commission selected the following topics as the most important: the retention of fragments within the sodium, including operation with defective fuel elements; the construction and testing of control systems; natural circulation as a means of emergency cooling; and the removal of fragments and radioactive conversion products from the coolant, the gas system, and the equipment [see At. Energ., 40, No. 1. 84 (1976)].

2. A technical conference of specialists on the exchange of material of fast-reactor fuel-element shells was held at Obninsk in July 1976. Agreement was reached as to the range of specimens that were to be exchanged, the period of the exchange (the first quarter of 1977), and the inventory and conditions of the experiments to be carried out by the two sides. There was a discussion of the results on the properties of materials used in the shells and cases of fuel-element assemblies in the USA and the USSR [see At. Energ., 41, No. 5, 367 (1976)].

3. A seminar on improvements in reliability and accident prevention in the use of steam generators for fast reactors was held at Dmitrovgrad in July 1976. The seminar led to the constitution of a technical conference of specialists, at which agreed programs of cooperation were developed on the following topics: investigation of the effects of reactions for small and large leakage of water into the sodium; methods of detecting leakage of water and sodium in steam generators; carbon transfer in the second sodium loop of fast reactors.

4. The specification and exchange of tube specimens from steam generators and intermediate heat exchangers not normally in contact with sodium was agreed upon. The specimens were used in the programs on small

Translated from Atomnaya Énergiya, Vol. 42, No. 4, pp. 344-346, April, 1977.

TABLE 1. State of US Fast-Reactor Program

Stage of program	FFTF	CRBRP	PLBR	CBR
Design	Close to completion	Detailed design of installation developed	Design preliminaries	General problem formulated
Technical programs	Complete	Successfully completed	Formulation of requirements complete	
Test bed	In use	Modeled	Proposals formulated	

leakage and carbon transfer (item 3). In the first half of 1977, it was hoped to reach agreement on the conditions of exchange of specimens usually in contact with sodium.

5. Results of physical calculations of a standard fast reactor were exchanged.

Both sides expressed satisfaction at the work accomplished.

The program of Soviet–American cooperation on fast reactors with sodium coolant in 1977-1978 provides for bilateral seminars on reactor physics (USSR, 1977); on the development, production, and testing of sodium components excluding the steam generators (USA, 1977); on steam generators (USA, 1978); on fuel-element shell materials (USSR, 1978); and also on the materials of the joint program (items 2 and 3 above).

American Development Program of LMFBR Fast Reactor with Sodium Coolant

The current concern of the American LMFBR program is to develop and demonstrate the feasibility of nuclear power plants with LMFBR and then to prepare for the mass production of the LMFBR. The program has been mapped out up to the year 2000, with minimal financial outlay and wide support from industry. There are five main stages of the program. The first envisages the construction and the start-up, in 1980, of the FFTF reactor with a power of 400 MW (therm.) for testing fuels and materials (Hanford Engineering Laboratory); the second should involve the creation and start-up, in 1983, of a CRBRP demonstration reactor of power 350 MW (el.) on the Clinch River, not far from Oak Ridge. The third stage will consist of the design and start-up, in 1988, of a PLBR reactor of around 1000 MW (el.), the prototype of the large commercial LMFBR. The fourth stage will be the start-up, in 1993, of the CBR-1 reactor of 1500 MW (el.), the first reactor of the commercial LMFBR series, and the fifth stage is the introduction, up to the year 2000, of 30-60 GW (el.), i.e., 20-40 commercial CBR-1 reactors.

The strategy of the program is based on a comparison of the presently known reserves of fissile uranium (3.7 million tons, calculated in terms of U_3O_8) with the fuel requirements of US nuclear power generation. It is assumed that the introduction of a commercial LMFBR in 1993 will allow the ore requirements to be kept at the level of the known reserves until the year 2000.

The LMFBR program (Table 1) may conveniently be divided into the development of the design (detailed design of the installation, licensing, placing orders for the equipment, construction, testing, start-up, running-in to full power), the technical programs (physics, materials, chemistry, fuel, components, safety, fuel cycle), and the test-bed stage (testing of the equipment).

The creation of the FFTF, CRBRP, and PLBR installations (Table 2) has been allocated 8.6 billion dollars (design 2.6, technical programs 3.7, test bed 2.3), of which 4 billion dollars has already been spent.

TABLE 2. Characteristics of Planned and Constructed Installations

Parameters	FFTF	CRBRP	PLBR	CBR
Power, MW	400 (therm)	350	1 000	1500
Mean fuel consumption, MW · day/ton	50 000	80 000	100 000	—
Doubling time, yr	—	25—30	20	12—15
Fuel charge, tons	2,9	4,6	12	—
Date of start-up	1980	1983	1988	1993

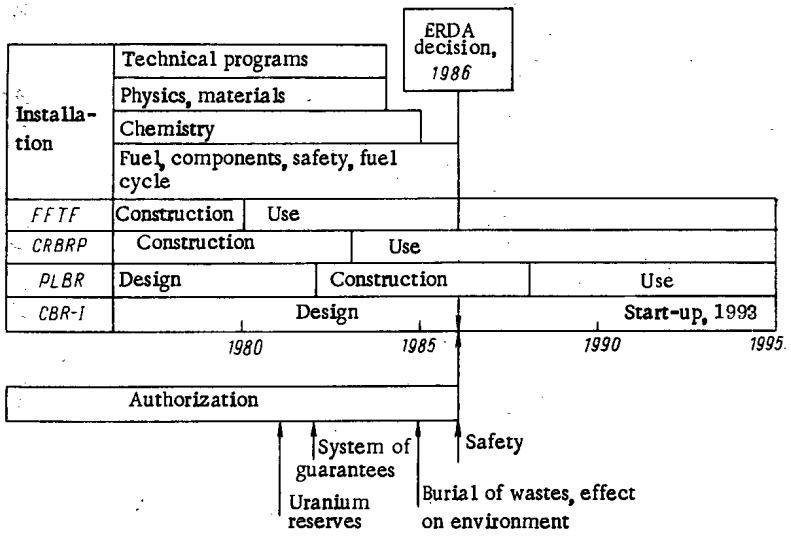

Fig. 1. Diagram of work on LMFBR program.

The critical moment of the program will come in 1986, when the ERDA leadership will be ready to make a decision on the implementation of a broad program of breeder reactors. By this time, the main technical program must have been concluded and approval (authorization) must have been obtained for programs on estimates of the US uranium resources, the development of a system of guarantees on the safety of nuclear fuel, the burial of radioactive waste, the effect of nuclear power stations on human health and the surrounding environment, and nuclear-power-station safety (see Fig. 1).

At present, work on the construction of the FFTF reactor is 62% complete and the procurement plan of the equipment is 98% complete. More than half the basic equipment for the CRBRP reactor is at the stage of being made or ordered. However, work on the constructional platform has not yet begun, because of a delay in ERDA authorization for "nonnuclear" work. Calculations of the safety and environmental impact are being considered by the Licensing Commission. It has been noted that obtaining a license is the most difficult step in CRBRP design, delaying the remaining work.

General Electric, Atomics International, and Westinghouse Electric are carrying out preliminary design work on the PLBR reactor to determine its main parameters and the requirements for the technical program. This stage should be concluded in 1978; however, it has already been decided that the PLBR will be a loop reactor of power around 1000 MW (el.). The main aim in producing the PLBR is to establish the confidence of the energy utilities in fast reactors and to estimate the potential for industry in the production of equipment for the high-power LMFBR. The design stage should end in 1982 and the technical programs in 1984. The delivery of the equipment to the constructional platform will begin in 1985. Before the end of 1976 preliminary estimates of expenditure will be made, and the administrative structure for design control will be decided.

It is intended to produce the main equipment and assemblies of the installation in "commercial" form, i.e., so that it can be used directly in the commercial CBR-1 reactor.

By 1986 the design of the CBR-1 reactor should be finished, but a decision as to its construction depends on the decision of the ERDA leadership. Other CBR reactors are also at the design and licensing stage.

The energy utilities, ERDA, national and engineering laboratories, and industry participate directly in the US LMFBR program. Their participation in the program is distributed as follows. The energy utilities formulate the requirement for commercial reactors, participate in the financing of the demonstration projects, and serve as the link between the LMFBR program and industry. ERDA ensures the implementation and control of the program and is the source of finance. The national and engineering laboratories carry out the technical programs and control all the test laboratories and test beds. Industry develops the demonstration project, including the programs to produce assemblies and components, and to increase the output power.

It should be noted that the American program is undergoing a time of definite change, associated with a reexamination of the strategy of the program, the wish to reduce financial outlay, the results of completion of the technical programs and the test-bed tests, the industrial potential, experience of the use of fast reactors in other countries, and the attitude of the US public to the LMFBR program. In particular, the data for the

introduction of the FFTF and PLBR reactors has been shifted from 1978 to 1980 and from 1986 to 1988, respectively; the decision to construct a PCTF reactor of 300 MW (therm.) has been reversed, pending tests of the steam-generator module; and plans to construct (after CRBRP) three demonstration reactors of power up to 500 MW (el.) are being replaced by the PLBR-reactor project.

The ERDA leadership regards the LMFBR program as intensive but possible. The decade from 1976 to 1986 should see the creation of a strong base for the fast-reactor program. If the program runs to schedule, then in 90 years' time, the USA will be close to introducing commercial power stations with breeder reactors.

SOVIET — CANADIAN SEMINAR ON THE VIBRATION OF STEAM-GENERATOR TUBES AND FUEL-ELEMENT ASSEMBLIES IN NUCLEAR POWER STATIONS

I. N. Testov and V. G. Federov

There have been two seminars on this theme: in Sept. 1975 in Moscow and in Oct. 1976 in Canada. At the first of these, 16 Soviet and 18 Canadian papers were presented and discussed; at the second, 18 Soviet and 17 Canadian papers. At present there are broad and specifically designed programs of investigation of the basis of vibrational strength in nuclear power stations, with particular reference to steam-generator tubes and fuel-element assemblies. In spite of the significant differences in the construction of Soviet and Canadian nuclear power stations, at the last seminar the most important common problems in this area were discussed: in particular, programs of investigation and methods suitable for the vibrational strength of structures; modeling of vibrations and hydrodynamics and the reliability of transfer of results of model experiments to actual structures; measurements of vibrations of the elements; construction and fitting out of test beds; and the investigation of fretting as applied to steam-generator tubes and fuel elements.

Canadian investigators have been studying the vibration and fretting of fuel-element assemblies, culminating in the development of the complex program Vimod, consisting of three interrelated programs: 1) Strum (Structure Module), the investigation of the parameters of free vibration of the fuel-element assemblies; this program, which uses the method of finite elements, has already been developed for the fuel-element assemblies and horizontal fuel channels of the Bruce reactor; 2) Huform (Hydrodynamic Force Module), the determination of the field of hydrodynamic perturbing forces; Canadian specialists have already begun work on this program; 3) Frem (Fretting Module), the correlation of vibration and fretting; work on this program begins at the end of 1977. The Vimod program as a whole will be used to analyze the likelihood of breakdown due to fretting and to develop design criteria for fuel elements.

The results of vibrational testing of the fuel elements of channels of the CANDU reactor are of interest. Since the actual fuel assemblies are constructed as simple aggregates of rods of a single type (of length 0.5 m), the transfer of results of model experiments to the actual reactor is significantly simplified.

Analysis of the structural tendencies in the modification of standard Canadian fuel assemblies in terms of the character and number of investigations shows that considerable continuity is ensured in the construction of the assemblies, and hence it is possible to pass from a purely empirical basis to the maximum use of all the available data, and the construction of an experimental model of the fretting of fuel assemblies should be accomplished in the near future.

Experimental work by D. Gorman on models of typical tube bundles, in connection with the limiting velocity of transverse flow of the heat carrier showed that the regions of stable vibration and hydroelastic instability of the tubes must be separated by a straight line on the Connors diagram, but the best correlation of the data was obtained for a coefficient of 3.3 (Gorman's experiment) and not 9.9 (Connors' data).

Translated from Atomnaya Énergiya, Vol. 42, No. 4, pp. 346-347, April, 1977.

A considerable number of Soviet papers were devoted to the following lines of research in the vibrations of heat-exchanger tubes:

1) the experimental study of eddy breakaway and vibrations in models of tube assemblies with various geometrical parameters, determining the Strouhal number and the critical rate of hydroelastic excitation of vibrations;

2) the determination of the permissible coefficient of divergence of the frequency of the tube characteristic vibrations from the Karman eddy-breakaway frequency, the choice of suitable gaps between tubes and apertures of the spacing lattice, and the establishing of the load criterion of the vibrations;

3) the reproduction in models of the intensity and frequency spectrum of the vibrations observed in actual tube assemblies;

4) the modeling of the vibrations of tubes immersed in heat carrier of various densities.

In several papers Soviet specialists considered a set of investigations to establish the vibrational strength of the in-reactor equipment used in the VVÉR-440 reactor.

The Canadian specialists also showed interest in Soviet papers on the vibration of fuel elements in a heat-carrier current.

CONFERENCE OF IAEA EXPERTS ON THE PROTECTION OF THE POPULATION IN RADIATION ACCIDENTS

Yu. V. Sivintsev

The second conference of experts on the preparation of a handbook on the protection of the population in radiation accidents was held on Nov. 15-19, 1976, at Ankara in Turkey (the first was held in Dec. 1975 at Vienna). The participants were 42 experts from the 15 member countries of the International Atomic-Energy Agency (IAEA), and administrators of that agency and of two international organizations (Euratom and the World Health Organization).

The main aim of the conference was to discuss the structure and content of a handbook on the protection of the population in the event of a radiation accident. This term denotes those accidents at nuclear installations (e.g., power stations) which result in the release of large quantities of radioactive material outside the limits of the protected region, leading to a risk of radiational injury of part of the population. The handbook under preparation is intended to provide a set of recommendations for countries which have nuclear installations on planning measures to protect the population in the event of a radiation accident. In the course of the conference, 24 documents were published, and roughly 70% of the text of the recommendations was prepared. The radiational safety unit of IAEA proposes to develop new material for the project and to submit it to experts of the participant nations in the first half of 1977. In addition, a third conference is planned for the final work on the handbook project.

In the course of the Ankara conference, it was decided to exclude from the test of the recommendations any quantitative information, and to include only two basic figures: 1) the appearance of malignant neoplasm is reliably established at large doses of radiation (100 rad); 2) the irradiation of the whole body by a dose of more than 100 rad in all cases must be the signal for the implementation of protective measures. More detailed radiobiological data will form Appendix A of the handbook.

The remaining quantitative information, in particular, on derived accidental standards, will form Appendix B to the final text of the handbook. The main material in this appendix will be quantitative values from the 1975 report by the UK Medical Research Council on criteria for the protection of the population after accidental release of radioactive materials.

Translated from Atomnaya Énergiya, Vol. 42, No. 4, pp. 347, April, 1977.

The IAEA administration is to prepare and distribute to the member countries an inquiry into the quantitative criteria developed and used to estimate the scale of radiation accidents and the implementation of accident-prevention measures for the protection of the population. A summary of this material will form Appendix C to the final text of the handbook.

THIRD INTERNATIONAL SUMMER SCHOOL ON RADIATION PROTECTION

N. G. Gusev

The aim of the school, which took place from Aug. 24 to Sept. 3, 1976, in Gertseg Novi (Yugoslavia), was to provide scientific and consultative – procedural assistance to nations developing nuclear power in solving problems of radiation protection. Like its predecessors, the third school was organized by the B. Kidrich Institute of Nuclear Physics (Yugoslavia) under the aegis, and with the assistance, of the IAEA. It was attended by around 100 people from 18 countries and two international organizations (IAEA and the UN NKDAR). In all, 39 papers were heard and discussed.

The papers relating to radiation safety may be briefly mentioned. K. Morgan (USA) reported on various sources of ionizing radiation and levels of radiation raising problems of radiation safety. In a sample of workers at the Colorado uranium mine (4000 people from a personnel of 15,000-20,000), 170 cases of lung cancer were found, although only in individual cases was the radon concentration above the permitted working limit ($3 \cdot 10^{-11}$ Ci/liter). The mean individual radiation dose among US nuclear-power-station personnel is 1 rem/yr, while between 1969 and 1973 the collective dose (calculated per power station) rose from 188 to 404 man-rem/yr. Morgan suggested limits of 40 and 400 man-rem/yr on the collective radiation dose of the personnel and the surrounding population, respectively, in the case of a nuclear power station of 1000 MW (el.). Another paper by Morgan considered the dose – effect problem and noted, in particular, that not all radiation effects increase linearly with dose. Skin inflammations, cataracts, nausea (for a single dose of 20 rem at 0.01%) and finally radiation death (for a total single dose of 300-500 rem) have a threshold dependence. It has recently been established that the yield of somatic injuries at 1 rad in a low dose (or dose rate), and in particular for α radiation, is higher than would be expected on the linear hypothesis. The risk of the appearance of leukemia in children between the ages one and four who have an allergy is larger by a factor of 3.7 than for all children of the same age group. If these children are irradiated in utero, the risk rises to $24.6 \cdot 10^{-6}$ cases/rad.

V. Klener (Czechoslovakia) presented three review papers on the risk of somatic, genetic, and teratogenic effects of radiation. According to these data, the risk of the appearance of malignant neoplasm is $150 \cdot 10^{-6}$ cases/rem with a time of latency of the effect of 40-50 years.

TABLE 1. Population Dose Caused by Globally Distributed Radionuclides Normalized to 1 MW (el.)

Nuclide	Rate of discharge	Dose, man-rem/MW·yr
^{85}Kr	400	0,16
^{3}H	20	0,06
^{14}C	0,02	2*

*This figure for ^{14}C is calculated for 500 years of irradiation. The dose to total decay is 9 man-rem/MW·yr.

Translated from Atomnaya Énergiya, Vol. 42, No. 4, pp. 347-349, April, 1977.

Klener's second paper gave risk coefficients for the appearance of genetic effects calculated for a double dose of 20 rad. In the opinion of V. Snyder (USA), the total risk coefficient of lethal outcomes may be taken as $(1.5\text{-}2)\cdot10^{-4}$ cases for a 1-rem dose. For the somatic consequences, D. Beninson (UN NKDAR) recommended the adoption of a risk coefficient for lethal outcomes $R = 1\cdot10^{-4}$ cases/rem. In another paper by Beninson, estimates of the collective radiation dose of personnel, calculated per MW (el.) of power developed for the total fuel cycle, gave the following results, man-rem/MW·yr:

Uranium mine	0.08
Cycle from mine to fuel-reprocessing plant	0.25
Reactors:	
light-water (USA)	1.3
gas-cooled (UK)	0.73
gas-cooled (Japan)	1.2
Fuel-reprocessing plant (NKDAR data)	1.6
Fuel transportation	0.001
Total cycle in nuclear industry (NKDAR data)	2-3

Beninson's data (Table 1) may be used to make rough predictions of the risks of using nuclear energy.

The individual and general risks of various sicknesses and death from natural causes characteristic for other modern occupations were discussed in a paper by M. Delplas (France).

A paper by B. Lindell (Sweden) examined the use of risk–benefit calculations for the whole fuel cycle of the nuclear industry and the principles of the calculation of the maximum permissible discharge (MPD) of radionuclides on the basis of the radiological capacity of the surrounding environment. The same ideas were developed in a paper by R. Coulomb (France), which discussed the behavior of transuranium radionuclides in marine waters. The concentration factors in marine hydrobionts were found to be 70 for fish, 200 for molluscs, 500 for crustacea, 1175 for algae, 1495 for sponges, and 4290 for lichens. B. Argie (France) generalized data on radioactive wastes and the radiation dose of personnel at French nuclear power stations over the last three years. In 1975, the collective radiation dose of personnel, normalized to 1 MW (el.), was 0.29 man-rem/MW·yr.

Speaking of the problem of control in the environment, O. Ilari reported that in Italy the working limits for environmental contamination are: ^{3}H $3\cdot10^{-6}$ Ci/liter of water; ^{90}Sr $1\cdot10^{-8}$ Ci/kg of fish and $4\cdot10^{-9}$ Ci/liter of milk; ^{131}I $2\cdot10^{-9}$ Ci/kg of fish and $4\cdot10^{-10}$ Ci/liter of milk. Papers by L. Farge (IAEA) considered the effect on the environment of noxious wastes in the production of electrical energy by various means, and also gave a review of models of the dispersal of aerosols in the atmosphere.

J. Swiebach (German Federal Republic) provided data on the activity of the primary heat carrier of nuclear power stations: according to the sum of iodine isotopes, 0.01; ^{131}I 10^{-4}–10^{-3}; corrosion products 10^{-6}; ^{239}Np 10^{-6}–10^{-4}; ^{3}H 10^{-4}–10^{-3} Ci/liter. In the water of the first loop, ^{239}Pu may also be found. The same paper gave figures for the minimum limit of detection of modern instruments: for continuous γ-spectroscopic monitoring of a mixture of radioactive inert gases (RIG) 10^{-11} and for ^{135}Xe $2\cdot10^{-10}$ Ci/liter; for a mixture of β-active aerosols by γ spectroscopy of filters obtained in a week-long test, 10^{-17}–$4\cdot10^{-16}$ Ci/liter; for a ^{131}I aerosol (measurements of a filter obtained in a seven-day test), $4\cdot10^{-17}$ Ci/liter; ^{3}H in the gas phase 10^{-11} Ci/liter; α-active aerosols (three-month test), $4\cdot10^{-17}$ Ci/liter.

In liquid wastes, laboratory methods are able to measure samples of specific activity as follows: ^{3}H $1\cdot10^{-9}$; ^{51}Cr $5\cdot10^{-9}$; ^{60}Co $1\cdot10^{-9}$; $^{89,90}Sr$ $2\cdot10^{-11}$; ^{131}I $7\cdot10^{-10}$; ^{137}Cs $8\cdot10^{-10}$ Ci/liter water. In 1971-1975 the rate of discharge of gaseous wastes from seven reactors was as follows: RIG 120-35,200; short-lived aerosols 0.003-88; long-lived aerosols 0.008-0.046; ^{131}I 0.001-1.3; ^{3}H 15-100 Ci/yr. In 1974, 427 Ci ^{3}H and 4.6 Ci of fission and corrosion products were released in liquid states.

According to the data of G. Lusen (France), the liquid-metal heat carrier of the Phoenix reactor of power 590 MW (therm.) and 264 MW (el.) has specific activity 6.2 Ci/kg for ^{24}Na and 10^{-4} Ci/kg for ^{22}Na, specific activity in the second loop $8\cdot10^{-7}$ Ci/kg for ^{24}Na, mean individual radiation dose of the personnel 0.015 rem/yr (maximum 0.29 rem/yr), and collective radiation dose of the personnel, for 248 people, 3.69 man-rem/yr. For the Phoenix reactor, situated in a densely populated area, the RIG MPD is 85,000 Ci/yr, which is less by a factor of 100 than the MPD of reactors in less populated areas. The actual discharge does not exceed 140 Ci/yr. A second paper by Lusen gave technical characteristics of the Superphoenix reactor of power 1200 MW (el.), and described the technical means by which the discharge of gaseous radionuclides to the external atmosphere is kept

below 360 Ci/yr (mainly ^{85}Kr and ^{133}Xe), while the amounts of iodine nuclides and tritium are negligibly small. The intention is to keep the levels of irradiation of the population in the area around the power station below 1% of the dose of natural radiation.

N. G. Gusev (USSR) outlined the physical principles of a method of calculating the individual and population doses caused by gas and aerosol discharge from a nuclear power station. The paper contained considerable original material. Another paper by Gusev described the use of this method to estimate the radiational danger to the population in accidental discharges of sodium by fast breeder reactors.

P. Markovich (Yugoslavia) reported the use of SI units in radiometry and radiology. The International Commission on Radiational Units and Measurements (ICRU) proposed in 1975 that the unit of absorbed dose be called the Gray (Gy): 1 Gy = 100 rad = 1 J/kg. The name proposed for the unit of activity is the Becquerel (Bq): 1 Bq = 1 sec^{-1} = $2.703 \cdot 10^{-11}$ Ci.

In the view of the ICRU, the units that are not consistent with the SI system – the rad, the roentgen, and the curie – should be replaced by the Gray, the C/kg, and the Becquerel over a period of not less than 10 years. I. Dvornik (Yugoslavia) presented an interesting report on accident dose meters of small range with inflexibility. Sources of nonionizing radiation were characterized in three papers by V. Hamm (USA), which considered the biological effects of UV, visible, IR, and laser radiation. Three papers by D. Sleaney (USA) discussed the dosimetry of nonionizing radiation and the regulation of protection against UV, visible, and IR radiation.

The proceedings of the Third International School on Radiational Protection will be published by the B. Kidrich Institute of Nuclear Physics.

D. Eadie et al.

STATISTICAL METHODS IN PHYSICS*

Reviewed by G. A. Ososkov

Unlike nany others, the present book – the text of lectures given in 1968-1969 to scientists at CERN by the statistician D. Eadie and four physicists specializing in high-energy investigations – provides an adequate treatment of the problems of probability theory and statistics as they affect experimental and theoretical physicists.

The main strength of this book is its practical character, which is especially apparent in the choice of a large number of examples from high-energy physics. These examples, together with many useful practical recommendations on the choice of methods of estimating parameters or criteria so as to verify hypotheses, are of great interest as an expression of the rich experience of one of the largest international scientific centers.

The book consists of 11 chapters, a bibliography, and an alphabetical index. In addition, the editor of the Russian translation, A. A. Tyapkin, has included in the book a large appendix (in three sections) and also supplementary bibliographical material, and has inserted a number of footnotes in the text.

The first chapter is an introduction, in which the technical terms used in the book are defined, a list of required expressions is given, and the authors' view of the differences between the Bayes and anti-Bayes approaches to the theory of estimates is given. As well as stressing that the use of the Bayes theorem is restricted, although completely competent when there is a priori knowledge of the parameters to be estimated, the authors use the idea of Hodges and Lehmann [J. Hodges and E. Lehmann, "The use of previous experience in reaching statistical decisions," Ann. Math. Stat., 23, 396 (1952)] on the generalization of the Bayes approach to the case when a priori data are absent, by introducing so-called subjective probabilities, and in what follows carry out parallel treatments by the two approaches. These questions are discussed in detail in the first section of the appendix.

Chapters two to five are devoted to probability theory, the basic ideas of which are outlined in the second chapter.

In the third chapter, various ideas of convergence are introduced, and the law of large numbers is formulated. The central limit theorem is also stated and proved for the case of identically distributed independent terms.

In the fourth chapter, after a description of the properties of the better-known discrete and continuous distributions, examples of distributions encountered in practice are given, together with methods involving them.

The authors attach great value to the idea of information on the parameter under investigation contained in the selected data; in the fifth chapter, following R. Fisher, information is introduced as the mean value of the second derivative of the probability function with respect to the parameter. After studying the properties of information, the idea of sufficient statistics is introduced, and the relation between the two ideas is investigated.

In the remaining six chapters of the book, the methods of mathematical statistics are outlined, beginning in chapter six with the theory of solutions. The seventh chapter develops the theory of estimates and describes their properties, methods of obtaining estimates, and asymptotic distributions. The eighth and ninth chapters

*Atomizdat, Moscow (1976).

Translated from Atomnaya Énergiya, Vol. 42, No. 4, pp. 349-350, April, 1977.

give a more detailed investigation of the properties of estimates and the requirements placed on them, descriptions and comparisons of various methods of obtaining estimates, and valuable practical recommendations of their use; the eighth chapter is concerned with accurate estimates and the ninth with ranges of values. Particular attention is given to the subject of the verification of hypotheses and the comparison of experimental data with theoretical distribution laws by means of consistency criteria. Various means of verification are given in the tenth chapter for simple hypotheses. The powers of various verification criteria are compared and successive criteria are explained. In the eleventh chapter, consistency criteria independent of the form of the distribution are described. A special paragraph is devoted to the real problem of the resolution of a fine structure superimposed on a certain background and other frequently occurring problems.

In the appendix to the book, as well as the very useful section mentioned above, on the main problems of the theory of estimates, there is also a section (by V. S. Kurbatov and A. A. Tyapkin) devoted to the problem of subtracting the background in estimating parameters by the maximum-probability method. The method proposed in this section is distinguished by its simplicity since no parametrization of the curve is required to describe the background experiment and even the smoothness of the background, and it reduces to the direct analysis of sets of events obtained in the main and background experiments.

The editor of the translation has included in the appendix a third section (by I. N. Silin) outlining the valuable practical experience of JINR, where very effective methods of minimizing nonlinear functions have been developed and appropriate programs devised.

The difficult work of translating this book, which occupies a position at the boundary of mathematics with physics, was carried out by V. S. Kurbatov at an adequately high level. There are a few inadequacies to be noted: in addition to a number of misprints, the translation of the heading of paragraph 4.3.3 is plainly inadequate, the bibliography contains errors, and there are several infelicities of style. It is also regrettable that the translator and editor were unable to include in the Russian text several of the features of the original which would make the book a more convenient work of reference. In the translation, the detailed list of practical examples used with the section in which they are to be found has disappeared, and the index has been needlessly shortened. It is also surprising that so few copies of the book have been produced, making it at once a bibliographical rarity, despite the poor quality of the paper on which it has been printed.

However, all these points in no way reduce the general high estimate of the book, which will certainly be used by a wide circle of readers and will facilitate a further increase in the level of mathematical culture relating to the treatment of experimental data.

FACHWÖRTER DER KRAFTWERKSTECHNIK. TEIL II. KERNKRAFTWERKE. DEUTSCH – ENGLISCH*

This dictionary contains around 9000 terms in German and English on various aspects of nuclear power and associated fields. It may be useful to working scientists, translators, editors, and specialists constantly working with non-Russian literature on this subject.

*German–English Dictionary of Technical Terms in Power-Station Technology, Vol. II, Nuclear Power Stations, Verlag K. Thiemig, Munich (1974).

Translated from Atomnaya Énergiya, Vol. 42, No. 4. p. 350, April, 1977.

W. Oldekor

EINFÜHRUNG IN DIE KERNREAKTOR- UND KERNKRAFTWERKSTECHNIK*

Like all the others in this series on various problems of the use of atomic energy, these two volumes are written for a wide circle of readers. The first part, consisting of five chapters, is devoted to the theory of nuclear reactors and, in spite of the simplified presentation, requires from the reader a certain preliminary knowledge.

The introductory chapter gives brief characteristics of power reactors of various kinds, but there is no mention of channel reactors. The next chapter contains information on the structure of atoms and nuclei, radioactivity, neutron-induced reactions, and reaction cross section, and examines the fission chain reaction. The third chapter is devoted to the diffusion and retardation of neutrons. The reader encounters the idea of the neutron distribution function, neutron fluxes and currents, the diffusion equation, scattering and resonance absorption of neutrons, and their albedo and growth. The physics of thermal reactors is discussed in the fourth chapter, which gives formulas to determine the coefficient of neutron multiplication, the effects and coefficients of reactivity, neutron distributions, and also numerical examples, mainly for light-water reactors.

Sufficient attention is given to the kinetics and dynamics of reactors, and to their instrumentation and regulation (the fifth chapter).

In the second volume of the book, approximate methods are presented for heat-engineering calculations of light-water reactors (the sixth chapter), a brief account is given of the constructional and nuclear materials used in reactor design and also methods of obtaining, enriching, and reprocessing uranium after its use in reactors (the seventh chapter).

Radiation protection and the reliability of nuclear power stations are treated in the eighth chapter, which describes the characteristics and sources of radioactive radiation, methods of attenuating radiation, and permissible radiation levels; in addition, possible accidents of light-water reactors are described, and the reliability of the reactor vessel is analyzed.

The ninth chapter gives a classification of the most widely used power reactors, including high-temperature and fast reactors, and indicates their constructional features and typical characteristics.

The book concludes with a small chapter outlining elementary methods of calculating the capacity of nuclear power stations to generate electrical energy.

At the end of each volume there is a bibliography and an index.

*Introduction to the Technology of Nuclear Reactors and Nuclear Power Stations, Vols. I and II, Verlag K. Thiemig, Munich (1975).

Translated from Atomnaya Énergiya, Vol. 42, No. 4, p. 350, April, 1977.

engineering science

continued
from back cover

Title	# of Issues	Subscription Price
Metallurgist *Metallurg*	12	$225.00
Metal Science and Heat Treatment *Metallovedenie i termicheskaya obrabotka metallov*	12	$215.00
Polymer Mechanics *Mekhanika polimerov*	6	$195.00
Problems of Information Transmission *Problemy peredachi informatsii*	4	$175.00
Programming and Computer Software *Programmirovanie*	6	$95.00
Protection of Metals *Zashchita metallov*	6	$195.00
Radiophysics and Quantum Electronics (Formerly Soviet Radiophysics) *Izvestiya VUZ. radiofizika*	12	$225.00
Refractories *Ogneupory*	12	$195.00
Soil Mechanics and Foundation Engineering *Osnovaniya, fundamenty i mekhanika gruntov*	6	$195.00
Soviet Applied Mechanics *Prikladnaya mekhanika*	12	$225.00
Soviet Atomic Energy *Atomnaya energiya*	12 (2 vols./yr. 6 issues ea.)	$235.00
Soviet Journal of Glass Physics and Chemistry *Fizika i khimiya stekla*	6	$ 95.00
Soviet Journal of Nondestructive Testing (Formerly Defectoscopy) *Defektoskopiya*	6	$225.00
Soviet Materials Science *Fiziko-khimicheskaya mekhanika materialov*	6	$195.00
Soviet Microelectronics *Mikroélektronika*	6	$135.00
Soviet Mining Science *Fiziko-tekhnicheskie problemy razrabotki poleznykh iskopaemykh*	6	$225.00
Soviet Powder Metallurgy and Metal Ceramics *Poroshkovaya metallurgiya*	12	$245.00
Strength of Materials *Problemy prochnosti*	12	$295.00
Theoretical Foundations of Chemical Engineering *Teoreticheskie osnovy khimicheskoi tekhnologii*	6	$195.00
Water Resources *Vodnye Resursy*	6	$190.00

SEND FOR YOUR
FREE EXAMINATION COPIES

Plenum Publishing Corporation

Plenum Press • Consultants Bureau
• IFI/Plenum Data Corporation

227 WEST 17th STREET
NEW YORK, N. Y. 10011

United Kingdom: Black Arrow House
2 Chandos Road, London NW10 6NR England

Back volumes are available. For further information, please contact the Publishers.

Declassified and Approved For Release 2013/04/01 : CIA-RDP10-02196R000700090004-5

breaking the language barrier

WITH COVER-TO-COVER ENGLISH TRANSLATIONS OF SOVIET JOURNALS

in engineering science

Title	# of Issues	Subscription Price
Automation and Remote Control *Avtomatika i telemekhanika*	24	$260.00
Biomedical Engineering *Meditsinskaya tekhnika*	6	$195.00
Chemical and Petroleum Engineering *Khimicheskoe i neftyanoe mashinostroenie*	12	$275.00
Chemistry and Technology of Fuels and Oils *Khimiya i tekhnologiya topliv i masel*	12	$275.00
Combustion, Explosion, and Shock Waves *Fizika goreniya i vzryva*	6	$195.00
Cosmic Research (Formerly Artificial Earth Satellites) *Kosmicheskie issledovaniya*	6	$215.00
Cybernetics *Kibernetika*	6	$195.00
Doklady Chemical Technology *Doklady Akademii Nauk SSSR*	2	$65.00
Fibre Chemistry *Khimicheskie volokna*	6	$175.00
Fluid Dynamics *Izvestiya Akademii Nauk SSSR mekhanika zhidkosti i gaza*	6	$225.00
Functional Analysis and Its Applications *Funktsional'nyi analiz i ego prilozheniya*	4	$150.00
Glass and Ceramics *Steklo i keramika*	12	$245.00
High Temperature *Teplofizika vysokikh temperatur*	6	$195.00
Industrial Laboratory *Zavodskaya laboratoriya*	12	$215.00
Inorganic Materials *Izvestiya Akademii Nauk SSSR, Seriya neorganicheskie materialy*	12	$275.00
Instruments and Experimental Techniques *Pribory i tekhnika eksperimenta*	12	$265.00
Journal of Applied Mechanics and Technical Physics *Zhurnal prikladnoi mekhaniki i tekhnicheskoi fiziki*	6	$225.00
Journal of Engineering Physics *Inzhenerno-fizicheskii zhurnal*	12 (2 vols./yr; 6 issues ea.)	$225.00
Magnetohydrodynamics *Magnitnaya gidrodinamika*	4	$175.00
Measurement Techniques *Izmeritel'naya tekhnika*	12	$195.00

SEND FOR YOUR FREE EXAMINATION COPIES

Back volumes are available. For further information, please contact the Publishers.

continued on inside back cover

Declassified and Approved For Release 2013/04/01 : CIA-RDP10-02196R000700090004-5